Distribution Agreement

In presenting this thesis or dissertation as a partial fulfillment of the requirements for an advanced degree from Emory University, I hereby grant to Emory University and its agents the non-exclusive license to archive, make accessible, and display my thesis or dissertation in whole or in part in all forms of media, now or hereafter known, including display on the world wide web. I understand that I may select some access restrictions as part of the online submission of this thesis or dissertation. I retain all ownership rights to the copyright of the thesis or dissertation. I also retain the right to use in future works (such as articles or books) all or part of this thesis or dissertation.

Signature:

_____ _____

David Ehrlich Date

Critical Periods in the Development of Amygdala Inhibition: The Effects of Prenatal Stress

By

David Ehrlich
Doctor of Philosophy

Graduate Division of Biological and Biomedical Science
Neuroscience

_____
Donald Rainnie, Ph.D.
Advisor

_____
Kerry Ressler, Ph.D.
Committee Member

_____
Peter Wenner, Ph.D.
Committee Member

_____
Gretchen Neigh, Ph.D.
Committee Member

_____
Andrew Jenkins, Ph.D.
Committee Member

Accepted:

_____
Lisa A. Tedesco, Ph.D.
Dean of the James T. Laney School of Graduate Studies

_____
Date

Critical Periods in the Development of Amygdala Inhibition: The Effects of Prenatal Stress

By

David Ehrlich
B.S. Neuroscience, Brown University, 2007

Advisor: Donald Rainnie, Ph.D.

An abstract of
A dissertation submitted to the Faculty of the
James T. Laney School of Graduate Studies of Emory University
in partial fulfillment of the requirements for the degree of
Doctor of Philosophy in

Graduate Division of Biological and Biomedical Science
Neuroscience
2013

Abstract

Critical Periods in the Development of Amygdala Inhibition: Effects of Prenatal Stress

By

David Ehrlich

The amygdala plays a key role in emotional processing, and dysfunction of the amygdala is implicated in a variety of psychiatric disorders. Growing evidence suggests many disorders, including anxiety, depression, autism, and schizophrenia, are neurodevelopmental in origin. During development, brain circuits undergo "sensitive periods" when environmental factors have potent effects that include long-term consequences for emotional processing. We hypothesized that a risk factor for psychiatric disorders, prenatal stress, alters the trajectory of amygdala maturation and thereby influences emotional outcomes. In order to test this hypothesis, however, it was necessary to first understand how the amygdala typically develops. While a number of gross structural and functional changes have been identified in the normally developing amygdala, no studies have characterized amygdala development in terms of the function of neurons. Here, we report the first findings of changes to electrophysiology of the developing amygdala. We used patch clamp in ex vivo rat brain slices to describe the electrophysiology of amygdala neurons, discovering a number of changes. Amygdala neurons exhibited profound maturation of their intrinsic properties from birth through infancy, including reduced excitability, faster action potentials produced at higher rates, and altered expression of membrane currents and the ion channels that mediate them. Developing amygdala neurons also showed corresponding morphological changes, including expansion of dendritic arbors and the emergence of dendritic spines. In addition, synapses for the neurotransmitter gamma-aminobutyric acid (GABA) exhibited changes to kinetics, excitability, and synaptic plasticity. GABA regulates a variety of neurodevelopmental processes, including cell proliferation, migration, and differentiation, as well as synapse maturation, suggesting perturbation of the GABA system could alter amygdala development. We found that GABAergic function in the amygdala was altered by exposure to prenatal stress, with deficits emerging during infancy that preceded long-term changes to neuron excitability. Furthermore, these changes to amygdala maturation correspond with deficits in amygdala-dependent, emotional behavior. In sum, we have provided the first account of physiological development of amygdala neurons, and identified ways in which this process is perturbed by a risk factor for psychiatric illness.

Critical Periods in the Development of Amygdala Inhibition: The Effects of Prenatal Stress

By

David Ehrlich
B.S. Neuroscience, Brown University, 2007

Advisor: Donald Rainnie, Ph.D.

A dissertation submitted to the Faculty of the
James T. Laney School of Graduate Studies of Emory University
in partial fulfillment of the requirements for the degree of
Doctor of Philosophy in

Graduate Division of Biological and Biomedical Science
Neuroscience
2013

Acknowledgements

I would like to thank my thesis committee for their patient and generous guidance and their commitment to my development as a scientist. This work would not have been possible without funding from the National Institutes of Mental Health, the Yerkes National Primate Research Center animal care and veterinary staff, or the support, training, and motivation of the entire Rainnie Lab, including Dr. Chen-Chen Li, Teresa Madsen, Sarah Dewitt, Tom Hennessey, Dr. Stefanie Ritter, Dr. Andrea Crowell, and Wei Liu. Special thanks are owed to Drs. Ji-Dong Guo, Rimi Hazra, and Joanna Dabrowska for sharing an abundance of technical expertise. Drs. Yoland Smith, Ronald Calabrese, Larry Young, and Shawn Hochman, along with Gary Longstreet and Sonia Hayden, constituted a support system much appreciated and often necessitated. The students of the Emory Neuroscience program, including Dr. Damon Lamb, Christopher Makinson, and Mallory Bowers, were an endless source of scientific inspiration, motivation, and perspective. Distinct gratitude is reserved for Steve Ryan, for a productive partnership with a rare mix of heated debate, mutual respect, and true compromise. Finally, to the mentor who inspired these strangers to a common cause and served as a constant advocate and selfless patron: thank you for everything.

In dedication to my mother, who taught me to formulate hypotheses,

my father, who taught me to test them,

and my siblings, who showed me why bother.

Table of Contents

List of Tables and Figures

Abbreviations

AHP, afterhyperpolarization

ASD, autism spectrum disorder

BLA, basolateral amygdala

CP, critical period

E#, embryonic day #

ELS, early life stress

fAHP, fast AHP

GABA, γ-aminobutyric acid

ISI, inter-spike interval

LTP, long-term potentiation

mAHP, medium AHP

MPO, membrane potential oscillation

NS, not significant

P#, postnatal day #

PS, prenatal stress

PV^+, parvalbumin-expressing

R_{in}, input resistance

STD, short-term depression

STF, short-term facilitation

STP, short-term plasticity

SZ, schizophrenia

τ_{memb}, membrane time constant

Chapter 1: The Basolateral Amygdala and Early-Life Stress in Anxiety Disorder Etiology

1.1 Neurodevelopmental Basis of Anxiety Disorders

1.1.1 Emergence of Anxiety Disorders in Children and Adolescents

Psychiatric disorders are increasingly considered developmental phenomena, largely due to high prevalence in juveniles. Of all adults with a mental disorder, over 50% were first diagnosed before 15 years of age (Kim-Cohen et al., 2003). In terms of cases of specific disorders, an estimated 50% of anxiety disorders emerge by age 11, 90% of impulse control disorders by age 19, and 25% of mood disorder cases by age 18. The most prevalent psychiatric disorders in children are, by most accounts, anxiety disorders, due to their early onset and high lifetime prevalence of nearly 30% (Kessler et al., 2005). For example, around 15% of children and adolescents are diagnosed with specific phobias, nearly 10% with social phobias, and around 5% with separation anxiety disorder (Beesdo-Baum and Knappe, 2012).

Anxiety disorders in children pose a significant societal burden, due not only to excessive expression of fear that detracts from quality of life and can require treatment and care, but also to the effects on other health outcomes. Although there are a number of appropriate, age-specific fears that normally manifest during temporal windows throughout development (Gullone, 2000), the expression of excessive or age-inappropriate fears can occur throughout most of life. While the symptoms may change with age, the fearful responses experienced in those with anxiety disorders often continue into adulthood. Furthermore, anxiety disorders in youths contribute to the emergence of secondary psychological complications that include other anxiety disorders, depressive disorders, and substance abuse (Beesdo-Baum and Knappe, 2012). Because of high rates of homo- and heterotypic continuity for anxiety disorders, there is great need for treatments of juvenile anxiety that can intervene and potentially halt the progression of psychiatric illness.

The early emergence of anxiety disorders and the limited treatment options targeted to juvenile anxiety disorders highlight the need for research targeted specifically at their pathogenesis in early life (Cartwright-Hatton et al., 2006). The current conceptualization of

anxiety in juveniles is based almost exclusively on models of adult anxiety disorders. Reframing anxiety disorders as developmental phenomena with distinct pathology in adults and children will be a critical step toward understanding their etiology (Cartwright-Hatton, 2006). Many potentially promising treatments for juvenile anxiety exist, but treatment efficacy is difficult to evaluate because of a limited understanding of the pathophysiology of anxiety disorders in the immature brain (Reinblatt and Riddle, 2007). These limitations stem from a lack of basic research targeted to the development of emotion; the normative development of brain regions that process emotion serves as a platform for the actions of genetic and environmental factors that promote emergence of neurodevelopmental disorders.

1.1.2 Early Life Sensitivity to Stress

One well-documented risk factor for anxiety disorders is exposure to stress. Although the response to an acute stressor is often adaptive, enabling an organism to mobilize an appropriate reaction to the stressor, exposure to chronic or particularly potent stressors is capable of permanently influencing an organism's stress response and emotional behavior. Anxiety disorders can be conceptualized as hyper-activation of certain components of the stress response, and chronic stress has been proposed to predicate anxiety disorders through sensitization to subsequent stressors (Chrousos and Gold, 1992; McEwen, 2004, 2007).

An association between stress and emotional dysfunction is present at all ages, but the effects of stress are particularly robust when exposure occurs during development. The timing of stress exposure is a critical factor, along with duration and intensity, in determining the effects on the brain and emotional outcomes (for review, see Lupien et al., 2009). Early life stress (ELS) is a well-documented risk factor for anxiety disorders, as well as depression, substance abuse, attention deficit hyperactivity, and autism spectrum disorders (MacMillan et al., 2001; Welberg and Seckl, 2001; Nemeroff, 2004; Moffitt et al., 2007; Kinney et al., 2008; Ronald et al., 2010; Wang et al., 2013). Studies in numerous animal models, including rodents and primates, confirm

the potency of ELS in promoting emotional deficits and abnormal stress reactivity later in life (Sanchez et al., 2001; Teicher et al., 2003). In line with the allostatic load model, that the cumulative burden of stress over one's lifetime drives dysfunctional stress reactivity and psychiatric illness, the later-life stress response is influenced by ELS (Graham et al., 1999; McEwen, 2004; Heim et al., 2008; Juster et al., 2010).

1.1.2.1 Effects of Early Life Stress

Animal studies have proven extremely useful in characterizing the effects of ELS, particularly in recognizing the variability and complexity of those effects. Many such studies have recapitulated a number of long-term behavioral deficits caused by ELS in humans; these studies have also identified a variety of neurological and physiological effects discussed in detail below (Maccari and Morley-Fletcher, 2007; Weinstock, 2008).

The specific effects of ELS are dependent on the developmental timing of stress exposure. While direct stress to a child is the prototypical form of ELS, the indirect stress exposure of a fetus, termed prenatal stress (PS), in some cases has more pronounced effects than early postnatal stress (Estanislau and Morato, 2005). A number of studies have linked stress exposure in pregnant mothers to a host of deficits in their offspring (Kofman, 2002; Van den Bergh et al., 2005; Talge et al., 2007), including anxiety (Weinstock, 2001; O'Connor et al., 2003; Van den Bergh and Marcoen, 2004), depression (Weinstock, 2001; Huizink et al., 2007; Markham and Koenig, 2011), schizophrenia (Koenig et al., 2002; Khashan et al., 2008), attention deficit hyperactivity disorder (Huizink et al., 2007; Ronald et al., 2010), and autism spectrum disorders (Kinney et al., 2008; Ronald et al., 2010), as well as developmental delays and altered stress reactivity (Huizink et al., 2003; Bergman et al., 2007; Glover et al., 2010).

To add another layer of complexity, the impact of PS varies with a number of factors, including the timing of stress exposure during pregnancy. For example, stress to mothers during early pregnancy alters stress reactivity and stress neurotransmitter and hormone systems in the

brains of the offspring (Mueller and Bale, 2008). In contrast, stress towards the end of pregnancy causes developmental delays in offspring, influencing a number of physiological and behavioral milestones (Barlow et al., 1978).

The effects of PS also depend on the quality of the stressor. For example, PS that occurs at unpredictable intervals results in developmental delays in rats, while predictable PS does not (Fride and Weinstock, 1984). However, there may be an interaction between stressor predictability and timing on offspring outcomes. Another study in rats comparing predictable and unpredictable stress restricted to the last week of gestation found opposite results: that the predictable stressor elicited the most robust changes in anxiety-like behavior and stress reactivity (Richardson et al., 2006). Comparing studies with different stress paradigms is not straightforward, as stressor intensity controls the long-term effects. Mild PS in some cases has little impact on the offspring (Mabandla et al., 2008), but can also promote fearful behaviors later in life (Griffin et al., 2003; Dickerson et al., 2005). Together, these studies highlight the potent but complex effects of PS, which depends on the timing, potency, and predictability of the stressor during pregnancy.

The impact of PS also depends on the sex of the offspring (Darnaudery and Maccari, 2008). One study found early gestation stress altered behavioral and endocrine components of the stress response and emotional behavior in male, but not female, mouse offspring (Mueller and Bale, 2008). The effects of slightly later gestational stress, presented from E10 to E18, were also detected in male but not female rat offspring, manifesting as emotional and memory deficits at 4 and 6 weeks of age, respectively (Nishio et al., 2001). However, another study found that stress in developing rats, from embryonic day (E)10 to E19 (of the 22-23 day long gestation), increased anxiety-like behavior selectively in female offspring at 4 weeks of age (Baker et al., 2008). Finally, restraint stress from E14 to E21 in rats resulted in a more pronounced increase in anxiety-like behavior in female offspring, but spatial memory deficits selectively in male offspring at 5 weeks of age (Zagron and Weinstock, 2006). Interestingly, the placentas of male but not female

offspring exhibited altered protein expression following early PS (Mueller and Bale, 2008). These findings suggest there are sex differences in the basic mechanisms by which PS alters neurodevelopment, but the effects on each sex vary depending on the age and type of stress exposure.

While the work summarized in this section suggests PS contributes solely to negative outcomes, contrasting reports support a role for some types of PS in promoting resiliency (see **Section 1.4.2**).

1.1.2.2 Maturation of the Stress Response

In order to understand how ELS contributes to the pathogenesis of anxiety disorders, it is necessary to consider the normative and maladaptive function of stress systems. Anxiety disorders can be considered as improper mobilization of the cognitive aspects of the stress response (Charney and Deutch, 1996). The perception of a stressor, defined as an actual or hypothetical disturbance of an individual's environment, leads to the shift of resources towards body systems necessary for immediate survival. The 'stress response' is initiated by activation of a variety of brain regions and involves release of myriad neurotransmitters and hormones. Corticotropin-releasing factor (CRF) is a neurotransmitter that coordinates many of the behavioral, endocrine, and autonomic aspects of the stress response (Vale et al., 1981; Dunn and Berridge, 1990; Owens and Nemeroff, 1991; Smagin et al., 2001). The perception of a stressor triggers immediate release of CRF from the hypothalamus and extended amygdala, which activates the hypothalamic-pituitary-adrenal (HPA) axis. The HPA axis, in turn, stimulates many physiological components of the stress response, including release of catecholamine neurotransmitters and activation of the sympathetic nervous system (for review, see Joels and Baram, 2009). HPA axis activation induces the release from the adrenal glands of hormones of the glucocorticoid family (cortisol in humans, corticosterone in rodents). Glucocorticoids elicit peripheral effects contributing to the stress response, but also pass through the blood-brain barrier

and activate receptors in the brain that provide negative feedback on the HPA axis (Zarrow et al., 1970; Joels and Baram, 2009). Dysfunctional CRF release and activation of the HPA axis have been implicated in the pathophysiology of both anxiety and depressive disorders (Arborelius et al., 1999; Yehuda, 2001; Nemeroff and Vale, 2005).

The function of the HPA axis is not consistent throughout life, and developmental changes in the stress response may contribute to vulnerability to early-life stress. Normative increases in stress reactivity occur during childhood and adolescence, and may generally be adaptive for the novel experiences of this developmental period (Spear, 2009). For example, prepubertal rodents exhibit a prolonged response to acute stress compared to adults, corresponding with increased activation of the paraventricular nucleus of the hypothalamus (Romeo et al., 2006). However, this window of stress hyper-reactivity may intensify a propensity for excessive anxiety in at-risk individuals (Spear, 2009). In contrast, infancy seems to represent a period of reduced sensitivity to stress. In rats, the stress response reaches maturity at the age of weaning (Takahashi et al., 1991). In contrast, during infancy, in rodents there exists a period of reduced responsiveness to stressors, called the "stress hypo-responsive period" (SHRP) or "stress non-responsive period" (Sapolsky and Meaney, 1986). An analogous window of reduced stress reactivity is thought to be expressed in infant humans as well (Gunnar and Quevedo, 2007). Rat pups during this period have low basal and stress-induced cortisol levels (for review, see Levine, 2005). The SHRP is thought to involve active suppression of the stress response (Levine, 2001).

1.1.2.3 Mediators of Early Life Stress Sensitivity

The potent effects of ELS may be explained by heightened sensitivity of the immature brain to chemical mediators of the stress response. The SHRP has been suggested to protect the developing brain from stress hormones (Sapolsky and Meaney, 1986; Francis et al., 1999b), and particularly stressful experiences can elicit a stress response during the SHRP and may thereby cause later life deficits (Levine, 1967; Ladd et al., 2004). The SHRP may be necessary because

the effects of CRF are more potent in the immature brain – infants are far more sensitive than adults to the pro-convulsant effects of CRF, in part because they possess a much higher density of CRF receptors in the brain (Baram and Schultz, 1991; for review, see Korosi and Baram, 2008). Expression of the CRF1 receptor peaks at 180% of adult values during infancy in the amygdala, a critical brain region for the expression and sensitivity to stress that is introduced in **Section 1.2** (Avishai-Eliner et al., 1996). During development from conception through P21, transient overexpression of CRF in the amygdala and throughout the forebrain is anxiogenic later in life, suggesting early CRF sensitivity of the brain may be a key mediator of ELS effects (Kolber et al., 2010).

The effects of PS are mediated, at least in part, by exposure of the fetus to maternal glucocorticoids (Barbazanges et al., 1996; Talge et al., 2007; Field and Diego, 2008). However, the role of glucorcorticoids is still unclear, considering maternal cortisol responses to stress are reduced late in pregnancy, but early in pregnancy, maternal cortisol may be less accessible to the fetus (Talge et al., 2007). One explanation is that, because PS can reduce expression of 11-βHSD2, the placental enzyme responsible for metabolizing cortisol and insulating the fetus (for review, see O'Donnell et al., 2009), chronic PS may weaken the placental barrier and subsequently influence the fetus late in gestation.

PS may also influence offspring through effects on maternal behavior, which has been shown to influence the development of the stress response in the offspring. Variations in maternal care are thought to reflect aspects of the environment, and as such can influence emotional behavior in the offspring (for review, see Zhang et al., 2006). In support of the notion that maternal behavior mediates some effects of PS, cross-fostering to control dams can attenuate some effects of late PS (Barlow et al., 1978; Maccari et al., 1995; however, see Del Cerro et al., 2010). Furthermore, fostering offspring of control dams to dams exposed to stress during pregnancy introduces some mild effects of PS. These findings suggest the effects of PS are

mediated both directly at the time of stress and indirectly by maternal behavior after birth (Barlow et al., 1978).

1.1.3 'Critical Periods' in Development as Windows of Vulnerability

In order to understand how ELS contributes to anxiety disorder etiology, it is necessary to consider its effects in the context of ongoing development of the nervous system. Developmental changes in brain function have been hypothesized to increase an organism's sensitivity to environmental influences (Casey et al., 2000). This notion is exemplified by 'critical periods' (CP), defined as specific developmental windows when ongoing changes align to produce heightened sensitivity to stimuli. Our understanding of CPs has been derived mostly from research in development of the visual system. During visual development, temporary occlusion of a single eye leads to permanent loss of acuity in that eye, which is achieved through re-organization of visual cortex to provide less cortical area for the processing of information from the occluded eye (Wiesel and Hubel, 1963). This effect can only be achieved during a specific developmental window, due to heightened sensitivity to the visual occlusion because of ongoing reorganization of synapses in the visual cortex that naturally occurs during said window (for review, see Hensch, 2005).

It is possible to extend this concept of CPs to the study of emotional development, raising the hope of identifying developmental windows and corresponding processes that are most vulnerable to risk-factors for psychiatric disease. CPs in the development of emotional behaviors have been suggested to reflect CPs for underlying emotional brain circuits (Machado and Bachevalier, 2003). Human studies are beginning to provide support for considering CPs as windows of vulnerability for the effects of ELS (Andersen et al., 2008). However, interpreting the impact of ELS on the development of healthy and maladaptive emotion requires consideration of normative brain development, with specific focus on windows of heightened plasticity and the changing brain circuits that may exhibit CPs for stress sensitivity. To this end, **Section 1.2**

introduces the basolateral amygdala, a brain region that is implicated in the pathophysiology of anxiety disorders, undergoes protracted and marked development, and is sensitive to the effects of stress across the lifespan.

1.2 Juvenile and Adult Anxiety Disorders Involve Dysfunction of the Amygdala

The amygdala is a temporal lobe structure critically involved in emotional processing and behavior. The involvement of the amygdala in social and emotional cognition was first described through gross experimental and specific lesions, (Rosvold et al., 1954; Pellegrino, 1968; Kling et al., 1970; Adolphs et al., 1994; Adolphs et al., 1998; Aggleton and Saunders, 2000). We now know the amygdala functions to assign emotional valence to sensory input, including social stimuli (Adolphs et al., 2000; Davis and Whalen, 2001; Adolphs, 2010) and plays a key role in both the experience and learning of fear and safety (Goddard, 1964; Davis, 2000; LeDoux, 2000). The amygdala contributes not only to the perception and processing of negative stimuli, but we now know it is involved in positive emotional responses including reward (Breiter et al., 1996; Maren, 2003; Hennenlotter et al., 2005; Costafreda et al., 2008).

The amygdala is comprised of many distinct nuclei that act together in a well described circuit, together known as the extended amygdala. Aligned with its role in sensory processing, the amygdala receives input from a number of primary and higher-order sensory regions, the majority of which enters at its basolateral complex, which includes the basolateral nucleus of the amygdala (BLA; McDonald, 1998). The BLA is critical for the production of appropriate emotional responses and the processing of emotional memories (Davis et al., 2003; LeDoux, 2007; Pape and Pare, 2010; Stuber et al., 2011). The BLA not only receives input from a wide variety of brain regions, but also has widespread output: it innervates amygdala output nuclei like the central nucleus (CeA) and the bed nucleus of the stria terminalis (BNST), which mediate fearful and anxious behaviors (for review, see Walker and Davis, 2008); innervates sensory areas to influence sensory perception and memory (Pessoa and Adolphs, 2010; Chavez et al., 2013; Chen

et al., 2013); and innervates the nucleus accumbens to regulate the reward system (Ambroggi et al., 2008; Stuber et al., 2011).

1.2.1 Implicating Amygdala Dysfunction in Anxiety Disorders

The amygdala contributes to the pathophysiology of both adult and juvenile anxiety disorders. The amygdala as a whole was first implicated in anxiety because lesions in humans have anxiolytic effects (Narabayashi et al., 1963). A variety of studies have, more recently, implicated amygdala dysfunction, particularly that of the BLA, in the pathophysiology of anxiety disorders (Davis et al., 1994; Quirk and Gehlert, 2003; Rainnie et al., 2004; Boyle, 2013). Furthermore, changes to amygdala function following traumatic events may underlie disorders like PTSD (Bremner, 2007; Rainnie and Ressler, 2009), consistent with the allostatic load model (McEwen, 2007).

The amygdala, along with other brain structures involved in emotional regulation like the prefrontal and cingulate cortices and the hippocampus, is implicated in the pathophysiology a variety of juvenile affective disorders (Mana et al., 2010). Functional imaging studies indicate that children and adolescents with anxiety disorders exhibit increased amygdala activation, consistent with findings in adults. Excessive activation of the amygdala is also observed in healthy juveniles at high risk for anxiety, including children of parents with anxiety disorders, suggesting amygdala hyper-reactivity is not only a symptom but a risk-factor for anxiety disorders (for review, see Blackford and Pine, 2012). Anxious children show exaggerated amygdala responses to fearful faces, while children with major depression have blunted amygdala responses to the same stimuli. The degree of amygdala hyper-activation positively correlates with the severity of anxiety symptoms (Thomas et al., 2001b).

Hyper-activation of the amygdala in adolescence may be due to limited top-down control of its activity by frontal cortices. In its role as a hub, the BLA innervates the amygdala output regions, the CeA and BNST, and can regulate the activity of the amygdala as a whole (**Figure**

1.1). Via inputs to the BLA, frontal cortices including the medial, ventrolateral, and ventromedial prefrontal cortices (mPFC, vlPFC, and vmPFC) and the anterior cingulate cortex regulate amygdala function and emotional reactivity (Ochsner and Gross, 2005; Eippert et al., 2007; Goldin et al., 2009; Sotres-Bayon and Quirk, 2010; Schulze et al., 2011). An imbalance in the activity of the amygdala and prefrontal cortex during adolescence, brought about by relatively delayed cortical development (Van Eden and Uylings, 1985; Bourgeois et al., 1994), may underlie the heightened emotionality and susceptibility to psychiatric disease onset during adolescence (Drevets, 2003; Yurgelun-Todd, 2007; Casey et al., 2010; Somerville et al., 2010). Further supporting the late emergence of BLA-PFC interactions, projections from the BLA to the mPFC and cingulate cortex continue to mature and increase in density during adolescence (Cunningham et al., 2002, 2008).

Indeed, a number of studies show deficits in PFC function, particularly in terms of its regulation of the amygdala, in juveniles with anxiety disorders. Negative functional connectivity of the amygdala and vlPFC, indicative of cortical suppression of amygdala activity, is diminished in the youths with generalized anxiety disorder and correlates with symptom severity and amygdala response to angry faces (Monk et al., 2008). Adolescents with higher trait anxiety exhibit less habituation of amygdala responses in repeated emotional tests, also correlating with diminished functional connectivity of the amygdala and vlPFC (Hare et al., 2008).

Diminished top-down regulation of the amygdala, caused by excessive stress, may promote the emergence of anxiety disorders. Chronic stress reduces the influence of vmPFC afferents on amygdala sensitivity to emotional stimuli (Correll et al., 2005). Importantly, children previously exposed to socioemotional deprivation as orphans exhibit diminished integrity of the fiber bundle connecting the amygdala and PFC, the uncinate fasciculus (Eluvathingal et al., 2006; Govindan et al., 2010). These studies suggest chronic stress and ELS can cause deficits in the regulation of the amygdala by frontal cortices.

As explained in **Section 1.2.2**, the amygdala plays a role initiating the stress response, and in turn its function and physiology can be altered by stress. Towards understanding how stress exposure early in life alters emotional development, **Section 1.3** covers the normative development of the amygdala and **Section 1.4** details how that development is altered by ELS.

1.2.2 The BLA in the Responses to Acute and Chronic Stress

The amygdala helps coordinate many aspects of the stress response and is situated to do so via widespread connectivity throughout the brain (Goldstein et al., 1996; Herman et al., 2003; Jankord and Herman, 2008; Dedovic et al., 2009). The BLA sends projections to the CeA and BNST, which in turn target the hypothalamus and brainstem nuclei to activate the stress response (for review, see Walker and Davis, 2008). The CeA and BNST are thought to be involved in phasic and sustained fear responses, respectively, with the latter more akin to anxiety (*ibid*.). The amygdala may contribute, more specifically, to initiating the response to psychological, rather than physical, stressors (for review, see Herman and Cullinan, 1997). Traumatic experiences correspond with reductions in amygdala volume and decreased amygdala reactivity, suggesting effectors of the stress response can, in turn, alter amygdala function (for review, see Shin et al., 2006).

Many chemical mediators of the stress response influence the function of neurons in the amygdala (Rodrigues et al., 2009). In vitro application of corticosterone reduces inhibitory synaptic transmission, mediated by the neurotransmitter γ-aminobutyric acid (GABA), in the BLA (Duvarci and Pare, 2007). Norepinephrine, a mediator of the stress response, suppresses GABAergic transmission in the amygdala and promotes synaptic plasticity (Tully et al., 2007). However, some of the most robust effects on amygdala function are caused by CRF, the stress neurohormone. CRF is released in the amygdala following acute stress and contributes to the behavioral aspects of the stress response, including anxiety-like behaviors (Merlo Pich et al., 1995; Gray and Bingaman, 1996; Sajdyk et al., 1999; Cook, 2004). Furthermore, CRF release in

the BLA promotes aversive memory formation (Roozendaal et al., 2002). The effects of acute CRF exposure are explained, in part, by its impact on the function of BLA principal neurons, including increased excitability and reduced action potential slow afterhyperpolarization (Rainnie et al., 1992), as well as enhanced sensitivity to afferent stimulation (Ugolini et al., 2008). These effects on amygdala inputs and neuronal excitability, combined with attenuation of GABAergic transmission in the BLA, promote synaptic plasticity and thereby contribute to stress-induced facilitation of the learning of fearful associations (Rodriguez Manzanares et al., 2005).

The effects of acute and chronic stress can differ wildly, with chronic exposure to stress often found to be detrimental (Brunson et al., 2003). There are mixed reports of the effects of chronic stress on HPA axis function (Miller et al., 2007), suggesting the link between chronic stress and psychopathology may occur elsewhere in the brain. Following chronic stress, exaggerated responses to subsequent stressors and psychiatric disorder pathogenesis may be due to well-documented alterations to amygdala function (McEwen, 2007; Roozendaal et al., 2009). Specifically, stress-induced release of CRF has been hypothesized to induce plasticity in the BLA that contributes to the persistent overexpression of anxiety (Shekhar et al., 2005). Chronic stress in rats increases dendritic arborization and spine density of BLA principal neurons (Vyas et al., 2002; Vyas et al., 2006; Cui et al., 2008). Chronic activation of CRF receptors in the BLA has a long-lasting (>30 day) anxiogenic effect, with a long-term attenuation of GABAergic transmission in the BLA that causes hyper-excitability (Rainnie et al., 2004).

Even weak or acute activation of the stress response can cause deficits in amygdala function. Subthreshold activation of CRF receptors in the BLA, which does not cause acute behavioral effects, sensitizes animals to panicogenic agents (Sajdyk et al., 1999). Like CRF, subthreshold doses of GABA receptor antagonists in the BLA ‘prime’ anxiety-like behavior and physiological aspects of the stress response (Sanders et al., 1995). This suggests the long-term effects of CRF in the amygdala may act via alterations in GABAergic transmission. Acute stress may also promote anxiety through actions on the amygdala; for instance, long term enhancement

of fear learning by acute stress exposure coincides with reduced expression of GABA receptor subunits in the BLA (Ponomarev et al., 2010).

1.2.3 GABA, a Key Regulator of BLA Function

As mentioned above, GABAergic transmission in the BLA is sensitive to acute and chronic stress. This is relevant to the pathogenesis of anxiety for two reasons: 1) GABA is a key neurotransmitter in the amygdala that is linked to adult anxiety, and 2) GABA systems are classically regulated by brain development. For these reasons, GABAergic dysfunction is proposed to be a key mediator of neurodevelopmental disorders (Chattopadhyaya and Cristo, 2012; King et al., 2013).

GABAergic transmission has been well characterized in the mature BLA (Washburn and Moises, 1992; Martina et al., 2001). GABAergic transmission, which mediates all of the fast synaptic inhibition in the amygdala, occurs primarily from BLA interneurons. The BLA is a cortical-like structure, with a similar distribution of cell types as the neocortex and hippocampus – a mix of principal neurons and inhibitory, GABAergic interneurons (Carlsen and Heimer, 1988). Principal neurons of the BLA are excitatory, projection neurons that constitute approximately 80-85% of its total cell population and mediate all of the output of the nucleus. The remainder is local-circuit interneurons that release GABA and inhibit the neighboring principal neurons (McDonald, 1985; Rainnie et al., 1993). GABAergic fibers in the BLA mainly originate from local interneurons, but also include extrinsic inhibitory inputs from nearby paracapsular intercalated cells, as well as the basal forebrain (Marowsky et al., 2005) (Mascagni and McDonald, 2009). BLA interneurons are highly interconnected, being targets of BLA principal neurons and extrinsic excitatory fibers; activation of excitatory inputs to the BLA elicits robust feed-forward inhibition that limits the response of the amygdala (Rainnie et al., 1991a).

GABA determines the excitability of the amygdala and thereby regulates emotional behavior and learning (Shekhar et al., 2003; Ehrlich et al., 2009). A balance of excitatory and

inhibitory synaptic transmission is critical for the function of local circuits in the brain (Shu et al., 2003). Activation of amygdala principal neurons is thought to bidirectionally influence anxiety states and aversive learning; GABAergic transmission in the amygdala is suggested to alleviate anxiety by reducing excitability of the nucleus as a whole. To this end, blocking GABA receptors in the BLA promotes fearful and anxious behaviors (for review, see Quirk and Gehlert, 2003), whereas enhancing GABA function attenuates these behaviors (Davis et al., 1994; Sanders and Shekhar, 1995). Furthermore, ablation of a subset of BLA interneurons reduces sociability (Truitt et al., 2007). GABA receptor activation blocks signal propagation throughout the amygdala (Wang et al., 2001), and loss of GABAergic transmission in the amygdala results in generalization of fearful associations (Shaban et al., 2006). Acute stress induces GABA release in the amygdala (Cook, 2004), but chronic stress attenuates GABA release caused by subsequent stressors, suggesting reductions in amygdala GABAergic transmission may contribute to stress allostasis (Reznikov et al., 2008). GABAergic transmission in the amygdala is, for all these reasons, a classic target of anxiolytic drugs, including benzodiazepines and barbiturates (Sandford et al., 2000).

Described further in **Section 1.3.3.1**, the amygdala plays a well-defined role in a form of associative fear learning called classical or Pavlovian fear conditioning. In classical fear conditioning, a benign (conditioned) stimulus is repeatedly presented along with a noxious (unconditioned) stimulus, and the conditioned stimulus comes to independently elicit a fear response. Synaptic input representing the conditioned and unconditioned stimuli converge in the BLA, where synaptic plasticity is thought to enable the conditioned stimulus to elicit the same response as the unconditioned stimulus (Fendt and Fanselow, 1999; Davis, 2000; LeDoux, 2007). GABA receptors exert control over classical fear conditioning, including the acquisition and expression of memories for the fear association (Ehrlich et al., 2009).

Not only does BLA inhibition regulate fear learning, but it is also essential for the learned suppression of conditioned fear known as ‘extinction.’ Learning to extinguish fearful associations

is particularly relevant for anxiety disorders, which involve excessive fear responses to benign stimuli that must be curbed by treatment (Coles and Heimberg, 2002; Lissek et al., 2005; Rainnie and Ressler, 2009). In extinction training, the formerly conditioned CS is repeatedly presented without the US, and over time the fearful response is curbed as the CS loses predictive value. This learning depends on the formation of a new memory in the BLA that inhibits the fearful memory (Rescorla, 2001; Barad et al., 2006; Bouton et al., 2006; Myers and Davis, 2007), and requires strengthening of GABAergic synapses in the amygdala (Lin et al., 2009). Furthermore, infusion of a GABA receptor agonist in the BLA enhances extinction (Akirav et al., 2006). Fear extinction enhances expression in the amygdala of genes related to GABAergic function, and fear conditioning causes a downregulation of GABA-related genes, suggesting the amygdala GABA system can be bidirectionally modulated to control the balance of fear and safety learning (Heldt and Ressler, 2007).

1.2.3.1 Parvalbumin Interneurons Organize BLA Activity

The most common class of interneuron found in the amygdala, cerebral cortex, and hippocampus is identified by its expression of the calcium-binding protein, parvalbumin (McDonald and Pearson, 1989; Baimbridge et al., 1992; Kemppainen and Pitkanen, 2000; McDonald and Mascagni, 2001; Schwaller et al., 2002). Parvalbumin-expressing (PV^+) interneurons comprise a large portion of basket cells, which form periosmatic baskets on principal neurons that provide robust inhibition at the soma (Somogyi et al., 1983; Bartos and Elgueta, 2012). In the BLA, these neurons have a variety of electrophysiological properties and include both burst-firing and stutter-firing interneurons (Rainnie et al., 2006). PV^+ neurons in the BLA and elsewhere in the brain innervate hundreds of neighboring neurons and can form multiple synapses on each of those neurons (Tamas et al., 1997; Wang et al., 2002; Rainnie et al., 2006).

As shown in the BLA and elsewhere, the diverse projections of PV^+ interneurons are useful for coordinating the activity of groups of principal neurons (Chapter 6; Cobb et al., 1995;

Miles et al., 1996; Ryan et al., 2012). PV^+ basket cells control rhythms in neural networks, organizing their target neurons into oscillations that are critical for network function (for review, see Freund and Katona, 2007). In the hippocampus, PV^+ neurons contribute to gamma oscillations in the hippocampus and thereby support memory function (Bartos et al., 2002; Fuchs et al., 2007; Sohal et al., 2009). In the BLA and throughout the brain, PV^+ neurons form a syncytium with dendritic and axonal gap junctions, coordinating their activity and supporting their role in oscillation production (Muller et al., 2005). Supporting the critical role of PV^+ interneurons in the BLA circuit, acute stress and a variety of anxiogenic agents cause activation of parvalbumin neurons in the rat BLA as measured by immediate early genes (Reznikov et al., 2008; Hale et al., 2010).

While parvalbumin is typically considered solely a neuronal marker, its expression does influence the function of interneurons. Parvalbumin functions as a so-called "slow-onset" calcium buffer in synaptic terminals, and genetic deletion of parvalbumin enhances short-term facilitation of synapses, strengthening repetitive GABAergic release events (Caillard et al., 2000; Vreugdenhil et al., 2003; Collin et al., 2005; Orduz et al., 2013). However, in neurons with low parvalbumin concentrations, it has no effect on synaptic transmission (Eggermann and Jonas, 2012). Furthermore, the concentration of parvalbumin in individual neurons and its variability across neurons differs by brain region (*ibid.*). Increases in parvalbumin concentration also reduce the excitability of fast-spiking interneurons (Bischop et al., 2012; Orduz et al., 2013). Together these data support a role for the expression of parvalbumin protein in reducing GABAergic transmission through synaptic depression and reducing interneuron excitability. In line with this logic, an inbred rat strain with high emotionality and anxiety has greater density of PV^+ neurons in the BLA (Yilmazer-Hanke et al., 2002).

1.2.3.2 GABA Promotes Network Oscillations Observed During Fear

As mentioned above, PV^+ interneurons play an important role in organizing neurons into network oscillations. These neurons exemplify the complex role of GABA in the brain; this neurotransmitter not only serves to dampen the activity of amygdala neurons, but can also promote BLA activation through the organization of neuron firing (Chapter 6; Ryan et al., 2012). Coordinated inhibitory input across multiple neurons is a common mechanism to synchronize their action potential firing and generate network oscillations (Soltesz and Deschenes, 1993; Buzsaki, 1997; Penttonen et al., 1998; Pouille and Scanziani, 2001; Person and Perkel, 2005; Sohal et al., 2006; Szucs et al., 2009). Optogenetic silencing of PV^+ neurons in awake, behaving mice influences the phase of ongoing theta (6-10 Hz) oscillations, supporting a role for these neurons in coordinating slow network oscillations (Royer et al., 2012).

Recent evidence suggests oscillatory activity of neurons in the BLA plays a key role in regulating affect in awake, behaving animals (for review, see Pape and Pare, 2010). More specifically, it is now evident that the amygdala, hippocampus, and prefrontal cortex produce coordinated high delta / low theta (4-5 Hz) oscillations during acquisition (Madsen and Rainnie, 2009) and retrieval (Sangha et al., 2009) of learned fear, which then diminish over the course of subsequent extinction learning. The importance of network oscillations for BLA function emphasizes the critical role PV^+ interneurons play in amygdala function. As discussed in the following section, the developmental emergence of PV^+ interneurons is one of many indicators of the changing function of the amygdala throughout postnatal life.

1.3 Maturation of Amygdala Physiology and Function

Towards the goal of understanding the etiology of anxiety disorders and interpreting the effects of ELS within a developmental framework, this section describes the current state of knowledge regarding amygdala development – in terms of function, physiology, morphology, connectivity, and synaptic transmission. **Section 1.3.1** contains an argument for the role of

amygdala development in shaping emotional outcomes. Then in **Sections 1.3.2** and **1.3.3**, respectively, the current knowledge is presented regarding developmental changes to the function of the primate and rodent amygdala. To facilitate comparisons across species, it is useful to consider the following developmental time points: a baby rat has comparable cortical maturity to a newborn human around postnatal day (P)12, which coincides with opening of the eyes and the onset of the capacity to hear; rats are weaned around P21, compared to around 6 months of age for rhesus macaques and humans; rats reach sexual maturity between P40 and P60, compared to 4-5 years old for macaques; rat life expectancy is around 3 years, while macaques typically live less than 40 years (Cork and Walker, 1993; Prather et al., 2001; Coe and Shirtcliff, 2004; Quinn, 2005; Tritsch and Bergles, 2010). Here, we will focus on postnatal periods including infancy and early adolescence, when the BLA undergoes rapid and drastic maturation.

1.3.1 A Critical Period for Amygdala Influence on Emotional Development

The importance of understanding the normative trajectory of brain development follows logically from a neuroconstructivist approach to studying anxiety disorders. Simply put, neuroconstructivism posits that brain function, genes, and environmental factors actively interact to shape brain development (Karmiloff-Smith, 2009). As such, understanding the function and physiology of a region in the mature brain is insufficient for interpreting that region's contribution to the function of the immature brain or the etiology of developmental disorders. **Section 1.3** therefore serves to identify putative CPs in amygdala development, windows of profound change when the contribution of this brain region to emotional processing is in flux. These CPs constitute the most likely periods when perturbations to amygdala function emerge in terms of behavioral deficits or influence the wiring of the limbic system.

A number of studies of amygdala lesions support a neuroconstructivist approach to emotional development, suggesting the function of the immature amygdala coordinates some aspects of emotional development. Specifically, these studies highlight differences in the effects

of lesions of the amygdala during development and in adulthood. Comparing amygdala lesions in early development and adulthood illustrates that humans with early amygdala damage have worse memory for emotionally arousing stimuli (Shaw et al., 2005). In addition, amygdala lesions later in life interfere minimally with recognition of emotional facial expressions (Hamann and Adolphs, 1999), contrasted with the profound effect of congenital amygdala lesions (Adolphs et al., 1994). Similar findings exist for nonhuman primates: lesions of the macaque amygdala in infancy impact emotional and social behavior distinctly from lesions in adulthood (Prather et al., 2001). Furthermore, adolescent lesions of the macaque amygdala have milder effects than neonatal lesions, which promote lower social dominance, reduced aggression, and enhanced social fear (Bachevalier and Malkova, 2006). Finally, while ablating the amygdala of a rat at P21 impacts its social behavior, if ablation occurs at an earlier point in development, at P7, the deficits are more severe and also impact the animal's stress response (Wolterink et al., 2001). These studies suggest the amygdala functions during brain development to organize the formation of emotional circuits in the brain, and early life changes to amygdala function are therefore of great importance for emotional outcomes.

1.3.2 Development of the Human Amygdala

Human imaging studies have identified a number of gross developmental changes to amygdala structure and function, in general identifying childhood and adolescence as a period of accelerated amygdala growth. The basic structure of the amygdala can be detected at birth (Humphrey, 1968; Ulfig et al., 2003). Nonhuman primate studies suggest that the amygdala develops most quickly during infancy (Payne et al., 2010), but its development is protracted. The amygdala enlarges through adolescence relative to the rest of the temporal lobe (Giedd et al., 1996). Late maturation of the amygdala is evidenced by studies of white matter density; the frontal and temporal lobes gain white matter relatively late in human development (Deoni et al., 2011).

In terms of function, the amygdala is active in childhood and adolescence but its specific function changes. The amygdala is activated in response to emotional faces during childhood and adolescence (Baird et al., 1999; Thomas et al., 2001a), and also contributes to fear conditioning as early as adolescence (Monk et al., 2003b). However, with age comes increased integration of the amygdala into limbic circuitry. Compared to adults, children show significantly weaker functional connectivity of the amygdala with limbic structures, the vmPFC, and polymodal association cortices. Interestingly, the role of the BLA seems to become more specified with age, as children show greater intrinsic connectivity between the BLA and CeA, as well as greater overlap in their functional connectivity with target regions (Qin et al., 2012).

As described in **Section 1.2.1**, a wealth of studies have identified greater responsiveness of the adolescent amygdala to social stimuli with a negative emotional valence (Baird et al., 1999; Monk et al., 2003a; Killgore and Yurgelun-Todd, 2004; Guyer et al., 2008) and diminished functional connectivity of the PFC and amygdala. This increased amygdala activity during adolescence may reflect development of the amygdala before the emergence of top-down control from higher-order cortical areas, especially the prefrontal cortex, that serve to inhibit the amygdala in adulthood (for review, see Casey et al., 2008).

1.3.3 Development of the Rodent Amygdala

1.3.3.1 Development of Amygdala Neuron Morphology and Physiology

Studies of the rodent amygdala have provided a much finer resolution description of amygdala development, identifying changes to the structure and function of individual neurons throughout infancy and into adolescence. Morphological studies have revealed the structure of the BLA in rodents does not begin to stabilize until at least P28. The basolateral complex of the amygdala emerges by E17 in rats (Berdel et al., 1997b), and the majority of neurogenesis there occurs between E14 and E16 (Bayer et al., 1993). The BLA specifically increases in volume until the third postnatal week (Berdel et al., 1997a; Chareyron et al., 2012). Neuronal density is reduced in half between P7 and P14 (Berdel et al., 1997a). From birth to P7, the cross-sectional

area of BLA neurons doubles, but at P7 the majority of neurons are still small and have only one or two main dendrites (*ibid.*). By P14, the cross-sectional area of neurons is the same as in the adult BLA. A Golgi-Cox study of developing BLA neurons found an expansion of dendrites during the first few postnatal weeks (Escobar and Salas, 1993).

Concomitant with changes to the structure of the BLA as a whole and its constituent neurons are a variety of changes to the connectivity of BLA neurons. There is a three-fold increase in total synapses in the BLA from P7 to P28, as measured by synaptophysin staining (Morys et al., 1998), reflecting increased intrinsic connectivity as well as maturation of inputs to the amygdala. Tract-tracing studies have shown that putative glutamatergic inputs to the BLA from the PFC and thalamus mature between P7 and P13 (Bouwmeester et al., 2002b) and stabilize by P25, before undergoing pruning in late adolescence (Cressman et al., 2010). Dopaminergic and noradrenergic inputs to the BLA become more dense between P14 and P20 (Brummelte and Teuchert-Noodt, 2006), and vesicular monoamine transporter 2 (VMAT2) is present in the BLA as early as E17, supporting a role for these monoamines in the early development of the BLA (Lebrand et al., 1998). Amygdala efferents also become refined postnatally; projections from the BLA to PFC seem to develop particularly late, during the second and third postnatal weeks, while projections to the thalamus and nucleus accumbens have mature morphology and density as early as P7 (Verwer et al., 1996; Bouwmeester et al., 2002a). Furthermore, studies with a trans-synaptic tracer injected into the stomach showed that efferents of the amygdala mature during the first postnatal week, as labeling of the amygdala was much greater at P8 than P4 (Rinaman et al., 2000). These studies suggest the wiring of the BLA changes postnatally, but no studies have characterized the development of dendritic spines. Dendritic spines provide a means of compartmentalization of biochemical and electrical signals related to neurotransmission, and should therefore reflect the maturation of amygdala connectivity (Shepherd, 1996; Lee et al., 2012). In **Chapter 3**, we address the knowledge gap

regarding the morphology of BLA principal neurons, as none of these studies addressed specific neuronal subtypes, both in terms of dendritic arborization and spine expression.

While much attention has been paid to the development of amygdala morphology, very little is known concerning amygdala neuron physiology throughout development. No study has yet to characterize the intrinsic physiology of BLA principal neurons during development. We address this knowledge gap in **Chapter 2**. The few electrophysiological studies performed in the developing BLA have identified changes to synaptic plasticity. Thalamic inputs to the BLA exhibit long-term potentiation (LTP) following high-frequency stimulation at P28, but not at P60 (Pan et al., 2009). Similarly, before P10, high-frequency stimulation of cortical input to the BLA results in LTP, while after P10 this same protocol elicits long-term depression (LTD; Thompson et al., 2008). In adulthood, GABAergic inhibition limits amygdala excitability and prevents LTP; therefore, this switch is likely driven by developmental changes to GABAergic transmission in the BLA, which are described in the following section and further characterized in **Chapter 4**.

1.3.3.2 Emergence of Amygdala Inhibition and Developmental Critical Periods

The structure and function of the GABAergic system undergo protracted development that lasts well into postnatal life. As described in **Section 1.2.3**, GABA is the sole mediator of fast synaptic inhibition in the adult BLA, and it regulates amygdala function in a variety of important ways. However, the function of this neurotransmitter system is classically regulated throughout development (Ben-Ari et al., 2012; Kilb, 2012). The extent of maturation of GABAergic transmission in the amygdala is largely unknown, despite early GABA dysregulation being implicated in the pathophysiology of neurodevelopmental disorders (Chattopadhyaya and Cristo, 2012; King et al., 2013). This section details what is known regarding GABAergic development in the BLA, as well as in the brain at large, to identify knowledge gaps related to the etiology of anxiety disorders.

GABAergic transmission is present very early, but plays distinct roles in the immature and mature brain. GABAergic neurons arise from the medial and caudal ganglionic eminences

and migrate throughout the brain during embryogenesis (Miyoshi et al., 2007; Miyoshi et al., 2010). GABAergic synapses have been identified in the brain as early as E16 by some measures (Konig et al., 1975; De Felipe et al., 1997). In the embryo and early postnatally, GABA performs distinct functions from in the adult brain; GABA is implicated in a variety of neurodevelopmental processes including cell proliferation, migration, and differentiation, synapse maturation and stabilization, and circuit wiring (Owens and Kriegstein, 2002; Huang and Scheiffele, 2008; Le Magueresse and Monyer, 2013). GABAergic transmission has also been shown to influence the function of neuronal stem cells and neuroblasts (LoTurco et al., 1995; Owens et al., 1996; Manent et al., 2005).

Postnatally, a number of structural and functional changes occur to GABAergic synapses and neurons. Refinement of structures and processes in postsynaptic neurons leads to refinement of GABAergic transmission (Le Magueresse et al., 2011). These synapses increase in density and have release events at higher frequencies across the first postnatal month (Luhmann and Prince, 1991). The postsynaptic currents elicited by GABAergic synapses become faster with age, influencing the duration of inhibition as well as the entrainment of action potentials and oscillations (Pouille and Scanziani, 2001; Tamas et al., 2004). Specifically in the BLA, there is a significant increase in the density of GABAergic fibers from P14 to P21, while the density of GABAergic cell bodies decreases (Brummelte et al., 2007). As discussed below, there are a number of postnatal changes to parvalbumin-expressing interneurons, which form perisomatic basket synapses and regulate network oscillations; these neurons only emerge in the BLA around P17, and do not reach mature levels until P30 (Berdel and Morys, 2000; Davila et al., 2008).

In general, GABAergic terminals early in development have high release probability and high neurotransmitter output, but revert to lower release probability and output in adulthood; these high output, immature synapses exhibit short-term depression, when the response becomes weaker upon rapid, repeated synapse activation (for review, see Zucker and Regehr, 2002). Variations in short-term plasticity alter temporal filtering mechanisms of synapses (Buonomano,

2000; Fortune and Rose, 2001; Pfister et al., 2010), and short-term depression of GABAergic synapses specifically promotes high-pass filtering of excitatory transmission and increases the information transmitted by bursts of action potentials (Abbott and Regehr, 2004; George et al., 2011).

The ionotropic receptor for GABA, the $GABA_A$ receptor, which mediates all fast inhibition in the adult amygdala, is not inhibitory early in development. GABAA receptors are excitatory at birth and assume their mature function postnatally (for review, see Ben-Ari et al., 2012). The switch from excitatory to inhibitory GABA results from changes to the concentration gradient of chloride, the major ion mediating $GABA_A$ currents. At birth, there is greater expression of sodium-potassium-chloride cotransporter 1 (NKCC1), which accumulates intracellular chloride and renders $GABA_A$ receptors excitatory. In adulthood, potassium-chloride cotransporter 2 (KCC2) is expressed more highly, extruding chloride from the cell and rendering $GABA_A$ receptors inhibitory (Ben-Ari et al., 2012). Excitatory GABA early in development is thought to promote calcium influx and modulate neuronal growth and synapse formation (Ben-Ari et al., 1997).

GABAergic transmission also plays a role in coordinating brain development. Activation of GABAergic synapses directly influences the development of those synapses (Akerman and Cline, 2007; Chattopadhyaya et al., 2007; Huang, 2009), but also organizes circuit maturation during CPs. One well-established trigger for the onset of CPs, or developmental windows of high plasticity, is activity at $GABA_A$ receptors (for review, see Hensch, 2005). Transplantation of interneurons restores CP plasticity, suggesting the development of inhibitory neurons specifically triggers this plasticity (Southwell et al., 2010).

Two specific, overlapping GABAergic circuits are implicated in regulating CP timing – $GABA_A$ receptors containing the α1 subunit as well as PV^+ interneurons. $GABA_A$ receptors are pentameric channels composed of subunits from a variety of families, including α, β, γ, δ, ε, θ, π, and ρ. The most common subtype configuration includes 2 α, 2 β, and 1 γ subunit. The α subunits

influence the kinetics, localization, and drug sensitivity of $GABA_A$ receptors (Nusser et al., 1996; Hevers and Luddens, 2002). There are six known α-subunits, and the relative expression of these subunits changes throughout development. As the brain develops, expression shifts from the α2 subunit toward the α1 subunit, which confers faster kinetics (Dunning et al., 1999; Cohen et al., 2000; Bosman et al., 2002; Mohler et al., 2004; Bosman et al., 2005b; Eyre et al., 2012). Emergence of the α1 subunit has specifically been linked to CP timing. Selective deletion of fast synaptic GABA activity prevents CP onset (Hensch et al., 1998), and activation of receptors containing the α1 subunit directly influences CP onset (Huntsman et al., 1994; Fagiolini et al., 2004). Further supporting a role for the α1 subunit in postnatal development, genetic deletion of this subunit preserves GABAergic terminals early in postnatal development, but GABAergic transmission is perturbed by P11 and lost by P18 (Fritschy et al., 2006).

The α1 subunit is the most highly expressed α-subunit in the mature brain, being included in 60% of adult $GABA_A$ receptors and having dense immunoreactivity and in-situ hybridization throughout the adult brain (Hornung and Fritschy, 1996; Davis et al., 2000) (Laurie et al., 1992, 1331359; Hornung and Fritschy, 1996; Davis et al., 2000). The adult, mouse BLA contains high expression of the α1 subunit (Heldt and Ressler, 2007; Pirker et al., 2000, 11113332) and postsynaptic currents (PSCs) mediated by both α1- and α2-containing $GABA_A$ receptors (Marowsky et al., 2004). During the first three weeks after birth, α1 mRNA emerges and reaches full expression in the rat BLA (Zhang et al., 1992). Supporting a role for the α1 subunit in BLA development, transgenic mice lacking this subunit exhibit enhanced conditioned fear as adults (Wiltgen et al., 2009). Conversely, knockdown of α1 in the BLA selectively during adulthood has not been shown to impact emotional behavior (Heldt and Ressler, 2010), raising the possibility that changes in α1 expression in the BLA have the most potent effect during development, when inhibitory synaptic transmission is helping to organize amygdala maturation.

As described in **Section 1.2.3.1**, PV^+ interneurons are a subtype of basket cells that play a fundamental role in the function of cortical-like circuits, including the BLA. These interneurons

and their function primarily emerge postnatally and also influence circuit development, likely through their interaction with $GABA_A$ receptors containing α1 subunits. In the hippocampus, release sites of PV^+ interneurons have a high abundance of $GABA_A$ receptor α1 subunits, relative to synapses of other interneuron subtypes (Nusser et al., 1996; Fritschy et al., 1998; Pawelzik et al., 1999; Thomson et al., 2000; Nyiri et al., 2001; Klausberger et al., 2002).

In the BLA, PV^+ interneurons do not emerge until P17 and reach maturity at P30 (Berdel and Morys, 2000), during the same window when α1 expression emerges. In contrast, principal neurons are numerous in the BLA at birth *(Berdel et al., 1997a)* and interneurons containing the calcium binding proteins calbindin and calretinin can be found in the incipient BLA as early as E14-15 (Legaz et al., 2005). While maturation of PV^+ interneurons specifically in the BLA has not been studied, a similar population in the mouse neocortex matures significantly from P7 to P21, showing increased high frequency spike discharge, alterations to intrinsic membrane properties (Goldberg et al., 2011) and faster action potentials (Lazarus and Huang, 2011). A similar developmental trajectory is observed in these interneurons in the rat striatum (Plotkin et al., 2005). The axonal arbors of basket cells expand markedly between P7 and P28 (Doischer et al., 2008) as their synapses on pyramidal cells increase in strength (Kuhlman et al., 2010).

PV^+ interneurons associate with another marker of circuit maturity, specializations of the extracellular matrix known as perineuronal nets (PNNs). PNNs are found in the adult BLA in humans, rhesus macaques, and rodents (Hartig et al., 1995; Pantazopoulos et al., 2008; Gogolla et al., 2009). These structures are responsible for the stabilization of synapses and are preferentially found on fast-spiking basket cells that express parvalbumin, and degradation of PNNs increases the excitability of these interneurons (Dityatev et al., 2007). The formation of PNNs during development and the subsequent increase in activation of PV^+ interneurons contribute to the closing of CP plasticity (Pizzorusso et al., 2002; Hensch, 2005; Nowicka et al., 2009). Importantly, reducing excitability of PV^+ interneurons by disrupting PNNs causes re-opening of these CPs (Pizzorusso et al., 2002), and disruption of PNNs and CP reopening are caused by

$GABA_A$ receptor antagonists (Harauzov et al., 2010). As discussed in the following section, their emergence triggers developmental changes in emotional learning (Gogolla et al., 2009).

1.3.3.3 Changing Contributions of the Amygdala to Emotional Behavior

Postnatal development also involves a number of changes to the expression of emotional behaviors as well as the contribution of the amygdala to those behaviors (for reviews, see Landers (for reviews, see Wiedenmayer, 2009; Landers and Sullivan, 2012; King et al., 2013). As one example, development of the amygdala is suggested to underlie changes to avoidance behavior (Ernst and Fudge, 2009). Rat pups exhibit an unlearned defensive behavior, freezing in the presence of an adult male, around P12 but not earlier (Takahashi, 1992). Also beginning at P12, exposure to an adult male elicits activation of the amygdala, suggesting changes in the function or connectivity of the amygdala contribute to this behavioral emergence (Moriceau et al., 2004).

The contribution of the developing BLA to emotional behavior has been studied in depth using classical fear conditioning (described in **Section 1.2.3**), the learned association of a benign, 'conditioned' stimulus with a noxious, 'unconditioned' stimulus (Fendt and Fanselow, 1999; Davis, 2000; LeDoux, 2000). Fear conditioning studies in humans have shown that conditioned responses increase across childhood (Gao et al., 2010). Studies of fear conditioning and the well characterized, underlying neural circuit nicely illustrate the contribution of amygdala development to a CP for emotional learning in infancy. For example, while pairing an odor (conditioned stimulus, CS) with a shock (unconditioned stimulus, US) leads to avoidance of the odor in rats as young as P10, just two days earlier, at P8, this pairing leads to paradoxical approach to the CS (Sullivan et al., 2000). Furthermore, the paradigm at P10 but not P8 causes activation of the BLA, as measured by immediate early gene expression. This early appetitive conditioning to shocks likely follows from an inability to categorize sensory stimuli; rats at P3 and P6 exhibit the same responses to milk infusions and footshocks, and not until P12 do pups exhibit appropriate and distinct responses to these stimuli (Camp and Rudy, 1988). The deficit in

assigning emotional valence to perceptual stimuli early in development suggests a lack of mature functionality of the amygdala.

The amygdala directly controls the CP for the approach behavior following fear conditioning, acting downstream of the stress response. Infusion of glucocorticoids into the amygdala during training leads to precocious avoidance behavior and amygdala activation at P8, while infusion of a glucocorticoid receptor antagonist into the amygdala during training reproduces the immature approach behavior after P10 (Moriceau et al., 2006). Similarly, administration of exogenous glucocorticoids causes precocious activation of the amygdala and defensive behavior following exposure to a predator odor at P8 (Moriceau et al., 2004), and andrenalectomy blocks the emergence of this response (Takahashi and Rubin, 1993). These findings support the notion that the CP is defined by the emergence of stress-induced glucocorticoid release in the amygdala, although changes to the amygdala may also act upstream of glucocorticoid release. The SHRP ends around P12 (described in **Section 1.1.2.2**), and one main function may be to suppress amygdala activation before this age (Moriceau et al., 2004).

Maturation of the dopamine system also plays a role in this fear learning CP during infancy. The paradoxical approach behavior at P8 corresponds with reduced dopamine efflux in the amygdala. Furthermore, glucocorticoid infusion into the amygdala at P8 increases dopamine efflux, and dopamine receptor antagonists block the glucocorticoid-induced, precocious aversion (Barr et al., 2009).

While aversive conditioning to odors is possible as early as P10, more complex behavioral responses emerge later, as the amygdala circuit continues to develop. Defensive behaviors including freezing responses and heart rate suppression emerge around 2 weeks after birth (Campbell and Ampuero, 1985; Hunt, 1999) and CS-induced potentiation of startle responses emerges between P18 and P23, depending on the modality of the conditioned stimulus (Hunt et al., 1994; Barnet and Hunt, 2006). Also, at two weeks-old, rats do not exhibit trace conditioning, when the CS and US are presented with a fixed delay, but develop this capacity

gradually over the subsequent two weeks (Moye and Rudy, 1987; Barnet and Hunt, 2005). Finally, the expression of contextual fear memories is temporarily suppressed in mice around P30, along with learning-induced synaptic changes in the BLA (Pattwell et al., 2011). The delayed development of the capacity to learn and express fearful associations is likely due to protracted maturation of amygdala circuitry.

There is a developmental profile for the contribution of the amygdala not only to fear conditioning, but also to the learned suppression of conditioned fear known as extinction (described in **Section 1.2.3**). The argument for extinction involving suppression, rather than erasure, of fear conditioning stems from the persistent fear-inducing capacity of the CS; after a period following extinction training, conditioned fear responses can recover due to re-exposure to the US without the CS, termed "reinstatement," or following exposure to the environmental context of the CS-US pairing, termed "renewal" (Bouton et al., 2006; Myers and Davis, 2007). However, early in development extinction seems to constitute permanent erasure of fear, as animals younger than P24 do not exhibit reinstatement or renewal of extinguished fear (Kim and Richardson, 2007, 2008). Developmental changes in synaptic plasticity in the BLA are implicated in this switch, as NMDA receptors are required for extinction at P24 but not the fear erasure exhibited at P17 (Langton et al., 2007). Interestingly, inactivation of the mPFC interferes with extinction at P24 but not at P17, suggesting the late development of connectivity of the BLA and mPFC also influences the mechanism of extinction (however, see Nair et al., 2001; Kim et al., 2009; Sotres-Bayon and Quirk, 2010).

A number of studies specifically implicate maturation of the amygdala GABA system in the development of fear learning. The emergence of conditioned avoidance at P10 corresponds with a switch in synaptic plasticity in the BLA; tetanic stimulation of the external capsule induces LTP in the BLA before P7 and LTD at P10, but application of a $GABA_A$ receptor antagonist in adulthood restores the immature form of synaptic plasticity (Thompson et al., 2008). Nearly every study of LTP in the adult BLA includes application of $GABA_A$ antagonists because stimulation of

BLA inputs elicits feed-forward inhibition that shunts excitatory input and blocks LTP (Rainnie et al., 1991a; McKernan and Shinnick-Gallagher, 1997; Weisskopf et al., 1999; Li et al., 2011). That $GABA_A$ receptor antagonists are not required to elicit LTP at P7 suggests feed-forward inhibition in the BLA may not be present at this young age. GABAergic inhibition not only suppresses LTP in the adult BLA, but also prevents generalization of conditioned fear to non-presented stimuli, a process implicated in anxiety disorders (Shaban et al., 2006; Bergado-Acosta et al., 2008). Interestingly, juvenile mice exhibit generalization of conditioned fear (Ito et al., 2009) which may be due to immature GABA circuits being unable to limit synaptic plasticity in the amygdala. Amygdala $GABA_A$ receptors are also required at P18 for infantile amnesia, the short-term suppression of learned fear associations during infancy (Kim et al., 2006b; Tang et al., 2007).

Developmental changes to GABAergic transmission in the amygdala are also implicated in the maturation of fear extinction, which is a GABA-receptor dependent phenomenon in adulthood (see **Section 1.2.3**). The switch in extinction mechanisms, from erasure to suppression, likely depends on maturation of amygdala inhibition, as activation of amygdala $GABA_A$ receptors is required for extinction at P24 but not the fear erasure exhibited at P17 (Kim and Richardson, 2007, 2010). Furthermore, PNNs (described in **Section 1.2.3.1**) emerge around P24 and their degradation in adult animals reverts extinction to the immature, erasure mechanism (Gogolla et al., 2009).

1.4 Impact of Early Life Experience on Amygdala Development

It is now possible to describe the effects of ELS on the amygdala, using the normative development of the amygdala as a context. As discussed in **Section 1.3.1**, the complex and interdependent processes of brain development make single time points of little value for understanding outcomes. Specific changes to amygdala function caused by ELS are hypothesized to be most impactful during CPs in development. It is necessary to consider the direct effects of

ELS during those windows, not in adulthood, to understand the trajectory over which anxiety disorders can be instantiated and thereby prevented. To this end, the various effects of ELS on the amygdala will be outlined, with greater preference placed on those spanning developmental CPs (**Section 1.4.1**) but some attention paid to those with limited developmental perspective (**Section 1.4.2**). Finally, environmental factors that have been shown to promote resiliency will be presented in **Section 1.4.3**, to contrast the effects of ELS and identify targets for intervention in anxiety disorder pathogenesis.

1.4.1 Early Life Stress and the Trajectory of Amygdala Development

As discussed above, amygdala dysfunction following ELS has been suggested to contribute to the pathogenesis of psychiatric disorders (Heim and Nemeroff, 2002; Zhang et al., 2004; Sadler et al., 2011; Blackford and Pine, 2012; Callaghan et al., 2013). The specific effects of ELS on the amygdala and the contribution of those effects to disease risk are complex; not only the timing of exposure to ELS, but also the timing of measurement, influences the effects on the biology of the amygdala (Tottenham and Sheridan, 2009). Therefore, this section will outline the current state of knowledge regarding the effects of ELS on the trajectory of amygdala development and summarize what conclusions can be drawn from this sparse and sometimes contradictory literature.

Studies investigating the trajectory of amygdala development following ELS in terms of volume have identified age-specific effects that emphasize the importance of considering trajectories. A longitudinal study of human families found that maternal cortisol early in pregnancy positively correlated with amygdala volume in offspring at 7 years old, which partly mediated the association between maternal cortisol and affective problems in the children (Buss et al., 2012). Further study of human development found adverse caregiving increased amygdala volumes during childhood (Mehta et al., 2009; Tottenham et al., 2010). Parallel findings in rodents support the increase of developing amygdala volume following ELS: PS increased the

volume, neuron density, and glia density of the rat BLA specifically in adolescence (at P25 but not P7, P45, or P60; Kraszpulski et al., 2006). Interestingly, childhood trauma reduces amygdala volume in adults with psychiatric disorders (Driessen et al., 2000; Schmahl et al., 2003), however a number of studies have failed to replicate this finding (Bremner et al., 1997; Stein et al., 1997; De Bellis et al., 1999; Andersen et al., 2008). One explanation for the discrepant findings in children and adults is that ELS increases amygdala volume in childhood, possibly via excessive or accelerated growth, but robust synaptic pruning or cell death lead to reduced volumes by adulthood. Thus, increased amygdala volume in childhood may contribute to the pathogenesis of psychiatric disorders or serve as a marker of risk, but further developmental processes during adolescence contribute to the final outcome.

One particular study supports the idea that adolescent development contributes to amygdala outcomes. Stress exposure during adolescence (P27-29) was shown to impact emotional behavior in adulthood, including enhancing cued fear conditioning, impairing avoidance learning, and reducing exploratory behavior. In addition, the stress exposure enhanced expression in the BLA, within 4 days and persisting into adulthood, of a neuronal cell adhesion molecule, L1. Expression of L1 normally wanes into adulthood, but adolescent stress opposes this effect. L1 is involved in several neurodevelopmental processes including neurite outgrowth, axon guidance, and cell adhesion, so persistent expression in adulthood may contribute to alterations of neuron density and volume of the BLA (Tsoory et al., 2010). The effects of juvenile stress and ELS may interact to produce the complex trajectory suggested to contribute to anxiety disorder pathogenesis. Furthermore, ELS may enhance stress reactivity in adolescence, increasing the likelihood juvenile stress alters subsequent amygdala development.

A number of animal studies have suggested the effects of PS are mediated by changes in stress sensitivity at the level of the amygdala. Exposure throughout pregnancy to glucocorticoids increases expression of glucocorticoid receptors in the BLA of adult offspring, and also reduces exploratory behavior (Welberg et al., 2001). Changes in the CRF system may also contribute, as

late prenatal stress (from E14-21) increases CRF content in and release from the amygdala in adulthood (Cratty et al., 1995). The effects of PS may be directly mediated by exposure of the fetus to stress hormones. In support of this argument, glucocorticoid receptor expression is increased in the BLA of adult offspring following prenatal inhibition of the placental barrier enzyme for maternal stress hormones, 11β-hydroxysteroid dehydrogenase 2 (Welberg et al., 2000). However, because these studies only measured effects in adulthood, they do not preclude that increased stress sensitivity in childhood or adolescence contribute to the deficits observed, or whether changes in amygdala reactivity to stress may emerge downstream of other effects on the brain. In fact, ELS may perturb stress reactivity of the developing BLA through effects on serotonin release, which provides negative feedback on the stress response (for review, see Joels and Baram, 2009). ELS from P16 to P20 reduces the concentration in the amygdala of serotonin and its main metabolite (Matsui et al., 2010). Further supporting the need to consider developmental timing of stress and its effects, the same stressor applied from P11 to P15 has the opposite effect on these molecules in the amygdala (*ibid*.)

1.4.1.1 ELS Causes Precocious Amygdala Development

Many effects of ELS on the amygdala can be simplified as accelerated maturation. For instance, exposure to ELS causes precocious activation of the amygdala to fearful faces. Typically, adults exhibit greater amygdala activation to fearful faces than neutral faces, while children do not (Davis and Whalen, 2001; Thomas et al., 2001a). However, children exposed to ELS, exhibit the adult phenotype: greater amygdala activation to fearful than neutral faces (Maheu et al., 2010; Tottenham et al., 2011). The hypothesized precocious development of the BLA following ELS is supported by studies of CPs in the development of two amygdala-dependent behaviors: the emergence of avoidance learning and the switch in fear extinction mechanism from erasure to suppression.

As described in **Section 1.3.3.3**, the rodent amygdala is not activated in response to footshocks at P8, and stimuli that are aversively conditioned at this age elicit an approach response (Sullivan et al., 2000). ELS from P1 to P7 caused precocious expression of aversive learning and amygdala activation at P8, an effect blocked by glucocorticoid receptor antagonists at the time of training (Moriceau et al., 2009). This study suggests ELS accelerates development of the stress response, which causes precocious activation of the amygdala. It is important to note that changes to the amygdala itself may act upstream of the altered stress response. Acute stress later in development can also cause precocious fear learning, in this case the expression of fear-potentiation of startle responses at P20 instead of P22, suggesting ELS may generally act to accelerate amygdala activation and fear learning (Yap and Richardson, 2007).

ELS also leads to precocious expression of the mature form of extinction learning. As described in **Section 1.3.3.3**, extinction of conditioned fear at P17 leads to fear erasure, but extinction at P24 consists of suppression of conditioned fear that allows for fear renewal and reinstatement (Kim and Richardson, 2007, 2008). However, precocious expression at P17 of mature extinction, allowing for fear renewal and reinstatement, is caused by ELS (Callaghan and Richardson, 2011). In this case, ELS consists of separation of the pup from the mother from P2-14. In addition, maternally separated rats exhibit much longer retention of fear that is conditioned at P17 (Callaghan and Richardson, 2012). Interestingly, recent work suggests the precocious fear learning and extinction caused by chronic ELS can be mimicked by a stressor lasting only 24 hours (Cowan et al., 2013).

Precocious activation of the amygdala following ELS may be due to accelerated integration into the fear circuit. Another form of ELS, early weaning at P14, causes anxiety-like behavior as early as P21 and accelerates myelination of the BLA (Ono et al., 2008). We propose strengthening the early connections of the BLA comes at the expense of the connections that form late in development, including those with the frontal cortices. In other words, ELS shifts amygdala connectivity towards brain regions it interacts with early, at the expense of those

connections that typically emerge late. Human imaging studies support this hypothesis; ELS diminishes the integrity of fiber bundles connecting the amygdala and PFC (Eluvathingal et al., 2006; Govindan et al., 2010). This hypothesis fits with the model for diminished top-down control of the amygdala in adolescence contributing to psychopathology (Correll et al., 2005; Casey et al., 2010).

Decreased receptivity following ELS of the BLA to late-developing inputs could theoretically be achieved through precocious closing of a CP of plasticity. As explained in **Section 1.3.3.2**, developmental CPs can be closed due to activation of $GABA_A$ receptors, specifically those containing the α1 subunit (Huntsman et al., 1994; Hensch et al., 1998; Fagiolini et al., 2004). In addition, CP closure coincides with the emergence of PNNs on PV^+ interneurons (Pizzorusso et al., 2002; Hensch, 2005; Dityatev et al., 2007; Nowicka et al., 2009), which themselves preferentially innervate α1-containing synapses (Nusser et al., 1996; Fritschy et al., 1998; Pawelzik et al., 1999; Thomson et al., 2000; Nyiri et al., 2001; Klausberger et al., 2002). In the following section, the potential link between ELS and altered CP timing is supported with evidence for experience-dependent regulation of GABAergic function and CP timing.

1.4.1.2 Experience-Dependent Changes to Critical Period Timing

ELS is likely to alter the development of BLA inhibition, because early sensory experience is known to influence the development of GABAergic transmission and neurons in brain regions involved in processing that information in the adult. For example, early auditory experience influences the development of GABAergic synapse strength and the localization and kinetics of $GABA_A$ receptors (for review, see Sanes and Kotak, 2011). Specifically, hearing loss during a developmental CP prevents the typical, age-dependent increase in the strength of inhibitory synapses and density of $GABA_A$ receptors and the loss of short-term synaptic depression (*ibid.*). Furthermore, deprivation during CPs in a variety of sensory modalities reduces the content of GABA and its synthesizing enzymes (Hendry and Jones, 1986; Benevento et al.,

1995; Jiao et al., 2006) and the density of GABAergic neurons and synapses in sensory cortex (Gabbott and Stewart, 1987; Micheva and Beaulieu, 1995). Sensory experience triggers balancing of levels of inhibition and excitation in the cortex, which leads to improved circuit performance (Dorrn et al., 2010).

The effects of sensory experience on CP expression also include changes to PV^+ interneurons and PNNs. Sensory deprivation delays the emergence of parvalbumin expression and the formation of perisomatic baskets on pyramidal neurons (Chattopadhyaya et al., 2004; Jiao et al., 2006). In songbirds, song learning corresponds with increased PNN expression on PV^+ interneurons in a brain area involved in said learning. Furthermore, song deprivation reduces the expression of both parvalbumin and PNNs (Balmer et al., 2009).

Early stressful experience may trigger changes in BLA inhibition by altering neuronal activity in the developing amygdala. Numerous studies have identified a direct impact of synaptic transmission on GABAergic circuit development, with blockade of $GABA_A$ receptor activation mimicking the effects of sensory deprivation (for reviews, see Akerman and Cline, 2007; Katagiri et al., 2007; Huang, 2009). For instance, blockade of activity in developing cultured networks leads to the loss of GABA and GABAergic neurons (Ramakers et al., 1994; de Lima et al., 2004). Reducing neurotransmission during development also delays the emergence of parvalbumin (Patz et al., 2004) and reduces PNN expression (Dityatev et al., 2007). Genetic knockdown of GABA synthesizing enzymes interferes with the formation of perisomatic basket synapses, which are preferentially innervated by PV^+ interneurons (Chattopadhyaya et al., 2007). Promoting GABAergic transmission by blocking reuptake or applying receptor agonists rescued this deficit, further implicating GABAergic transmission in promoting GABAergic synapse formation and maintenance. GABAergic transmission in the embryonic brain promotes survival of PV^+ interneurons (Luk and Sadikot, 2001). GABA is excitatory early in development not only for principal neurons, but also for incipient PV^+ interneurons, suggesting GABA release may promote parvalbumin neuron survival through direct synaptic effects on these neurons (Sauer and

Bartos, 2010). In support of this notion, the maturation of GABA expression depends on activity-induced calcium influx (Spitzer et al., 1993).

Some effects of neurotransmission on the maturation and survival of interneurons are mediated by brain-derived neurotrophic factor (BDNF), which is secreted in response to neuronal activity (Rutherford et al., 1997; de Lima et al., 2004). BDNF secretion can be caused by activation of GABA receptors (Fiorentino et al., 2009). BDNF accelerates the emergence of developmental CPs, parvalbumin expression, and perisomatic baskets (Huang et al., 1999; Patz et al., 2004; Fiorentino et al., 2009). It also accelerates the maturation of cultured PV^+ interneurons, increasing their somatic diameter, dendritic branching, action potential frequency, and synaptic strength (Berghuis et al., 2004). In addition, another target-derived signaling molecule that interacts with BDNF, bone morphogenetic protein 4 (BMP4), promotes parvalbumin emergence and increases the density of PV^+ interneurons in the mature cortex (Mukhopadhyay et al., 2009; Takatoh and Wang, 2012).

Thus, changes in neuronal activity or GABAergic transmission in the developing BLA following ELS could influence BDNF secretion and alter the maturation of PV^+ interneurons and the timing of CPs. In fact, the developing amygdala may be more likely to experience stress-induced changes in its activity; for instance, chronic stress in adolescents increases the spontaneous activity of neurons in the BLA and impairs fear extinction, but the same stressor in adulthood recapitulates neither effect (Zhang and Rosenkranz, 2012, 2013). This study comprises our entire, limited knowledge regarding the development of amygdala neuron activity. No study has yet to describe the developmental trajectory of BLA neuron electrophysiology, let alone when the effects of ELS may first perturb this process. We address this knowledge gap in **Chapter 2**, providing a foundation to interpret the effects of ELS on amygdala inhibition and, therefore, CPs in emotional development.

1.4.1.3 ELS Alters Development of the BLA GABA System

Similar to research on the effects of ELS on the activity of developing amygdala neurons, studies on the effects on development of GABA systems in the BLA are lacking. One study found PS reduces the expression of the $GABA_A$ receptor γ2 subunit at P14 and P22, but no consistent effect on the α1 subunit was detected (Laloux et al., 2012). Several more have described changes in adulthood, but the time course and therefore the effects on developmental CPs are unknown. For instance, ELS increases the number of PV^+ interneurons in the adult BLA nearly 4-fold (however, see Giachino et al., 2007; Seidel et al., 2008). Stress from P27-30 reduced the expression in the adult amygdala of the $GABA_A$ receptor α1 subunit relative to α3, promoting an immature phenotype (Jacobson-Pick et al., 2008). A similar reduction of α1 expression in the adult BLA is caused by poor maternal care (Caldji et al., 2003). In addition, reduced α1 expression due to ELS has been observed in the adult hippocampus (Hsu et al., 2003). These findings seem contradictory, since PV^+ neurons preferentially innervate α1-containing synapses, but the two measures are influenced oppositely by ELS. Further studies are needed to characterize the trajectory of ELS effects on amygdala inhibition, particularly PV^+ interneuron, PNN, and $GABA_A$ receptor α1 subunit emergence, to identify the potential impact on developmental CPs. We address this knowledge gap in **Chapter 5**.

1.4.2 Experiential Factors Promoting Resiliency

A large number of studies have attempted to elucidate the mechanisms by which ELS leads to vulnerability for psychiatric illness. However, the identification of early life factors that promote resiliency will be equally important for devising interventional treatment. Conceptual models of fetal programming suggest early exposure to stress can program subsequent stress responses to adapt the offspring and improve reproductive fitness for highly stressful environments (for review, see Glover, 2011). While many reports discussed in **Section 1.1.2.1** find negative outcomes following PS, contrasting reports support a role for some types of PS in

promoting resiliency by buffering against later life stress (Lyons et al., 2009; Green et al., 2011). There may in fact be a nonlinear relationship between ELS and anxiety outcomes, such that moderate PS exposure is protective for offspring (Edge et al., 2009). Genetic factors likely moderate the impact of ELS, contributing to individual variation in risk and resiliency (for review, see Gillespie et al., 2009).

Resiliency can also be promoted by exposure to certain types of parenting early in life. Variations in maternal care are meaningful for the development of emotional behavior and stress responses in the offspring. Diorio and Meaney argue for the adaptive nature of this sensitivity to maternal behavior, such that care can reflect the inherent risk in the environment and promote behavioral responses with immediate adaptive value, sometimes at the cost for emotional dysfunction later in life (2007). Specific types of maternal care are known to affect the development of the HPA axis in offspring (for review, see Francis et al., 1999a). For instance, early maternal nurturing in rhesus monkeys buffers HPA axis responses (Sanchez, 2006) and reduces the expression of glucocorticoids and CRF (Korosi and Baram, 2009). Importantly, stress reactivity can also be reduced by other forms of early experience, as environmental enrichment at the time of weaning is anxiolytic and reduces CRF receptor expression in the BLA (Sztainberg et al., 2010).

Maternal care seems to promote resiliency by moderating the effects of ELS on the amygdala. For example, while rats normally exhibit conditioned avoidance starting at P10 (switched from attraction learning, see **Section 1.3.3.3**) the presence of a rat's mother or the mother's odor is sufficient at P15 to reproduce the immature, attraction learning. Maternal presence acts by suppressing shock-induced glucocorticoid release, which prevents amygdala activation and, therefore, fear conditioning (Moriceau and Sullivan, 2006). Maternal care can therefore serve to dampen amygdala activation, which may prevent the stress-induced, precocious maturation of the amygdala described in **Section 1.4.1.1**.

Maternal care can also influence outcomes of the amygdala GABA system. Types of naturally occurring maternal care that reduce fearfulness and HPA axis activation in adulthood also increase expression in the BLA of $GABA_A$ receptor α1, α5, and γ2 subunits (Caldji et al., 2003). Interestingly, increased γ2 subunit expression in the BLA and a corresponding reduction of anxiety-like behavior can also be elicited by simply handling animals in infancy (Caldji et al., 2000). These findings strikingly contrast those on the effects of ELS, which reduces γ2 and α1 subunit expression in the BLA (Caldji et al., 2003; Jacobson-Pick et al., 2008; Laloux et al., 2012). Early life factors promoting resiliency may do so by opposing the effects of ELS on GABAergic transmission in the developing amygdala.

1.5 Conceptual Summary

This chapter has established several important points moving forward: 1) it is important to consider trajectories of development to understand the etiology of neurodevelopmental disorders, 2) dysfunction of the BLA is implicated in the pathophysiology of several neurodevelopmental disorders, including anxiety disorders, 3) the changes that occur in the developing amygdala likely contribute to early life emergence of anxiety disorders and vulnerability to risk factors, 4) understanding how risk factors like ELS influence amygdala development will require filling large knowledge gaps concerning the normative development of amygdala neurons and physiology, and 5) GABAergic transmission is a prime candidate to mediate the effects of ELS because it regulates both the maturation of neural circuits and adult BLA function.

The remainder of this thesis describes individual studies that address knowledge gaps concerning BLA function and development, focusing on the GABA system and the effects of PS. **Chapters 2 & 3** address the normative maturation of BLA principal neuron electrophysiology and morphology, respectively. **Chapter 4** describes the maturation of GABAergic transmission in the BLA. Using those studies as a foundation, the effects of PS on the trajectory of BLA

development is covered in **Chapter 5**, again with special attention paid to GABAergic transmission and PV^+ interneurons. Considering the changes to BLA neurons and GABAergic transmission following PS, the function of PV^+ interneurons in the BLA is explored **Chapter 6**. Finally, **Chapter 7** includes a summary of findings, with focus on integrating the effects of PS with the normative changes to BLA physiology and function.

Figure 1.1: Schematic of connections of the basolateral amygdala.

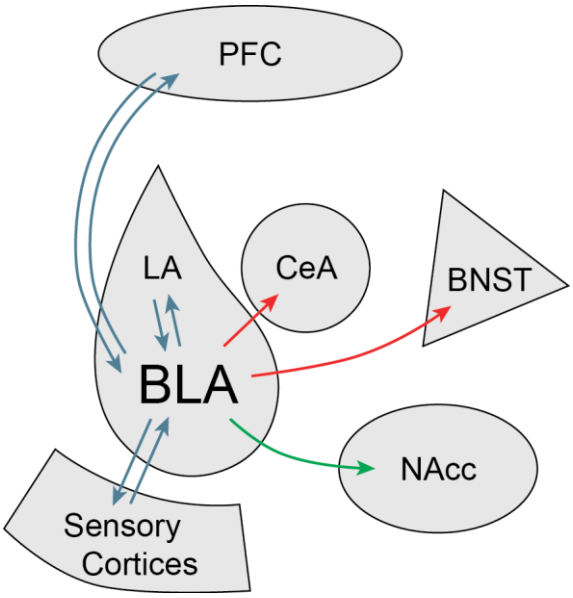

Figure 1.1: Schematic of connections of the basolateral amygdala. The basolateral amygdala (BLA) has reciprocal connections with upstream brain regions including primary sensory cortices, prefrontal cortices (PFC) which provide top-down control (including medial, ventromedial, and ventrolateral PFC as well as anterior cingulate cortex), and the lateral amygdala (LA). The BLA sends afferents for regulating emotional behavior to the central amygdala (CeA) and bed nucleus of the stria terminalis (BNST), which promote behavioral responses to aversive stimuli (connections depicted in red), and to the nucleus accumbens (NAcc), which promote behavioral responses to appetitive stimuli (connections depicted in green).

Chapter 2: Postnatal development of electrophysiological properties of principal neurons in the rat basolateral amygdala[1]

[1] Adapted from: Ehrlich DE*, Ryan SJ*, Rainnie DG (2012). *Postnatal development of electrophysiological properties of principal neurons in the rat basolateral amygdala*. J Physiol 590 (19); 4819-38.

2.1 Abstract

The basolateral amygdala (BLA) is critically involved in the pathophysiology of psychiatric disorders, which often emerge during brain development. Several studies have characterized postnatal changes to the morphology and biochemistry of BLA neurons, and many more have identified sensitive periods of emotional maturation. However, it is impossible to determine how BLA development contributes to emotional development or the etiology of psychiatric disorders because no study has characterized the physiological maturation of BLA neurons. We addressed this critical knowledge gap using whole-cell patch clamp recording in rat BLA principal neurons to measure electrophysiological properties at postnatal day 7 (P7), P10, P14, P21, P28, and after P35. We show that intrinsic properties of these neurons undergo significant transitions before P21 and reach maturity around P28. Specifically, we observed significant reductions in input resistance and membrane time-constant of nearly ten- and four-fold, respectively, from P7 to P28. The frequency selectivity of these neurons to input also changed significantly, with peak resonance frequency increasing from 1.0 Hz at P7 to 5.7 Hz at P28. In the same period, maximal firing frequency significantly increased and doublets and triplets of action potentials emerged. Concomitantly, individual action potentials became significantly faster, firing threshold hyperpolarized 6.7 mV, the medium AHP became faster and shallower, and a fast AHP emerged. These results demonstrate neurons of the BLA undergo vast change throughout postnatal development, and studies of emotional development and treatments for juvenile psychiatric disorders should consider the dynamic physiology of the immature BLA.

2.2 Introduction

The mechanisms by which early-life experiences impact the developing amygdala remain largely unknown because our understanding of amygdala physiology is based almost exclusively on research conducted in adult animals. Consequently, to better understand how early-life events can impact affective behavior later in life, a critical first step is to chart the normative developmental trajectory of the amygdala. Here we provide the first evidence for electrophysiological changes in the developing amygdala.

The few studies that have addressed other aspects of amygdala development reveal a highly dynamic neuronal environment in juvenile rodents, which does not begin to stabilize until at least postnatal day 28 (P28) (Morys et al., 1998; Berdel and Morys, 2000; Brummelte et al., 2007; Davila et al., 2008). As mentioned in **Chapter 1**, the neuronal composition of the BLA is highly dynamic during the first postnatal month. Numerous in the BLA from birth, principal neurons account for about 85% of all neurons in the adult BLA (McDonald, 1985; McDonald and Pearson, 1989; Berdel et al., 1997a). In contrast, interneurons expressing parvalbumin and/or calbindin, which comprise the majority of interneurons, first appear in the BLA around P14 and do not reach mature levels until about P25-30 (Berdel and Morys, 2000). In parallel with these changes, the number of synaptic contacts in the BLA nearly triples, while cell soma size doubles, and neuronal density halves between P7 and P14 (Berdel et al., 1997a; Morys et al., 1998). These changes are, in turn, mirrored by changes in thalamic and cortical inputs, which only emerge at P7 and are continually refined until P26 (Bouwmeester et al., 2002b). Finally, the protein expression of key ion channels in BLA neurons changes on a similar time scale (Vacher et al., 2006).

We and others have shown that the normal function of the adult BLA is tightly regulated by a reciprocal interaction between principal neurons and GABAergic interneurons (See **Chapter 1.2.3**; Rainnie (See Chapter 1.2.3; Rainnie et al., 1991b, a; Ehrlich et al., 2009; Ryan et al., 2012).

Given the studies outlined above, the neural circuitry of the BLA, and hence its function, would be predicted to change dramatically across development. As outlined in **Chapter 1.3.3.1**, at P7, rats approach an aversively-conditioned stimulus, only expressing the mature avoidance behavior after P10 (Sullivan et al., 2000). Similarly, adult-like expression of fear-potentiated startle does not emerge until P23 (Hunt et al., 1994; Richardson et al., 2000). Other aspects of conditioned fear, including the emergence of trace conditioning and reinstatement, change on a similar time-scale (Campbell and Ampuero, 1985; Moye and Rudy, 1987; Kim and Richardson, 2007).

Despite the compelling evidence of early-life transitions in BLA function, no study to date has examined how changes in the physiological properties of individual BLA neurons contribute to these critical periods of development. This information is essential if we are to understand how the adult BLA becomes organized, how it comes to communicate with other brain regions, and how early-life perturbations could influence mature BLA function. We have begun to address this knowledge gap using whole-cell patch clamp recording to characterize the physiological development of BLA principal neurons during the first postnatal month. We show that these neurons undergo significant transitions in intrinsic properties which define their sensitivity to input and characteristic activity, including passive and oscillatory membrane properties, action potential waveform, and spike-train characteristics.

2.3 Methods

2.3.1 Ethical approval

All experimental protocols strictly conform to National Institutes of Health guidelines for the Care and Use of Laboratory Animals, and were approved by the Institutional Animal Care and Use Committee of Emory University.

2.3.2 Animals

Rats born in-house to time-mated Sprague-Dawley female rats (embryonic day 14 on arrival, Charles River, Wilmington, MA) were used in all experiments. Pups were housed with the dam prior to weaning on postnatal day 22 (P22) or P23 (considering P1 as day of birth). After weaning, rats were isolated by sex and housed 3-4 per cage with access to food and water ad libitum. Animals attributed to each recording day (P7, P10, P14, P21, and P28) were recorded on that day or the following day (P7-8, P10-11, P14-15, P21-22, and P28-29, respectively).

2.3.3 Slice preparation

Slices containing the BLA were obtained as previously described (Rainnie, 1999b). Briefly, animals were decapitated under isoflurane anesthesia (Fisher Scientific, Hanoverpark, IL, USA) if older than 11 days, and the brains rapidly removed and immersed in ice cold, 95/5% oxygen/carbon dioxide-perfused "cutting solution" with the following composition (in mM): NaCl (130), $NaHCO_3$ (30), KCl (3.50), KH_2PO4 (1.10), $MgCl_2$ (6.0), $CaCl_2$ (1.0), glucose (10), ascorbate (0.4), thiourea (0.8), sodium pyruvate (2.0), and kynurenic acid (2.0). Coronal slices containing the BLA were cut at a thickness of 300-350 μM using a Leica VTS-1000 vibratome (Leica Microsystems Inc., Bannockburn, IL, USA). Slices were kept in oxygenated cutting solution at 32 °C for 1 h before transferring to regular artificial cerebrospinal fluid (ACSF) containing (in mM): NaCl (130), $NaHCO_3$ (30), KCl (3.50), KH_2PO_4 (1.10), $MgCl_2$ (1.30), $CaCl_2$ (2.50), glucose (10), ascorbate (0.4), thiourea (0.8), sodium pyruvate (2.0).

2.3.4 Patch clamp recording

Individual slices were transferred to a recording chamber mounted on the fixed stage of a Leica DMLFS microscope (Leica Microsystems Inc., Bannockburn, IL, USA) and maintained fully submerged and continuously perfused with oxygenated 32 °C ACSF at a flow rate of 1–2 mL/min. The BLA was identified under 10x magnification. Individual BLA neurons were

identified at 40x using differential interference contrast (DIC) optics and infrared (IR) illumination with an IR sensitive CCD camera (Orca ER, Hamamatsu, Tokyo Japan). A subset of neurons was filled using patch solution with added biocytin (0.3%) to confirm localization within the BLA. After some recordings, cytosol was recovered and screened using single-cell reverse-transcriptase PCR, as described previously (Hazra et al., 2011), to confirm the presence of the glutamate transporter, VGluT, which was seen in 58/60 neurons tested across all ages. Patch pipettes were pulled from borosilicate glass and had a resistance of 4–6 MΩ. Patch electrode solution had the following composition (in mM): K-gluconate (130), KCl (2), HEPES (10), $MgCl_2$ (3), K-ATP (2), Na-GTP (0.2), and phosphocreatine (5), titrated to pH 7.3 with KOH, and 290 mOsm. Data acquisition was performed using either a MultiClamp 700A or an Axopatch 1D amplifier in conjunction with pClamp 10.2 software and a DigiData 1322A AD/DA interface (Molecular Devices, Burlingame, CA, USA). Whole-cell patch clamp recordings were obtained and filtered at 2 kHz and digitized at 10 kHz. The membrane potential was held at −60 mV for all neurons if not specified. Cells were excluded if they did not meet the following criteria: a stable resting membrane potential more negative than −55 mV; access resistance lower than 30 MΩ; stable access resistance throughout recording, changing less than 15%; action potentials crossing 0 mV. Where indicated, Cs^+ (5 mM, Sigma Aldrich, St. Louis, MO) was administered through bath application.

2.3.5 Data Analysis

Data were analyzed by importing the raw voltage and current traces into Matlab (Mathworks, Natick, MA, USA) using scripts provided with sigTOOL (http://sigtool.sourceforge.net/, developed at King's College, London) and processed with customized scripts (available upon request). To characterize neurons in current clamp, first, a series of ten hyperpolarizing and depolarizing, 1 second long, square-wave current steps were injected. They were scaled so that, for each cell, the peak voltage deflections were to

approximately -80 mV and -40 mV (amplitude of negative current injections ranged from a minimum of -20 pA at P7 to a maximum of -1000 pA at P28, and positive current injections from +16 pA at P7 to +800 pA at P28). Second, linear ramps of depolarizing current were injected, lasting 250 ms and scaled to depolarize the neuron to -35 mV and elicit an action potential within the final 50 ms (peak current ranged from a minimum of +85 pA at P7 to a maximum of 555 pA at P28).

2.3.6 Membrane Properties and Intrinsic Currents

Input resistance and time constant were calculated using the deflection (approx. 5 mV) in response to the smallest, hyperpolarizing current step (minimum of -4 pA at P7, maximum of -200 pA at P28). Time constant was defined as the time necessary for the cell to reach 63.2% of its maximal deflection; input resistance was calculated as the ratio of peak voltage deflection to the current injected. To measure the hyperpolarization-activated, non-specific cation current, I_h, neurons were voltage clamped at a holding potential of -60 mV and stepped to -100 mV for 600 ms in the presence of 1 µM TTX. The waveform of the I_h current was generated by subtracting a current trace measured in the presence of bath-applied, 5mM Cs^+, known to block I_h, from that measured in its absence. This subtraction current was used to measure amplitude and activation time constants of I_h. A two-term exponential fit (**Equation 2.1**, k = 1) was used to extract fast and slow time constants of I_h activation, except at P7, where two terms over-parameterized the fit and a one-term exponential (**Equation 2.1**, k = 2) was used instead.

Equation 2.1 $$f(t) = \sum_{i=1}^{k} A_i \times e^{-t/\tau_i} + C$$

2.3.7 Action Potentials and Spike Trains

Action potentials were detected using a heuristic to locate peaks in the second derivative of the membrane potential waveform. The time of the peak was assigned to be the time of spike initiation and the voltage assigned as action potential threshold, which correlated well with visual inspection of the data. Since the sampling rate used here was not fast compared to the frequency of the action potential waveform (10 kHz compared to ~1 kHz), linear interpolation between data points was used to enhance the temporal resolution of measurements of 10-90% rise time, 90-10% decay time, and half-maximal width. These parameters and average action potential waveforms were calculated using spikes collected in the ramp protocol described above. Fast and medium afterhyperpolarizations (AHPs) were measured on spike-triggered averages from every spike captured (at least 8) during a 1 minute recording from neurons clamped manually at action potential threshold with DC current injection. Fast AHP peak was measured at a local minimum directly following spike re-polarization, if visibly distinct from the medium AHP and occurring within 15 ms of spike initiation. Medium AHP peak was measured at the minimum voltage following the spike, if it occurred within 150 ms of spike initiation (Storm, 1989).

Data on spike trains were collected from responses to the depolarizing, 1 second-long, square-wave current injections described above. Spike trains were included in the analysis if the mean of their inter-spike membrane potential fell within one standard deviation of the spike threshold measured for each age. Inter-spike intervals (ISIs) were calculated using the times for spike initiation in these traces, and the instantaneous firing frequency of the spike train was calculated as the reciprocal of these ISIs.

2.3.8 Resonance and Oscillations

Resonance was assessed by injecting neurons with a ZAP current, a sinusoidal current of fixed amplitude that sweeps logarithmically from 0.1 to 12 Hz over 30 seconds. The amplitude of the current was adjusted to elicit a 20 mV maximal depolarization from a baseline potential of -70 mV. Impedance was calculated as a function of input frequency for each neuron by deriving a power spectrum for the voltage response to the ZAP current, using fast Fourier transforms in the Chronux toolbox for Matlab (Bokil et al., 2010), and normalizing it to the power spectrum of the injected current. In order to extract peak values from noisy power spectra and generate averages, the raw impedance traces were fit with a 6^{th} order polynomial. Prominence was calculated using power spectra as the proportion of total power in the entire range considered (1-10 Hz) found in a given frequency band (1-2, 2-4, 4-6, 6-8, or 8-10 Hz). The change in prominence due to Cs^+ application was calculated as a ratio of the power in a given frequency band in Cs^+ and TTX to that in TTX alone. Correlation analysis of the relationship between membrane time constant (τ_{memb}) and peak resonance frequency was performed using GraphPad Prism 4 (GraphPad Software Inc., La Jolla, CA, USA). The presence of membrane potential oscillations (MPOs) in recordings of neurons gradually depolarized to action potential threshold was assessed by an observer blinded to age group. Spike-triggered averages of these depolarized traces were generated using Matlab to observe phase relationships between action potentials and putative MPOs.

2.3.9 Statistics

Data points greater than 2 standard deviations from the mean were deemed outliers and removed from statistical analysis. All data sets were tested for normality using the Shapiro-Wilk test ($\alpha = 0.05$) and for homoscedasticity using Levene's test ($\alpha = 0.0001$), implemented in Matlab. Data sets for mAHP and fAHP amplitude, maximal firing rate, peak resonance frequency, and I_h amplitude passed the Shapiro-Wilk and Levene's tests, so one-way ANOVA with Tukey's post-

hoc tests ($\alpha = 0.05$) were used to assess significance. To account for age-dependent changes in variance, values of R_{in}, τ_{memb}, and action potential rise- and decay-times were log-transformed before statistical analysis. Because the data sets for 6 of 7 basic electrophysiological parameters (R_{in}, τ_{memb}, action potential half-width, rise-time, decay-time, and first inter-spike interval, but not action potential threshold) failed either the Shapiro-Wilk or Levene's test, all of these data sets were analyzed using the Kruskal-Wallis test for overall effect of age on each parameter ($\alpha = 0.05$). The Kruskal-Wallis test was also used for mAHP and fAHP times-to-peak. When a main effect was found, pair-wise comparisons were made for each age group with two nearest older and younger groups (i.e. P21 vs. P10, 14, 28, and >35) using Wilcoxon rank sum tests (Matlab) with a Bonferroni correction for the resulting 9 comparisons ($\alpha = 0.0056$). Significant changes in prominence were assessed using a two-way, repeated measures ANOVA with Bonferroni post-hoc tests, with frequency band as a within-subjects factor and age as a between-subjects factor. Peak resonance frequency was exponentially correlated with τ_{memb} using a least-squares method with Equation 2.1 ($k = 1$) in GraphPad for all data from P14, P21, and P28.

An analysis of the effects of sex on physiological maturation was performed using a two-way ANOVA with factors of sex and age for the following parameters using GraphPad: R_{in}, τ_{memb}, action potential threshold, half-width, rise-time, decay-time, and first inter-spike interval. Significance was assessed for a main effect of sex in each parameter ($\alpha = 0.05$). This analysis included 16 male and female neurons from 5 male and 3 female rats at P14, 12 male and female neurons from 3 male and 2 female rats at P21, and 12 male and 8 female neurons from 4 male and 2 female rats at P28. No neurons were included from P7 or P10 due to difficulty assessing sex in the young rats. A posthoc power analysis for the effect of sex was conducted using G*Power (Faul et al., 2007) with $\alpha = 0.05$.

2.4 Results

Data were collected from a total of 499 BLA neurons from 93 rats on postnatal day 7 (P7), P10, P14, P21, and P28. Also included were data from 53 neurons from 26 older animals (P>35) for comparison with the preadolescent data. To make gross comparisons of neural properties across development, we first examined the voltage response of patch clamped principal neurons to transient (1s) hyperpolarizing and depolarizing current injections at P7, P14, P21, and P28. As illustrated in **Figure 2.1,** BLA principal neurons at each developmental time-point had distinct voltage responses to DC current injection. The most obvious changes were to input resistance (R_{in}), membrane time-constant (τ_{memb}), the depolarizing voltage sag upon membrane potential hyperpolarization likely caused by I_h, and the pattern of action potentials. Below we quantify these and many other physiological changes to BLA principal neurons across the first postnatal month.

2.4.1 Postnatal Maturation of Passive Membrane Properties

We measured the passive electrical properties of principal neurons at all time-points when manually held at -60 mV with DC current injection. Here, R_{in} and τ_{memb} were estimated from small, <5 mV hyperpolarizing voltage deflections elicited by transient current injection. We observed a significant reduction in R_{in} of nearly ten-fold across the first postnatal month (**Figure 2.2A;** $p < 0.001$, Kruskal-Wallis, $\chi^2_5 = 241.8$), with the greatest changes occurring before P21. There was a more than two-fold reduction in R_{in} from P7 to P14, and a nearly three-fold reduction from P14 to P21. Specifically, R_{in} decreased significantly from a median value of 523.7 MΩ at P7 (n = 45) to 374.8 MΩ at P10 (n = 37), 238.4 MΩ at P14 (n = 54), 88.0 MΩ at P21 (n = 43), and 55.9 MΩ at P28 (n = 58; Wilcoxon rank sum post-hoc tests). By P28, R_{in} had achieved its mature value and was not significantly different ($p > 0.05$) from neurons aged >P35 (52.67 MΩ, n = 56). Membrane time-constant followed a similar developmental trajectory to R_{in} (**Figure 2.2B,**

C), with a nearly four-fold reduction from P7 to P28. Overall there was a significant effect of age (Kruskal-Wallis, $\chi^2_5 = 221.4$), with a nearly two-fold reduction from P7 to P14 and another two-fold decrease from P14 to P28. Whereas the change from P7 to P10 was not significant ($p > 0.05$, Wilcoxon rank sum post-hoc tests; median = 59.1 ms at P7, n = 45; 50.5 ms at P10, n = 39), there was a significant ($p < 0.001$) decrease from P10 to P14 (32.0 ms, n = 53), P14 to P21 (18.0 ms, n = 45), and P21 to P28 (15.1 ms, n = 56). Similar to R_{in}, τ_{memb} reached its mature value by P28 and did not change significantly between P28 and >P35 (15.1 ms, n = 54; $p > 0.05$). Having observed significant age-dependent changes in the passive membrane properties of BLA principal neurons, we next examined concomitant changes in active properties, beginning with the voltage-gated current, I_h.

2.4.2 Postnatal Maturation of Intrinsic Currents

2.4.2.1 Development of the Voltage-Gated Current, I_h

One current which classically contributes to passive membrane properties like R_{in} and τ_{memb} is the hyperpolarization-activated cation current, I_h. This current mediates a depolarizing voltage sag observed in response to hyperpolarization from rest that is readily apparent at all ages (**Figure 2.1**). When neurons were manually held at -60 mV and the amplitude of the transient hyperpolarizing current steps adjusted to elicit peak voltage deflections to -80 mV, the depolarizing sags observed in the voltage response had a similar amplitude at all time-points (**Figure 2.3A**); however, the rate of onset of the sag increased with age. Significantly, the voltage sag was abolished at all ages by bath application of 5 mM Cs^+, suggesting it is likely mediated by activation of I_h. An example of the Cs^+ blockade of the depolarizing sag at P28 is illustrated in **Figure 2.3A**, upper trace. Considering the differences in R_{in} across ages and the visible differences in the kinetics of the voltage sag, we next quantified the maturation of I_h in voltage clamp.

To quantify the amplitude and kinetics of I_h activation, the membrane potential was stepped from -60 to -100 mV, both before and after application of 5 mM Cs^+, and the resulting currents were then subtracted to isolate I_h. The mean isolated I_h for each time-point is illustrated in **Figure 2.3B**. Analysis of the peak amplitude revealed a steady increase of I_h amplitude across the entire first postnatal month (**Figure 2.3C**), such that the mean I_h amplitude was 91.5 ± 28.1 pA at P7 (n = 10), 359.8 ± 82.3 pA at P14 (n = 14), 518.1 ± 239.2 pA at P21 (n = 11), and 641.9 ± 239.8 pA at P28 (n = 11). Notably, significant transitions occurred from P7 to P14 and from P14 to P28 ($p < 0.01$, One-way ANOVA with Tukey's post-hoc, $F_{3,42} = 19.93$). The activation kinetics of I_h were estimated by fitting its charging curve with a two-term exponential equation, except at P7, when the curve was sufficiently parameterized with a one-term exponential. The fast time constant decreased from 25.4 ± 6.3 ms at P14 (n = 19) to 19.6 ± 2.4 ms at P21 (n = 15), but remained steady between P21 and P28 (19.1 ± 2.7 ms, n = 13; **Figure 2.3D**, black squares). The single time constant at P7 was 188.5 ± 61.1ms (n = 11), which was similar to the slow time constant of activation for the other ages (253.5 ± 65.2 at P14, 252.9 ± 127.7 at P21, and 361.7 ± 340 at P28; **Figure 2.3D**, black triangles).

2.4.2.2 Development of Intrinsic Resonance

Membrane properties like τ_{memb} and active currents like I_h help shape intrinsic resonance, which acts as a band-pass filter to enhance responsiveness to synaptic input at particular frequencies. BLA principal neurons in the adult rat, guinea pig, and primate exhibit a preferred resonance frequency between 2.5 and 6 Hz (Pape and Driesang, 1998; Ryan et al., 2012). Resonance properties of neurons likely contribute to the production of network oscillations (Lampl and Yarom, 1997; Desmaisons et al., 1999; Richardson et al., 2003; Tohidi and Nadim, 2009), and recent evidence suggests that network oscillations in the BLA at the frequency of principal neuron resonance are intimately related to fear memory formation and expression (Popa et al., 2010; Lesting et al., 2011). Considering the potential contribution of BLA principal neuron

resonance to the generation of fear expression and learning, we next examined the ontogeny of resonance properties in these neurons.

By injecting a sinusoidal ZAP current of increasing frequency (see Methods) we were able to determine the peak resonance frequency, the input frequency that elicits the greatest membrane deflection, of BLA principal neurons across development. As illustrated in **Figure 2.4A,** the population responses to ZAP currents at P7, P14, P21, and P28 clearly showed a shift in the resonance frequency of principal neurons, with more mature neurons showing higher resonance frequencies. By taking the ratio of power spectra for output voltage and ZAP input current, we generated functions of impedance vs. input frequency (**Figure 2.4B**). Here, the peak resonance frequency increased sharply and significantly until P21 ($p < 0.001$, One-Way ANOVA with Tukey's post-tests, $F_{3,91} = 74.31$), with values (mean ± SD) of 0.97 ± 0.33 Hz at P7 (n = 21), 2.63 ± 1.48 Hz at P14 (n = 24), 5.47 ± 1.30 Hz at P21 (n = 21), and 5.69 ± 1.49 Hz at P28 (n = 29; **Figure 2.4C**).

To determine how developmental changes in I_h may contribute to the maturation of resonance, we blocked I_h using Cs^+ and measured changes in the responses to ZAP currents across the first postnatal month (**Figure 2.5A**). At all ages, Cs^+ application reduced the peak resonance frequency to below 1 Hz (0.60 ± 0.09 Hz at P7 (n = 8), 0.67 ± 0.22 Hz at P14 (n = 9), 0.85 ± 0.29 Hz at P21 (n = 8), and 0.94 ± 0.49 Hz at P28 (n = 11)). However, the effect of Cs^+ blockade on resonance involves more than a change in peak frequency; therefore, to highlight differences in the contribution of I_h to resonance across ages, we quantified the effect of Cs^+ on prominence, the proportion of total power between 1 and 10 Hz found in a given frequency band (1-2, 2-4, 4-6, 6-8, or 8-10 Hz)(Burton et al., 2008).

As shown in **Figure 2.5B**, the change in prominence due to Cs^+ application varied by age as an inverted 'U' with Cs^+ having relatively little impact at P7 and causing robust changes at P14, then having a progressively weaker effect at later time-points. There were significant main effects on change in prominence of frequency band ($F_{4,272} = 518.1$, $p < 0.0001$, Two-way

ANOVA with repeated measures) and age ($F_{3,272} = 28.9$, $p < 0.0001$), as well as a significant interaction effect ($F_{12,272} = 40.9$, $p < 0.0001$). Specifically, at P7 Cs^+ increased prominence (mean ± SD) at 1-2 Hz by 32.9 ± 20.1% and reduced prominence in the higher bands by between 1 and 3% each (n = 18). Compared to at P7, Cs^+ application at P14 caused a significantly greater increase in prominence in the 1-2 and 2-4 Hz bands (+157.3 ± 49.4% and +28.2 ± 12.6 % respectively; $p < 0.001$, Bonferroni post-hoc tests), and a significantly greater reduction in the 4-6, 6-8, and 8-10 Hz bands (-31.8 ± 7.5%, -53.0 ± 9.0%, and -58.3 ± 7.6%, respectively; n = 19; $p < 0.01$). The effect of Cs^+ at P21 was significantly weaker than at P14 ($p < 0.001$) in the 1-2, 4-6, and 6-8 Hz bands and significantly greater ($p < 0.01$) in the 2-4 Hz band (+113.9 ± 43.1% at 1-2 Hz, +44.6 ± 16.3% at 2-4 Hz, -9.5 ± 6.7% at 4-6 Hz, -35.0 ± 9.3% at 6-8 Hz, and -46.5 ± 11.5% at 8-10 Hz; n = 19). The trend continued at P28, with Cs^+ having a weaker effect than at P21. Specifically, Cs^+ caused a significantly smaller increase in prominence in the 1-2 Hz band ($p < 0.001$; +68.9 ± 27.4%) but effects in the remaining bands were not significantly different than at P21 (+33.4 ± 13.5% at 2-4 Hz, -2.2 ± 4.3% at 4-6 Hz, -23.7 ± 8.9% at 6-8 Hz, and -34.8 ± 11.8% at 8-10 Hz; n = 16).

The effects of Cs^+ on resonance were largely attributable to a direct effect on τ_{memb}. In control conditions, peak resonance frequency was correlated with τ_{memb} using a standard exponential equation (see Methods), yielding a R^2 value of 0.76 with $A_1 = 12.42$, $\tau_1 = 17.24$, and $C = 0.28$ (**Figure 2.5C**). Application of Cs^+ increased τ_{memb} at P14, P21, and P28 by an average of 67.0, 19.0, and 24.5 ms, respectively, causing a corresponding reduction in peak resonance frequency at each age (**Figure 2.5D**). Based on these observed changes to oscillatory properties of BLA principal neurons, we next characterized the maturation of spontaneous expression of membrane oscillations.

2.4.2.3 Development of Spontaneous Membrane Potential Oscillations

The oscillatory properties of adult BLA principal neurons manifest not only as resonance, but also as spontaneous membrane potential oscillations (MPO; Pape and Driesang, 1998; Ryan et al., 2012). These MPOs can influence spike-timing and interact with resonance to filter synaptic input based on frequency (Desmaisons et al., 1999; Izhikevich, 2002; Sancristobal et al., 2010). Furthermore, we have recently shown that phase-locked MPOs and coordinated spiking in adult BLA principal neurons are promoted by spontaneous, synchronous inhibitory postsynaptic potentials, highlighting a mechanism by which MPOs could contribute to network oscillations in the BLA (Ryan et al., 2012). We were therefore interested in the ontogeny of network oscillations in the BLA, and next examined the expression of MPOs in neurons at P7, 14, 21, and 28. Here, principal neurons were depolarized to action potential threshold with DC current injection. As illustrated in **Figure 2.6A**, neurons at P7 were more likely to fire action potentials in bursts, whereas P28 neurons had a more stable membrane potential and fired sporadically (**Figure 2.6A**). When depolarized to threshold, neurons also became more likely to exhibit spontaneous MPOs across the first postnatal month (**Figure 2.6B, C**). A blinded, qualitative analysis of current-clamp recordings near threshold revealed that only 5% of BLA principal neurons exhibited spontaneous MPOs at P7 (n = 20) and P10 (n = 19), but MPOs were present in 23% of neurons at P14 (n = 26), 64% at P21 (n = 25), and 60% at P28 (n = 48). Moreover, when we measured the frequency of spontaneous MPOs for neurons with a discernible peak in the power spectrum of their activity during a low-spiking period at threshold, we observed that it increased with development (3.8 ± 1.0 Hz at P14, n = 3; 3.7 ± 1.9 Hz at P21, n = 12; 4.4 ± 1.9 Hz at P28, n = 22). In other brain regions, MPOs are capable of organizing action potential timing (Llinas et al., 1991; Gutfreund et al., 1995; Desmaisons et al., 1999), and the same appears to be true in the BLA. An example of this is illustrated in **Figure 2.6D,** which shows a spike-triggered average from a P28 neuron.

2.4.3 Postnatal Maturation of Spiking

2.4.3.1 Development of Spike Trains

Having observed significant developmental changes in the sensitivity of BLA principal neurons to input as well as gross changes in action potential output (see **Figures 2.1** and **2.6A**), we next quantified the maturation of action potential trains across the first postnatal month. Here, spike trains were elicited with a transient, 1s, square-wave depolarizing current injection to action potential threshold. As illustrated in **Figure 2.7** (inset), there was a gradual emergence across the first postnatal month of doublet and triplet firing at the onsets of the spike trains. Moreover, analysis of the instantaneous firing rates based on the first 6 inter-spike-intervals (ISIs) for principal neurons at P7, 14, 21, and 28 revealed that at P7 the firing rate was relatively consistent across the entire train, starting at 29.7 ± 13.3 Hz and stabilizing at 16.8 ± 8.1 Hz by the third interval (**Figure 2.7A**). By P14, doublets became more apparent with an initial firing rate of 62.2 ± 52.1 Hz that dropped to 17.3 ± 12.5 Hz by the second interval. At P21, the doublet became faster and a triplet emerged in some neurons, with firing rates of 138.8 ± 77.9 and 45.0 ± 44.5 Hz for the first and second intervals, respectively, which stabilized around 20 Hz for the remainder of the train. Firing at P28 was very similar to that at P21, with slightly faster rates for the first pair of spikes (166.9 ± 95.3 Hz). We quantified the emergence of doublets using the first ISI, which significantly decreased from P14 to 21 and from P21 to 28 (**Figure 2.7B**; $p < 0.001$, Kruskal-Wallis with Wilcoxon rank sum post-hoc tests, $\chi^2_5 = 194.0$). Every transition between neighboring pairs of time-points was significant as well ($p < 0.001$).

We next measured the input-output relationship for action potential generation at P7, 14, 21, and 28 (n = 7, all groups), using 1 s, square-wave current injections applied from a resting membrane potential of -60 mV. As illustrated in **Figure 2.7C**, as neurons matured they required more current to generate the same output frequency. Interestingly, although the maximal firing frequency (mean ± SD) significantly increased ($p < 0.001$, One-way ANOVA with Tukey's post-

hoc tests, $F_{3,23} = 25.96$) from P7 (15.9 ± 3.3 Hz) to P14 (33.9 ± 7.3 Hz), the transitions ($p > 0.05$) from P14 to P21 (34.7 ± 3.7 Hz) and from P21 to P28 (36.5 ± 4.2 Hz) were not significant.

2.4.3.2 Development of the Action Potential Waveform

We reasoned that the observed changes in spike trains were likely due, in part, to maturation of the waveform of individual action potentials. Consequently, to quantify changes in action potential waveform, neurons were probed with a depolarizing current ramp lasting 250 ms, whose amplitude was adjusted to elicit a single action potential. **Figure 2.8A** illustrates the mean action potential waveforms from each age group. As can be seen, action potential threshold exhibited a significant, negative shift of approximately 7 mV from P7 to P28 (Kruskal-Wallis, χ^2_5 = 164.5, **Figure 2.8B**). The median threshold was -33.5 mV at P7 (n = 51), -34.7 mV at P10 (n = 35), -37.0 mV at P14 (n = 52), -40.9 mV at P21 (n = 43), -40.3 mV at P28 (n = 56), and -41.3 mV at >P35 (n = 55). Statistically significant transitions occurred from P10 to P14 and P14 to P21 ($p < 0.001$, Wilcoxon rank sum post-hoc tests). In addition, action potentials became much faster; the action potential half-width decreased between P7 and P28 (**Figure 2.8C)**, with the value at each time-point being significantly faster than at the previous ($p < 0.01$, Kruskal-Wallis with Wilcoxon rank sum post-hoc tests, $\chi^2_5 = 217.8$). The median half-width was 1.39 ms at P7 (n = 49), 1.23 ms at P10 (n = 35), 1.11 ms at P14 (n = 52), 0.90 ms at P21 (n = 44), 0.76 ms at P28 (n = 56), and 0.83 ms at P>35 (n = 57). Action potential 10-90% rise-time also decreased over this window, but the change was more gradual (**Figure 2.8D**). Here, the median rise-time was 0.56 ms at P7 (n = 51), 0.47 ms at P10 (n = 37), 0.42 ms at P14 (n = 55), 0.37 ms at P21 (n = 45), 0.30 ms at P28 (n = 57), and 0.32 ms at P>35 (n = 55). The only significant neighboring comparison in rise-time was between P21 and P28 ($p < 0.001$, Kruskal-Wallis with Wilcoxon rank sum post-hoc tests, $\chi^2_5 = 134.7$), but every transition across two time-points was significant ($p < 0.001$). Finally, the 90-10% decay-time also decreased more than two-fold from P7 to P28 (**Figure 2.8E**) and decreased significantly between every neighboring pair of time-points aside from P10 to 14

($p < 0.001$, Kruskal-Wallis with Wilcoxon rank sum post-hoc tests, $\chi^2_5 = 201.6$). Here, the median decay-time was 1.64 ms at P7 (n =50), 1.30 ms at P10 (n = 36), 1.07 ms at P14 (n = 53), 0.83 ms at P21 (n = 43), 0.66 ms at P28 (n = 56), and 0.86 ms at P>35 (n = 56).

2.4.3.3 Development of Afterhyperpolarization

The maturation of action potential duration strongly suggested that calcium influx due to individual spikes would also change significantly. Hence, we next examined the developmental expression of post-spike afterhyperpolarizations (AHPs), which have been shown to have some calcium-dependency in amygdala principal neurons (Faber and Sah, 2002) and could further contribute to the observed changes in spike trains. As expected, AHP expression also matured across the first postnatal month, with clear changes in both the fast and medium AHP (fAHP and mAHP, respectively). **Figure 2.9A** illustrates representative AHPs of BLA principal neurons at P7, 14, 21, and 28. As can be seen, the mAHP is already present at P7, whereas a distinct fAHP does not appear until P21. As shown in **Figure 2.9B**, the mAHP became faster and more shallow from P7 to P28, with times-to-peak of 91.4 ± 11.8 ms at P7 (n = 8), 69.0 ± 5.8 ms at P14 (n = 15), 59.8 ± 3.8 ms at P21 (n = 22), and 57.2 ± 3.6 ms at P28 (n = 42). The amplitude of the mAHP was -14.9 ± 2.4 mV at P7, -13.2 ± 1.9 mV at P14, -12.4 ± 2.6 mV at P21, and -11.1 ± 1.9 mV at P28. There was a significant effect of age on mAHP amplitude ($p < 0.001$, One-way ANOVA, $F_{3,83} = 8.95$) and duration ($p < 0.01$, Kruskal-Wallis, $\chi^2_3 = 11.45$). The fAHP emerged at P14 (**Figure 2.9C**), with 33% of neurons exhibiting a fAHP. The proportion increased to 68% by P21 and to 74% by P28. The fAHP became faster across this period, with times-to-peak (mean ± SEM) of 2.8 ± 0.1 ms at P14 (n = 5 of 15), 2.4 ± 0.1 ms at P21 (n = 15 of 22), and 2.4 ± 0.1 ms at P28 (n = 31 of 42). The fAHP also became deeper, with amplitudes (mean ± SD) of -2.8 ± 2.6 mV at P14, -5.2 ± 2.3 mV at P21, and -6.1 ± 3.1 mV at P28. The effect of age was not significant for fAHP amplitude ($p = 0.052$, One-way ANOVA, $F_{2,48} = 3.147$) and duration ($p = 0.061$, Kruskal-Wallis, $\chi^2_2 = 5.61$).

2.4.4 No Effect of Sex on Postnatal Changes in Physiological Properties

Due to differences in emotional processing and development of emotional behaviors across sexes, there is great interest in sex differences in amygdala maturation. Therefore, we performed a statistical analysis to assess sex differences in many of the physiological properties discussed above. Using a two-way ANOVA with factors of age and sex, we compared groups of between 8 and 16 neurons per sex at P14, 21, and 28. We found no main effect of sex ($p > 0.05$) in any of the parameters tested (R_{in}, τ_{memb}, action potential threshold, half-width, 10-90% rise-time, 90-10% decay-time, and first ISI). We conducted a post-hoc power analysis using G*Power (Faul et al., 2007) to assess whether we had sufficient power to detect an effect of sex. The power to detect a large effect size ($f = 0.40$, Cohen, 1988) was 0.94, but the power to detect a medium-sized effect ($f = 0.25$) was 0.59. Therefore, we cannot rule out the possibility of an effect of sex on these parameters in development, but expect such an effect would not be large. It is important to note that all measures were taken before sexual maturity, and large effects of sex may emerge by adulthood.

2.5 Discussion

In this study, we have provided the first evidence that physiological properties of principal neurons in the rat BLA undergo significant change during the first postnatal month. Characterizing how neurons of the amygdala develop is fundamental to understanding normative emotional development and, in turn, how risk factors and genetic predispositions are translated into developmental emotional disorders like anxiety, depression, autism spectrum disorders, and schizophrenia (Pine, 2002; Kim-Cohen et al., 2003; Kessler et al., 2005; Monk, 2008). Emotional processing, in particular fear learning, is critically dependent on the BLA (Davis, 2000; LeDoux, 2000), and the rapid and robust changes to fear learning observed during the first postnatal month in rats suggest the BLA develops profoundly during this period (Campbell and Ampuero, 1985;

Moye and Rudy, 1987; Hunt et al., 1994; Sullivan et al., 2000; Kim and Richardson, 2007). To facilitate comparisons of the timing of our observations to milestones in other species, consider that an infant rat first opens its eyes and reaches comparable cortical maturity to a newborn human at around two weeks after birth, is weaned around three, and reaches sexual maturity between six and eight (Quinn, 2005). In our hands, BLA principal neurons exhibited the greatest physiological changes between P7 and P21. Furthermore, neuronal physiology at P28 very closely resembled that of neurons recorded after P35, as well as previous reports of adult BLA principal neurons. These findings suggest that the electrophysiological properties of neurons in the human amygdala may undergo the largest transitions before one year of age and continue to develop into early adolescence. All of these changes support the notion that the BLA and its contribution to emotional processing are in flux well into postnatal life, marking a period of vulnerability for the circuit and long-term emotional outcomes (Spear, 2009).

2.5.1 Maturation of passive membrane properties

The most fundamental aspect of physiology in which we observed changes was passive membrane properties. For both input resistance (R_{in}) and membrane time constant (τ_{memb}), a great proportion of maturation took place by P21. In fact, R_{in} decreased 6-fold and τ_{memb} more than 3-fold between P7 and P21. The values we report for R_{in} and τ_{memb} at P28 and >P35 match those reported previously for adult BLA principal neurons (Rainnie et al., 1993), suggesting these neurons are physiologically mature by P28. These trajectories are also comparable to those seen in sensorimotor (McCormick and Prince, 1987) and prefrontal cortex (Zhang, 2004) as well as thalamus (Ramoa and McCormick, 1994). The decreases in R_{in} and τ_{memb} are consistent with the observed increase in cross-sectional area of BLA neurons (Berdel et al., 1997b) and likely involve insertion of ion channels into the membrane. The developmental reduction of R_{in} would, in isolation, reduce responsiveness to synaptic input, and may serve as a homeostatic mechanism to compensate for increasing synaptic strength, as seen elsewhere (Zhang, 2004). The larger τ_{memb}

in younger neurons means their voltage responses to synaptic input would be slower, promoting temporal summation of inputs. However, this would also reduce temporal precision of action potentials, meaning preadolescent amygdala neurons may be less able to coordinate action potentials and take advantage of temporal coding and spike-timing dependent plasticity.

2.5.2 Maturation of membrane potential oscillations and resonance

Passive membrane properties like τ_{memb} also help shape oscillatory properties of neurons, which influence the sensitivity of neurons to input and production of action potentials based on frequency. Over the first postnatal month, the proportion of BLA principal neurons expressing spontaneous membrane potential oscillations (MPOs) increased substantially and the frequency of those MPOs increased. Spontaneous MPOs are expressed in adult BLA principal neurons in the guinea pig at a proportion comparable to that seen here at P21 and P28 (Pape et al., 1998). The change in frequency with development was not significant, although similar trends have been observed in entorhinal cortex (Boehlen et al., 2010) and midbrain (Wu et al., 2001). Interestingly, the MPO was abolished by application of 1 µM tetrodotoxin (unpublished observation), suggesting the oscillation is promoted by synaptic activity.

Maturation of intrinsic oscillatory activity in BLA principal neurons also manifests as a change in the preferred resonance frequency. Intrinsic resonance has a similar time-course of development to the MPO, expressing a mature phenotype in the BLA at P21. Resonance and MPOs also exhibit coordinated development in neurons of the entorhinal cortex (Burton et al., 2008; Boehlen et al., 2010). These two phenomena are mediated by a similar set of voltage-gated currents and have similar frequency preference (Lampl and Yarom, 1997; Hutcheon and Yarom, 2000; Erchova et al., 2004). The mean peak resonance frequency we report here for BLA principal neurons at P28, 5.69 Hz, differs substantially from those reported for the guinea pig, 2.5 Hz (Pape and Driesang, 1998), and the adult rat, 4.2 Hz (Chapter 6; Ryan et al., 2012). While these differences could be due to continued maturation of oscillatory properties after P28, we

believe it is more likely due to differences in species or recording voltage, which is known to impact resonance (Pape and Driesang, 1998; Tseng and Nadim, 2010).

Spontaneous MPOs can directly influence spike timing (Desmaisons et al., 1999; Richardson et al., 2003), and in our hands, action potentials were phase-locked with the peak of the spontaneous MPO in some neurons at P28. Oscillatory properties of individual neurons contribute to the production of network oscillations (Lampl and Yarom, 1997; Tohidi and Nadim, 2009), which are an important component of communication between distant brain regions (Engel et al., 2001; Singer, 2009; Canolty and Knight, 2010; Fujisawa and Buzsaki, 2011). Coherent oscillations are expressed by the amygdala and downstream target regions, including the hippocampus and prefrontal cortex, during fear acquisition and expression (Madsen and Rainnie, 2009; Sangha et al., 2009; Pape and Pare, 2010). Importantly, the frequency of these coherent oscillations overlaps with the frequency of peak resonance and spontaneous MPOs in BLA principal neurons at P28, suggesting the emergence of these properties contributes to the mature expression of fear. Theta oscillations in local field potentials from the hippocampus increase in frequency throughout the third and fourth postnatal weeks, corresponding with emergence of mature network properties (Wills et al., 2010). This finding further supports a role for development of the oscillatory properties of individual neurons in network function and mature behavior.

Considering the importance of oscillatory properties of individual neurons for the generation of network oscillations (Lampl and Yarom, 1997; Desmaisons et al., 1999; Richardson et al., 2003; Tohidi and Nadim, 2009), their emergence in the BLA should correspond with that of principal neuron resonance. Based on electroencephalograms of the developing rat brain, no discernible network oscillations are observed in the BLA from birth through P14. Prominent oscillations emerge by this age in other regions including cortex, hippocampus and thalamus (Snead and Stephens, 1983), suggesting network oscillations in the BLA develop relatively late. We argue that network oscillations in the amygdala are promoted by organization of principal

neuron MPOs by synaptic input from parvalbumin-expressing interneurons (Ryan et al., 2012). Interestingly, these interneurons emerge in the BLA at P17 and reach mature expression by P21 (Berdel and Morys, 2000), when mature oscillatory properties would render BLA principal neurons more susceptible to organization by parvalbumin interneurons.

2.5.3 Maturation of I_h and its contribution to resonance

The observed changes to resonance, as well as to passive membrane properties, were likely influenced by maturation of the voltage-sensitive current, I_h. This current is critically involved in the expression of resonance properties (Hutcheon et al., 1996a; Hu et al., 2002; Marcelin et al., 2012) and contributes to input resistance at rest (Surges et al., 2004). Here we have shown an increase in amplitude and a decrease in activation time constant of I_h across the first postnatal month, as shown previously in other brain regions (Vasilyev and Barish, 2002; Khurana et al., 2012). The interaction of a 7-fold increase in I_h current amplitude across this window with a nearly 10-fold reduction of R_{in} explains the fairly consistent amplitude of voltage sag at all ages. Consistent sag amplitude across the first postnatal month was also observed in entorhinal cortex despite increasing I_h conductance (Burton et al., 2008).

The amplitude of I_h may be regulated throughout the first postnatal month to homeostatically maintain a consistent resting membrane potential. There are, however, visible changes in the voltage waveform of I_h because of faster I_h activation and τ_{memb}. Changes to I_h in the BLA may be due to transitions in the expression of subtypes of HCN, the channel mediating I_h, as in thalamic and hippocampal neurons (Bender et al., 2001; Kanyshkova et al., 2009). I_h activation kinetics were assessed by fitting the Cs^+ subtraction current with a two-term exponential equation at P14, P21, and P28, since I_h has previously been shown to have two distinct activation time constants (Pena et al., 2006). It is not clear why I_h at P7 appeared to have only a single activation time constant. While Cs^+ is not selective for HCN channels, we believe the subtraction currents are largely comprised of I_h. The hyperpolarization-activated current we

observed likely involved activation of voltage-gated K^+ channels, which can also be sensitive to Cs^+. However, for Cs^+ to affect those channels, it must enter the cell, which is unlikely at the voltages used for this protocol. Assessed by blockade with Cs^+, I_h makes a substantial contribution to resonance as early as P14. From P14 to P28, Cs^+ shifted the peak resonance toward lower frequencies, but at P7, there was little impact. Interestingly, the greatest effects on resonance of I_h blockade were seen at P14, when the resonance in Cs^+ resembled that seen at P7 in control conditions. This suggests I_h emerges as a major contributor to resonance between P7 and P14. Starting at P21, Cs^+ did not functionally abolish resonance by enhancing power preferentially in the lowest frequencies, as it did at P14. Cs^+ application had a diminishing effect on resonance with age following P14, suggesting other currents begin to play a greater role in shaping resonance. Although the amplitude of I_h continues to increase beyond P14, the concurrent reduction of input resistance and the compensatory effect of other emerging currents may mitigate the effects of Cs^+ application on resonance.

Considering the unique role I_h plays in shaping resonance at P14, at that age we expect profound sensitivity of resonance to neuromodulators that influence cAMP, a classic modulator of I_h. Developmental changes in neuromodulators contribute to maturation of I_h around P14 in the medial superior olive, further suggesting neuromodulation is relevant for neuronal function at that age (Khurana et al., 2012). Interestingly, I_h conductance in BLA principal neurons is reduced by the anxiolytic neurotransmitter neuropeptide Y and enhanced by the anxiogenic neurotransmitter corticotrophin-releasing factor (Giesbrecht et al., 2010).

Changes to resonance due to blockade of I_h are indirect and largely attributable to effects on τ_{memb}. There is a close relationship between τ_{memb} and peak resonance frequency (Hutcheon and Yarom, 2000), and the magnitude of resonance is linearly correlated with I_h amplitude (Marcelin et al., 2012). We showed that blockade of I_h directly impacts τ_{memb} but does not maintain the fitted relationship between τ_{memb} and peak resonance frequency, suggesting that, aside from passively contributing to resonance through τ_{memb}, I_h contributes actively through its

voltage-dependence and activation kinetics. In hippocampal pyramidal neurons, the amplitude of I_h is tightly correlated with the magnitude of the resonance peak (Marcelin et al., 2012).

2.5.4 Maturation of trains of action potentials

As expected, trains of action potentials elicited by direct current injection changed qualitatively across the first postnatal month. At P7, neurons exhibited a consistent action potential frequency throughout trains; as the animals aged, the frequency of the first two to three spikes increased dramatically, such that mature cells exhibited doublets or triplets at the onset of firing. Spike doublets have been documented in adult neurons of the basolateral (Rainnie et al., 1993) and lateral (Driesang and Pape, 2000) nuclei of the amygdala, and are thought to improve the fidelity of synaptic transmission (Lisman, 1997). Furthermore, doublets have been suggested to promote network oscillations and bridge the temporal gap between inputs to the amygdala representing conditioned and unconditioned stimuli during fear conditioning (Driesang and Pape, 2000). Interestingly, changes in dendritic morphology can directly affect spiking properties, including doublet firing (Mainen and Sejnowski, 1996), and experiments are underway to characterize morphological changes in these neurons during development.

In this study, maximal firing rate reached maturity in P14 cells, while in cortical pyramidal neurons, maximal firing rates have been reported to reach mature values as early as P2 (McCormick and Prince, 1987). This disparity is consistent with the late development of emotional processing relative to sensorimotor processing. The consistency of firing rates after P14 may be afforded by strengthening of I_A through insertion of K_v4 channels into the membrane (Vacher et al., 2006) to compensate for reduced medium afterhyperpolarizations (mAHPs).

It is important to note that, while spike trains elicited with square current pulses were relatively consistent across the first postnatal month, there were profound changes in the spontaneous activity of neurons depolarized to near threshold with direct current. Specifically, neurons at P7 exhibited highly erratic membrane potentials characterized by waves of

depolarization, likely involving activation of low-threshold calcium currents, which resulted in bursts of action potentials and periods of quiescence. Throughout the first postnatal month, membrane potentials became more stable near threshold. It is possible that the erratic membrane potentials in immature neurons were due to instability of the seal or physical qualities of the membrane. This is likely not the case based on the high R_{in} and repetitive firing exhibited at P7, properties indicative of a healthy membrane and seal. Furthermore, the membrane potential at P7 was stabilized by application of TTX (unpublished observation), suggesting the volatility was introduced by synaptic or intrinsic currents.

2.5.5 Maturation of action potentials and AHPs

There were also many developmental changes to properties of individual action potentials, including threshold, kinetics, and AHPs. Action potential threshold hyperpolarized until P21, potentially counteracting the effects of reduced R_{in} on neuronal excitability and acting to maintain consistent firing activity. The value we report for mature threshold (-41 mV) differed from the threshold values previously reported for mature BLA principal neurons (mean of -52 mV, (Rainnie et al., 1993), but this difference may be due to methods of recording (whole-cell patch vs. sharp) or analysis. Action potentials rise-time, decay-time and half-width were halved from P7 to P28, with the majority of change occurring by P21. Thalamic neurons also achieve mature action potential durations around P21 (Ramoa and McCormick, 1994), while neocortical projection neurons do so somewhat earlier, at approximately P14 (McCormick and Prince, 1987). Faster action potentials would allow for faster firing rates and may also impact calcium influx due to spiking, which could impact AHPs of action potentials.

Across the first postnatal month, AHPs matured in two ways: mAHPs became significantly faster and shallower while fast AHPs (fAHPs) became faster and deeper. Fast AHPs were not present at P7 but were present in two thirds of neurons by P21, when they exhibited adult-like waveforms. The emergence of fAHPs corresponds with faster action potential

repolarization, and these phenomena are likely both due to maturation of fast voltage-gated potassium currents. A reduction in mAHP duration across the first postnatal month has also been observed in entorhinal cortex (Burton et al., 2008). Medium AHPs can normalize inter-spike intervals and promote regular firing, hindering temporal coding mechanisms in favor of rate coding (Prescott and Sejnowski, 2008); smaller mAHPs in adult principal neurons are therefore another factor, along with smaller τ_{memb} and more prominent oscillations, that could promote temporal coding in mature emotional processing. Both fAHPs and mAHPs have been reported in adult BLA principal neurons (Rainnie et al., 1993), and the reported values suggest the trends we observed in AHP amplitude and duration continue past P28. A subset of adult BLA principal neurons has been shown to also express a slow AHP (Rainnie et al., 1993; Faber and Sah, 2002). Unfortunately, we were unable to assess the presence of a sAHP in immature BLA principal neurons with our data set. Future studies should address whether the presence of a sAHP emerges during postnatal development, as this could shed light on the developmental differentiation of principal neuron subtypes.

The trajectory of fAHP maturation corresponds with a reduction of the first inter-spike interval, such that almost all neurons at P28 have a fAHP and fire doublets. Interestingly, reduction of fAHP amplitude in the lateral amygdala through modulation of BK channels has been shown following stress and linked to anxiety (Guo et al., 2012), suggesting doublets are relevant for amygdala function. While the emergence of a fAHP likely involves changes in currents like BK, we cannot make any direct claims regarding the quantity or quality of underlying currents because we measured voltage deflections. Furthermore, because these voltage deflections are measured relative to action potential threshold, which is itself changing across development, the interaction of AHPs with currents regulating inter-spike interval may vary with age.

2.5.6 Maturation of amygdala connectivity and neuronal morphology

The BLA contributes to a network of brain regions that produce and regulate emotional behavior, including the prefrontal cortex, which itself develops substantially during the first postnatal month (Van Eden and Uylings, 1985; Bourgeois et al., 1994; Anderson et al., 1995; Rakic, 1995; Gourley et al., 2012). Afferents from cortical areas, including the prefrontal and auditory cortices, do not emerge in the BLA until around P13, while thalamic afferents are present as early as P7 (Bouwmeester et al., 2002b). Interestingly, a functional interaction of the prefrontal cortex and BLA also develops late; the medial prefrontal cortex does not contribute to extinction learning until P24 (Kim et al., 2009).

The interaction of the BLA with other brain regions that process emotion depends on the function BLA principal neurons. We have provided evidence that neurons of the BLA are not physiologically mature at birth, and have argued that postnatal changes in amygdala function and emotional processing are likely driven by drastic changes to the physiology of amygdala neurons. These physiological changes may be driven by developmental changes to the morphology or ion channel expression of these neurons. Changes to the size of the soma or extent of dendritic arborization can alter the electrophysiological properties of neurons. In terms of ion channels, we described maturation in the BLA of the properties of I_h, which suggests there are concomitant changes to the underlying ion channels; in addition, many other currents shape the properties we have shown to mature in BLA principal neurons, suggesting a host of changes to gene expression during development.

Several studies have addressed these aspects of amygdala development. The BLA increases in volume from embryonic day 17 until P14 (Berdel et al., 1997b), although the total number of neurons reaches the mature value at P7. From birth to P7, the cross-sectional area of rat BLA neurons doubles, but at P7 the majority of neurons are still small and have only one or two main dendrites (Berdel et al., 1997a). By P14, the cross-sectional area is the same as in the

adult. A 3-fold increase in total synapses in the BLA from P7 to P28, as measured by synaptophysin staining (Morys et al., 1998), probably reflects increased intrinsic connectivity as well as maturation of inputs to the amygdala. Interestingly, in terms of BLA volume and number of neurons, throughout development no differences were observed across sex (Rubinow and Juraska, 2009), corroborating our findings of no sex differences in principal neuron physiology.

Despite the number of studies addressing BLA neuron morphology during development, none have employed modern techniques to characterize dendritic arborization of estimate soma volume, necessary information to understand the factors driving the maturation of BLA neuron physiology and connectivity. Furthermore, the postnatal emergence of afferents from throughout the brain and the increase in synaptophysin staining suggest robust changes to the inputs to BLA neurons, which should be reflected not only in dendritic arborization but also in the expression of dendritic spines. In order to better identify how the amygdala circuit becomes organized and functions during postnatal development, we addressed the morphology and ion channel expression in this neuronal population throughout development. Our findings are summarized in **Chapter 3**.

Figure 2.1: Maturation of physiological properties of BLA principal neurons across the first postnatal month

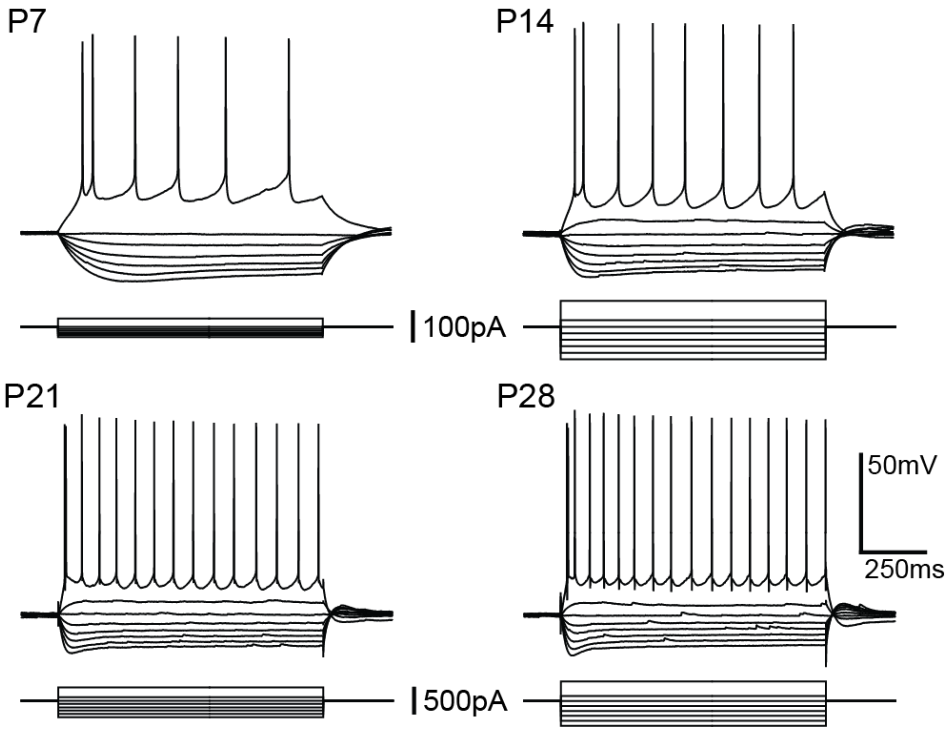

Figure 2.1: Maturation of physiological properties of BLA principal neurons across the first postnatal month. Illustrated are representative voltage responses to a series of transient (1 s) hyperpolarizing and depolarizing current steps, depicting age-dependent changes in the active and passive membrane properties of BLA principal neurons. All neurons were held at -60 mV with direct current injection. The amplitudes of current injection were adjusted for each neuron to normalize the voltage deflections. Note the difference in scale for the current injections of the neurons depicted in the top panel (postnatal day 7 (P7, left) and 14 (right)) and those depicted in the bottom panel (P21 (left) and 28 (right)).

Figure 2.2: Input resistance and membrane time constant decrease with age

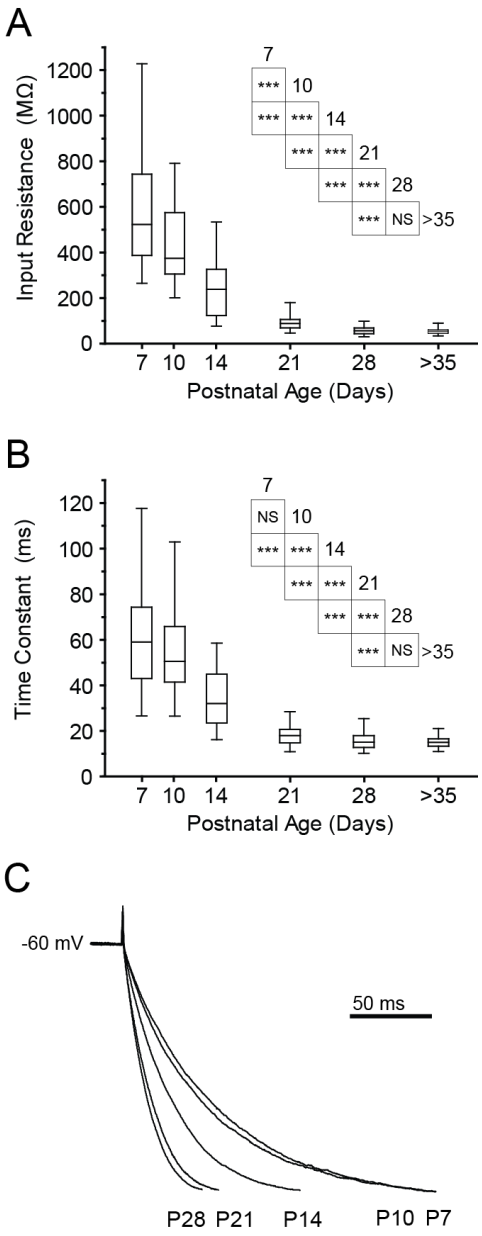

Figure 2.2: Input resistance and membrane time constant decrease with age. (A, B) Box and whisker plots show input resistance (A) and membrane time-constant (B) of BLA principal neurons across the first postnatal month and in adulthood (n = 45 (P7), 37-39 (P10), 53-54 (P14), 43-45 (P21), 56-58 (P28), and 54-56 (P>35)). Significance was assessed using a Wilcoxon rank-sum test and pairwise comparisons were made for each age group with up to four neighboring time-points (see inset tables for results) using a Bonferroni correction for the resulting 9 comparisons (***, $p < 0.001$; NS: not significant, $p > 0.05$). (C) Maturation of membrane time-constant is illustrated with the average, normalized membrane charging in response to a small, hyperpolarizing current step (approximately 5 mV deflection) for each developmental time point (n = 48 (P7), 28 (P10), 56 (P14), 45 (P21), and 58 (P28)).

Figure 2.3: Developmental increase in I_h amplitude and kinetics in BLA principal neurons

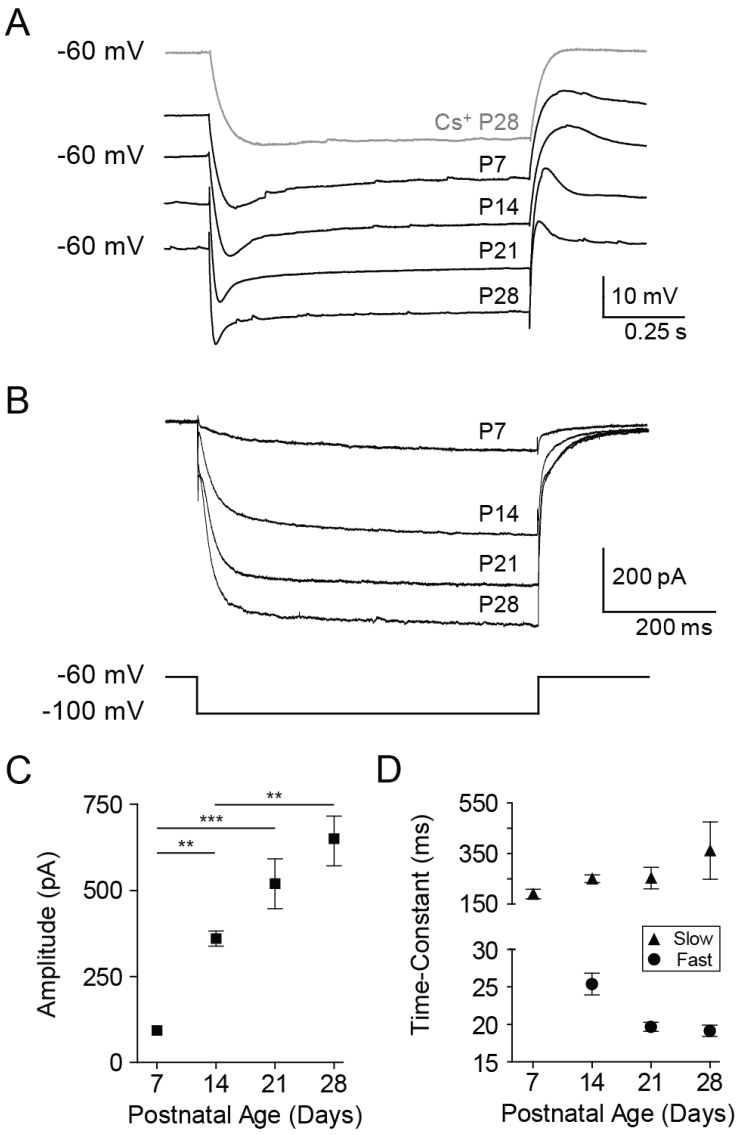

Figure 2.3: Developmental increase in I_h amplitude and kinetics in BLA principal neurons. (A) Representative voltage responses of neurons to a hyperpolarizing, square step of magnitude adjusted to elicit a 20 mV peak deflection. Neurons were recorded in the presence of 1 μM TTX at each time point, and blockade of I_h by 5 mM cesium (Cs^+) is depicted for a neuron at P28. Neurons had baseline membrane potential adjusted to -60 mV with direct current. (B) Voltage-clamp recordings following Cs^+ application (5 mM) subtracted from those prior to Cs^+ application depict the maturation of a Cs^+-sensitive current. Neurons were held at -60 mV and stepped to -100 mV, and all recordings were performed in the presence of 1 μM TTX (n = 10 (P7), 14 (P14), 11 (P21), 11 (P28)). (C) Peak amplitudes of subtraction currents from B are plotted as mean ± SEM for each time point. Significance was assessed using a one-way ANOVA with Bonferonni's post-tests, and pairwise comparisons were made for each age group with up to three neighboring time-points (see inset table for results; ***, $p < 0.001$; **, $p < 0.01$; NS: not significant, $p > 0.05$). (D) Plotted as mean ± SEM for each age, the time constant of I_h activation was measured from a double exponential fit to the subtraction currents in B at all ages except P7, which was sufficiently fit with a single exponential.

Figure 2.4: Maturation of intrinsic resonance towards higher frequencies

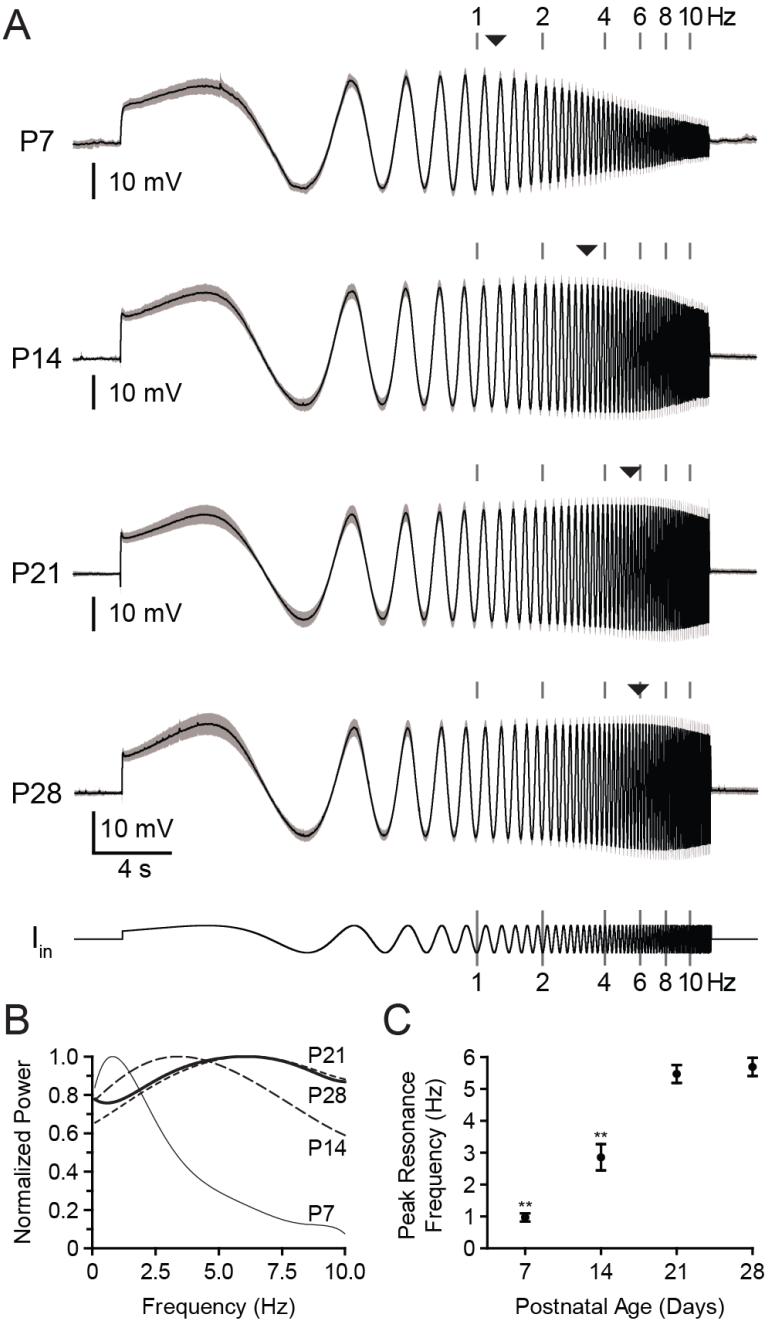

Figure 2.4: Maturation of intrinsic resonance towards higher frequencies. (A) Membrane potential response, shown as mean (black line) and standard deviation (grey band), to a ZAP current (I_{in}, fixed amplitude and logarithmically increasing frequency, shown at bottom) is depicted for each age (n = 22 (P7), 24 (P14), 22 (P21), and 32 (P28)). Neurons were first hyperpolarized to -70 mV with direct current, and ZAP current amplitude was adjusted for each neuron to elicit a 20 mV depolarizing deflection. Instantaneous frequency of the injected current is highlighted with gray bars above each trace, and the mean, peak resonance frequency for each age is depicted amid the gray bars with a black triangle. (B) Relative impedance for input from 0.1-10 Hz, calculated by normalizing the power spectra of the voltage responses in A to the power spectra of injected current, were fit with polynomials and plotted as the mean (n consistent with A). (C) Peak resonance frequency is plotted as mean ± SEM, measured at the maximum of each neuron's individual power spectrum (n = 21 at P7, 24 at P14, 21 at P21, and 29 at P28). Statistical significance was assessed with a one-way ANOVA using Bonferroni's post-tests to compare all data sets (** denotes $p < 0.001$ versus all other groups).

Figure 2.5: Contribution of I_h to intrinsic resonance of BLA principal neurons changes with age

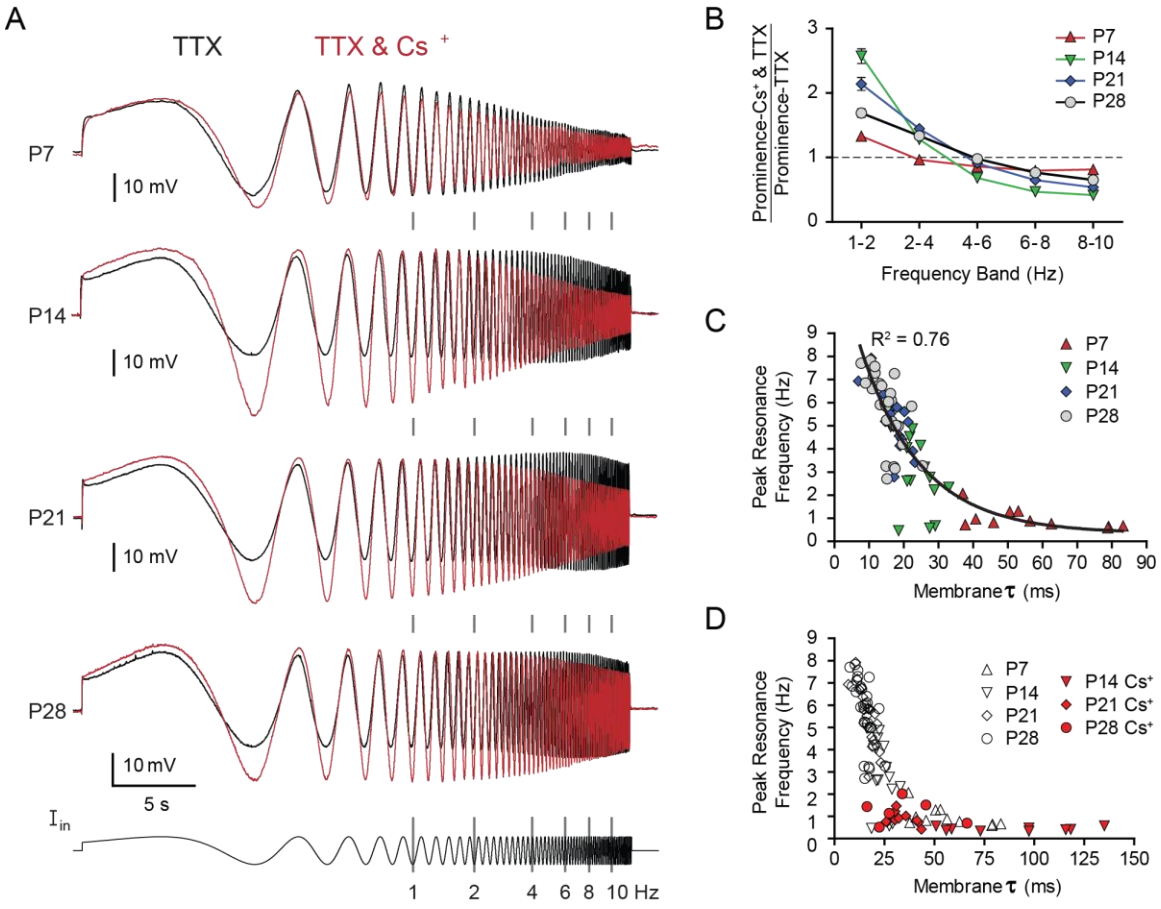

Figure 2.5: Contribution of I_h to intrinsic resonance of BLA principal neurons changes with age. (A) Mean membrane potential response to a ZAP current (I_{in}, fixed amplitude and logarithmically increasing frequency, shown at bottom) in 1 μM TTX alone (black line, taken from Figure 6) or with 5 mM Cs+ (red line) is depicted for each age (in Cs+, n = 19 at P7, 21 at P14, 20 at P21, and 17 at P28). Neurons were first hyperpolarized to -70 mV with direct current, and ZAP current amplitude was adjusted for each neuron and condition to elicit a 20 mV, maximal depolarizing deflection. Instantaneous frequency of the injected current is highlighted with gray bars between traces. (B) Effect of Cs^+ application on prominence, calculated as ratio of the prominence before and after Cs+ application, plotted as mean & SEM at P7, P14, P21, and P28. (C, D) Peak resonance frequency is plotted against membrane time constant (τ) for neurons at each time point, recorded in TTX alone (C, D) or following application of 5 mM Cs^+ (D). A black line depicts the results of an exponential regression (R2 = 0.76) of the data shown in C.

Figure 2.6: Spontaneous membrane potential oscillations emerge as BLA principal neurons develop

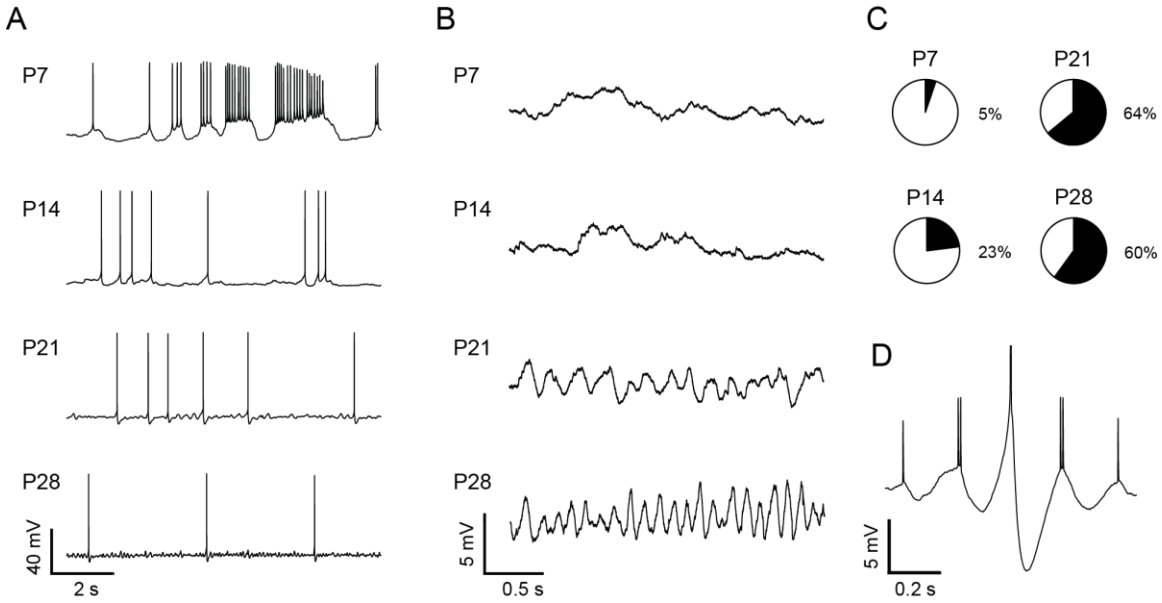

Figure 2.6: Spontaneous membrane potential oscillations emerge as BLA principal neurons develop. (A, B) Representative current-clamp recordings, shown at two scales, of neurons depolarized to action potential threshold with direct current, highlighting maturation of spiking pattern (A) and spontaneous membrane potential oscillations (B). (C) Pie charts depict the proportion of neurons expressing spontaneous membrane potential oscillations at each time-point (n = 20 (P7), 26 (P14), 25 (P21), and 48 (P28)). (D) Representative spike-triggered average from a 30 s recording of a P28 neuron held near threshold, displaying entrainment of spiking to a spontaneous membrane potential oscillation.

Figure 2.7: Maturation of spike trains in BLA principal neurons

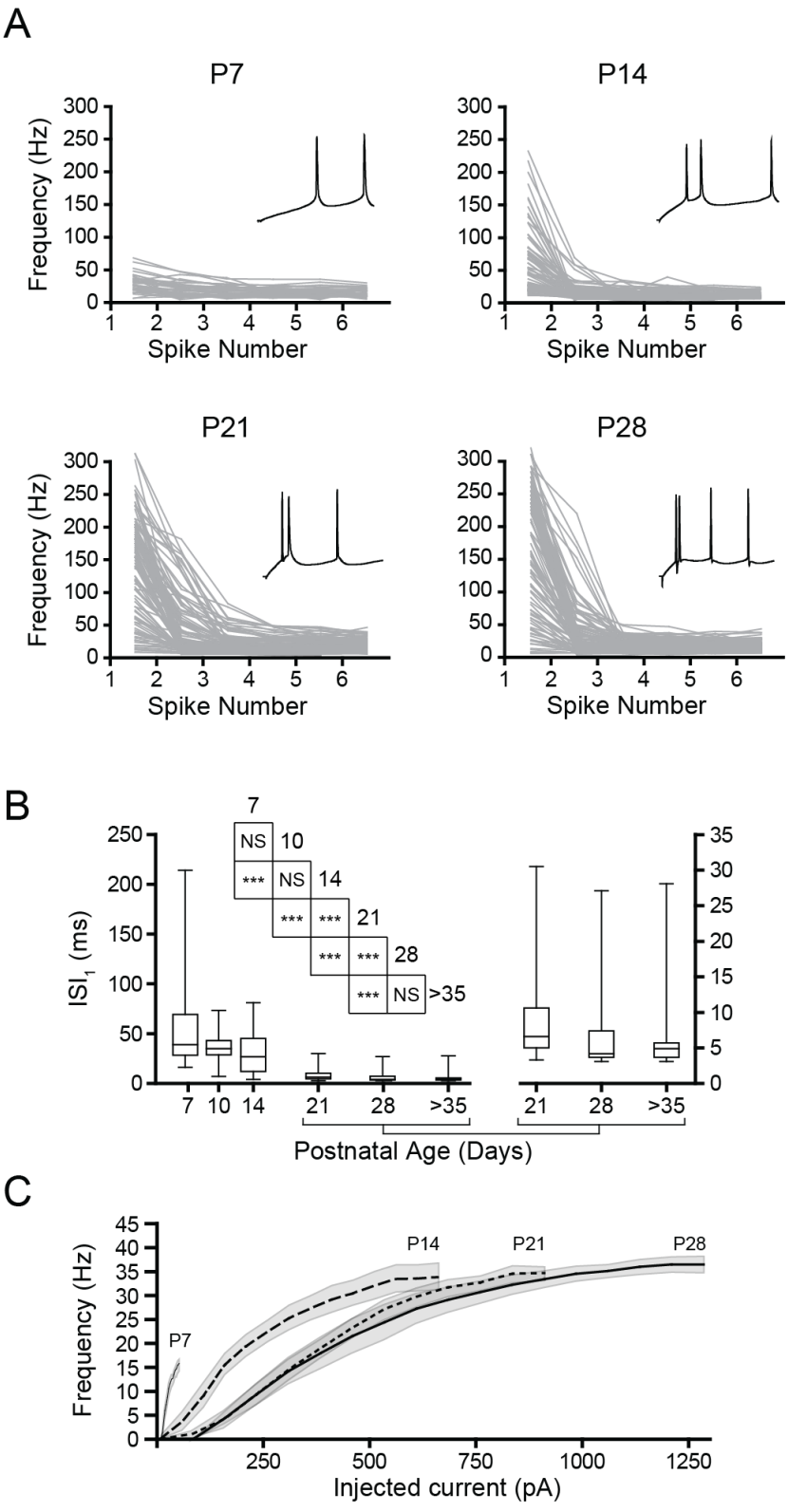

Figure 2.7: Maturation of spike trains in BLA principal neurons. (A) Instantaneous action potential frequency is plotted for individual neurons (grey lines) and group mean (black lines) at each time point. Neurons were depolarized such that the mean inter-spike membrane potential was near spike threshold (see Methods for details). The start of a representative spike train is inset in each plot to highlight differences in initial spike rate (n = 39 (P7), 75 (P14), 97 (P21), and 103 (P28) trains). (B) First interspike-interval for the spike trains in A is depicted in a box and whisker plot, with the later time-points shown on both y-axes (n = 45 (P7), 37 (P10), 53 (P14), 43 (P21), 54 (P28), and 59 (P>35)). Significance was assessed using a Wilcoxon rank-sum test and pairwise comparisons were made for each age group with up to four neighboring time-points (see inset table for results) using a Bonferroni correction for the resulting 9 comparisons (***, $p < 0.001$; NS: not significant, $p > 0.05$). (C) Input-output curves for neurons at each time point are depicted as mean (line) and standard deviation (grey band) of average firing frequency in response to a 1 s square current step from holding potential at -60 mV (n = 7 for all time points).

Figure 2.8: Action potentials of BLA principal neurons develop a more hyperpolarized threshold and become faster with age

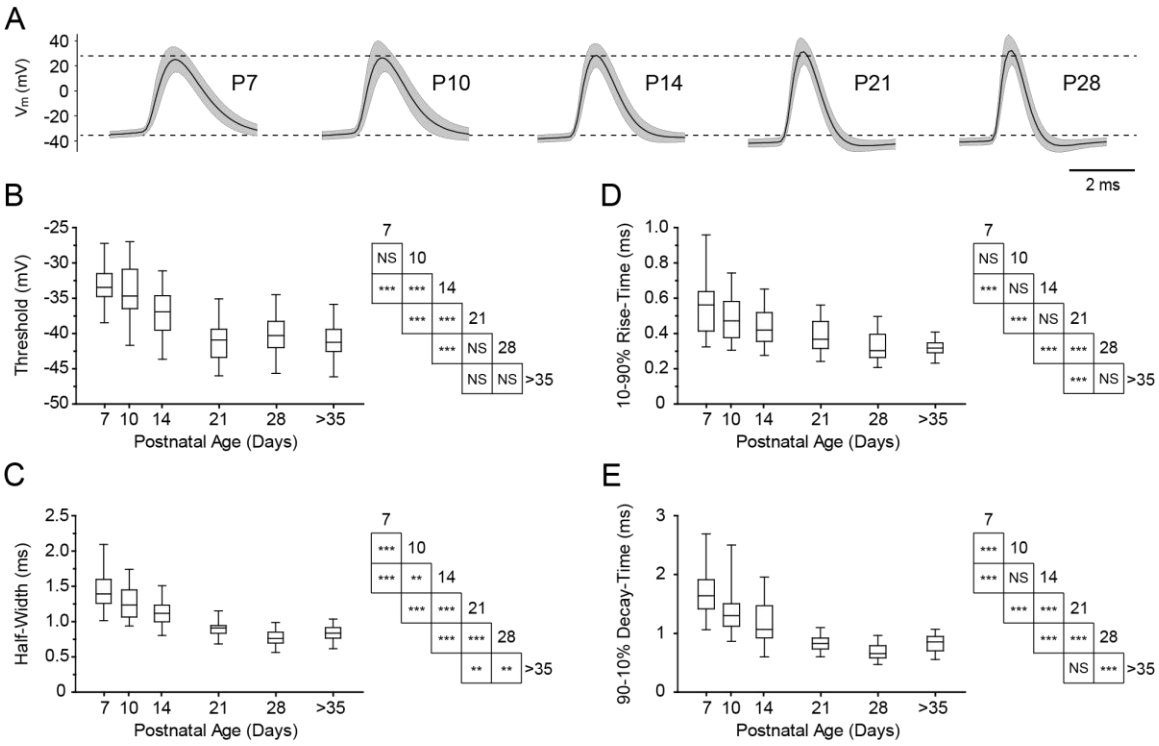

Figure 2.8: Action potentials of BLA principal neurons develop a more hyperpolarized threshold and become faster with age. (A) Action potential waveform, depicted as mean (black line) and standard deviation (grey band), for neurons across postnatal development (n = 48 (P7), 34 (P10), 46 (P14), 40 (P21), 54 (P28)). (B-E) Box and whisker plots depict action potential threshold (B), half-width (C), 10-90% rise-time (D), and 90-10% decay time (E) for neurons at each time point (n = 49-51 (P7), n = 35-37 (P10), n = 52-55 (P14), n = 43-45 (P21), n = 56-57 (P28), and n = 55-57 (P>35)). Significance was assessed using a Wilcoxon rank-sum test and pairwise comparisons were made for each age group with up to four neighboring time-points (see inset tables for results) using a Bonferroni correction for the resulting 9 comparisons (***, $p < 0.001$; **, $p < 0.01$; NS: not significant, $p > 0.05$).

Figure 2.9: Action potential medium AHP matures and a fast AHP emerges with age

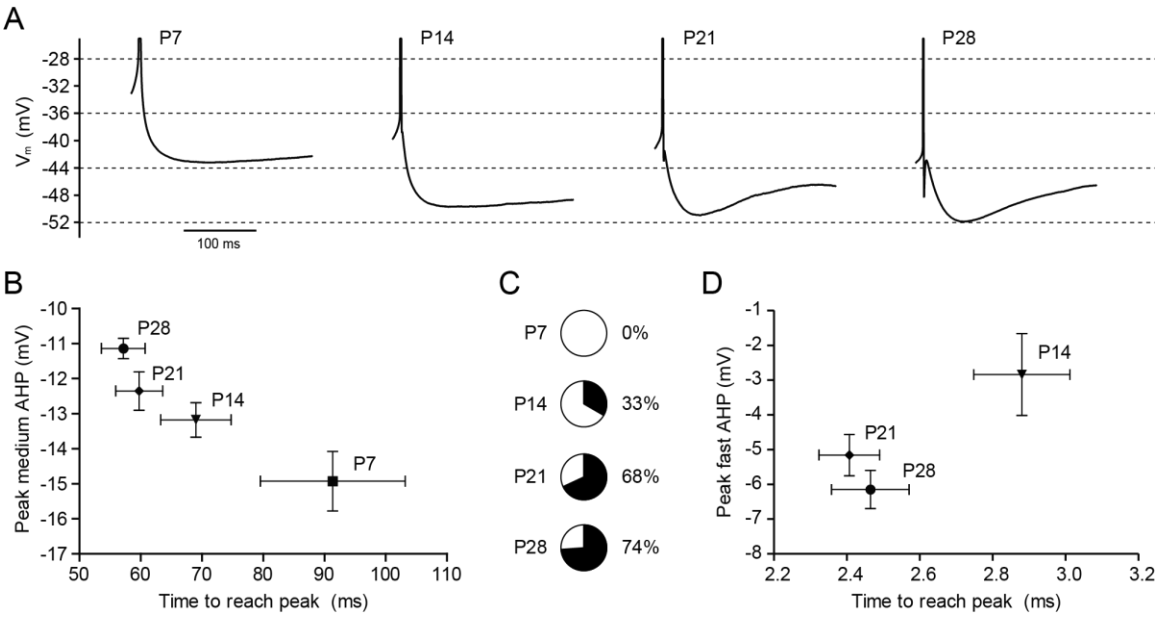

Figure 2.9: Action potential medium AHP matures and a fast AHP emerges with age. (A) Changes in afterhyperpolarization (AHP) waveform are illustrated by spike-triggered averages (from at least 8 action potentials) of one free-firing, representative neuron for each time point. (B, D) Derived from spike-triggered averages, the voltage difference between a neuron's action potential threshold and its medium (B) or fast (D) AHP peak (mean ± SEM) is plotted versus time elapsed from spike initiation to AHP peak (mean ± SEM) for each time point (n = 8 (P7), 15 (P14), 22 (P21), and 31 (P28)). There was a significant effect of age on mAHP amplitude ($p < 0.001$, One-way ANOVA) and duration ($p < 0.01$, Kruskal-Wallis). Only neurons with a discernible fast AHP were included in analysis for D, and the proportions of neurons expressing a fast AHP at each time point are depicted as pie charts (C).

Chapter 3: Morphology and Ion Channel Expression of Developing Principal Neurons in the Rat Basolateral Amygdala[2]

[2]Adapted from: Ryan SJ*, Ehrlich DE*, Hazra R, Guo JD, Rainnie DG (2013). *Morphology and Ion Channel Expression of Developing Principal Neurons in the Rat Basolateral Amygdala*. Under revision at J Comp Neurol.

3.1 Abstract

The basolateral nucleus of the amygdala (BLA) assigns emotional valence to sensory stimuli, and many amygdala-dependent behaviors undergo marked development during postnatal life. We recently showed principal neurons in the rat BLA undergo dramatic changes to their electrophysiological properties during the first postnatal month, but no study to date has thoroughly characterized changes to morphology or gene expression that may underlie the functional development of this neuronal population. We addressed this knowledge gap with reconstructions of biocytin-filled principal neurons in the rat BLA and single-cell RT-PCR at postnatal days 7 (P7), 14, 21, 28, and 60. BLA principal neurons underwent a number of morphological changes, including a two-fold increase in soma volume from P7 to P21 followed by a comparable decrease by P60. Dendritic arbors expanded significantly during the first postnatal month and achieved a mature distribution around P28, in terms of total dendritic length and distance from soma. The number of primary dendrites and branch points were consistent with age, but branch points were found farther from the soma in older animals. Dendrites of BLA principal neurons at P7 had few spines, and spine density increased nearly five-fold by P21. Corresponding with these morphological changes were shifts in the expression of transcripts for voltage-gated ion channels, with a number of subtypes present at P7 or P14 replaced by P28. Together, these developmental transitions in BLA principal neuron morphology and gene expression help explain a number of concomitant electrophysiological changes and identify a critical period in amygdala development.

3.2 Introduction

The amygdala is critical for the expression of normative and maladaptive emotional behaviors, but relatively few studies have characterized how BLA structure and function change with age. Many prior studies addressing maturation of the BLA have been performed in rats. These studies have identified a window during the first postnatal month wherein the morphology and physiology of the nucleus undergo rapid and pronounced change. In particular, during this window the volume of the BLA increases while the density of neurons is reduced by half (Morys et al., 1998; Rubinow and Juraska, 2009; Chareyron et al., 2012). Neurons in the BLA grow during this period, with somas and dendritic arbors expanding (Escobar and Salas, 1993). We characterized the developmental changes to electrophysiological properties of BLA principal neurons, which comprise approximately 85% of BLA neurons and mediate virtually all output of the nucleus (Chapter 2; Ehrlich et al., 2012). Specifically, we showed that BLA principal neurons exhibit significant changes to their excitability and sensitivity to synaptic input across the first postnatal month, including a ten-fold reduction in input resistance and a hyperpolarization of action potential threshold greater than 5 mV. There are also concomitant changes to the waveform and patterning of action potential output, including the emergence of a fast after-hyperpolarization and spike doublets.

While previous studies have addressed gross morphological changes to the BLA and its component neurons throughout postnatal development, several important knowledge gaps remain. The only study to date examining the morphology of individual neurons in the BLA was not specific to principal neurons and did not address features such as the quantity or branching of dendritic material or the expression of spines (Escobar and Salas, 1993). Developmental changes to these features should substantially alter neuronal function, as the surface area of BLA principal neurons and the types of ion channels inserted into their membranes directly impact neurophysiology, including firing patterns (Mainen and Sejnowski, 1996). We have addressed

this knowledge gap by characterizing BLA principal neuron morphology throughout the first postnatal month and in adulthood. Additionally, we identified corresponding changes to the expression of subtypes for various voltage-gated ion channels. Specifically, we used whole cell patch clamp at postnatal days 7, 14, 21, 28, and 60 to fill neurons with biocytin for post-hoc morphological reconstruction and analysis. We also recovered principal neuron cytosol for analysis with single-cell RT-PCR, testing for the expression of transcripts for voltage-gated ion channels in the HCN, K_{IR}, K_V, and Ca_V families. Here, we describe a number of changes to the soma, dendritic arbor, dendritic spines, and ion channel expression in developing BLA principal neurons.

3.3 Methods

3.3.1 Ethical approval

All experimental protocols strictly conform to National Institutes of Health guidelines for the Care and Use of Laboratory Animals, and were approved by the Institutional Animal Care and Use Committee of Emory University.

3.3.2 Animals

Male rats born in-house to time-mated Sprague–Dawley female rats (embryonic day 5 on arrival from Charles River, Wilmington, MA, USA) were used in all experiments. Pups were housed with the dam prior to weaning on postnatal day (P)22 or P23 (considering P1 as day of birth). After weaning, rats were isolated by sex and housed three to four per cage with access to food and water *ad libitum*. Animals attributed to each developmental time-point (P7, P14, P21, P28, and P60) were used on that day or the following day (P7–8, P14–15, P21–22, P28–29, and P60-61, respectively).

3.3.3 Slice Physiology

To perform neuronal reconstructions at each time-point, we performed whole-cell patch clamp to identify BLA principal neurons based on electrophysiological properties as described previously (Ehrlich et al., 2012) and to visualize neurons, biocytin (0.35%, Sigma-Aldrich, St Louis, MO, USA) was included in the patch recording solution. Acute brain slices containing the BLA were obtained as previously described (Rainnie, 1999b). Briefly, animals were decapitated under isoflurane anesthesia (Fisher Scientific, Hanoverpark, IL, USA) if older than 11 days, and the brains rapidly removed and immersed in ice cold, 95% oxygen–5% carbon dioxide-perfused 'cutting solution' with the following composition (in mM): NaCl (130), $NaHCO_3$ (30), KCl (3.50), KH_2PO4 (1.10), $MgCl_2$ (6.0), $CaCl_2$ (1.0), glucose (10), ascorbate (0.4), thiourea (0.8), sodium pyruvate (2.0) and kynurenic acid (2.0). Coronal slices containing the BLA were cut at a thickness of 300–350 μm using a Leica VTS-1000 vibrating blade microtome (Leica Microsystems Inc., Bannockburn, IL, USA). Slices were kept in oxygenated cutting solution at 32°C for 1 h before transferring to regular artificial cerebrospinal fluid (ACSF) containing (in mM): NaCl (130), $NaHCO_3$ (30), KCl (3.50), KH_2PO_4 (1.10), $MgCl_2$ (1.30), $CaCl_2$ (2.50), glucose (10), ascorbate (0.4), thiourea (0.8) and sodium pyruvate (2.0).

3.3.4 Patch clamp recording

Individual slices were transferred to a recording chamber mounted on the fixed stage of a Leica DMLFS microscope (Leica Microsystems Inc., Bannockburn, IL, USA) and maintained fully submerged and continuously perfused with oxygenated 32°C ACSF at a flow rate of 1–2 mL min^{-1}. The BLA was identified under 10x magnification. Individual BLA neurons were identified at 40x using differential interference contrast (DIC) optics and infrared (IR) illumination with an IR sensitive CCD camera (Orca ER, Hamamatsu, Tokyo Japan). Patch pipettes were pulled from borosilicate glass and had a resistance of 4–6 MΩ. Patch electrode solution had the following composition (in mM): potassium gluconate (130), KCl (2), HEPES (10), $MgCl_2$ (3), K-ATP (2),

Na-GTP (0.2), phosphocreatine (5), and 0.35% biocytin, titrated to pH 7.3 with KOH, and 290 mosmol L^{-1}. Data acquisition was performed using either a MultiClamp 700A or an Axopatch 1D amplifier in conjunction with pCLAMP 10.2 software and a DigiData 1322A AD/DA interface (Molecular Devices, Sunnyvale, CA, USA). Whole-cell patch clamp recordings were obtained and low-pass filtered at 2 kHz and digitized at 10 kHz. The membrane potential was held at −60 mV for all neurons if not specified. Cells were excluded if they did not meet the following criteria: a stable resting membrane potential more negative than −55 mV; access resistance lower than 30 MΩ; stable access resistance throughout recording, changing less than 15%; and action potentials crossing 0 mV. The identity of BLA principal neurons was verified by injecting a series of 10 hyperpolarizing and depolarizing, 1 s long, square-wave current steps. They were scaled so that, for each cell, the peak voltage deflections were to approximately −80 mV and −40 mV. Traces were analyzed using Clampfit 10.2 (Molecular Devices, Sunnyvale, CA, USA).

3.3.5 Histochemical Processing

Patched neurons were labeled with biocytin (Sigma-Aldrich, St Louis, MO, USA) included in the patch pipette recording solution. After neurons were recorded for at least 15 minutes, slices were fixed in 10% buffered formalin (Fisher Scientific, Hanoverpark, IL, USA) for 12-72 hours, and then transferred to cryo-protectant for storage at -20 C. After three consecutive 10 minute washes in 0.05 M phosphate buffered saline (PBS), slices were permeabilized for 30 minutes in phosphate buffered saline (PBS) and 0.5% Triton X-100 (Sigma-Aldrich, St Louis, MO, USA). Slices were then treated with Alexa Fluor 488-conjugated Streptavidin (Invitrogen, Grand Island, New York, USA) diluted to 1:1000 in PBS with Triton X-100 overnight at room temperature. Slices were then washed 2 times for 1 hour each in 0.05 M PBS and washed for 10 minutes in 0.05 M phosphate buffer. Finally, the slices were mounted on glass slides, air dried for two to twelve hours, and cover-slipped with mowiol mounting medium (Sigma-Aldrich, St Louis, MO, USA).

3.3.6 Neuronal reconstruction and Data Analysis

For morphological analysis, the dendritic arbor of each neuron was first reconstructed by hand using the Neurolucida neuron tracing software (MicroBrightField, Colchester, VT) from single z-stack images taken at 10x magnification with a 0.4 μm step size using a Leica DM5500B spinning disk confocal microscope (Leica Microsystems Inc., Bannockburn, IL, USA) and SimplePCI data acquisition software (Compix, Sewickley, PA). Slices were examined live at 63x to support tracing of fine or overlapping dendritic segments. Reconstructions of neuronal somas were performed using AutoNeuron workflow in Neurolucida from image stacks obtained with a 63x objective. Quantitative analysis of reconstructions was performed using Neurolucida Explorer (MicroBrightField). The volume and surface area of somas were estimated using the 'Marker and Region Analysis' subroutine to provide a 3-D contour summary. Dendritic length and branching were analyzed in Neurolucida Explorer using Sholl analyses with ring radius increments of 2 μm, and data were analyzed in Matlab (The MathWorks, Natick, MA, USA). Corrections were not made for shrinkage due to tissue processing.

To estimate the average spine density for BLA principal neurons, we manually counted dendritic spines with Neurolucida on image stacks of dendrite segments taken at 100x magnification. For each neuron, 10 dendritic segments were analyzed and the counter was blinded to the originating neuron of each segment. The 10 segments for counting were chosen pseudo-randomly using a custom Matlab script (available upon request), which selected random locations throughout the dendritic arbor that were separated from each other by a minimum of 50 μm. Dendritic spines were counted on segments centered on each of these 10 locations, spanning 50 μm (or less if near an ending) along a random path through the dendritic arbor. Total spine number was estimated for each neuron individually using the product of average spine density and aggregate dendritic length, defined as the sum of the lengths of all dendritic segments.

3.3.7 Single Cell RT-PCR

At the end of a subset of patch clamp recording sessions without biocytin present in the patch solution, the cell cytoplasm was aspirated into the patch recording pipette by applying gentle negative pressure under visual control. Pipettes contained ~5 μL of RNase-free patch solution. The contents of the patch pipette were expelled into a microcentrifuge tube containing 5 μL of the reverse transcription cocktail (Applied Biosystems, Foster City, CA, USA), and the reverse transcription product was amplified in triplicate and screened for 18S rRNA. Only those cell samples positive for 18S rRNA were subjected to amplification with primers. All cells were screened for the vesicular glutamate transporter 1 (VGLUT1) expression to confirm a glutamatergic phenotype, and all 46 neurons presented here were positive. The procedure used to determine mRNA transcript expression in single cells has been described in detail previously (Hazra et al., 2011). The sequences for the oligonucleotide primers are listed in **Table 3.1**. PCR products were visualized by staining with ethidium bromide and separated by electrophoresis in a 1% agarose gel.

3.3.8 Statistics

To compensate for age-dependent changes in variance (assessed using Bartlett's test with GraphPad, GraphPad Software Inc., La Jolla, CA, USA), data for soma volume, critical value of dendritic length, dendritic spine density, and total spine estimate were log-transformed before statistical analysis. Unless otherwise noted, data are presented as mean ± SEM. The values for aggregate dendritic length, critical value of dendritic length, dendritic spine density, and total dendritic spine estimate were fit with a Boltzman sigmoidal equation (**Equation 3.1**) in GraphPad. Most data sets were analyzed with a One-way ANOVA to determine effects of age (GraphPad). Data from Sholl analyses were analyzed with Two-way ANOVA to determine effects of age and distance from soma. Single-cell RT-PCR data were analyzed using logistic regression with a binomial distribution in R (The R Foundation for Statistical Computing,

Vienna, Austria), with gene expression as the dependent variable (no expression defined as 0, expression defined as 1) and age as the independent variable.

Equation 3.1 $y = A_2 + (A_1 - A_2)/(1 + e^{(V_{1/2} - x)/\alpha})$

3.4 Results

In total, 40 neurons from 15 male rats were filled with biocytin at postnatal day 7 (P7), P14, P21, P28, and P60 (8 per time-point). In addition, we characterized mRNA expression at each time-point using single cell reverse transcription – polymerase chain reaction (scRT-PCR) after recovering mRNA from BLA principal neurons at P7, P14, P21, and P28 (n = 11 to 12 neurons from 1 animal per time-point). Basic electrophysiological properties were measured and found to be consistent with previously reported values (Ehrlich et al., 2012). Brain slices containing filled, recorded neurons were stained and neurons visualized post-hoc to make neuronal reconstructions (see Methods). Representative neuronal reconstructions are depicted for each time-point in **Figure 3.1**, and illustrate a variety of developmental changes to BLA principal neuron morphology that are quantified in detail below. Principal neurons at all ages lacked a consistent orientation in the slice.

3.4.1 Soma size

We first quantified somatic volume and surface area of BLA principal neurons throughout postnatal development (**Figure 3.2**). Somatic diameters ranged between 10 and 16 µm and somatic volume changed significantly during postnatal development (**Figure 3.2A**, $P < 0.0001$, One-way ANOVA, $F_{4,29} = 12.97$), gradually increasing across the first postnatal month and then decreasing by adulthood. Mean somatic volume increased by 94% from P7 to P21, followed by a 39% reduction by P60. Somatic volume also exhibited an inverted-U relationship with age, increasing significantly from 793.9 ± 56.1 μm^3 (mean ± SEM) at P7 (n = 7) to 1291.5 ±

60.7 μm^3 at P14 (n = 7; Tukey's *post hoc* test, P < 0.01), 1541.5 ± 156.8 μm^3 at P21 (n = 7, P < 0.001), and 1507.1 ± 61.8 μm^3 at P28 (n = 6, P < 0.001). However, by P60, somatic volume measured 946.0 ± 103.7 μm^3 (n = 7), constituting a significant decrease from P14 (P < 0.05), P21 (P < 0.01), and P28 (P < 0.01).

A similar trajectory was exhibited by somatic surface area, which also changed significantly across postnatal development (**Figure 3.2B**, P < 0.001, One-way ANOVA, $F_{4,29}$ = 6.143). Somatic surface area increased from 376.5 ± 27.1 μm^2 at P7 (n = 7) to 498.3 ± 25.8 μm^2 at P14 (n = 7), and significantly increased from P7 to 536.0 ± 52.2 μm^2 at P21 (n = 7; Tukey's *post hoc* test, P < 0.05) and 558.5 ± 20.0 μm^2 at P28 (n = 6; P < 0.01). By P60, the somatic surface area of 390.2 ± 29.9 μm^2 was comparable to that at P7 and constituted a significant decrease from P21 (P < 0.05), and P28 (P < 0.05).

3.4.2 Growth and Retraction of Dendritic Arbor

Extensive remodeling of dendritic architecture of BLA principal neurons also occurred across postnatal development (**Figure 3.3**). The aggregate length of dendrites for each neuron changed significantly with age (P < 0.0001, One-way ANOVA, $F_{4,34}$ = 23.27), increasing more than threefold across the first postnatal month (**Figure 3.3A**). Aggregate dendritic length increased significantly from 2.106 ± 0.168 mm at P7 (n = 7) to 4.863 ± 0.466 mm at P14 (n = 8; Tukey's *post hoc* test, P < 0.001), 6.185 ± 0.358 mm at P21 (n = 8; P < 0.001), 6.809 ± 0.402 mm at P28 (n = 8; P < 0.001), and 6.378 ± 0.409 mm at P60 (n = 8; P < 0.001). The aggregate dendritic length also increased significantly from P14 to P28 (P < 0.01). The distribution of aggregate dendritic length vs. age was fit with a sigmoidal Boltzmann function (**Eqn. 3.1**), which estimated the inflection point at $V_{1/2}$ = 10.92 days with a slope of α = 3.48 days. The lower asymptote of aggregate length was estimated to be A_2 = 659.8 µm and the upper asymptote to be A_1 = 6578 µm. The goodness of fit was R^2 = 0.726.

The observed increase in aggregate dendritic length with age corresponded with an

increased distance of that material to the soma (**Figure 3.3B**). Using a Sholl analysis with concentric rings of 4 μm thickness, we were able to determine the critical value for dendritic length, defined as the radius of the Sholl ring with the greatest amount of dendritic length. With age, dendrites became concentrated farther from the soma, with the critical value increasing significantly across the first postnatal month ($P < 0.0001$, One-way ANOVA, $F_{4,33} = 10.69$). Specifically, the critical value for dendritic length increased from 32.3 ± 2.9 μm at P7 (n = 7) to 52.0 ± 5.7 μm at P14 (n = 8) and increased significantly to 71.7 ± 10.1 μm at P21 (n = 7; Tukey's *post hoc* test, $P < 0.01$ vs P7), 91.0 ± 9.6 μm at P28 (n = 8; $P < 0.001$), and 93.0 ± 11.8 μm at P60 (n = 8; $P < 0.001$). The critical value also increased significantly from P14 to P28 and P60 ($P < 0.05$). As for the aggregate dendritic length values, the distribution of critical value vs. age was fit with a sigmoidal Boltzmann function (**Eqn. 3.1**), which estimated the inflection point at $V_{1/2} = 16.37$ days with a slope of $\alpha = 4.91$ days. The lower asymptote for critical value was estimated to be $A_2 = 23.70$ μm and the upper asymptote to be $A_1 = 94.26$ μm. The goodness of fit was $R^2 = 0.507$.

The proximity of dendrites to the soma matures in a specific pattern, exemplified by the representative reconstructions in **Figure 3.1**. Across the first few postnatal weeks, dendrites extend farther from the soma. From P21 to P28 there is expansion of dendrites near the soma, and by P60 there is a reduction of dendrites in the most proximal and distal portions of the arbor. Using Sholl analysis, we identified specific portions of the dendritic arbor where significant growth and retraction occur during postnatal development (**Figure 3.3D**; Two-way ANOVA with Bonferroni *post hoc* tests; main effect of age: $P < 0.0001$, $F_{4,1155} = 85.67$; main effect of distance from soma: $P < 0.0001$, $F_{34,1155} = 187.8$; interaction effect: $P < 0.0001$, $F_{136,1155} = 6.586$). In P7 neurons (n = 7), more than 99.7% of dendritic length is found within 200 μm of the soma. By P14, the proportion found within 200 μm drops to 89.8%, while 99.8% of dendritic length is found within 400 μm of the soma. From P7 to P14, there is also a significant expansion of dendrites in the region 40 to 180 μm from the soma ($P < 0.01$). By P21, only 93.5% of dendritic

material is found within 400 µm of the soma, with the remainder extending as far as 660 µm from the soma. From P14 to P21, significant growth of dendrites occurs in the region 140 to 220 µm from the soma ($P < 0.01$). At P28, dendritic arbors occupy a similar space as those at P21, extending as far as 680 µm from the soma, with 96.5% of dendritic length found within 400 µm of the soma. The greater proportion of dendrites within 400 µm of the soma at P28 corresponds with a significant increase from P21 in dendrites found in the region 80 to 120 µm from the soma ($P < 0.001$). The developmental expansion of dendrites in this window is reversed by P60, which exhibits a significant decrease from P28 in the region 60 to 120 µm from the soma ($P < 0.05$). By P60, the reduction in dendritic length also occurs in the most distal parts of the arbor, with 99.4% of dendritic length being found within 400 µm of the soma.

We also examined the pattern of dendrite maturation by considering the growth of specific orders of dendritic branches (**Figure 3.3C**). When we normalized the aggregate dendritic length for individual orders of branches to the total for all branch orders of a neuron, we found the majority of dendritic length in second through sixth order dendrites. The total length of dendrites varied significantly by branch order, but age did not significantly affect this distribution (Two-way ANOVA; main effect of branch order: $P < 0.0001$, $F_{8,268} = 52.96$; main effect of age: $P > 0.05$, $F_{4,268} = 0.28$).

3.4.3 Maturation of Dendritic Branching

We also investigated the maturation of branch points in the dendritic arbor, because the location of branch points determines the relationship between dendrite order and proximity to the soma (**Figure 3.4**). The number of primary dendrites was consistent throughout postnatal development (**Figure 3.4A**; $P > 0.05$, Kruskal-Wallis, $H(4) = 5.93$; mean ± SD: 7 ± 2.4 at P7, 5.75 ± 1.5 at P14, 5.5 ± 1.1 at P21, 6.1 ± 1.5 at P28, and 7.75 ± 2.4 at P60; n = 8). We analyzed the total number of branch points in the dendritic arbor for neurons at each time-point, and found no significant effect of age (**Figure 3.4B**; $P > 0.05$, Kruskal-Wallis, $H(4) = 7.10$; mean ± SD: 42

± 18.0 at P7, 34.7 ± 13.3 at P14, 35.0 ± 8.5 at P21, 45.0 ± 8.8 at P28, and 34.5 ± 8.8 at P60; n = 7-8). Furthermore, we quantified the proximity of branch points to the soma using a Sholl analysis with 40 µm thick rings. We found significant changes in the proximity of branch points to the soma with age (**Figure 3.4C**; Two-way ANOVA with Bonferroni *post hoc* tests; main effect of distance from soma: $P < 0.0001$, $F_{15,512} = 185.6$; interaction of age and distance from soma: $P < 0.0001$, $F_{60,512} = 3.998$). In P7 neurons, branch points were found very close to the soma, with 65.1 ± 9.4% occurring within 40 µm of the soma and 99.3 ± 0.7% occurring within 160 µm (mean ± SEM, n = 7). With age, branch points transitioned away from the soma: by P14, branch points were found more distally, extending as far as 320 µm from the soma, and with significantly fewer within 40 µm (45.3 ± 6.6%, $P < 0.001$, n = 7). The proportion of branch points within 40 µm of the soma decreases further from P14 to P21 (40.0 ± 6.4%, n = 7), and decreases significantly from P14 to P28 (33.5 ± 5.5%, $P < 0.001$, n = 8) and P60 (31.6 ± 3.4%, $P < 0.001$, n = 8). Conversely, the proportion of branch points located more distally increases significantly with age. Specifically, in P7 neurons 4.4 ± 1.8% of branch points are located 80 to 120 µm from the soma, while this number increases to 10.1 ± 1.7% at P14 and significantly increases to 14.7 ± 3.5% at P21 ($P < 0.05$), 17.8 ± 3.6% at P28 ($P < 0.001$), and 18.8 ± 3.1% at P60 ($P < 0.001$). A similar trend occurs for branch points located 120 to 160 µm from the soma (see **Figure 3.4C**).

3.4.4 Developmental Emergence of Dendritic Spines

We next investigated the maturation of dendritic spines (**Figure 3.5**), which were much more apparent on the arbors of neurons at later time-points. Neurons at P7 frequently possessed smooth dendrites with few spines, while neurons at P21 and older had spine-laden dendrites (**Figure 3.5A**). To quantify the emergence of dendritic spines with age, we counted spines on 10 random segments of dendrite for neurons at each time-point (see Methods). We found that the density of dendritic spines changed significantly with age, increasing nearly six-fold across the time period studied, reaching adult levels at the end of the first postnatal month (**Figure 3.5B**; $P <$

0.0001, One-way ANOVA, $F_{4,25} = 59.41$; n = 6 neurons per time-point). Specifically, neurons at P7 had a spine density of 0.21 ± 0.03 spines/µm (mean ± SEM) which increased significantly to 0.53 ± 0.05 spines/µm at P14 ($P < 0.001$), 1.03 ± 0.12 at P21 ($P < 0.001$), 1.18 ± 0.05 at P28 ($P < 0.001$), and 1.29 ± 0.07 at P60 ($P < 0.001$). Spine density also increased significantly from P14 to all later time points ($P < 0.001$). The distribution of dendritic spine density vs. age was fit with a sigmoidal Boltzmann function (**Eqn. 3.1**), which estimated the inflection point at $V_{1/2} = 15.97$ days with a slope of $\alpha = 3.89$ days. The lower asymptote for spine density was estimated to be $A_2 = 0.10$ spines and the upper asymptote to be $A_1 = 1.26$ spines. The goodness of fit was $R^2 = 0.868$.

Using our measurements of mean spine density and the aggregate dendritic length from our reconstructions, we were able to estimate the total number of dendritic spines for each neuron (**Figure 3.5C**). These estimates suggest the total number of spines is more than fifteen times larger at P60 than at P7, as the number of spines increases significantly across postnatal development ($P < 0.0001$, One-way ANOVA, $F_{4,25} = 59.92$; n = 6). Specifically, neurons at P7 had an estimated 533 ± 146 spines (mean ± SEM) which increased significantly to 2530 ± 392 spines at P14 ($P < 0.001$), 6204 ± 512 at P21 ($P < 0.001$), 7675 ± 704 at P28 ($P < 0.001$), and 8357 ± 999 at P60 ($P < 0.001$). Total spine number also increased significantly from P14 to all later time-points ($P < 0.01$). As with spine density, the distribution of total dendritic spines vs. age was fit with a sigmoidal Boltzmann function (**Eqn. 3.1**), which estimated the inflection point at $V_{1/2} = 17.0$ days with a slope of $\alpha = 3.80$ days. The lower asymptote for spine density was constrained at $A_2 = 0$ spines and the upper asymptote was estimated to be $A_1 = 8256.0$ spines. The goodness of fit was $R^2 = 0.826$.

3.4.5 Expression of Ion Channel Transcripts

We next investigated the expression of ion channel mRNA transcripts, which are thought to endow principal neurons with their basic electrophysiological properties. Our previous study of

the electrophysiological properties of developing BLA principal neurons provided several candidate ion channels for further study. Here, we investigated the presence of transcripts for multiple ion channel subtypes by isolating cytosolic mRNA from individual BLA principal neurons throughout the first postnatal month (**Figure 3.6**). Specifically, we assessed the presence of mRNA transcripts for subtypes of 4 different ion channels: namely, the hyperpolarization-activated, cyclic nucleotide-gated (HCN) channel that mediates the H-current (I_H); the inwardly rectifying potassium channel, K_{IR}; the voltage-gated potassium channels mediating the A-current (I_A); and the voltage-gated calcium channels mediating the T-current (I_T).

3.4.5.1 HCN Subtype Expression

Four subtypes of HCN channel (HCN 1-4) mediate I_H and are primarily differentiated by their differing gating kinetics (Pena et al., 2006). We previously reported a decrease in the activation time-constant for I_H across the first postnatal month, leading us to hypothesize that HCN subtype expression may also change across development (Ehrlich et al., 2012). Consistent with our hypothesis, a developmental transition in the expression of mRNA for I_H channel subtypes was observed in BLA principal neurons (**Figure 3.6A**). HCN2 and HCN4 were the only HCN subtypes present at P7, and at this age they were mutually exclusive, being expressed by 6/11 and 5/11 neurons, respectively. At P14 no HCN2 transcript expression was detected, however we did detect HCN3 and HCN4 transcript expression in 6/11 and 7/ 11 neurons, respectively. At P21, transcripts for all three HCN subtypes found previously were expressed; HCN2 was detected in 4/12 neurons, HCN3 in 3/12, and HCN4 in 4/12. At P28, HCN1 expression emerged, being detected in 7/12 neurons, while HCN2 and HCN3 transcripts were detected in 5/12 and 9/12 neurons, respectively. HCN4 transcript expression was absent at P28.

3.4.5.2 K_{IR} Subunit Expression

K_{IR} channels are a family of inwardly-rectifying potassium channels. K_{IR}2.1-2.4 are responsible for the "anomalous rectifying current" that is, like I_H, activated at membrane

potentials hyperpolarized to rest. We also found changes in the expression of mRNA transcripts for these channel subunits (**Figure 3.6B**). At P7, $K_{IR}2.1$ was the only subunit expressed, and was found in all 11 neurons tested. At P14, $K_{IR}2.1$ was only expressed in 4/11 neurons, while $K_{IR}2.3$ expression emerged, being mutually exclusive with $K_{IR}2.1$ expression, and found in the remaining 7/11. $K_{IR}2.1$ and 2.3 were the only subunits expressed at P21, in 7/12 and 9/12 neurons, respectively. A similar pattern of expression was found at P28, with 7/12 neurons expressing $K_{IR}2.1$, 1/12 expressing $K_{IR}2.2$, and 8/12 expressing $K_{IR}2.3$. There was no detectable expression of $K_{IR}2.4$ transcripts during the first postnatal month.

3.4.5.3 K_V Subunit Expression

We also investigated the developmental expression of several voltage-gated potassium (K_V) channel subunits, specifically those channels mediating I_A. As illustrated in **Figure 3.6C**, $K_V1.4$ was expressed robustly and exclusively in immature neurons, being found in 10/11 neurons at P7, and 9/11 neurons at P14. However, at P21 and P28 $K_V1.4$ mRNA transcripts were not detectable in any neuron tested. Contrastingly, $K_V3.4$ transcripts were absent from neurons at P7 or P14, but were present in 10/12 and 12/12 neurons at P21 and P28, respectively. The pattern of expression for Kv4.1, 4.2, and 4.3 transcripts was consistent throughout development. $K_V4.1$ transcripts were expressed by 8/11 neurons at P7, 7/11 at P14, 6/12 at P21, and 6/12 at P28. $K_V4.2$ was expressed by all 11 neurons at P7, 9/11 at P14, all 12 at P21, and 6/12 at P28. $K_V4.3$ was expressed by 2/11 neurons at P7, 5/11 at P14, 5/12 at P21, and 4/12 at P28. Notably, expression of K_V 4.1 and 4.3 transcripts were mutually exclusive in most neurons, aside from a single neuron at each of P14, P21, and P28 that expresses both subunits.

3.4.5.4 Ca_V3 Subunit Expression

Finally, we examined expression of the three alpha subunits of the heteromeric channels that conduct the transient calcium current, I_T (**Figure 3.6D**). We found a clear shift in expression of Ca_V3 subunits from $Ca_V3.1$ to $Ca_V3.2$ with age. At P7 and P14, 10/11 neurons had detectable

expression of $Ca_V3.1$, while that proportion decreased to 2/12 at P21 and 0/12 at P28. Conversely, no neurons had detectable expression of $Ca_V3.2$ transcripts at P7 or P14, whereas 7/12 neurons showed expression at P21 and 4/12 neurons at P28 expressed $Ca_V3.2$ transcripts. Transcripts for $Ca_V3.3$ were not detected at any time-point.

3.5 Discussion

In this study, we presented a detailed analysis of the morphological properties of BLA principal neurons, conducted across the first two postnatal months in rats. During this window, BLA principal neurons exhibit a variety of structural changes with the most dramatic maturation occurring before P21. Significant morphological changes included: soma size developing as an inverted U with a peak at P28; a three-fold increase in aggregate dendritic length from P7 to P21; growth of distal dendrites until P21 followed by retraction at P28; a shift of branch points more distally in the dendritic arbor through P60; and an increase in the density of dendritic spines, reaching maturity around P28. During the first postnatal month, we also observed transitions in the expression of specific subtypes of voltage-gated ion channels, generally away from channels that operate at more depolarized voltages and with slower kinetics. Taken together, these developmental changes to principal neuron morphology and gene expression help explain a wealth of electrophysiological changes occurring in the first postnatal month, including dramatic changes to passive membrane properties, action potential waveform and patterning, and intrinsic frequency preference (Ehrlich et al., 2012). The structural and functional maturation of amygdala neurons may underlie a variety of developmental changes to emotional behavior (King et al., 2013), which also occur during the first postnatal month and include conditioned avoidance (Sullivan et al., 2000), fear-potentiated startle (Hunt et al., 1994; Richardson et al., 2000), trace conditioning (Moye and Rudy, 1987), and extinction (Kim and Richardson, 2007). Our observations suggest that developmental changes in the mammalian amygdala extend from birth until adolescence, based on developmental milestones in the rat (Quinn, 2005).

3.5.1 Somatic Development

The most basic metrics of morphological development we examined were somatic volume and surface area. Values for both measures increased dramatically from P7 to P28, with soma volume nearly doubling in this window. From P28 to P60, however, some volume and surface area decreased back to the values observed at P7. Our measurements of adult soma size are consistent with previous reports in rat amygdala (Chareyron et al., 2012) and somatosensory cortex (Romand et al., 2011). An early increase in soma size with a subsequent decrease has been observed in other brain regions in the rat (Vidal et al., 2004; Liao and Lee, 2012) and gerbil (Gleich and Strutz, 2002), while less expansive studies in rat motoneurons and cerebellar granule cells have corroborated the late decrease in soma size, suggesting a general principle of neuron development (Monteiro et al., 1998; Gleich and Strutz, 2002; Monteiro et al., 2005). In contrast, no significant effect of postnatal age was found on soma size in the macaque amygdala, although there was a peak during infancy (Chareyron et al., 2012). Nevertheless, we have shown that in rat BLA principal neurons the increase in soma size precedes the major period of dendritic outgrowth, while the soma shrinks once dendritic growth has ceased; this suggests the soma may enlarge specifically during a period of dendritic outgrowth, potentially to produce proteins or support the assembly of microtubules for dendritic growth (Baas and Lin, 2011). Interestingly, the soma is a key site for synaptic contacts from inhibitory basket cells, including parvalbumin-expressing interneurons, which increase in expression in the BLA until P30, when principal neurons reach a peak in soma surface area (Berdel and Morys, 2000).

3.5.2 Dendritic Morphology

Our data suggests almost all growth of the dendritic arbor of BLA principal neurons occurs by P28, with a large proportion occurring between P7 and P21. While the aggregate length of dendritic material reaches the mature value around P21, Sholl analyses suggest the dendritic arbor is still remodeled beyond this time-point, with dendrites retracting from P21 to P28. We

also used a Sholl analysis to compare the distribution of branch points throughout development. Interestingly, the proportion of dendritic length for each branch order was comparable across ages, suggesting there is an optimal distribution of branch points in the dendritic arbor that is maintained through development. The total number of branch points was consistent at every age, as was the number of primary dendrites. Our Sholl analysis further revealed a shift of branch points more distally with age. While P7 neurons have nearly two-thirds of their dendritic branch points within 40 μm of the soma, for P60 the proportion is below one-third. On the other hand, at P60 nearly one-sixth of branch points are found between 120 and 160 μm from the soma, a much greater proportion than at any earlier time-point. The net effect of these changes is that the critical value is found gradually farther from the soma until P28. Maturation of the dendritic arbor is dependent on the excitatory actions of GABA early in development, and loss of excitatory GABA in development severely limits dendritic arborization and complexity (Cancedda et al., 2007). We have reported that GABAergic transmission onto BLA principal neurons is excitatory at P7 but switches to inhibitory by P14, suggesting the first two postnatal weeks represent a critical period for dendrite maturation (Ehrlich et al., 2013). Furthermore, activation of $GABA_B$ receptors early in development has been shown to promote dendrite outgrowth, and we have previously demonstrated large $GABA_B$ responses in P7 and P14 BLA principal neurons that diminish by P21, when dendrite expansion ends (Bony et al., 2013; Ehrlich et al., 2013).

The developmental trajectory of dendritic arbor morphology we report here is corroborated by previous studies in the BLA and developmental studies of pyramidal neurons in other brain regions. A previous study of BLA principal neurons in adult rats found a comparable spatial distribution of dendrites to our P60 time-point using a traditional Sholl analysis (Yajeya et al., 1997). A morphological analysis of developing layer V pyramidal neurons in somatosensory cortex by Romand and colleagues revealed a very similar growth pattern in the distribution of dendritic material, although their Sholl curves were notably broader, likely due to larger aggregate dendritic lengths (2011). Stereological studies in the rat have also shown an increase in

the volume of the rat BLA between P7 and P21, consistent with an expansion of dendritic arbors of BLA neurons during this period (Chareyron et al., 2012). Furthermore, a Golgi-Cox study of developing BLA neurons, which reported the area encompassed by the dendritic arbor, found a similar expansion during the first few postnatal weeks, albeit with substantially smaller arbors (Escobar and Salas, 1993). Notably, previous Golgi-Cox studies of adult BLA neurons have estimated the aggregate dendritic length between 300 and 2000 μm (Tosevski et al., 2002; Johnson et al., 2009; Pillai et al., 2012; Torres-Garcia et al., 2012), which differs greatly from our measurement of ~6,400 microns at P60. We argue that the Golgi-Cox technique provides underestimates of dendritic length, possibly by selectively sampling smaller neurons or staining only proximal dendritic segments. However, it is possible we are overestimating the dendritic length due to bias in the visual selection of neurons for patch clamp.

The growth of the dendritic arbor in both quantity and complexity has substantial implications for neuronal physiology, particularly passive electrical properties. The increase in neuronal surface area across the first postnatal month undoubtedly contributes to the concurrent, nearly ten-fold decrease in input resistance and three-fold decrease in membrane time constant we previously reported in this cell population (Ehrlich et al., 2012). Furthermore, multi-compartment modeling has revealed that expansion of the dendritic arbor can promote the expression of doublets of action potentials, driven by depolarization of the soma due to a dendritic spike (Mainen and Sejnowski, 1996). In our hands, the expansion of the dendritic arbor of BLA principal neurons during the first postnatal month reported here does in fact correspond with the emergence of doublets (Ehrlich et al., 2012). In addition, expansion of the dendritic arbor has the potential to effectively increase the diversity of presynaptic partners or sensory modalities of input for a BLA principal neuron, due to the topographical organization of sensory input to the BLA (McDonald, 1998). Interestingly, these inputs also undergo developmental change; tract tracing studies have demonstrated thalamic afferents are present in the BLA at P7 and remain relatively unchanged with age, while cortical afferents continue to mature throughout the first

postnatal month (Bouwmeester et al., 2002b). It will be critical for future studies to address the sensitivity of this developmental trajectory to experience, considering the well documented effects of stressors on the dendritic arborization of principal neurons in the adult BLA (Roozendaal et al., 2009; Padival et al., 2013) and in the case of autism spectrum disorders and Fragile X syndrome (Kaufmann and Moser, 2000; Beckel-Mitchener and Greenough, 2004; Puram et al., 2011).

3.5.3 Dendritic Spine Emergence

As the dendritic arbor expands throughout the first postnatal month, BLA principal neurons come to express many more dendritic spines. We observed a progressive increase in the density of dendritic spines between P7 and P28, by which time spines are as dense as in adulthood (~1.2 spines/µm at P60). Comparable studies examining the development of dendritic spines in other brain regions have reported similar spine densities and developmental trajectories. For example, the spine density of layer V neurons in somatosensory cortex stabilizes around P21 at ~0.6 spines/µm (Romand et al., 2011). Previous measurements of spine density in the BLA have yielded values slightly lower than ours, ~0.7 spines/µm in late-adolescence (Torres-Garcia et al., 2012). This discrepancy may be because this study utilized the Golgi-Cox staining method, which, as discussed above, may be biased towards proximal dendrites.

Interestingly, previous studies of synapse formation in the developing BLA, measured by synaptophysin staining, show the number of presynaptic terminals reaches a peak at P14 (Morys et al., 1998), while our data show that dendritic spines reach about half their mature density at this age. Although synaptophysin is not specific for afferents of principal neurons or those targeting dendritic spines, this mismatch in synaptophysin and spine development suggests during the first few postnatal weeks glutamatergic presynaptic terminals may form synapses with dendritic shafts or release transmitter without direct synaptic contact. The emergence of dendritic spines corresponds with the age when glutamate removal from synapses switches from primarily

diffusion-based to uptake-dependent (Thomas et al., 2011). The early peak of synaptophysin expression may indicate an increase in glutamatergic transmission that could trigger the outgrowth of dendritic spines (Calabrese et al., 2006). In support of this notion, tract-tracing studies have shown that putative glutamatergic inputs to the BLA mature between P7 and P13 (Bouwmeester et al., 2002b) and stabilize by P25, before undergoing pruning in late adolescence (Cressman et al., 2010). Dopaminergic and noradrenergic inputs to the BLA, which largely target spine shafts and heads on distal dendrites (Muller et al., 2009; Muly et al., 2009; Zhang et al., 2013), become more dense between P14 and P20 (Brummelte and Teuchert-Noodt, 2006). Our own previous work demonstrates the presence of stimulation-evoked and spontaneous glutamatergic transmission onto BLA principal neurons as early as P7 (Ehrlich et al., 2013), when very few spines are present.

The emergence of dendritic spines in BLA principal neurons has numerous potential implications for neurotransmission in the amygdala. Glutamatergic afferents to the BLA are thought to provide representations for sensory stimuli that are critical to amygdala function, including noxious and neutral stimuli that undergo plasticity during associative fear learning (Rodrigues et al., 2004; Maren, 2005; Pape and Pare, 2010). Dendritic spines provide a means of compartmentalization of biochemical and electrical signals related to neurotransmission (Shepherd, 1996; Lee et al., 2012), meaning the lack of spines early in development should impact the specificity of synaptic plasticity. Coincidentally, during the same window when spines emerge and reach mature numbers, there is increased abundance in BLA synaptic terminals of zinc, which promotes long-term potentiation of glutamategic synapses in the BLA (Mizukawa et al., 1989; Li et al., 2011). Interestingly, juvenile mice exhibit generalization of conditioned fear, which could be related to poor specificity of synaptic plasticity (Ito et al., 2009). During infancy, rats also exhibit deficits to fear learning, and many forms of associative emotional learning emerge during the first few postnatal weeks (for review, see King et al., 2013). Perhaps most interesting is the observation that the amygdala is activated by odor-shock pairing after but not

before P10, corresponding with the emergence of aversive conditioning and a change in amygdala synaptic plasticity (Sullivan et al., 2000; Thompson et al., 2008), precisely when dendritic spines begin to emerge.

3.5.4 Voltage-gated Ion Channel Expression

In addition to the morphological changes we observed throughout development, we found a variety of changes in the expression of ion channel subtype mRNA transcripts in BLA principal neurons. These channels are distributed throughout the neuronal membrane and impact the electrophysiological function of BLA principal neurons. Using single-cell RT-PCR of patch clamped neurons at each time point, we found transitions in the expressed subtypes expressed of all the ion channels tested: HCN, K_{IR}, K_V, and Ca_V. The subtype changes, discussed individually below, correspond with and in many cases are corroborative of the maturation of membrane currents in these neurons. Further experiments will be required to determine whether quantitative changes are found for expression of mRNA for these ion channel subtypes and whether these translate to changes in protein and the function of ion channels using pharmacological manipulations. In addition, because we assessed gene expression on a binary scale and the technique has high potential for false negatives, we interpret these results as indications of trends in expression levels.

HCN channels mediate the H-current, a hyperpolarization-activated, nonselective cation current (Pena et al., 2006). We have shown a developmental shift in the expression of mRNA for HCN channel subtypes in BLA principal neurons from HCN4 to HCN1. Specifically, HCN4 mRNA was detected only at time-points before P28, while HCN1 mRNA emerged at P28. HCN4 has much slower kinetics and is classically expressed early in development, while HCN1 exhibits the fastest kinetics of the 4 subtypes and has stronger expression in the mature brain (Monteggia et al., 2000; Vasilyev and Barish, 2002; Surges et al., 2006; Bender and Baram, 2008; Kanyshkova et al., 2009). The shift in expression from HCN4 to HCN1 in BLA principal neurons

corresponds with the activation time-constant of I_H in these neurons (Ehrlich et al., 2012). The transition in I_h kinetics does not occur sharply between P21 and P28, as the expression of HCN4 and 1 mRNA would suggest, possibly due to contributions of HCN2 and HCN3 or more gradual changes in protein expression compared to mRNA. Future studies should address quantitative changes in HCN subtype mRNA expression, which the present study failed to capture.

The changes we observed in HCN transcript expression are likely to impact the function of principal neurons in the maturing BLA. I_h is known to contribute to input resistance at rest (Surges et al., 2004), oscillatory properties of neurons including resonance (Hutcheon et al., 1996a; Hu et al., 2002; Marcelin et al., 2012), and synaptic integration in dendrites (Atkinson and Williams, 2009). Interestingly, the first postnatal month also includes a dramatic shift in the intrinsic resonance frequency of BLA principal neurons towards higher frequencies that could engage HCN channels with faster kinetics (Ehrlich et al., 2012). Resonance to higher frequencies can also be promoted by a reduction of input resistance, which is likely promoted by the expansion of the dendritic arbor and increase in soma volume across the first postnatal month. HCN1 and 2 have been found in distal dendrites of adult pyramidal neurons (Notomi and Shigemoto, 2004), and HCN1 channels have been shown to impact synaptic transmission and plasticity in distal dendrites (Nolan et al., 2004). Interestingly, the expression of this subtype is lacking when dendrites are shorter early in development.

The $K_{IR}2$ subfamily of inwardly rectifying potassium channels also pass current at voltages hyperpolarized to rest. Consistent with previous observation (Hibino et al., 2010), expression of these channel subunits, which form homo- and hetero-tetramers, was limited to $K_{IR}2.1$ and 2.3 in BLA principal neurons. $K_{IR}2.3$ mRNA expression was absent at P7, but otherwise $K_{IR}2.1$ and 2.3 were expressed throughout postnatal development. In addition to their role regulating resting membrane potential and excitability of neurons (Isomoto et al., 1997; Hibino et al., 2010), $K_{IR}2.1$ and 2.3 are also found localized to the postsynaptic density in dendritic spines through an interaction with the scaffolding protein, PSD-95, where they regulate

local resting membrane potential (Inanobe et al., 2002). This interaction seems likely to occur in the amygdala, considering the concomitant emergence of K_V2.3 mRNA and dendritic spines. Notably, K_V2.3 becomes dissociated from PSD-95 following phosphorylation by protein kinase A (Cohen et al., 1996), which is activated in the BLA during stimulus-induced synaptic plasticity and may provide a mechanism for disinhibition of spines.

Similarly, the subunits for the tetrameric potassium channel mediating the A-type current also exhibited a distinct developmental trajectory. K_V1.4 subunit mRNA was detected in BLA principal neurons at P7 and 14, but was lost by P21, whereas K_V3.4 had an opposite profile of expression, only emerging at P21. Conversely, no significant change in mRNA expression was observed for K_V4.1, 4.2, and 4.3 transcripts at any time-point. In the adult BLA, a previous *in situ* hybridization study reported stronger expression of mRNA transcripts for K_V4.3 than 4.1 or 4.2 (Serodio and Rudy, 1998), but the study did not examine the expression profile across development. However, protein expression of K_V4 subunits has been shown to increase in the BLA gradually with age until P30, then increase drastically by P60, suggesting development of these channels may continue beyond the window studied here (Vacher et al., 2006). Similarly, in pyramidal neurons of rat somatosensory cortex, protein expression of K_V4.1, 4.2, and 4.3 increases across the first postnatal month as A-type potassium current increases in amplitude (Guan et al., 2011). While our results would predict a decrease in the contribution of K_V1.4 to the A-current in BLA principal neurons with age, Guan and colleagues reported this subunit contributes proportionally to the A-current throughout the first postnatal month.

The loss of K_V1.4 and emergence of K_V3.4 during the first postnatal month should impact the electrical properties of these neurons, considering the functional differences of the two channels. Specifically, K_V3.4 has more depolarized activation and inactivation curves than K_V1.4 (Chandy et al., 2012b, a), suggesting more mature BLA principal neurons would be less likely to activate A-current at voltages below action potential threshold, which hyperpolarizes with age (Ehrlich et al., 2012). In addition, K_V3.4 inactivates nearly five times faster than K_V1.4 (Chandy

et al., 2012b, a), which would potentially contribute to the faster action potential repolarization, larger spike after-hyperpolarization, and higher frequency action potential trains observed later in the first postnatal month (Ehrlich et al., 2012). Interestingly, $K_V1.4$ is targeted to axons in central neurons, suggesting the loss of this subunit with age may preferentially affect axon function or synaptic transmission (Sheng et al., 1992).

Classically opposed to the A-current is the calcium-mediated T-current, a low-voltage-activated current that is conducted by the Ca_V3 family of ion channels (Pape et al., 1994; Molineux et al., 2005; Hammack et al., 2007). Here we report a developmental shift in the Ca_V3 channel subunit composition, with mRNA transcripts for $Ca_V3.1$ expressed in almost all BLA principal neurons at P7 and P14. By P21, however, few neurons expressed mRNA transcripts for this subunit, and neurons began to express transcripts for $Ca_V3.2$. In situ hybridization studies in the adult rat brain show strong labeling for both transcripts in the BLA, as well as for $Ca_V3.3$ (Talley et al., 1999). Interestingly, the signal was strongest for the $Ca_V3.1$ subunit, suggesting other types of neurons in the BLA may prominently express this subunit. This discrepancy reinforces the need to assess levels of protein expression for the various subunits.

The T-current plays a variety of roles in neuronal function. Importantly, T-type calcium channels can be distributed throughout the dendritic arbor, where they contribute to dendritic calcium flux and back-propagation of action potentials (Errington et al., 2010). T-current and H-current in adult BLA principal neurons are critically involved in the generation of membrane potential oscillations that emerge during the first postnatal month (Chapters 2 and 6; Ehrlich et al., 2012; Ryan et al., 2012), and the shift from $Ca_V3.1$ to 3.2 may play a role. As mentioned above, T-type and A-type channels are classically opposed, and $Ca_V3.2$ has been shown to form a complex with $K_V4.2$ channels that allows the calcium influx from the T-current to modulate the activity of $K_V4.2$ channels (Anderson et al., 2010).

Here we have shown how the morphology and ion channel expression of BLA principal neurons mature radically across the first two postnatal months. We also discussed these changes

in the context of concurrent, substantial changes to neuronal physiology, animal behavior, and synaptic plasticity. Together, these findings clearly show that the first postnatal month of rodent development is a critical period in the development of brain regions that process emotion. However, while morphology and intrinsic electrophysiology influence neuronal function, the functional output of the amygdala, and therefore its contribution to emotional behavior, relies on synaptic transmission. Various neurotransmitters regulate the activity of BLA principal neurons and influence the maturation of neural circuits. In **Chapter 4**, we describe a number of developmental changes to the function in the BLA of GABA, a neurotransmitter that regulates amygdala excitability and the expression of fear and anxiety, and, most importantly, influences the timing of neural circuit development. Due to its role coordinating processes in brain development, changes to GABAergic transmission in the developing BLA may act upstream of the maturation of morphology and intrinsic physiology. Therefore, understanding the properties of the GABA system in the developing BLA will be necessary for understanding how early life experience can shape emotional development.

Table 3.1: PCR Primers used for single cell RT-PCR

Genes	**Accession No**.	**PCR product size (bp)**
18S rRNA	X01117	563
HCN 1	AF247450	405
HCN 2	AF247451	211
HCN 3	AF247452	335
HCN 4	AF247453	462
Ca_V 3.1	AF027984	407
Ca_V 3.2	AF290213	256
Ca_V 3.3	AF086827	556
K_V 1.4	X16002	434
K_V 3.4	X62841	676
K_V 4.1	M64226	467
K_V 4.2	S64320	265
K_V 4.3	U42975	296/386
Kir 2.1	X73052	413
Kir 2.2	NM010603	358
Kir 2.3	NM008427	204
Kir 2.4	NM45963	234
VGLUT1	NM053859	416

Figure 3.1: Soma and dendrites of BLA principal neurons grow during the first postnatal month

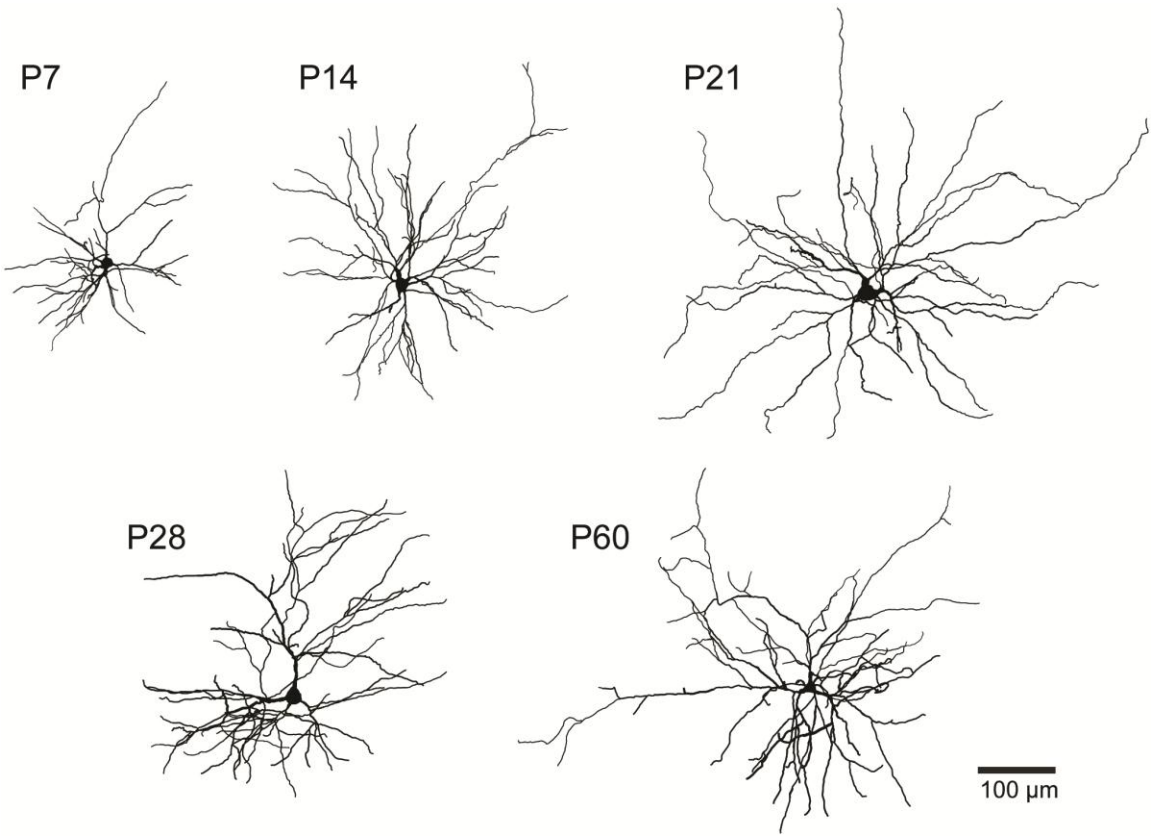

Figure 3.1: Soma and dendrites of BLA principal neurons grow during the first postnatal month. Reconstructions of representative, biocytin-filled BLA principal neurons at postnatal days 7 (P7), 14, 21, 28, and 60.

Figure 3.2: Soma size increases across the first postnatal month, then decreases in adulthood

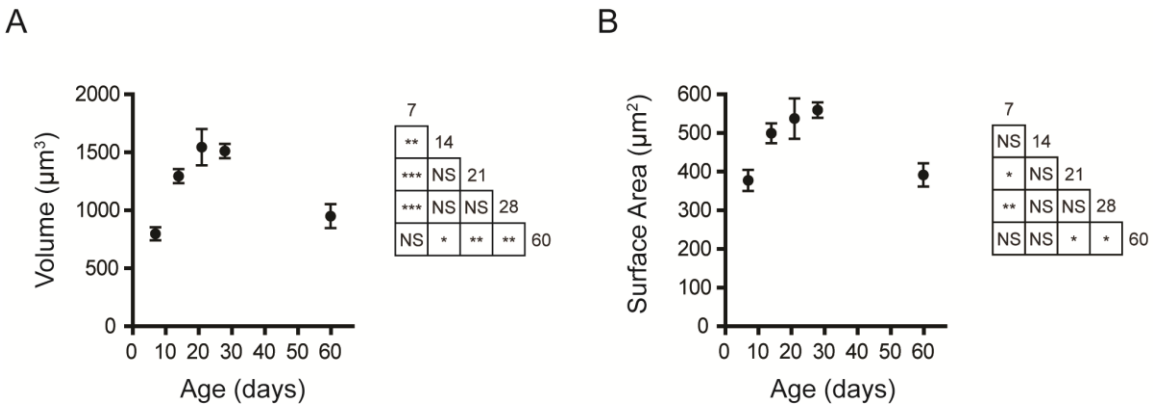

Figure 3.2: Soma size increases across the first postnatal month, then decreases in adulthood. (A, B) Soma volume (A) and surface area (B) of BLA principal neurons are depicted as mean ± SEM at postnatal days 7 (P7), 14, 21 and 28. At P7, P14, P21 and P60, n = 7; at P28, n = 6. * $P < 0.05$; ** $P < 0.01$. The results of Tukey's tests following one-way ANOVA are depicted in grids (* $P < 0.05$; ** $P < 0.01$; *** $P < 0.001$; NS: not significant).

Figure 3.3: Dendritic arbors expand with a specific pattern across postnatal development

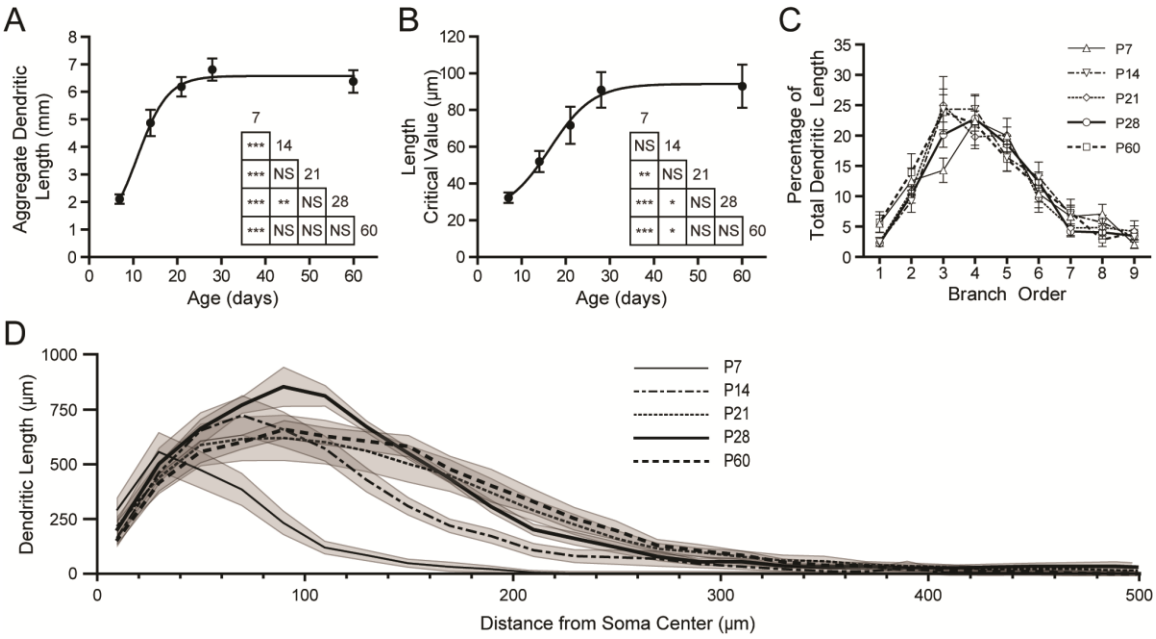

Figure 3.3: Dendritic arbors expand with a specific pattern across postnatal development. Sholl analysis was performed on reconstructed neurons with 20 μm steps between rings. (A, B) Aggregate length (A) and the critical value for length (B) of the dendritic arbor are plotted versus age as mean ± SEM, with a best-fit sigmioidal Boltzmann curve. The results of Tukey's tests following two-way ANOVA are depicted in inset grids (* $P < 0.05$; ** $P < 0.01$; *** $P < 0.001$; NS: not significant; n = 8 per time-point). (C) Percentage of total dendritic length found in branches of a given order is plotted as mean ± SEM for each age (n = 8 neurons per age). (D) The profile of dendritic length derived from the Sholl analysis is plotted as mean (black line) and SEM (grey band) versus distance from the center of the soma, illustrating the expansion and pruning of the dendritic arbor with age (n = 8).

Figure 3.4: Dendritic branch points become more distant from the soma during postnatal development

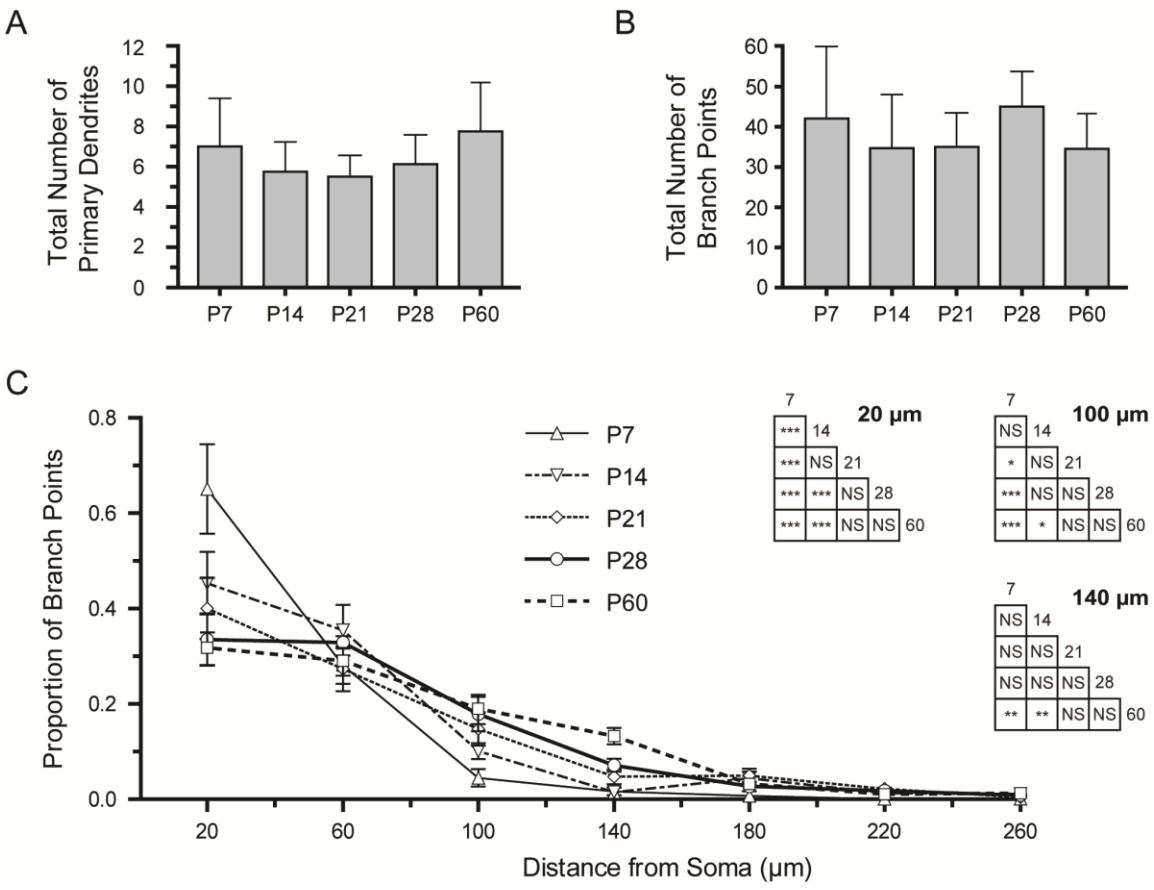

Figure 3.4: Dendritic branch points become more distant from the soma during postnatal development. (A, B) Bar graphs illustrate the mean ± SD of the total number of primary dendrites (A) and branch points (B) for BLA principal neurons at each time-point (n = 8). (C) The proximity of branch points to the soma was derived from Sholl analyses on reconstructed neurons with 40 µm thick rings, and the proportion of total branch points found in each ring is plotted as mean ± SEM (n = 8). The results of Tukey's tests following two-way ANOVA are depicted in inset grids for Sholl rings with significant effects of age, namely those centered at 20, 100, and 140 µm from the soma (* $P < 0.05$; ** $P < 0.01$; *** $P < 0.001$; NS: not significant).

Figure 3.5: Dendritic spines emerge the first month of postnatal development in BLA principal neurons

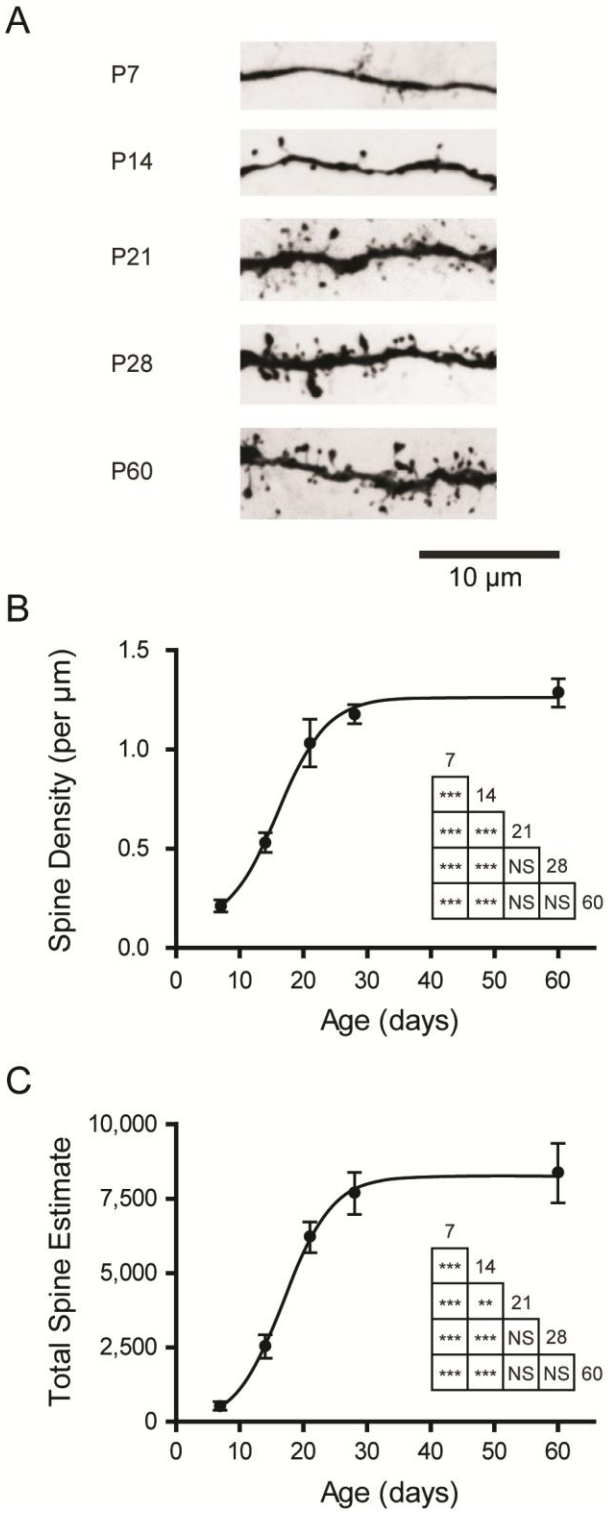

Figure 3.5: Dendritic spines emerge the first month of postnatal development in BLA principal neurons. (A) Representative photomicrographs of segments of dendrites from filled BLA principal neurons at each time-point. (B,C) Dendritic spine density and the estimated total number of spines are plotted as mean ± SEM for neurons at each time-point (n = 6). The results of Tukey's tests following one-way ANOVA are depicted in inset grids (* $P < 0.05$; ** $P < 0.01$; *** $P < 0.001$; NS: not significant).

Figure 3.6: Ion channel transcript expression in individual BLA principal neurons matures across the first postnatal month

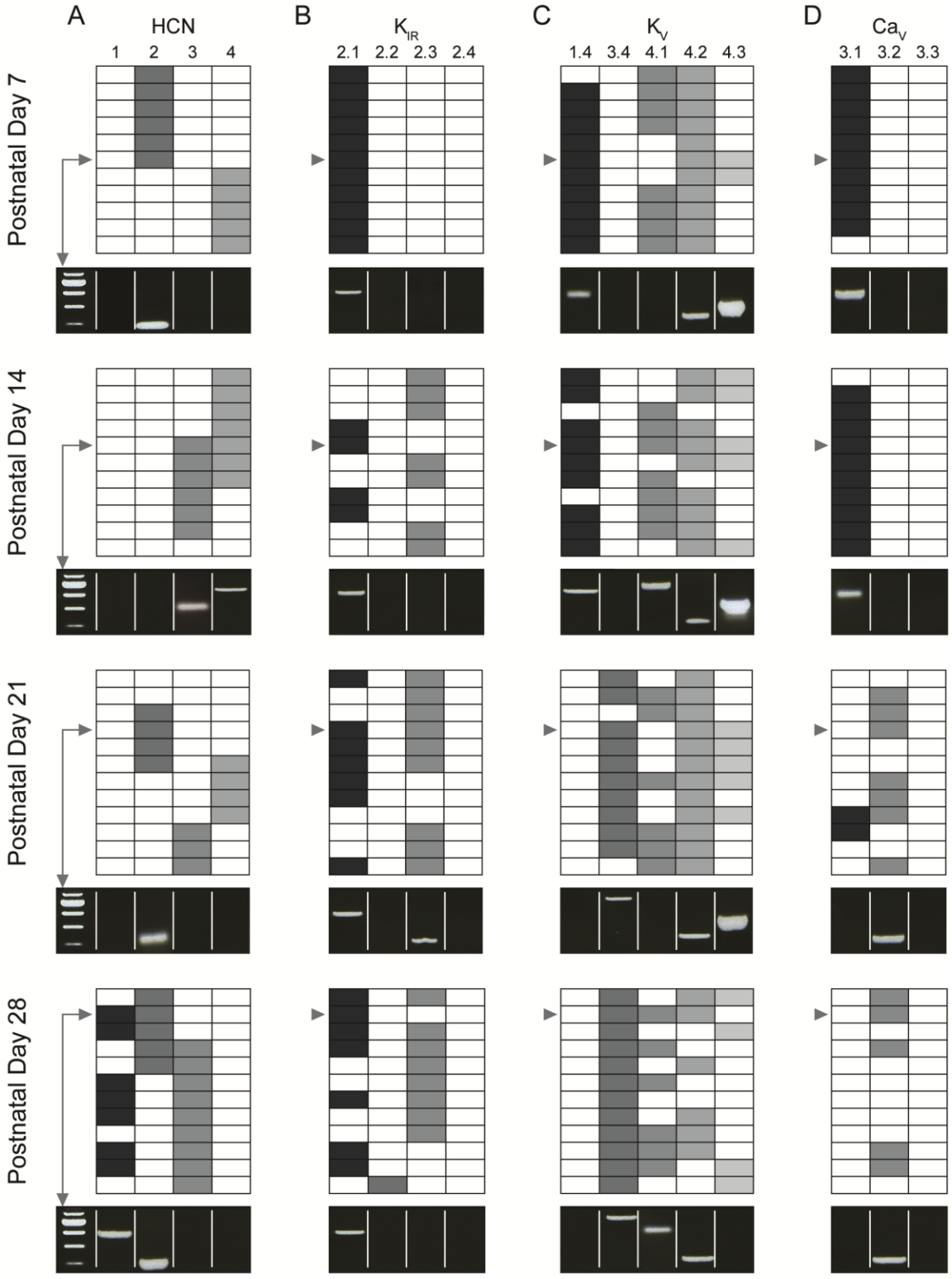

Figure 3.6: Ion channel transcript expression in individual BLA principal neurons matures across the first postnatal month. Single-cell RT-PCR results for BLA principal neurons are depicted for 11 to 12 neurons at each time-point, with filled blocks signifying detectable expression for a given transcript. The results for all genes from a single neuron are depicted in a single row, with varying shades of grey for contrast. Representative gel images are included at each age to illustrate the expression profile of a single neuron, indicated with a grey arrow.

Chapter 4: Postnatal maturation of GABAergic transmission in the rat basolateral amygdala[3]

[3]Adapted from: Ehrlich DE, Ryan SJ, Hazra R, Guo JD, Rainnie DG (2013). *Postnatal maturation of GABAergic transmission in the rat basolateral amygdala*. J Neurophysiol 110(4): 926-41.

4.1 Abstract

Many psychiatric disorders, including anxiety and autism spectrum disorders, have early ages of onset and high incidence in juveniles. To better treat and prevent these disorders, it is important to first understand normal development of brain circuits that process emotion. Healthy and maladaptive emotional processing involve the basolateral amygdala (BLA), dysfunction of which has been implicated in numerous psychiatric disorders. Normal function of the adult BLA relies on a fine balance of glutamatergic excitation and GABAergic inhibition. Elsewhere in the brain GABAergic transmission changes throughout development, but little is known about the maturation of GABAergic transmission in the BLA. Here we used whole cell patch-clamp recording and single-cell RT-PCR to study GABAergic transmission in rat BLA principal neurons at postnatal day (P)7, P14, P21, P28, and P35. $GABA_A$ currents exhibited a significant twofold reduction in rise time and nearly 25% reduction in decay time constant between P7 and P28. This corresponded with a shift in expression of $GABA_A$ receptor subunit mRNA from the α2- to the α1-subunit. The reversal potential for $GABA_A$ receptors transitioned from depolarizing to hyperpolarizing with age, from around −55 mV at P7 to −70 mV by P21. There was a corresponding shift in expression of opposing chloride pumps that influence the reversal, from NKCC1 to KCC2. Finally, we observed short-term depression of $GABA_A$ postsynaptic currents in immature neurons that was significantly and gradually abolished by P28. These findings reveal that in the developing BLA GABAergic transmission is highly dynamic, reaching maturity at the end of the first postnatal month.

4.2 Introduction

There is a critical need to characterize the developmental trajectory of the BLA and brain circuits that process emotion. Previously we have shown that the electrophysiological and morphological properties of neurons in the BLA change dramatically over the first postnatal month {Chapters 2 and 3`; \Ehrlich, 2012 #1297}. Here we focused on inhibitory synaptic transmission, which has been shown to be developmentally regulated (Ben-Ari et al., 2012; Kilb, 2012) and implicated in the pathophysiology of neurodevelopmental disorders (Chattopadhyaya and Cristo, 2012; King et al., 2013).

Inhibitory synaptic transmission has been well characterized in the mature BLA (Rainnie et al., 1991a; Washburn and Moises, 1992; Martina et al., 2001), playing a fundamental role in determining the excitability of the region and thereby regulating emotional behavior (Quirk and Gehlert, 2003; Shekhar et al., 2003; Ehrlich et al., 2009). Synaptic inhibition in the BLA is produced by intrinsic and extrinsic afferents activating local-circuit interneurons; these inhibitory neurons then release the neurotransmitter γ-aminobutyric acid (GABA) onto principal neurons, which comprise 80–85% of the BLA neuronal population (McDonald, 1985, 1996). Blocking $GABA_A$ receptors in the BLA promotes fearful and anxious behaviors (for review, see Quirk and Gehlert, 2003), whereas enhancing GABA function attenuates these behaviors (Davis et al., 1994; Sanders and Shekhar, 1995). GABAergic transmission in the BLA can also organize network activity; rhythmic inhibition of BLA principal neurons by burst-firing, parvalbumin-expressing interneurons can coordinate and synchronize firing of the principal neurons and may underlie network oscillations in the BLA related to fear (Chapter 6; Ryan et al., 2012).

In addition to regulating neuronal activity in the adult brain, $GABA_A$ receptors undergo functional maturation and serve to coordinate brain development. One well-established trigger for the onset of "critical periods," or developmental windows of high plasticity, is activity at $GABA_A$ receptors (Hensch, 2005). This action depends on the subunit composition of

$GABA_A$ receptors, which are comprised of five subunits and typically contain two α-, two β-, and one γ-subunit. There are six known α-subunits, and the relative expression of these subunits changes throughout development. The α-subunits influence the kinetics, localization, and drug sensitivity of $GABA_A$ receptors (Nusser et al., 1996; Hevers and Luddens, 2002). As the brain develops, expression shifts from high levels of the α2-subunit toward the α1-subunit, which confers faster kinetics (Hornung and Fritschy, 1996; Dunning et al., 1999; Davis et al., 2000; Bosman et al., 2002; Mohler et al., 2004; Eyre et al., 2012).

$GABA_A$ receptor function in the brain changes in another fundamental way, switching from excitatory at birth to inhibitory in adulthood (for review, see Ben-Ari et al., 2012). This switch is believed to result from developmental changes to the concentration gradient of chloride, the ion mediating $GABA_A$ currents. At birth, there is greater expression of sodium-potassium-chloride cotransporter 1 (NKCC1), which accumulates intracellular chloride and renders $GABA_A$ receptors excitatory. In adulthood, potassium-chloride cotransporter 2 (KCC2) is expressed more highly, extruding chloride from the cell and rendering $GABA_A$ receptors inhibitory (Ben-Ari et al., 2012). Excitatory GABA early in development is thought to promote calcium influx and modulate neuronal growth and synapse formation (Ben-Ari et al., 1997).

Aside from the precedent for GABAergic maturation observed elsewhere in the brain, there are good reasons to expect that similar changes occur in the developing BLA. For example, we recently showed that the electrophysiological properties of BLA principal neurons mature rapidly from postnatal day (P)7 to P21, including a 10-fold reduction in input resistance and a 3-fold reduction in membrane time constant, suggesting that the sensitivity to synaptic inhibition would also vary greatly (Ehrlich et al., 2012). There are also concurrent changes in the expression and connectivity of GABAergic interneurons in the BLA, including the emergence and maturation of parvalbumin-expressing interneurons between P14 and P30 (Berdel and Morys, 2000; Davila et al., 2008). Between P14 and P20, there is a significant increase in the density of GABAergic fibers and a decrease in the density of GABAergic cell bodies in the BLA

(Brummelte et al., 2007). Further evidence comes from the development of behaviors related to BLA function. There is a switch from paradoxical approach to an aversively conditioned stimulus to the mature, avoidance behavior at P10, corresponding with a change in synaptic plasticity that is reversed by $GABA_A$ blockade (Sullivan et al., 2000; Thompson et al., 2008). In addition, rats exhibit suppression of fear learned at P18 but not P23, a phenomenon called infantile amnesia that is $GABA_A$ receptor dependent (Kim et al., 2006b). The mechanisms of fear extinction also change in this window, becoming amygdala- and GABA dependent between P17 and P24 (Kim and Richardson, 2008). There are several additional examples of rapid, developmental changes to the expression and underlying physiology of fear learning (Campbell and Ampuero, 1985; Moye and Rudy, 1987; Hunt et al., 1994; Tang et al., 2007).

Despite the variety of documented changes to the BLA circuit and emotional behavior across the first postnatal month, and the critical role that synaptic inhibition plays in the function of the adult amygdala, no study to date has examined the developmental profile of GABAergic transmission in the immature BLA. To address this knowledge gap, we have used a combination of patch-clamp electrophysiology and single-cell reverse transcription-polymerase chain reaction (RT-PCR) to characterize the properties of synaptic inhibition of BLA principal neurons across the first postnatal month. Here we outline significant changes in terms of the kinetics, reversal potential, and short-term synaptic plasticity (STP) of $GABA_A$ receptor activation as well as underlying changes in gene expression. In this study we characterized normative amygdala development to enable future studies to address the contribution of the amygdala to both healthy and maladaptive emotional development.

4.3 Methods

4.3.1 Ethical approval.

All experimental protocols strictly conform to the National Institutes of Health *Guide for the Care and Use of Laboratory Animals* and were approved by the Institutional Animal Care and Use Committee of Emory University.

4.3.2 Animals.

Rats born in-house to time-mated female Sprague-Dawley rats (Charles River, Wilmington, MA) were used in all experiments. Pups were housed with the dam prior to weaning on P22 or P23 (considering P1 as day of birth). After weaning, rats were isolated by sex and housed three to four per cage with access to food and water ad libitum. Animals were killed for electrophysiological recordings at P7–10, P13–15, P20–22, P27–29, and P33–36, and for brevity these windows are described as single time points. To maximize the use of animals, experiments on $GABA_A$ reversal and for single-cell RT-PCR included data from the offspring of dams used as negative control subjects for other studies. In these cases, data were grouped because there was no observable difference in standard-raised animals and those born from dams receiving either manipulation.

4.3.3 Slice preparation.

Slices containing the BLA were obtained as previously described (Rainnie, 1999b). Briefly, animals were decapitated under isoflurane anesthesia (Fisher Scientific, Hanover Park, IL) if older than P11, and the brains were rapidly removed and immersed in ice-cold 95% oxygen-5% carbon dioxide-perfused "cutting solution" with the following composition (in mM): 130 NaCl, 30 $NaHCO_3$, 3.50 KCl, 1.10 KH_2PO_4, 6.0 $MgCl_2$, 1.0 $CaCl_2$, 10 glucose, 0.4 ascorbate, 0.8 thiourea, 2.0 sodium pyruvate, and 2.0 kynurenic acid. Coronal slices containing the BLA

were cut at a thickness of 300–350 μm with a Leica VTS-1000 vibrating blade microtome (Leica Microsystems, Bannockburn, IL). Slices were kept in oxygenated cutting solution at 32°C for 1 h before transfer to regular artificial cerebrospinal fluid (ACSF) containing (in mM) 130 NaCl, 30 $NaHCO_3$, 3.50 KCl, 1.10 KH_2PO_4, 1.30 $MgCl_2$, 2.50 $CaCl_2$, 10 glucose, 0.4 ascorbate, 0.8 thiourea, and 2.0 sodium pyruvate.

4.3.4 Whole-cell patch clamp.

Individual slices were transferred to a recording chamber mounted on the fixed stage of a Leica DMLFS microscope (Leica Microsystems) and maintained fully submerged and continuously perfused with oxygenated 32°C ACSF at a flow rate of 1–2 ml/min. The BLA was identified under ×10 magnification. Individual BLA neurons were identified at ×40 with differential interference contrast optics and infrared illumination with an infrared-sensitive CCD camera (Orca ER, Hamamatsu, Tokyo, Japan). Patch pipettes were pulled from borosilicate glass and had a resistance of 4–6 MΩ. We used two patch electrode solutions, one based on potassium gluconate for current-clamp recordings and one based on cesium gluconate for voltage-clamp recordings. The potassium gluconate patch solution had the following composition (in mM): 140 potassium gluconate, 2 KCl, 10 HEPES, 3 $MgCl_2$, 2 K-ATP, 0.2 Na-GTP, and 5 phosphocreatine, was titrated to pH 7.3 with KOH, and was 290 mosM. The cesium gluconate patch solution had the following composition (in mM): 131 CsOH, 131 gluconate, 10 HEPES, 2 $CaCl_2$, 10 glucose, 10 EGTA, 5 Mg-ATP, and 0.4 Na-GTP, was titrated to pH 7.3 with gluconate, and was 270 mosM. To visualize the recording sites of some neurons, 0.35% biocytin (Sigma-Aldrich, St. Louis, MO) was added to the patch solution and tissue was stained as previously described (Rainnie et al., 2006) and imaged at ×5 magnification on a Leica DM5500B microscope (Leica Microsystems) equipped with a CSU10B Spinning Disk (Yokagawa Electronic, Tokyo, Japan).

Data acquisition was performed with a MultiClamp 700A or Axopatch 1D amplifier in conjunction with pCLAMP 10.2 software and a DigiData 1322A AD/DA interface (Molecular

Devices, Sunnyvale, CA). Whole cell patch-clamp recordings were obtained, low-pass filtered at 2 kHz, and digitized at 10 kHz. Cells were excluded if they did not meet the following criteria: a resting membrane potential more negative than −55 mV and drifting <5 mV over the course of the recording session; access resistance lower than 30 MΩ; stable access resistance throughout recording, changing <15%; and action potentials crossing 0 mV. Recordings were only included from BLA principal neurons, which can be distinguished from BLA interneurons for electrophysiological recordings by a combination of their large somatic volume, low input resistance, slow action potentials, and relatively low synaptic input (Rainnie et al., 1993). Furthermore, we previously reported that 58 of 60 putative principal neurons recorded in the immature BLA were found positive for mRNA for the vesicular glutamate transporter by single-cell RT-PCR (Ehrlich et al., 2012).

4.3.5 Spontaneous inhibitory postsynaptic currents.

To quantify changes in the kinetics of $GABA_A$ inhibitory postsynaptic currents (IPSCs) in developing BLA principal neurons, spontaneous IPSCs were measured from 30-s-long recordings in voltage-clamp mode with a cesium gluconate-based patch solution. Outward synaptic currents were measured at −50 mV, unless discernible outward currents were observed at −60 mV. Neurons were only included in this analysis if their outward synaptic currents exhibited a reversal potential below −50 mV. Synaptic currents were selected by hand by a blinded experimenter from traces low-pass filtered at 500 Hz, and kinetics were analyzed off-line with Mini Analysis 6.0.3 (Synaptosoft, Decatur, GA). Event detection parameters were as follows: time before a peak for baseline (7.5 ms), period to search a decay time (50 ms), fraction of peak to find a decay time (0.368), and period to average a baseline (5 ms). Ten to ninety percent rise time and decay time constant were measured automatically based on the detected baseline and peak, using the time to reach 0.1 and 0.9 of the peak on the rising phase and 0.368 of the peak on the falling phase. An individual IPSC was excluded from analysis if its detected rise time was

longer than its decay time, and a neuron was excluded if it had fewer than five IPSCs for analysis. For illustration, IPSC waveforms were temporally aligned by rise time in MiniAnalysis and then smoothed with a sliding window of 2-ms width and averaged with MATLAB (The MathWorks, Natick, MA).

4.3.6 Stimulation-evoked postsynaptic potentials and currents.

To measure the duration of the network response and the reversal potential and STP of $GABA_A$ receptor-mediated events in BLA principal neurons, a bipolar stimulating electrode was placed in the dorsal end of the BLA, just medial to the external capsule (**Figure 4.1**). The initial, half-maximal response was recorded in current clamp when using potassium-based patch solution and voltage clamp when using cesium-based patch solution. Durations of the voltage-clamp responses were measured with Clampfit 10.2 (Molecular Devices) by an experimenter blind to postnatal age, from the stimulation artifact to the return to resting membrane potential, and the duration was averaged for the responses at −50, −60, and −70 mV.

To isolate from the initial response monosynaptic $GABA_A$ postsynaptic currents (PSCs) and potentials (PSPs), stimulation at 0.2 Hz was applied after application of a cocktail of synaptic blockers, including the AMPA/kainate receptor antagonist 6,7-dinitroquinoxaline-2,3-dione (DNQX, 20 μM; Sigma-Aldrich), the NMDA receptor antagonist 3-(2-carboxypiperazin-4-yl)propyl-1-phosphonic acid (RS-CPP, 10 μM; Tocris Bioscience, Bristol, UK), and the $GABA_B$ receptor antagonist (2*S*)-3-[[(1*S*)-1-(3,4-dichlorophenyl)ethyl]amino-2-hydroxypropyl] (phenylmethyl)phosphinic acid hydrochloride (CGP52432, 2 μM; Tocris). Placement of the stimulating electrode medial to the external capsule was often required to elicit a response in the presence of glutamatergic synaptic blockers. Stimulation intensity was adjusted to elicit a half-maximal response after application of blockers. To verify that the isolated response was purely $GABA_A$, some experiments culminated with the application of the $GABA_A$ antagonist 6-imino-3-(4-methoxyphenyl)-1(6*H*)-pyridazinebutanoic acid hydrobromide (SR95531, 5 μM; Tocris).

Reversal potential was estimated from $GABA_A$ PSPs evoked in neurons at least 15 min after patching with the potassium gluconate-based solution. Reversal potential was interpolated from stimulation responses in neurons adjusted with direct current injection to baseline recording potentials spanning the reversal, including three of the following: approximately −50, −60, −70, and −80 mV. The average response of five sweeps at each baseline potential was used for calculation with Clampfit.

To analyze STP of $GABA_A$ PSCs neurons were voltage-clamped at −50 or −60 mV, and only outward currents were used. Trains of five pulses at 10 and 20 Hz were evoked for each neuron, and five sweeps were presented at 0.1 Hz. The sweeps were averaged in Clampfit, and amplitudes were measured for each pulse from the 1 ms prior to the stimulation artifact to the absolute peak deflection. The ratios of the amplitudes of *pulse 2* and *pulse 5* to *pulse 1* were calculated at both frequencies and used for statistical analyses.

4.3.7 Picospritzer response.

The exogenous $GABA_A$ receptor agonist muscimol (Sigma-Aldrich) was focally applied to patch-clamped neurons with a picospritzer (Parker Hannifin, Cleveland, OH). After patching, the tip of a second pipette, identical to microelectrodes for patch clamping and filled with a solution of 100 μM muscimol dissolved in regular ACSF, was brought within 15 μm of the soma of the patched neuron. Five responses (0.1 Hz) to 5-ms puffs of muscimol at 5 PSI were recorded in voltage clamp at −50, −60, and −70 mV. The majority of responses were measured in the presence of bath-applied tetrodotoxin (TTX, 1 μM; Tocris), but there was no discernible difference with or without the drug, so data were pooled. Decay time constant was measured from the average response with a single-exponential fit in Clampfit. The reversal potential of the picospritzer response was estimated from the peak of the mean response at each recording voltage by interpolation. The peak conductance was calculated for, and averaged across, the response at each voltage, excluding any recordings made within 5 mV of the estimated reversal potential.

4.3.8 Single-cell and whole tissue RT-PCR.

To perform single-cell RT-PCR, at the end of the patch-clamp recording session the cell cytoplasm was aspirated into the patch recording pipette by applying gentle negative pressure under visual control. Pipettes contained ~5 μl of RNase-free patch solution. The contents of the patch pipette were expelled into a microcentrifuge tube containing 5 μl of the reverse transcription cocktail (Applied Biosystems, Foster City, CA). The reverse transcription product was amplified in triplicate and screened for 18S rRNA. Only those cell samples positive for 18S rRNA were subjected to amplification with primers. The procedure used to determine mRNA transcript expression in single cells has been described in detail previously (Hazra et al., 2011). The sequences for the oligonucleotide primers are detailed in **Table 4.1**. PCR products were visualized by staining with ethidium bromide and separated by electrophoresis in a 1% agarose gel. RT-PCR was also performed on whole BLA of P7 rats, from tissue isolated by microdissection from 300-μm-thick slices. The slices were made with the protocol for electrophysiological recording described above, and RNA isolation and RT-PCR were performed as described previously (Hazra et al., 2011).

4.3.9 Statistics.

All statistical analyses were performed with Prism 4 (GraphPad, LaJolla, CA). All tests for significant effects of age were performed with one-way ANOVAs, except for the effects of age on STP, which was tested with a two-way ANOVA with repeated measures, with the second factor being stimulation frequency. For all ANOVAs and posttests, significance was defined at $\alpha = 0.05$. To perform pairwise comparisons following significant main effects in ANOVA, Tukey's posttests were generally used. The only exception was the two-way ANOVA, which was followed by Bonferroni posttests comparing all pairs of group means. For the estimation of $GABA_A$ reversal potential, one data point in the P7 group was more than 2 standard deviations from the group mean and was therefore excluded from analysis. To perform a one-way ANOVA

on the peak conductance of IPSCs, data were log-transformed to correct for heteroscedasticity assessed with Bartlett's test.

4.4 Results

4.4.1 Compound synaptic response to local electrical stimulation.

In total, we made whole cell patch-clamp recordings from 170 BLA principal neurons from 62 rats of ages ranging from P7 to P36. We first investigated whether the response of the local BLA network to electrical stimulation changed during the first postnatal month (**Figure 4.2**). Here, we characterized the stimulation response in current clamp at three different baseline membrane potentials and found three distinct components (**Figure 4.2A**). The first, a fast excitatory component, was depolarizing at all ages and was blocked by the AMPA/kainate receptor antagonist DNQX (20 μM, data not shown). There was also a fast inhibitory response (**Figure 4.2A**, filled arrowheads) that shunted the glutamatergic component at all ages and was blocked by the specific $GABA_A$ receptor antagonist SR95531 (5 μM, data not shown). Finally, there was a second, slower inhibitory component (**Figure 4.2A**, open arrowheads) that was blocked by the specific $GABA_B$ receptor antagonist CGP52432 (2 μM, data not shown). With age, there was an apparent hyperpolarization of the reversal potential of the $GABA_A$ component and an apparent reduction of the amplitude and duration of the $GABA_B$ response. In P7 neurons, the stimulation response had a long duration, typically lasting >1 s (n = 18). By P14, the $GABA_B$ component generally had smaller amplitude and duration, lasting <1 s (n = 17). Responses were highly similar between P21 and P28, with a fast, inhibitory $GABA_A$ peak and a $GABA_B$ response that terminated within 500 ms of stimulation (n = 11 for P21, 8 for P28).

Between P7 and P28 the input resistance and membrane time constant of BLA principal neurons show 10- and 3-fold reduction, respectively (Ehrlich et al., 2012), which would dramatically alter the waveform of the evoked PSPs. Hence we next measured the properties of

evoked synaptic currents in voltage-clamp mode in another set of neurons. By blocking the $GABA_B$ component with a cesium-based patch solution, we were able to isolate the $GABA_A$ component of the evoked response (**Figure 4.2B**). Consistent with our current-clamp recordings, stimulation at holding potentials of −50, −60, and −70 mV reliably resulted in a fast excitatory PSC (EPSC) at every time point examined and a $GABA_A$ PSC that became faster with age. We measured the duration of the $GABA_A$ response, which exhibited a significant, threefold reduction across the first postnatal month (**Figure 4.2C**; 1-way ANOVA, $F_{3,60} = 5.81$, $P < 0.001$). A majority of the change occurred between P7 and P14, with a significant reduction in duration (mean ± SE) from 466.0 ± 49.1 ms at P7 ($n = 18$) to 280.9 ± 38.4 ms at P14 ($n = 17$; Tukey's posttest, $P < 0.01$). The duration was relatively stable from P14 to P21 and P28, with a value of 281.0 ± 36.6 ms at P21 ($n = 18$) and 219.6 ± 55.1 ms at P28 ($n = 11$). The stimulation response at P28 matched the biphasic response seen in adult BLA principal neurons, with a fast glutamatergic EPSC that is rapidly shunted by a GABAergic IPSC (see **Figure 4.2B**, *inset*). We hypothesized that the slow $GABA_A$ response in immature BLA neurons was due to slow individual $GABA_A$ PSCs or, alternatively, to the depolarized reversal potential of $GABA_A$ receptors removing a brake on network activity. Therefore, we next quantified the kinetics and reversal potential of isolated $GABA_A$ receptor-mediated currents in BLA principal neurons across the first postnatal month.

4.4.2 Kinetics of fast synaptic inhibition of BLA principal neurons.

To quantify changes to the kinetics of $GABA_A$ currents in BLA principal neurons we recorded spontaneous IPSCs (**Figure 4.3**). Across the first postnatal month, IPSCs became significantly faster with age until around P21 (**Figure 4.3A**). In particular, IPSC 10–90% rise time exhibited a significant decrease of more than twofold across the first postnatal month (**Figure 4.3B**; 1-way ANOVA, $F_{3,36} = 7.80$, $P < 0.001$). There was also a significant reduction across this window in the time constant of IPSC decay (**Figure 4.3C**; 1-way ANOVA, $F_{3,36} =$

3.45, $P < 0.05$) and a similar trend in IPSC half-width (**Figure 4.3D**). Specifically, spontaneous IPSCs of neurons at P7 were relatively slow, with a rise time (mean ± SE) of 2.29 ± 0.34 ms, a decay time constant of 5.76 ± 0.19 ms, and a half-width of 5.86 ± 0.59 ms ($n = 6$). By P14 rise time was reduced to 1.68 ± 0.14 ms, although decay time constant and half-width were relatively unchanged at 6.13 ± 0.43 ms and 5.70 ± 0.40 ms, respectively ($n = 16$). At P21 IPSCs were faster, with rise time reduced to 1.15 ± 0.12 ms, decay time constant reduced to 4.93 ± 0.22 ms, and half-width reduced to 4.65 ± 0.19 ms ($n= 11$). At P28 IPSCs showed kinetics similar to those at P21 and were significantly faster than at younger ages; rise time was 1.10 ± 0.12 ms (Tukey's posttests, $P < 0.001$ vs. P7 and $P < 0.01$ vs. P14), decay time constant was 4.59 ± 0.36 ms ($P < 0.05$ vs. P14), and half-width was 4.51 ± 0.42 ms (not significant; $n = 7$).

Unlike IPSC kinetics, there was no age-dependent change in the size of spontaneous IPSCs. We found no significant effect of age on peak conductance, although it tended to increase with age (**Figure 4.3E**; 1-way ANOVA, $F_{3,23} = 0.87$, $P > 0.05$; $n = 5$ or 6). At later time points there was an emergence of large IPSCs not observed at P7, but they were not frequent enough to significantly alter the mean conductance. Moreover, no significant difference was observed in the coefficient of variation of peak conductance for each neuron with age (**Figure 4.3F**; $F_{3,22} = 1.28$, $P > 0.05$; $n = 5$ or 6). There was a weak positive correlation of peak IPSC conductance and decay time constant ($R^2 < 0.2$ at each age; data not shown).

To exclude the possibility that the developmental change in IPSC kinetics was due to presynaptic effects, we also measured responses to focal application of the $GABA_A$ receptor agonist muscimol (**Figure 4.4**). As illustrated in Figure 4.4A, the tip of a pipette was placed near a patched BLA principal neuron, and 100 μM muscimol was picospritzed onto the soma. The muscimol response became much larger and faster with age, as seen in Figure 4.4, *B* and *C*. There was a significant overall effect of age on the decay time constant of the response, with a significant decrease between P14 and P21 (**Figure 4.4D**; 1-way ANOVA with Tukey's posttests, $F_{3,53} = 5.57$,$P < 0.01$). At P7, the decay time constant of the muscimol response was

407.7 ± 54.2 ms (mean ± SE, *n* = 12), which increased to 431.1 ± 34.7 ms at P14 (*n* = 16). The decay time constant then decreased significantly to 291.9 ± 20.3 ms at P21 ($P < 0.05$; *n* = 12) and 266.3 ± 24.6 ms at P28 ($P < 0.01$; *n* = 12). The inverse developmental trajectory was observed for the peak conductance of the muscimol response, which increased significantly with age and also transitioned abruptly from P14 to P21 (**Figure 4.4E**; 1-way ANOVA with Tukey's posttests, $F_{3,43} = 5.67$, $P < 0.01$). At P7 the peak conductance was 15.6 ± 4.1 nS (*n* = 10), which decreased to 13.8 ± 2.6 nS at P14 (*n* = 14). The peak conductance then increased significantly to 31.6 ± 5.5 nS at P21 ($P < 0.05$; *n* = 10) and 36.4 ± 7.1 nS at P28 ($P < 0.01$; *n* = 10).

The kinetics of $GABA_A$ receptors are influenced by their subunit composition, which is classically regulated during development. Hence we next used single-cell RT-PCR to identify developmental changes in the expression of $GABA_A$ receptor subunit mRNA in BLA principal neurons (**Figure 4.5**). There was an age-dependent increase in the proportion of neurons with detectable transcripts for 7 of the 13 $GABA_A$ receptor subunits tested: namely, α1, α2, α3 and α5, β2 and β3, and γ2 (**Figure 4.5A, B**; *n* = 10). No expression was detected for α4, α6, β1, γ3, or δ, and only one neuron at any age was found to express γ1 mRNA. There was no detectable expression of any subunit transcripts at P7; however, because rRNA for the housekeeper gene 18S was present in all cells used for this analysis, we assume this was due to limited sensitivity of the technique for low levels of transcript. As a positive control, we screened whole BLA tissue for mRNA of $GABA_A$receptor subunits (**Figure 4.5C**); as early as P7, the whole BLA contained detectable levels of mRNA for every subunit screened (*n* = 4).

Using single-cell RT PCR, we observed an increase in the expression of the α1 subunit, which confers faster IPSC kinetics, relative to that of α2, which confers slower IPSC kinetics. Specifically, while 4 of 10 neurons at P14 expressed α2 mRNA, 0 had expression for α1; by P28 the proportions for the subunits were comparable, with 4 and 6 of 10 neurons expressing α1 and α2, respectively. Interestingly, there was a strong clustering effect at P21 and P28, with the β3 subunit being expressed by 11 of 12 neurons with detectable expression of α2 but 0 of 7 with α1.

The β2- and γ2-subunits had the opposite pattern: β2 and γ2 were detected in 5 of 7 neurons with α1 expression, while 0 of 12 neurons with α2 also expressed β2 and only one expressed γ2. We address this clustering, as well as the relationship between the developmental trajectories of IPSC kinetics and subunit expression, in the Discussion.

4.4.3 Depolarized reversal potential of $GABA_A$ receptors in immature BLA principal neurons.

We next examined the effect of age on the $GABA_A$ reversal potential in BLA principal neurons (**Figure 4.6**). Here $GABA_A$ receptor-mediated inhibitory PSPs (IPSPs) were elicited with bipolar stimulation of the dorsolateral BLA in the presence of a cocktail of neurotransmitter receptor antagonists for AMPA/kainate, NMDA, and $GABA_B$ receptors (see Methods). The residual monosynaptic IPSP evoked in the presence of this cocktail was completely abolished by the $GABA_A$receptor antagonist SR95531 (5 μM, data not shown). The reversal potential of the $GABA_A$ response was estimated with peak IPSP amplitudes from stimulation at three different baseline membrane potentials. This approach corroborated our initial observations, with the $GABA_A$ reversal potential exhibiting a significant hyperpolarizing shift with age (**Figure 4.6A, B**; 1-way ANOVA, $F_{3,21} = 19.91$, $P < 0.0001$). For example, the reversal potential was significantly reduced from −54.3 ± 1.0 mV at P7 ($n = 8$) to −66.6 ± 2.3 mV at P14 (Tukey's posttests, $P < 0.001$; $n = 7$). From P14 onward, the mean reversal potential did not change significantly but became less variable across neurons, reaching −69.1 ± 2.0 mV at P21 ($n = 5$) and −69.7 ± 0.9 mV at P28 ($n = 5$). While the whole cell patch-clamp technique is not ideal for measuring $GABA_A$ reversal potentials because of dialysis of the intracellular chloride concentration (which would bias the results for every neuron, regardless of age, toward the Nernst reversal of approximately −33 mV), the observed trend of more hyperpolarizing $GABA_A$ responses with age was robust to the bias. Interestingly, despite the depolarized reversal potential of $GABA_A$receptors at P7, we were unable to elicit action potentials with these evoked,

isolated $GABA_A$ PSPs in P7 neurons, even when depolarized toward action potential threshold (n = 4, data not shown).

The reversal potential of the $GABA_A$-mediated IPSP is influenced by the intracellular concentration of chloride ions, which is tightly regulated by the activity of two selective ion pumps: NKCC1, which promotes excitatory $GABA_A$ receptor-mediated potentials, and KCC2, which facilitates an inhibitory response to $GABA_A$receptor activation. The expression of these pumps is developmentally regulated, and we were therefore interested in the developmental trajectory of chloride pump expression in BLA principal neurons. Using single-cell RT-PCR, we measured the expression at P7, P14, P21, and P28. Consistent with the depolarized reversal potential we observed in immature neurons, there was a shift in mRNA expression from NKCC1 to KCC2 between P7 and P21 (**Figure 4.6D**). Specifically, there was comparable expression of the two transcripts at P7, with 9 and 10 of 15 neurons expressing detectable levels of NKCC1 and KCC2, respectively. At P14, NKCC1 was more prominent, expressed by 17 of 20 neurons compared with only 5 of 20 with KCC2 expression. No NKCC1 transcripts were detected at P21 or P28, but the majority of neurons expressed KCC2 (21 of 23 at P21, 5 of 8 at P28).

4.4.4 Short-term plasticity of $GABA_A$ IPSCs.

The influence of GABA on BLA principal neuron activity depends not only on the amplitude, kinetics, and valence of individual synaptic events but also on the patterning and plasticity of these events. Therefore, we next characterized the development of STP of $GABA_A$ receptor-mediated synaptic transmission. Isolated $GABA_A$ receptor-mediated IPSCs were evoked, as before, in voltage-clamped neurons at P7, P14, P21, and P28 with electrical stimulation within the BLA and a cocktail of neurotransmitter antagonists. Trains of five pulses were evoked at 10 and 20 Hz, and the amplitudes of the $GABA_A$ IPSCs within each train were measured (**Figure 4.7**). At both 10- and 20-Hz stimulation, IPSCs at P7 exhibited robust short-term depression (**Figure 4.7A, B**). The depression was lost gradually with age. Because of this

gradation, we included a group of neurons at P35 to determine whether the trend reached an asymptote at P28.

To quantify the developmental changes, we used two metrics based on IPSC amplitudes: the early STP, defined as the ratio of the amplitudes of the second and first IPSCs in the train, and the late STP, defined as the ratio of the fifth and first IPSCs in the train (**Table 4.2**). For early STP, there was a significant main effect of age (2-way ANOVA with repeated measures, $F_{4,23}$ = 8.53, $P < 0.001$) but no effect of stimulation frequency (**Figure 4.7C**). All possible pairwise comparisons were made with Bonferroni posttests. For 10-Hz stimulation, early STP exhibited no significant developmental transitions. However, significant individual transitions were found for 20-Hz stimulation. Specifically, early STP for 20-Hz stimulation increased significantly from P7 to P21 ($P < 0.05$), P28 ($P < 0.001$), and P35 ($P < 0.001$). There were also significant increases from P14 to P28 ($P < 0.05$) and P35 ($P < 0.01$) and from P21 to P35 ($P < 0.01$). For both stimulation frequencies the values at P28 and P35 were highly similar, suggesting that the phenotype is stable beyond P28.

Late STP, the ratio of the fifth IPSC to the first, also exhibited robust synaptic depression in immature neurons that transitioned toward synaptic facilitation with age. A two-way ANOVA with repeated measures revealed significant main effects of age ($F_{4,23}$ = 3.709, $P < 0.05$) and stimulation frequency ($F_{1,23}$ = 14.58, $P < 0.001$) as well as a significant interaction effect ($F_{4,23}$ = 3.29, $P < 0.05$; **Figure 4.7D**). Pulse ratios for 20-Hz stimulation were generally smaller than those for 10 Hz. Late STP for 10-Hz stimulation exhibited an increase with age, although none of the individual transitions was statistically significant. For 20-Hz stimulation, late STP increased significantly from P7 to P28 ($P < 0.05$). For both stimulation frequencies, n = 3 neurons at P7, 5 at P14, 7 at P21, 6 at P28, and 7 at P35.

4.4.5 Spontaneous GABA activity is rhythmically organized throughout the first postnatal month.

Although we observed many differences in the character of GABAergic synaptic transmission with age, it is important to consider these changes in the context of normal GABA function. In slice preparations of the adult BLA, groups of principal neurons simultaneously receive rhythmic, compound synaptic events that consist mainly of $GABA_A$ receptor-mediated IPSCs but also include glutamatergic EPSCs. We have observed them not only in BLA slices from adult rats but also in rhesus macaques, where they promote intrinsic membrane potential oscillations and coordinate network activity (Chapter 6; Ryan et al., 2012). Considering the important functional role of these synaptic events, we characterized their expression during postnatal development (**Figure 4.8**). We observed rhythmic, compound IPSCs as early as P7 and at every time point studied (**Figure 4.8A, B**). As expected, the rhythmic PSCs were depolarizing from rest at P7 and became consistently hyperpolarizing by P21. The waveform changed with age, as rhythmic IPSCs at P7 were smooth while those at P28 were sharp, a cluster of many distinct release events (**Figure 4.8A**). Interestingly, the proportion of neurons receiving compound IPSCs was similar at all ages, with rhythmic events spontaneously observed in ~20–40% of neurons (6 of 14 neurons at P7, 6 of 28 at P14, 8 of 25 at P21, and 4 of 16 at P28; **Figure 4.8B**). Consistent with the mature BLA (Ryan et al., 2012), as early as P7 rhythmic IPSCs were perfectly synchronized across BLA principal neurons (**Figure 4.8C**).

4.5 Discussion

In this study, we provided the first evidence that synaptic transmission, in particular GABAergic transmission, undergoes significant change throughout BLA development. Similar to the intrinsic physiology of BLA principal neurons (Ehrlich et al., 2012), we demonstrated that inhibitory synaptic transmission reaches maturity ~3–4 wk after birth. Specifically,

$GABA_A$ receptor-mediated PSCs become faster and more hyperpolarizing and lose short-term depression with age until P21–P28, when rats are in late infancy (Quinn, 2005). In addition, these physiological changes correspond with maturation of the expression of genes that influence GABAergic function specifically in BLA principal neurons—in the case of PSC kinetics a change in $GABA_A$ receptor subunit expression and in the case of PSC reversal a shift in chloride transporter expression. Considering the critical role of GABAergic transmission in the function of BLA principal neurons and the nucleus in general, these changes likely contribute to the maturation of amygdala function throughout postnatal development.

4.5.1 Shift from depolarizing to hyperpolarizing $GABA_A$ transmission.

One of the most profound changes we observed in the developing BLA was a transition in the $GABA_A$ reversal potential. The reversal potential in principal neurons became more hyperpolarized with age, shifting from approximately −55 mV at P7 to −70 mV at P21. The magnitude and time course of this change matched those identified in cell-attached recordings of hippocampal pyramidal neurons, which exhibit a similar hyperpolarization of the $GABA_A$ reversal potential of ∼15 mV between birth and P17 (Tyzio et al., 2008). The existence of excitatory $GABA_A$ receptor-mediated potentials during brain development has been well documented (Ben-Ari, 2002; Owens and Kriegstein, 2002). In BLA principal neurons before P14, $GABA_A$ receptor activation caused depolarization, suggesting that these receptors play a different functional role early in development. Depolarizing $GABA_A$ receptors should render the BLA more excitable, which may be important for communication between the BLA and other limbic brain regions like the extended amygdala, hippocampus, and prefrontal cortex, before strong connections have been formed (Bouwmeester et al., 2002b). Despite the inability of $GABA_A$ receptor activation at P7, to drive action potential firing, GABA may be excitatory at that age through interactions with glutamatergic transmission (Gulledge and Stuart, 2003; Valeeva et al., 2010). One consequence of depolarizing $GABA_A$ receptors is that positive allosteric modulators

like barbiturates and benzodiazepines could paradoxically facilitate activation of BLA principal neurons during infancy, which could have important clinical ramifications, particularly in light of the role of the BLA as an epileptogenic locus and the incidence of infantile seizures (Racine et al., 1972; White and Price, 1993).

Depolarizing $GABA_A$ transmission likely serves an important function in normative brain development: $GABA_A$ receptors are thought to fulfill the role AMPA receptors play in the mature brain, providing sufficient postsynaptic depolarization to enable NMDA receptor activation and subsequent synaptic strengthening (Ben-Ari et al., 1997). This phenomenon likely occurs in the immature BLA when glutamate and GABA are simultaneously released during the rhythmic, compound PSCs we described here. Rhythmic, compound PSCs could serve this purpose in the BLA as early as P7, with 43% of neurons recorded at P7 receiving them. Supporting this notion, synaptic events in the immature hippocampus similar to our rhythmic PSCs, termed "giant depolarizing potentials," have been shown to promote synaptic strengthening (Mohajerani and Cherubini, 2006). This function of rhythmic PSCs is distinct from that proposed in the adult BLA, where rhythmic IPSCs promote intrinsic membrane potential oscillations and synchronize action potentials across BLA principal neurons (Chapter 6; Ryan et al., 2012). Supporting a distinct function for rhythmic PSCs in the immature and mature BLA, a much higher proportion (~80%) of BLA principal neurons receive these events in slices from adult animals (*ibid.*). Interestingly, mature oscillatory properties of BLA principal neurons are not present until around P21 (Chapter 2; Ehrlich et al., 2012), supporting convergent developmental timing of inhibitory GABA and membrane potential oscillations. In the mature BLA rhythmic IPSCs are driven by a syncytium of burst-firing parvalbumin interneurons (Rainnie et al., 2006), but parvalbumin expression does not emerge in the BLA until around P14 (Berdel and Morys, 2000); rhythmic PSCs at P7 may be driven by burst-firing interneurons that may later express parvalbumin.

A possible caveat to our measurements of reversal potential is that dialysis of the cytosol by our patch solution could alter the electrochemical gradients of ions passed by

$GABA_A$ receptors, particularly chloride. However, if dialysis had an effect, it would be to minimize differences across time points, shifting the reversal potential toward the Nernst reversal of chloride, approximately −33 mV for our patch solution and ACSF. The disparity between the observed reversals and the Nernst reversal, as well as the significant effect we found of age on $GABA_A$ reversal, suggests that the chloride concentration near $GABA_A$ receptors is locally regulated. Interestingly, there is a precedent for chloride reversal being robust to dialysis of the neuronal cytosol (Jarolimek et al., 1999; Gonzalez-Islas et al., 2009). Therefore, we are confident in our observations of a hyperpolarization of the $GABA_A$ reversal with age.

Hyperpolarization of the $GABA_A$ reversal potential with age is typically thought to result from a change in the expression of chloride pumps from NKCC1, which renders $GABA_A$ excitatory by extruding chloride, to KCC2, which renders it inhibitory by accumulating the ion intracellularly (Ben-Ari, 2002). Indeed, our single-cell RT-PCR study indicated that at P7 and P14 a high proportion of principal neurons express mRNA for NKCC1, but expression was undetectable by P21. In contrast, mRNA for KCC2 was prominent at P21 and P28. These changes in chloride pump expression are also consistent with those in other brain regions (Ben-Ari, 2002). Further experiments will be required to determine whether levels of protein expression follow suit and whether similar changes in chloride pump expression occur in BLA interneurons.

4.5.2 Development of a GABAergic shunt of the network response.

Corresponding with the emergence of inhibitory $GABA_A$ potentials was a shortening of the network response to local electrical stimulation. Specifically, in immature neurons low-frequency stimulation evoked slow, depolarizing $GABA_A$ responses and even slower, inhibitory $GABA_B$ responses resulting in a compound potential that could last between 1 and 2 s. By P21 the mature phenotype was present, in which stimulation evoked a fast, inhibitory $GABA_A$ response followed by a curtailed $GABA_B$ response, returning to baseline within 1 s (Rainnie et al., 1991a; Washburn and Moises, 1992). Although we have previously reported that

immature neurons have larger input resistances and membrane time constants (Ehrlich et al., 2012), this did not fully account for the slower synaptic potentials. Our voltage-clamp recordings also revealed a prolongation of stimulation-evoked $GABA_A$ currents in immature neurons.

The long duration of the network response in immature neurons likely results from the depolarized reversal potential of $GABA_A$ receptors. In adult BLA principal neurons, feed-forward activation of inhibitory $GABA_A$ receptors provides a fast shunt, limiting the extent of BLA activation (Rainnie et al., 1991a). As we have shown here, in immature BLA principal neurons $GABA_A$ is depolarizing, which should enable or even promote feed-forward excitation within the BLA. Without feed-forward $GABA_A$ receptor-mediated inhibition, in the immature BLA a different brake is afforded: potent activation of $GABA_B$ receptors. However, $GABA_B$ acts on a slower timescale than $GABA_A$, which would explain the long-duration network responses observed here. The strong $GABA_B$ receptor activation we found at P7 could mitigate the risk of hyperexcitability and excitotoxicity due to GABA release by opposing the depolarizing action of $GABA_A$ at this age.

$GABA_B$ receptors are thought to be localized extrasynaptically, and in adulthood they are activated when a train of stimuli releases sufficient GABA to spill over into the extrasynaptic compartment (Kim et al., 1997; Fritschy et al., 1999; Scanziani, 2000; Kulik et al., 2002; Beenhakker and Huguenard, 2010). The strong $GABA_B$ response to a single stimulation in the immature BLA suggests there is an age-dependent difference in the accessibility of GABA to $GABA_B$ receptors after stimulation. This developmental change must be interpreted in the context of the concurrent increase in input resistance, but the amplitude of $GABA_B$ relative to $GABA_A$ PSPs decreases considerably with age. This difference could be afforded by age-dependent changes in the architecture of GABAergic synapses. To support this notion, $GABA_B$ receptors in cerebellar neurons move from dendritic shafts at P7 to spines at P21 (Lujan and Shigemoto, 2006). Moreover, activation of metabotropic receptors with a single stimulation may be a general phenomenon early in development; we observed a muscarinic current that was

abolished by atropine (5 μM) and evoked by single stimulation in some neurons at P7 but not at any later time points (unpublished observation).

4.5.3 Faster IPSCs with age.

The function of GABA in the BLA also depends on the kinetics of $GABA_A$ receptor-mediated IPSCs, and we found significant developmental changes to their kinetics. Specifically, there was a nearly twofold reduction in spontaneous IPSC rise time from P7 to P21, when the mature, fast waveform was expressed. Decay time constant and IPSC half-width exhibited a similar trajectory. As with the decay time constant of spontaneous IPSCs, there was an abrupt decrease from P14 to P21 in the kinetics of the response to exogenous muscimol. Interestingly, while the peak conductance of the response to muscimol significantly increased with age, we found no age-dependent change in the peak conductance underlying spontaneous IPSCs. This effect may be due to the proximity of receptor activation to the soma, since the picospritzer pipette was placed close to the soma while IPSCs presumably originate throughout the dendritic arbor. This notion is supported by the fact that dendrites of BLA principal neurons expand greatly throughout the first postnatal month, with the total dendritic length increasing more than threefold as dendrites come to extend more than twice as far from the soma (**Chapter 3**). Furthermore, this difference may be due to a developmental change in the ratio of synaptic to extrasynaptic $GABA_A$receptors.

When considered in the context of a nearly threefold reduction in membrane time constant from P7 to P28, $GABA_A$ PSPs are likely much faster in the adult BLA (Chapter 2; Ehrlich et al., 2012). The presence of slow IPSCs early in development has been well documented throughout the brain (Draguhn and Heinemann, 1996; Hollrigel and Soltesz, 1997; Pouzat and Hestrin, 1997; Dunning et al., 1999). Comparable developmental changes were also found in the kinetics of miniature IPSCs in marmoset amygdala principal neurons, albeit on a different time course (Yamada et al., 2012). The kinetics of individual IPSCs should influence their effect on

spike timing (Pouille and Scanziani, 2001) and are known to regulate the ability of GABAergic afferents to entrain postsynaptic oscillations (Tamas et al., 2004). Furthermore, faster IPSCs should more precisely control the timing of spikes and membrane potential oscillations due to postinhibitory rebound (Ryan et al., 2012), promoting the viability of temporal coding mechanisms in the adult BLA.

The maturation of IPSC kinetics corresponds with changes to the expression of $GABA_A$ receptor subunits in BLA principal neurons. We observed an increase with age in the proportion of neurons expressing seven different $GABA_A$ subunits. The subunit mRNA we found in BLA principal neurons at P21 and P28 closely matches protein expression in the adult BLA, aside from the α4-, β1-, and δ-subunits (Sieghart and Sperk, 2002). Expression of α4, β1, and δ is likely found in other cell types. Expression of the α1-subunit, among others, emerged at P21, confirming results found with mRNA from whole BLA (Zhang et al., 1992). This change is well documented throughout the brain and is known to contribute to the faster kinetics observed with age (Hornung and Fritschy, 1996; Dunning et al., 1999; Davis et al., 2000; Okada et al., 2000; Vicini et al., 2001; Bosman et al., 2002; Mohler et al., 2004; Eyre et al., 2012). Developmental changes in subunit expression are also known to regulate channel localization and drug sensitivity (Nusser et al., 1996; Hevers and Luddens, 2002). Activation of receptors containing the $GABA_A$ receptor α1-subunit directly influence critical period onset (Huntsman et al., 1994; Fagiolini et al., 2004), suggesting that the emergence of α1 expression may trigger other aspects of emotional circuit development. Despite the apparent contribution of postsynaptic changes, identified with exogenous muscimol application, to the development of IPSC kinetics, the observed maturation of IPSC kinetics may be due, in part, to changes in the activity of different subtypes of interneurons. This notion is supported by the fact that interneurons exhibit specificity in the subunit composition of $GABA_A$ receptors to which they are apposed. For instance, in the hippocampus synapses formed by parvalbumin-expressing interneurons on pyramidal cell somas preferentially express the $GABA_A$ receptor α1-subunit (Klausberger et al., 2002). In the BLA,

parvalbumin-expressing interneurons do not emerge until P17 and reach maturity at P30 (Berdel and Morys, 2000), which corresponds with the emergence of α1 expression between P14 and P21 observed here.

We also observed clustering of subunit expression at P21 and P28, with α1-, β2-, and γ2-subunits primarily expressed in distinct neurons from α2, α3, α5, and β3. While this result was unexpected and curious considering the homogeneous population of $GABA_A$ PSCs we observed, there is some precedent for separation of α1 protein from other α-subunits (Hutcheon et al., 2004). There is an important caveat for interpreting this clustering, namely, the high rate of false negatives. Similarly, while neurons at P7 provided enough RNA to detect 18S and chloride pump expression, the lack of $GABA_A$ subunit mRNA detected is not evidence for an absolute lack of $GABA_A$ receptors. The presence of $GABA_A$ receptor-mediated PSCs and receptor subunit mRNA in whole tissue at P7 clearly refutes this, meaning that the developmental changes we see in subunit transcript expression are not concrete but indicate trends in expression levels. As with all single-cell RT-PCR results, it will be important to extend these findings by quantifying mRNA and protein expression in the developing BLA.

4.5.4 Short-term synaptic depression of $GABA_A$ IPSCs in immature BLA.

We also found distinct changes to GABAergic synaptic plasticity during development. At P7, $GABA_A$ inputs to BLA principal neurons exhibited robust early and late synaptic depression. Gradually with age the synaptic depression waned and shifted toward short-term facilitation. By P28, the amplitude of the response was maintained at the second pulse (early STP) and facilitated at the fifth (late STP). Comparable changes on a similar developmental trajectory have been observed for GABAergic and glutamatergic synapses in other brain regions (Pouzat and Hestrin, 1997; Reyes and Sakmann, 1999). For late STP, we observed facilitation at P28 that disappeared by P35; while this trend was not significant, it raises the interesting possibility of a temporary window with short-term facilitation around P28. There was also a significant effect of stimulation

frequency on late STP. Short-term depression is classically sensitive to stimulation frequency, likely because of the kinetics of depletion and restoration of releasable neurotransmitter pools (Zucker and Regehr, 2002; Elfant et al., 2008). Interestingly, for late STP there was also a significant interaction effect; the influence of stimulation frequency on STP decreased with age and may therefore be specific to short-term depression.

The developmental change in STP may be explained by several mechanisms, although the simplest involves a change in release probability—from high-release-probability, high-output GABAergic terminals in immature neurons to low release probability, low output in the mature BLA (for review, see Zucker and Regehr, 2002). High GABAergic output would be parsimonious with the robust activation of $GABA_B$receptors we observed in immature BLA principal neurons. In light of this hypothesis, future studies should address the contribution of parvalbumin expression to STP in the BLA. This calcium-binding protein directly influences STP and presynaptic calcium dynamics (Vreugdenhil et al., 2003; Collin et al., 2005), and its expression in the BLA changes during the first postnatal month (Berdel and Morys, 2000). We can rule out a contribution of presynaptic $GABA_B$ receptors to the observed short-term depression in younger animals, because CGP52432 was included in the bath during these experiments; however, presynaptic $GABA_A$ receptors can play a similar role (MacDermott et al., 1999). $GABA_A$ receptor desensitization is also known to contribute to short-term depression (Overstreet et al., 2000), although there is no precedent for a developmental change in this phenomenon. Finally, short-term depression of immature GABAergic IPSCs may involve ionic plasticity, a depolarization of the chloride reversal following strong $GABA_A$ activation (for review, see Raimondo et al., 2012). To better understand the maturation of STP we observed, future studies should differentiate the various interneuron subtypes found in the BLA, which play different roles in the network but were grouped in the population response used here.

STP affords synapses with a variety of temporal filtering mechanisms, suggesting that the BLA processes information and communicates using different mechanisms with age

(Buonomano, 2000; Fortune and Rose, 2001; Pfister et al., 2010). The role of synaptic filters in tuning the network to specific frequencies is particularly important because BLA oscillations have been implicated in the expression and consolidation of fear memories (Madsen and Rainnie, 2009; Sangha et al., 2009; Popa et al., 2010; Lesting et al., 2011) and BLA inhibition is thought to promote these oscillations (Chapter 6; Ryan et al., 2012). Short-term depression of inhibition, as we observed in the juvenile BLA, promotes high-pass filtering of excitatory input and increases the information transmitted by bursts (Abbott and Regehr, 2004; George et al., 2011). Therefore, short-term depression may provide salience for high-frequency and bursting activity in the immature BLA, possibly providing compensation for the reduced sensitivity to high-frequency input of immature BLA principal neurons (Ehrlich et al., 2012).

We have shown that synaptic inhibition in the developing BLA is not static but undergoes a number of profound changes that will directly influence BLA physiology and its contribution to emotional processing. The function of GABA receptors and, therefore, of the entire BLA are in flux during the first postnatal month, which likely contributes to the emotional changes observed during this window. Future studies should determine whether development of synaptic transmission in the amygdala contributes to the expression of critical periods that render the brain vulnerable to the pathogenesis of emotional disorders like anxiety, depression, and autism spectrum disorders. To improve our understanding of the etiology of psychiatric disorders, it will be important to characterize how the normative development of the amygdala is influenced by genetic predispositions and risk factors for psychiatric disease (Pine, 2002; Monk, 2008). To this end, in **Chapter 5** we describe the effects on BLA development of a risk-factor for neurodevelopmental disorders, prenatal stress.

Table 4.1 PCR primers used in this study.

Gene	Accession No.	Primer sequence	PCR product size (bp)
18S rRNA	X01117	Forward: 5'- CCGGCGGCTTTGGTGACTCTA-3' Reverse: 5'- GCTCGGGCCTGCTTTGAACA-3'	563
GABA*α*1	AY574250	F: 5'- TGCCCATGCCTGCCCACTAAAA-3' R: 5'- GCCATCCCACGCATACCCTCTCT-3'	511
GABA*α*2	P23576	F: 5'-CCA GTC AAT TGG GAA GGA GAC AAT-3' R: 5'-TAG GCG TTG TTC TGT ATC ATG ACG-3'	434
GABA*α*3	X51991	F: 5'-T GTT GTT GGG ACA GAG ATA ATC CG-3' R: 5'-CAC TGT TGG AGT TGA AGA AGC ACT-3'	549
GABA*α*4	P28471	F: 5'-AGC TGC CCC AGT ACT GAA GGA AAA-3' R: 5'-ACT GTT GTC TTA ATG CGC CCA AGT-3'	374
GABA*α*5	X51992	F: 5'-ACA GTA GGC ACT GAG AAC ATC AGC- 3' R: 5'-AGG ATG GGT CAA CTT CCC AGT TGT-3'	407
GABA*α*6	NM_021841	F: 5'- CAAGCTCAACTTGAAGATGAAGG-3' R: 5'-TCCATCCATAGGGAAGTTAACC-3'	416
GABAβ1	NM_012956	F: 5'- ACAGCTCCAATGAACCCAGCAA-3' R: 5'-TGCTCCCTCTCCTCCATTCCA-3'	521
GABAβ2	X15467	F: 5'- GGAGTGACAAAGATTGAGCTTCCT-3' R: 5'-GTCTCCAAGTCCCATTACTGCTTC-3'	564
GABAβ3	NM_017065	F: 5'- CCGTCTGGTCTCCAGGAATGTTGTC-3' R: 5'-CGATCATTCTTGGCCTTGGCTGT-3'	411
GABAγ1	NM_080586	F: 5'- CAATAAAGGAAAAACCACCAG-3' R: 5'- TGATTATATTGGACTAAGCCAGA-3'	374
GABAγ2	L08497	F: 5'-GTGAAGACAACTTCTGGTGACTATGTGGT-3' R: 5'-CATATTCTTCATCCCTCTCTTGAAGGTG-3'	415
GABAγ3	X63324	F: 5'- CTGCTGCTTCTCCTCTGCCTGTTC-3' R: 5'- GGTTGGGTGTGGTGATCCAGTGA-3'	423
GABAδ	NM_017289	F: 5′-AGCAGTGCCTGCCAGAGTAT-3′ R: 5′-CATGTAAAGCCGTCATGTGG-3′	563
KCC2	NM_134363.1	F: 5'-AGGTGGAAGTCGTGGAGATG-3' R: 5'- CGAGTGTTGGCTGGATTCTT-3'	190
NKCC1	NM_031798.1	F: 5'-CCTGATCTCTGCGGGTATCTTT-3' R: 5'-ACCTTTCGCAAACATCTGGAA-3'	130

Table 4.2 IPSC Amplitude Ratios for Short-term Plasticity.

	Early STP		Late STP	
	10 Hz	**20 Hz**	**10 Hz**	**20 Hz**
P7	0.84 ± 0.06	0.64 ± 0.08	0.77 ± 0.02	0.58 ± 0.05
P14	0.81 ± 0.05	0.78 ± 0.04	0.83 ± 0.07	0.76 ± 0.04
P21	0.91 ± 0.03	0.83 ± 0.05	1.03 ± 0.11	0.94 ± 0.08
P28	0.95 ± 0.03	0.97 ± 0.04	1.19 ± 0.08	1.06 ± 0.10
P35	0.95 ± 0.03	1.02 ± 0.06	0.91 ± 0.07	0.96 ± 0.07

Table 4.2 IPSC Amplitude Ratios for Short-term Plasticity. The ratios of IPSC amplitudes following 10 and 20 Hz stimulation are listed for each time-point as mean ± SEM. Early STP corresponds to the ratio of pulse 2 to pulse 1, and late STP to the ratio of pulse 5 to pulse 1. Statistical tests for significance are described in the Results.

Figure 4.1: Schematic of recording and stimulation sites

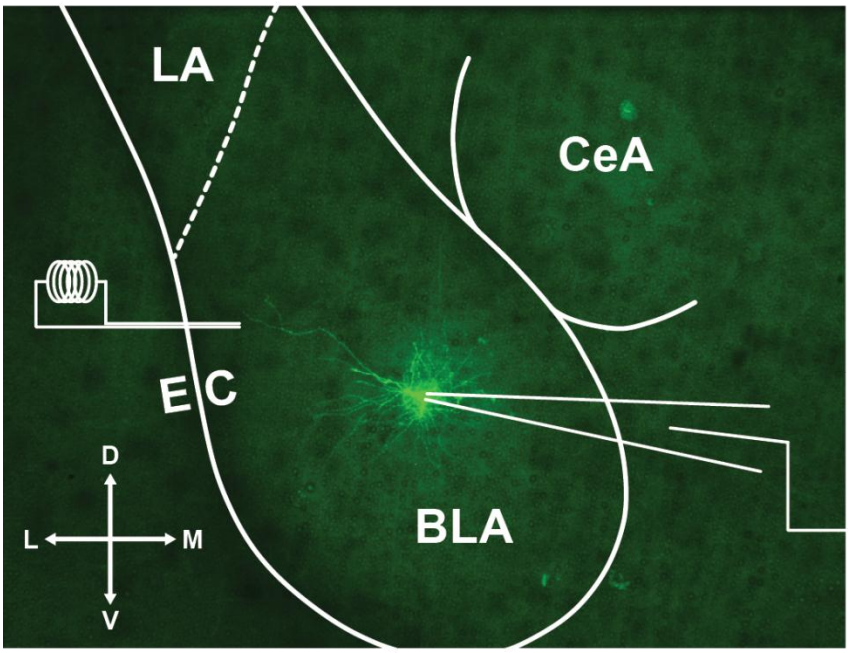

Figure 4.1: Schematic of recording and stimulation sites. A photomicrograph of a coronal slice of medial temporal lobe, depicting a representative, filled BLA principal neuron at P14 in the target recording site. The bipolar stimulating electrode was placed medial to the external capsule (EC) within the BLA. The lateral nucleus (LA) and central nucleus (CeA) of the amygdala are also labeled. The compass gives directions for dorsal (D), ventral (V), lateral (L), and medial (M).

Figure 4.2: Maturation of the stimulation response within the BLA

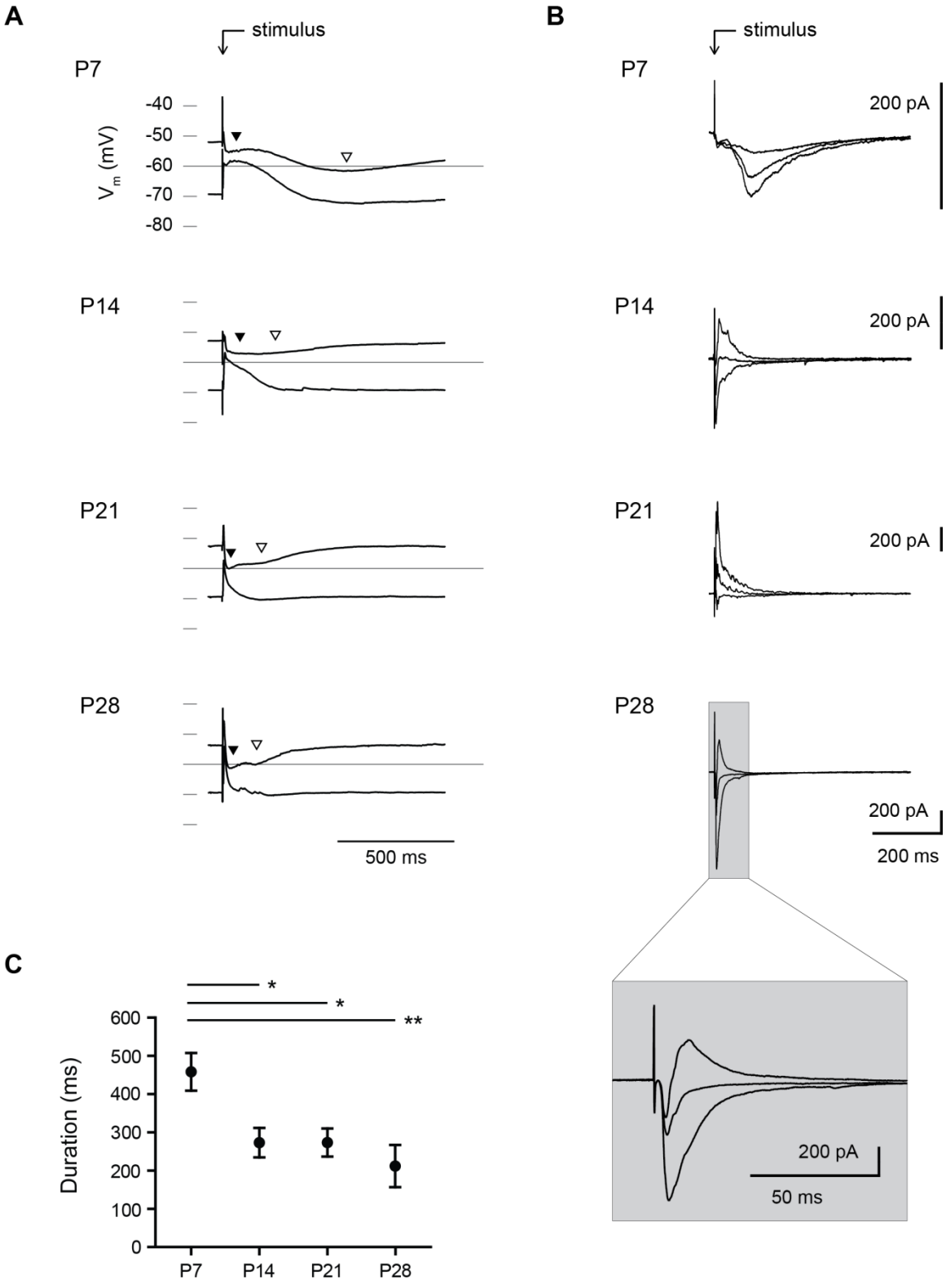

Figure 4.2: Maturation of the stimulation response within the BLA. (A,B) The average waveform of the response to five stimulations (0.1 Hz) of the dorsolateral BLA is shown for representative neurons at P7, P14, P21, and P28 from recordings in current clamp (A) and voltage clamp (B). Neurons in current clamp were adjusted before stimulation to a baseline membrane potential of approximately -50 or -70 mV, and the responses are plotted on a single voltage axis. Highlighted on the plots are the $GABA_A$ (closed arrowheads) and $GABA_B$ (open arrowheads) components of the response. Neurons in voltage clamp were recorded from holding potentials of -50, -60, and -70 mV, and baselines were subtracted for comparison. The $GABA_B$ component was blocked in the voltage clamp recordings to highlight the $GABA_A$ response. (C) The duration of the stimulation response in voltage clamp is plotted for each time-point as mean ± SEM. Significance was assessed with a one-way ANOVA ($F_{3,60} = 5.807$, $p < 0.001$) and Tukey's posttests (* $p < 0.05$, ** $p < 0.01$, n = 18 (P7), 17 (P14), 18 (P21), 11 (P28)).

Figure 4.3: Development of spontaneous IPSC kinetics across the first postnatal month

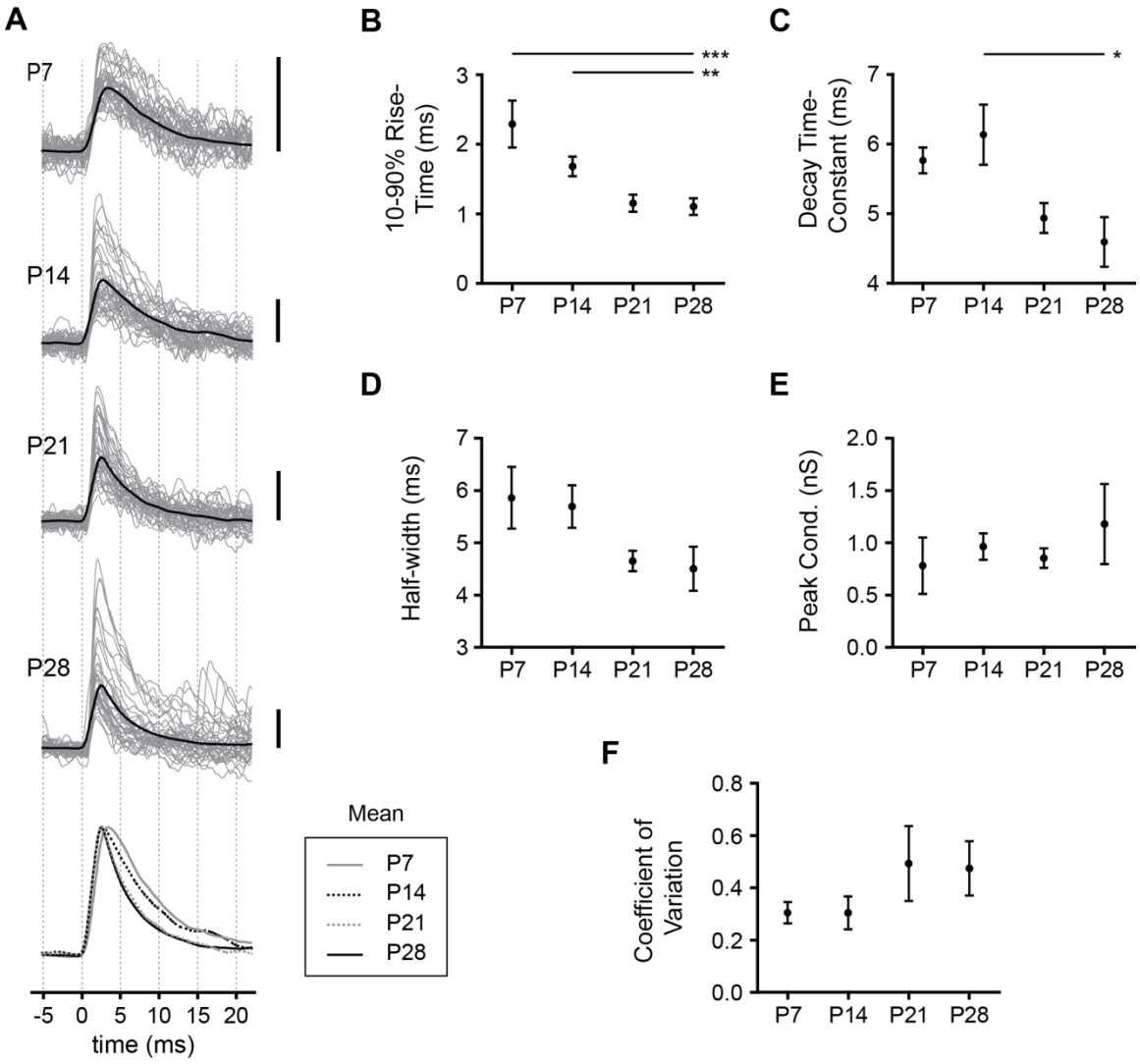

Figure 4.3: Development of spontaneous IPSC kinetics across the first postnatal month. (A) The waveforms of spontaneous IPSCs are illustrated for representative neurons at P7, P14, P21, and P28, depicted as the mean (black line) of all IPSCs recorded in a 30s window, as well as the first 40 IPSCs observed in these windows (grey lines). Scale bars represent 10 pA. Mean waveforms are superimposed (bottom) for comparison. (B-F) At each time-point, mean ± SEM is plotted for IPSC 10-90% rise-time (B), decay time-constant (C), half-width (D), and peak conductance (E), as well as the coefficient of variation of the peak conductance for each neuron (F). Significance was assessed using One-way ANOVAs and Tukey's posttests (* $p < 0.05$, ** $p < 0.01$, *** $p < 0.001$), identifying a significant main effect of age on IPSC rise-time ($F_{3,36} = 7.80$, $p < 0.001$) and decay time-constant ($F_{3,36} = 3.45$, $p < 0.05$), but not half-width (n = 6 (P7), 16 (P14), 11 (P21), 7 (P28)). No significant effect of age was detected for peak conductance ($F_{3,23} = 0.87$, $p > 0.05$) or coefficient of variation ($F_{3,22} = 1.28$, $p > 0.05$; n = 5-6).

Figure 4.4: Maturation of the response to exogenous $GABA_A$ agonist

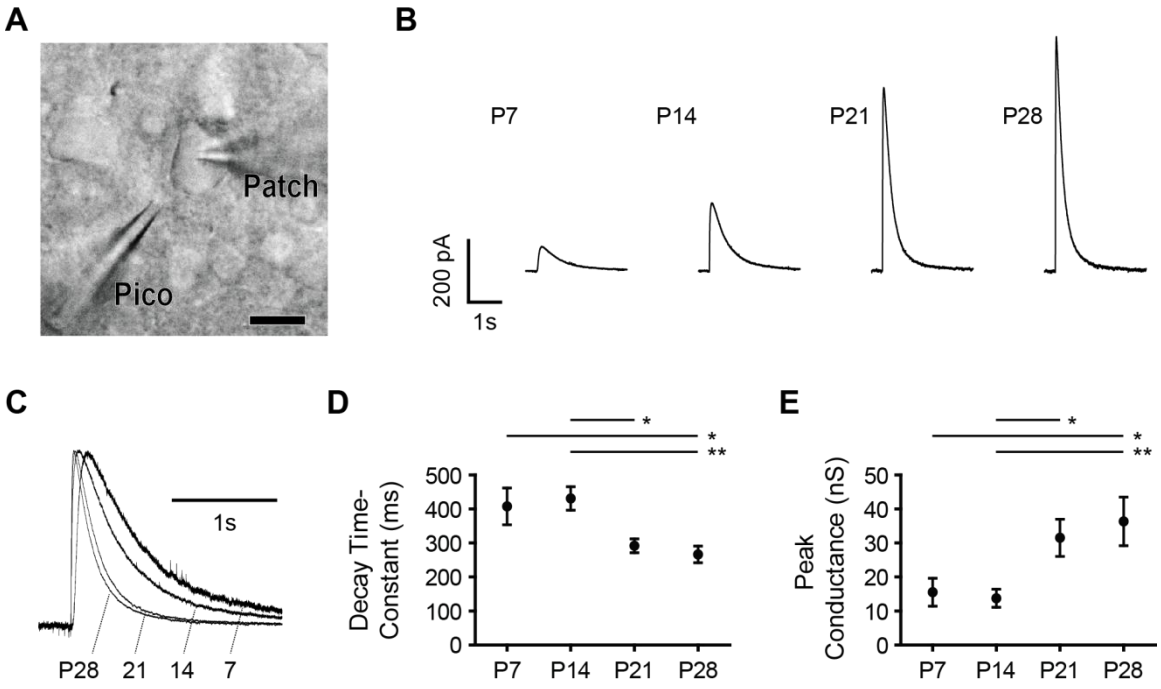

Figure 4.4: Maturation of the response to exogenous $GABA_A$ agonist. (A) BLA principal neurons at P7, P14, P21, and P28 were patch clamped with a patch electrode ('patch') and a microelectrode containing 100 μM muscimol ('pico') was brought in close proximity to the soma. Scale bar represents 10 μm. (B) Mean responses in voltage clamp at -50 mV to picospritzer application of muscimol in a representative neuron at each time-point. (C) Responses from panel B are normalized and superimposed to highlight decay kinetics. (D, E) The decay time-constant (D) and peak conductance (E) of the muscimol response are plotted as mean ± SEM for each time-point. Significance was assessed using One-way ANOVAs and Tukey's posttests (* $p < 0.05$, ** $p < 0.01$), identifying a significant main effect of age on decay time-constant ($F_{3,53} = 5.57$, $p < 0.01$; n = 12 (P7), 16 (P14), 13 (P21), 13 (P28)) and peak conductance ($F_{3,43} = 5.67$, $p < 0.01$; n = 10 (P7), 14 (P14), 10 (P21), 10 (P28)).

Figure 4.5: Development of $GABA_A$ receptor subunit gene expression

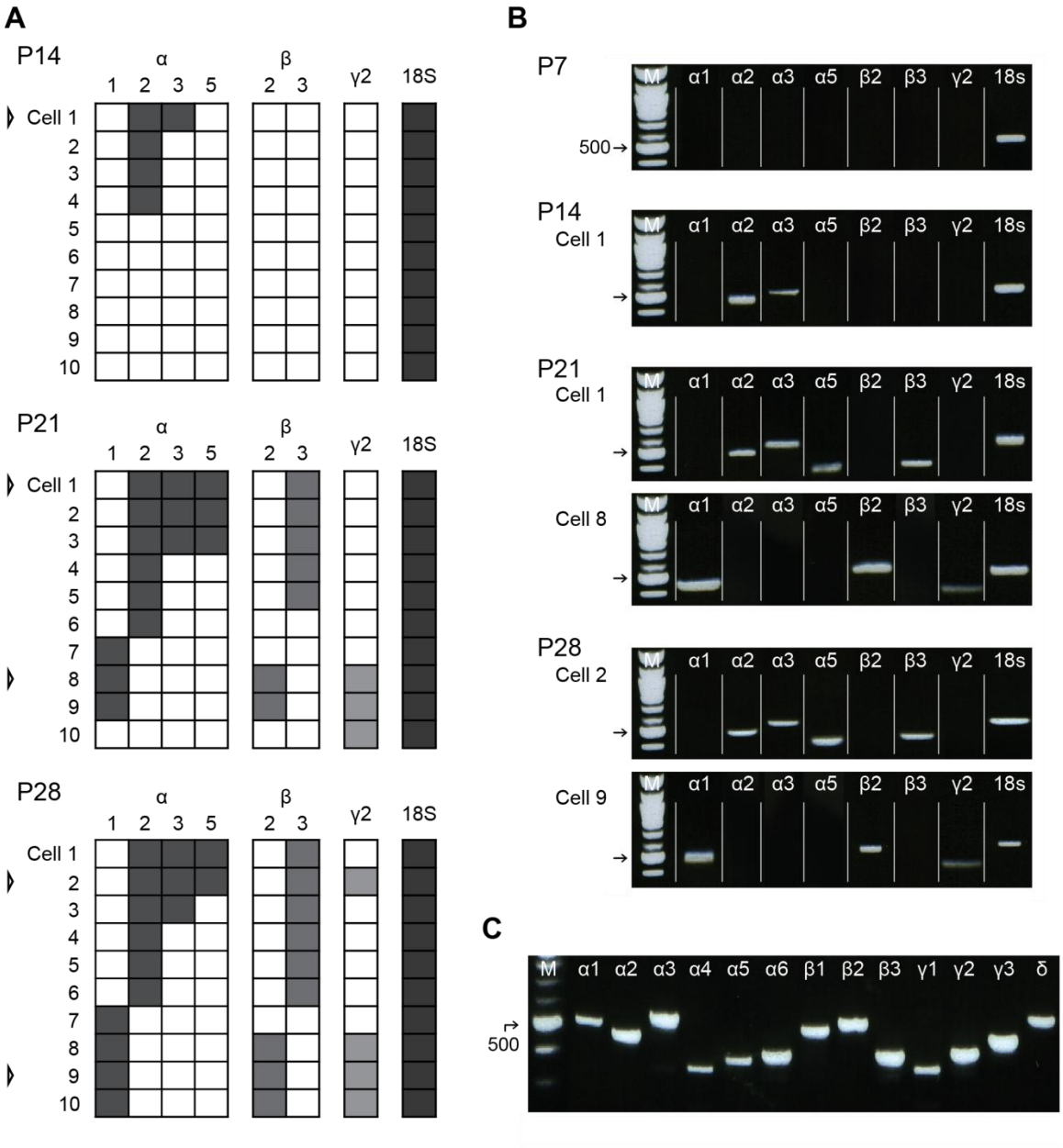

Figure 4.5: Development of $GABA_A$ receptor subunit gene expression. (A) The expression of mRNA for seven $GABA_A$ receptor subunits (α1, α 2, α 3, α 5, β2, β3, and γ2) are depicted for ten BLA principal neurons at P14, P21, and P28. Each row depicts the expression of each gene for a single neuron, with positive signal represented by a filled box. Ten neurons at P7 were also analyzed but are not presented because they lacked detectable expression for all genes but 18S. Only neurons with signal for the housekeeper gene 18S rRNA were included. Gel pictures are presented for representative neurons identified by open arrowheads. (B) Gel pictures depict the expression of particular receptor subunits for one to two representative neurons at each time-point, reassembled from gels organized by gene instead of individual neuron. (C) A gel picture showing detectable mRNA expression for all $GABA_A$ receptor subunits tested in whole-BLA from a representative animal at P7 (n = 4).

Figure 4.6: Maturation of $GABA_A$ reversal potential and chloride pump expression

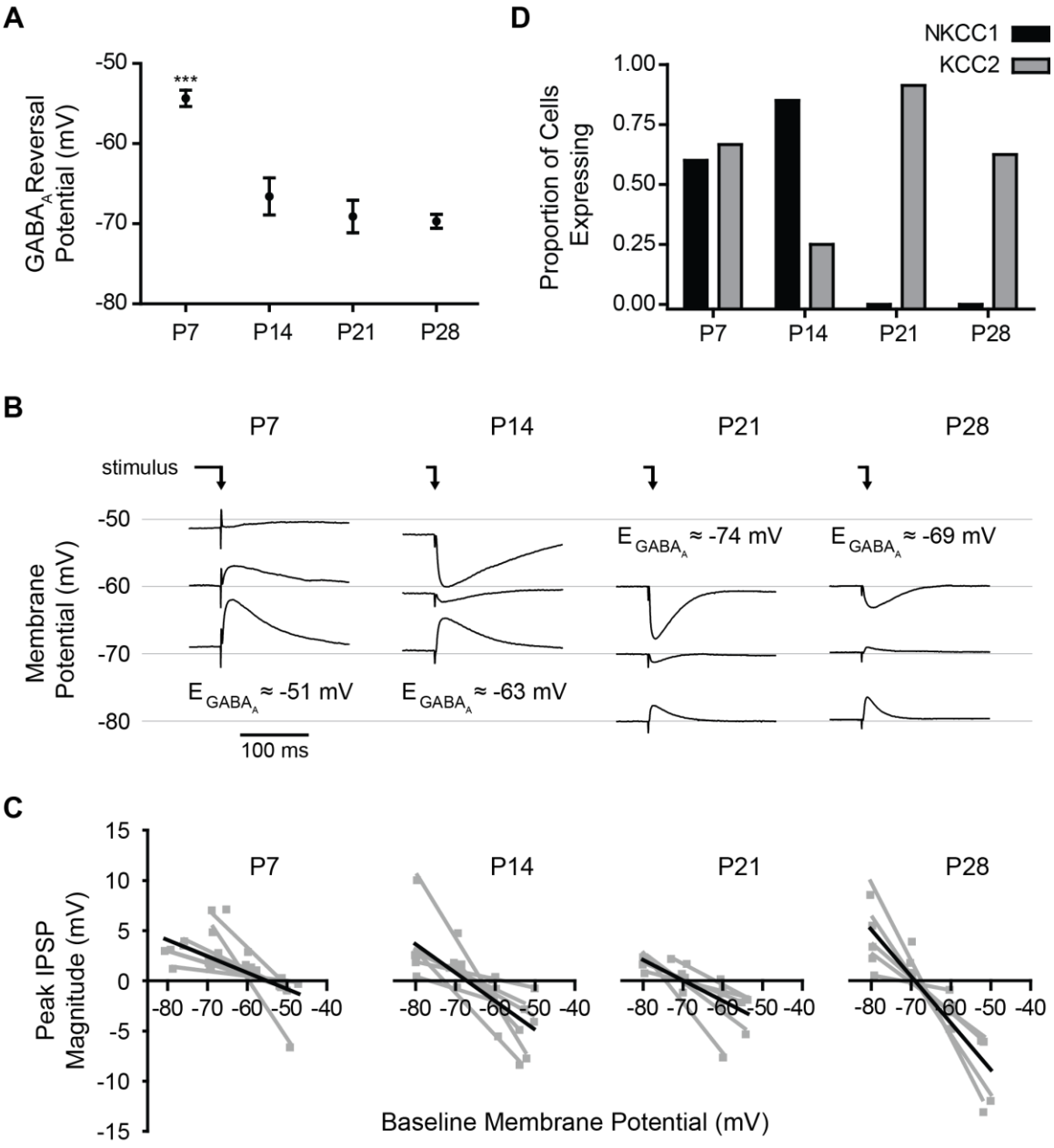

Figure 4.6: Maturation of $GABA_A$ reversal potential and chloride pump expression. (A,B) Reversal potential of evoked $GABA_A$ PSPs is plotted as mean ± SEM (A) for neurons at P7 (n = 8), P14 (n = 7), P21 (n = 5), and P28 (n = 5), and the average response at three different baseline membrane potentials is plotted for a representative neuron at each time-point (B). The reversal potentials shown in (B) are specific to the individual neurons depicted. Significance was assessed with a One-way ANOVA ($F_{3,21} = 19.91$) and pairwise comparisons were made with Tukey's posttests (***, $p < 0.001$ vs. P14, P21, and P28). The time of stimulation is depicted with an arrow. (C) The linear fits used to estimate $GABA_A$ reversal potential for each neuron are plotted in grey for neurons at each time-point, with the average line for each group plotted in black. (D) Expression of mRNA for the chloride pumps KCC2 and NKCC1, assessed in individual BLA principal neurons using single-cell RT-PCR, is plotted as the proportion of neurons with detectable expression at P7 (n = 15), P14 (n = 20), P21 (n = 23), and P28 (n = 8).

Figure 4.7: Development of short-term synaptic plasticity of IPSCs

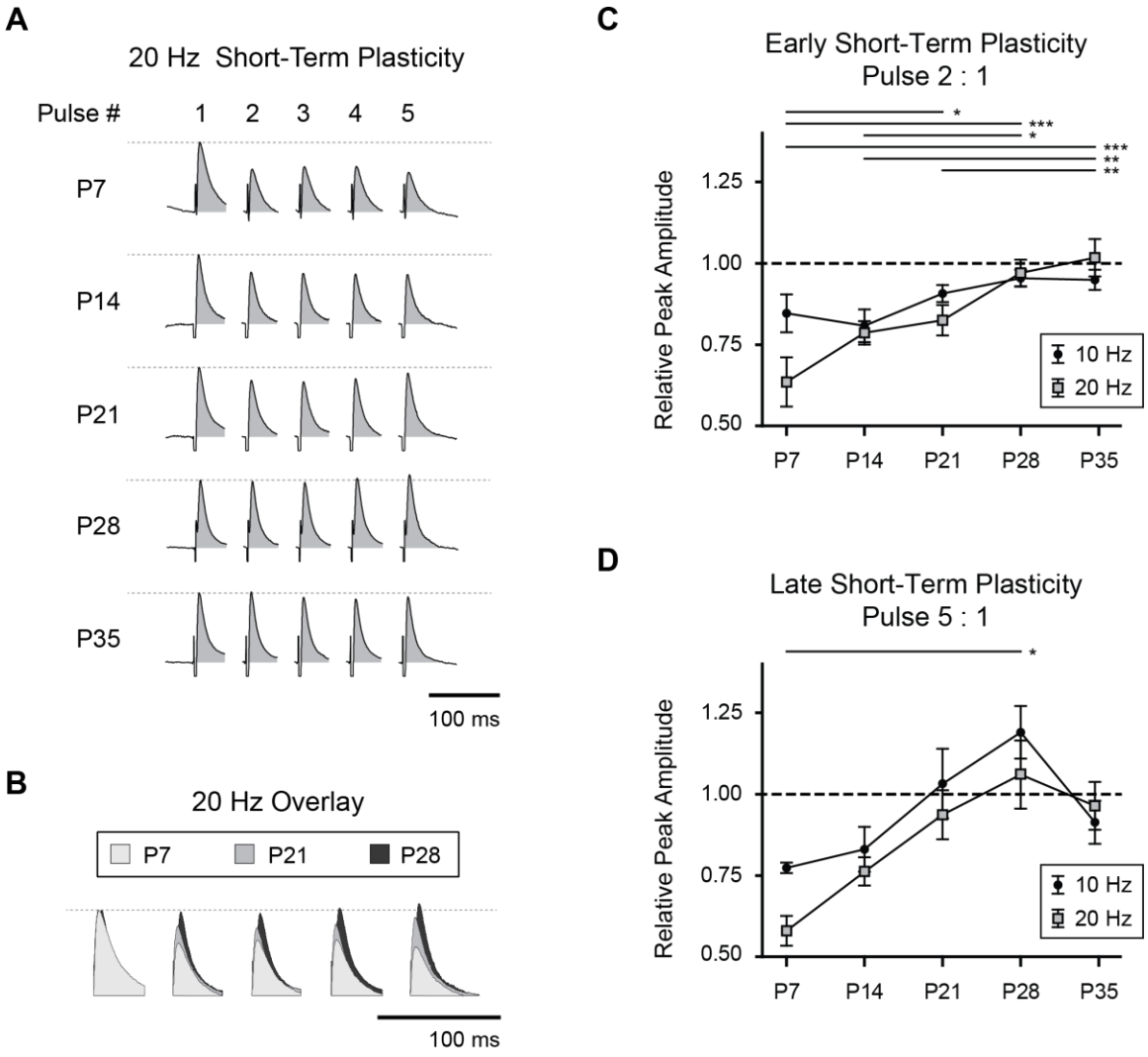

Figure 4.7: Development of short-term synaptic plasticity of IPSCs. (A) Short-term plasticity of $GABA_A$ IPSCs in representative neurons at P7, P14, P21, P28, and P35 are illustrated as the average response to stimulation of the dorsolateral BLA with 5 pulses at 20 Hz. Neurotransmitter receptor antagonists were used to isolate the $GABA_A$ component of the response (see Methods). Stimulation responses were aligned to and normalized by the first pulse, and stimulation artifacts were cropped for clarity. The area under the curve was filled to aid visual comparison across time-points. (B) As in *A*, average, normalized IPSCs in response to 20Hz stimulation are overlaid for comparison, taken from a representative neuron at P7, P21, and P28. (C, D) Short-term plasticity was quantified for 10 Hz and 20 Hz stimulation as a ratio of pulse amplitudes. The ratios of the second pulse (early STP, C) and fifth pulse (late STP, D) to the first pulse are plotted for each time-point as mean ± SEM. Significance was assessed with Two-way ANOVAs with repeated measures, and all pair-wise comparisons were made with Bonferroni posttests. Bars above each plot illustrate the significant pair-wise comparisons for stimulation at 20 Hz (* $p < 0.05$, ** $p < 0.01$, *** $p < 0.001$). No pair-wise comparisons for 10 Hz stimulation were significant. N = 3 (P7), 5 (P14), 7 (P21), 6 (P28), and 7 (P35).

Figure 4.8: Maturation of spontaneous, rhythmic IPSCs

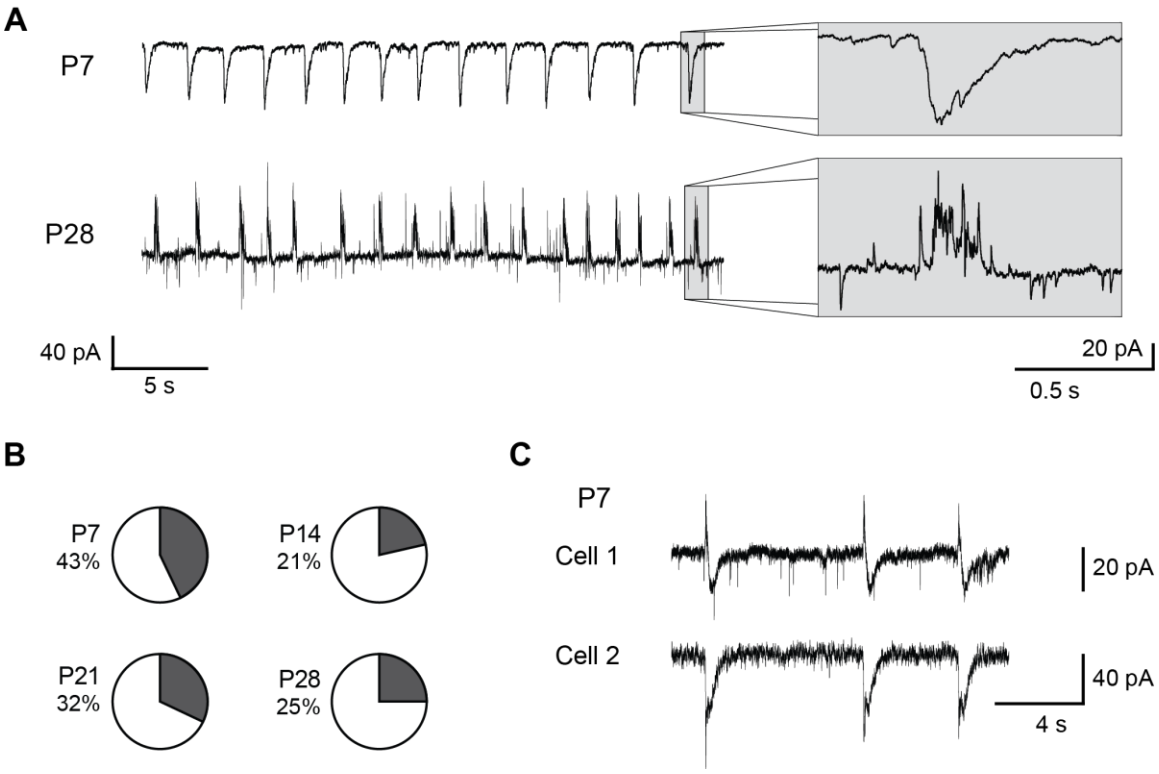

Figure 4.8: Maturation of spontaneous, rhythmic IPSCs. (A) Representative BLA principal neurons at P7 and P28 spontaneously exhibit rhythmic, compound IPSCs. Both neurons were recorded in voltage clamp with a holding potential of -60 mV. Insets highlight the waveform of individual events. (B) Pie charts depict the proportion of neurons spontaneously receiving rhythmic IPSCs at each time-point (n = 14 at P7, 28 at P14, 25 at P21, and 16 at P28). (C) Traces from a pair of simultaneously recorded BLA principal neurons illustrate that rhythmic IPSCs are synchronized across BLA principal neurons as early as P7.

Chapter 5: The Developmental Trajectory of Amygdala Neuron Excitability and GABAergic Transmission are Altered by Prenatal Stress

5.1 Abstract

The basolateral amygdala (BLA) plays a key role in emotional processing and is implicated in a variety of psychiatric disorders, many of which have early ages of onset and high incidence in juveniles. However, the cellular processes that contribute to the etiology of developmental psychiatric disorders are largely unknown. In **Chapters 2 and 3**, we showed principal neurons of the BLA undergo morphological and physiological transitions between postnatal days 7 (P7) and 21, including a 3x expansion of the dendritic arbor, 10x increase in dendritic spine density, and 10x decrease in input resistance. This developmental window coincides with maturation of GABAergic transmission, including a 15mV hyperpolarization of the $GABA_A$ reversal potential and a decrease in the duration of $GABA_A$ postsynaptic currents from P14 to P21, corresponding with the emergence of the fast $GABA_A$ receptor subunit, α1. We hypothesized that an early-life risk factor for anxiety disorders, prenatal stress (PS), alters the trajectory of BLA maturation. We tested this hypothesis by exposing pregnant dams to 30 min of daily unpredictable shock stress during gestational days 17-20. Male offspring of PS and control dams were sacrificed for whole-cell patch clamp studies at P10, 14, 17, 21, 28 & 60 to characterize the developmental trajectory of intrinsic membrane properties and synaptic transmission in BLA principal neurons. In adulthood, PS had an anxiolytic effect, as measured in the elevated plus-maze, and reduced sociability in the social choice test. Whole-cell patch clamp studies revealed no impact of PS on input resistance or membrane time-constant at any age. However, PS reduced neuronal excitability in several ways. PS caused an increase in the rheobase that began to emerge at P28 (2-way ANOVA, $p < 0.01$; N = 9-18); rheobase in PS neurons at P28 and P60 was 186 ± 21 and 323 ± 32 pA (mean ± SEM), respectively, compared to 170 ±19 and 176 ± 18 pA in controls. PS significantly increased action potential amplitude across all time-points (2-way ANOVA, $p < 0.05$; N = 10-19) including ~10mV increase at P17. In addition, neurons from PS animals exhibited slower $GABA_A$ receptor-mediated currents (2-way ANOVA,

$P < 0.01$) at P14 (decay time constant = 15.7 ± 1.9 ms, N = 20) compared to controls (9.8 ± 1.1 ms, N = 11). Finally, PS animals exhibited reduced expression in the BLA of the $GABA_A$ receptor α1 subunit, which plays a key role in coordinating developmental critical periods, as early as P17 and persisting into adulthood. We identified a number of effects of PS on the immature BLA that influence amygdala function during emotional development. These changes likely underlie the reduction in emotionality and sociability caused by PS, and may contribute to the etiology of psychiatric disorders, including autism and schizophrenia.

5.2 Introduction

Autism spectrum disorders (ASDs) and schizophrenia (SZ) are neurodevelopmental disorders characterized by deficits in social interaction and emotional behavior, and these disorders are thought to involve pathophysiology in parts of the brain that mediate socioemotional processing, including the amygdala (Baron-Cohen et al., 2000; Sweeten et al., 2002; Aleman and Kahn, 2005; Schultz, 2005; Shayegan and Stahl, 2005; Bachevalier and Loveland, 2006; Amaral et al., 2008; Benes, 2010; Bellani et al., 2013; Tottenham et al., 2013). While the specific causes of ASDs and SZ are likely distinct and include both genetic and environmental factors (State and Levitt, 2011; Geoffroy et al., 2013; van Dongen and Boomsma, 2013), both disorders share the risk factor of prenatal stress (PS; Koenig et al., 2002; Beversdorf et al., 2005; Khashan et al., 2008; Kinney et al., 2008; Ronald et al., 2010). Stress early in life is known to alter amygdala maturation (Ono et al., 2008; Moriceau et al., 2009; Maheu et al., 2010; Tottenham et al., 2011), and early life deficits in amygdala dysfunction could mediate the contribution of PS to these neurodevelopmental disorders.

The contribution of PS to ASD and SZ etiology may be mediated by changes to the coordination of amygdala development by the neurotransmitter GABA. Neurodevelopmental disorders are thought to follow from early life deficits in inhibitory GABA systems in the brain, because GABAergic neurotransmission plays an organizing role in nervous system development (Ramamoorthi and Lin, 2011; Sgado et al., 2011; Chattopadhyaya and Cristo, 2012; King et al., 2013). In the immature brain, GABAergic transmission regulates cell proliferation, migration and differentiation, synapse maturation and stabilization, and circuit wiring (Owens and Kriegstein, 2002; Huang and Scheiffele, 2008; Le Magueresse and Monyer, 2013). Furthermore, activation of GABA receptors control the timing of developmental critical periods, windows of heightened plasticity and sensitivity to external stimuli (Hensch, 2005); specifically, activation of $GABA_A$ receptors containing the α1 subunit closes critical periods (Fagiolini et al., 2004), which coincides

with the emergence of parvalbumin-expressing (PV^+) interneurons that preferentially innervate these receptors (Nusser et al., 1996; Fritschy et al., 1998; Pawelzik et al., 1999; Klausberger et al., 2002; Hensch, 2005; Nowicka et al., 2009). Therefore, if PS alters the development of GABAergic transmission and the expression of $GABA_A$ receptor α1 subunit and PV^+ interneurons in the amygdala, it may thereby influence critical periods to induce broad changes to emotional brain circuits. This mechanism has been broadly hypothesized for both SZ and ASD (Di Cristo, 2007; LeBlanc and Fagiolini, 2011; Volk and Lewis, 2013). Expression of the α1 subunit is reduced by 40% in cortex of human subjects with SZ (Glausier and Lewis, 2011), and genetic variation in $GABA_A$ receptor subunits has been associated with autism (Ma et al., 2005). In addition, dysfunction of PV^+ interneurons is proposed to underlie the deficits observed in SZ (Curley and Lewis, 2012).

In studying the effects of PS, we focused on the GABA system in the basolateral nucleus of the amygdala (BLA) for several reasons. The BLA is a hub in emotional processing with widespread connectivity in the brain that support its roles mediating fearful and anxious behavior (Davis et al., 2003; LeDoux, 2007; Pape and Pare, 2010; Stuber et al., 2011), regulating sensory perception and memory (Pessoa and Adolphs, 2010; Chavez et al., 2013; Chen et al., 2013), and influencing reward systems (Ambroggi et al., 2008; Stuber et al., 2011). Activity of the BLA is strictly regulated by GABAergic interneurons, especially those expressing parvalbumin (Rainnie et al., 1991a; Ehrlich et al., 2009; Ryan et al., 2012), and ablation of BLA interneurons causes deficits in social behavior (Truitt et al., 2007). We have recently demonstrated that GABAergic transmission in the rat BLA undergoes pronounced maturation in the first three postnatal weeks (Ehrlich et al., 2013), suggesting it contributes to amygdala development and may be sensitive to early life perturbation. Furthermore, neurons in the BLA mature with a similar time course, exhibiting robust changes to intrinsic electrophysiological properties and excitability (Ehrlich et al., 2012). Early postnatal changes to GABAergic function in the BLA may therefore influence the development of neurons in the amygdala.

A recent study in a rodent model of Fragile X syndrome, which often presents autistic-like features, found that expression in the BLA of the $GABA_A$ receptor α1 subunit failed to emerge during the second and third postnatal weeks (Vislay et al., 2013). The only related study of PS found reduced expression of the $GABA_A$ receptor γ2 subunit as early as two weeks after birth, but no consistent effect on the α1 subunit (Laloux et al., 2012). Various forms of early *post*natal stress reduce expression of the α1 subunit and increases the density of PV^+ interneurons in the adult BLA (Caldji et al., 2003; Jacobson-Pick et al., 2008; Seidel et al., 2008), but the effects on developing GABA circuits, specifically when they coordinate critical period plasticity, are largely unknown. Considering these studies, PS is likely to influence GABAergic transmission in the developing BLA, which could broadly influence outcomes for emotional brain circuitry.

Here we describe the effects of PS on the developmental trajectory of BLA neuron electrophysiology, focusing on intrinsic excitability and GABAergic transmission. Male offspring of rat dams exposed to unpredictable shock stress from embryonic day (E)17-20 were sacrificed for patch clamp recordings in acute brain slices, and electrophysiological responses were measured throughout amygdala development (at postnatal days (P)10, 14, 17, 21, 28) and in adulthood (day 60). Expression in the BLA of mRNA for the $GABA_A$ receptor α1 subunit was also measured at each time point using quantitative RT-PCR. These studies were paired with behavioral investigations to validate our PS paradigm as a model of risk for ASD and SZ. Offspring were tested for anxiety-like behavior on the elevated-plus maze in adulthood and isolation-induced ultrasonic vocalizations during infancy (Morgan et al., 1999; Shu et al., 2005) and sociability and social novelty preference were measured with the social choice test (Moy et al., 2004).

5.3 Methods

5.3.1 Ethical Approval

All experimental protocols strictly conform to the *Guidelines for the Care and Use of Laboratory Animals* of the National Institutes of Health, and were approved by the Emory University Institutional Animal Care and Use Committee.

5.3.2 Animals

Male rats born in-house to time-mated, Sprague-Dawley rats (embryonic day (E)4 on arrival, Charles River, Wilmington, MA, USA) were used in all experiments. Pups were housed with the dam prior to weaning on P22 or P23, with the day of birth considered P1. After weaning, rats were isolated by sex and housed three to four per cage with *ad libitum* access to food and water. Throughout this chapter, animal ages are attributed to a single day for brevity, but labels describe developmental windows as follows: 'P10' for P10-11, 'P14' for P13-14, 'P17' for P17-18, 'P21' for P21-22, 'P28' for P27-30, and 'P60' for P60-70.

5.3.3 Prenatal Stress

An unpredictable shock stress paradigm was applied as previously described (Hazra et al., 2012) to pregnant dams as follows. On E17-20, dams were placed in an operant conditioning chamber measuring 60 × 34 × 26 cm, with aluminum and polycarbonate walls (Lafayette Instruments, Lafayette, IN, USA). The floor of the chamber, composed of 0.4 cm-diameter stainless steel bars, conducted the electric shock. Dams in the PS group were allowed to habituate to the chamber for 5 min and then received two 8 min periods of shocks separated by an 8 min period without shocks (**Figure 5.1**). Each shock period consisted of 8 pseudo-randomly applied footshocks (0.5 s, 0.5 mA, inter-shock interval ranging from 30 to 90 s). Non-stressed control dams received the same handling procedures as the PS group and were placed in the shock

chamber for the same duration without shocks applied. After stress exposure on E20, dams were returned to their home cage and left to give birth and rear pups normally.

5.3.4 Electrophysiology

5.3.4.1 Tissue Preparation

Offspring of stress-exposed and control dams were used for electrophysiological studies. Slices were prepared from rats at various ages as previously described (Ehrlich et al., 2013). Briefly, animals were decapitated, with those beyond P11 under isoflurane anesthesia (Fisher Scientific, Hanover Park, IL), and brains were rapidly removed and immersed in ice-cold 95% oxygen-5% carbon dioxide-perfused "cutting solution" with the following composition (in mM): 130 NaCl, 30 $NaHCO_3$, 3.50 KCl, 1.10 KH_2PO_4, 6.0 $MgCl_2$, 1.0 $CaCl_2$, 10 glucose, 0.4 ascorbate, 0.8 thiourea, 2.0 sodium pyruvate, and 2.0 kynurenic acid. Coronal slices containing the basolateral nucleus of the amygdala (BLA) were cut at a thickness of 300–350 μm with a Leica VTS-1000 vibrating blade microtome (Leica Microsystems, Bannockburn, IL). Slices were incubated for 1h in oxygenated cutting solution at 32°C before being transferred to regular artificial cerebrospinal fluid (ACSF) containing (in mM) 130 NaCl, 30 $NaHCO_3$, 3.50 KCl, 1.10 KH_2PO_4, 1.30 $MgCl_2$, 2.50 $CaCl_2$, 10 glucose, 0.4 ascorbate, 0.8 thiourea, and 2.0 sodium pyruvate.

5.3.4.2 Whole Cell Patch Clamp

Individual slices were transferred to a recording chamber mounted on the fixed stage of a Leica DMLFS microscope (Leica Microsystems) and maintained fully submerged and continuously perfused with oxygenated 32°C ACSF at a flow rate of 1–2 ml/min. The BLA was identified under 10x magnification, and individual BLA neurons were identified at 40x with differential interference contrast optics and infrared illumination with an infrared-sensitive CCD camera (Orca ER, Hamamatsu, Tokyo, Japan). Patch pipettes of 4–6 MΩ were pulled from

borosilicate glass. Two patch electrode solutions were used, one based on potassium gluconate for current-clamp recordings and one based on cesium gluconate for voltage-clamp recordings. The potassium gluconate patch solution had the following composition (in mM): 140 potassium gluconate, 2 KCl, 10 HEPES, 3 $MgCl_2$, 2 K-ATP, 0.2 Na-GTP, and 5 phosphocreatine, was titrated to pH 7.3 with KOH, and was 290 mosM. The cesium gluconate patch solution had the following composition (in mM): 131 CsOH, 131 gluconate, 10 HEPES, 2 $CaCl_2$, 10 glucose, 10 EGTA, 5 Mg-ATP, and 0.4 Na-GTP, was titrated to pH 7.3 with gluconate, and was 270 mosM.

Data acquisition was performed with a MultiClamp 700A amplifier in conjunction with pCLAMP 10.2 software and a DigiData 1322A AD/DA interface (Molecular Devices, Sunnyvale, CA). Whole cell patch-clamp recordings were obtained, low-pass filtered at 2 kHz, and digitized at 10 kHz. Cells were excluded if they did not meet the following criteria: a resting membrane potential more negative than −50 mV and drifting <5 mV over the course of the recording session; access resistance lower than 30 MΩ; stable access resistance throughout recording, changing <15%; and action potentials crossing 0 mV. Recordings were only included from BLA principal neurons, whose physiological profile we have recently characterized during development; they can be distinguished from BLA interneurons for electrophysiological recordings by a combination of their large somatic volume, low input resistance, slow action potentials, and relatively infrequent synaptic input (Ehrlich et al., 2012). In that study, we reported 58 of 60 putative principal neurons recorded in the immature BLA were found positive for mRNA for the vesicular glutamate transporter by single-cell RT-PCR.

5.3.4.3 Intrinsic Properties

Raw voltage and current traces were imported into Matlab (The MathWorks, Natick, MA, USA) using scripts provided with sigTOOL (http://sigtool.sourceforge.net/, developed at King's College London) and processed with customized scripts developed in the Rainnie Lab (first reported in Hazra et al., 2011). To determine input resistance and membrane time constant

in current clamp, neurons were held at -60 mV with direct current injection and hyperpolarizing, 1 s-long, square-wave current steps were injected to elicit <5 mV voltage deflections. Input resistance was calculated as the ratio of peak voltage deflection to the current injected, averaged across 5 sweeps. The time constant was defined as the time necessary for the cell to reach 63.2% of its maximal deflection, averaged across 5 sweeps.

Action potential properties were measured from the responses to 5 linear ramps of depolarizing current, each lasting 250 ms and scaled to depolarize the neuron to approximately −35 mV and elicit an action potential within the final 50 ms. Action potential threshold was defined from a peak in the second derivative of the membrane potential waveform, which correlated well with visual inspection of the data. Linear interpolation between data points was used to enhance the temporal resolution of measurements of 10–90% rise time, 90–10% decay time and half-maximal width. Fast afterhyperpolarization (fAHP) peaks were measured from neurons free-firing near action potential threshold (at least 8 spikes) to remove the confound of current step artifacts, at a local minima following spike repolarization, if occurring within 15 ms of spike initiation and visibly distinct from the medium AHP.

Data on spike trains were collected from responses to depolarizing, 1 s-long, square-wave current injections with sweeps iterated at 0.1 Hz. Rheobase was measured at resting membrane potential with a series of current injections in increments of 5-20 pA depending on the age, and was defined as the magnitude of the injection of the first of two consecutive steps to elicit at least one action potential. F-I curves were generated from a series of sweeps that iterated beyond the magnitude required to elicit the maximum spike rate for each neuron, and data were excluded for current injections greater than the minimum current required to elicit the maximum spike rate. To facilitate plotting F-I curves, due to the diminishing number of cells with responses as current injection magnitude increased, data were not plotted at large current injection values for which less than half of neurons had responses at that time point. For neurons from animals at least 21 days old, neurons were excluded from plotting if they could not fire at least 30 spikes, based on

previous findings (Ehrlich et al., 2012). This resulted in the exclusion of 5 of 58 neurons at P21, 28 and 60 combined (3 from control animals, 2 from PS animals).

5.3.4.4 GABAergic Transmission

To elicit GABAergic postsynaptic currents (PSCs), a bipolar stimulating electrode was placed in the dorsal end of the BLA, just medial to the external capsule, and the $GABA_A$ component of the response was pharmacologically isolated as previously described (Ehrlich et al., 2013). Stimulation at 0.2 Hz was applied after application of the following cocktail of synaptic blockers: the AMPA/kainate receptor antagonist 6,7-dinitroquinoxaline-2,3-dione (DNQX, 20 μM; Sigma-Aldrich), the NMDA receptor antagonist 3-(2-carboxypiperazin-4-yl)propyl-1-phosphonic acid (RS-CPP, 10 μM; Tocris Bioscience, Bristol, UK), and the $GABA_B$ receptor antagonist (2*S*)-3-[[(1*S*)-1-(3,4-dichlorophenyl)ethyl]amino-2-hydroxypropyl] (phenylmethyl)phosphinic acid hydrochloride (CGP52432, 2 μM; Tocris). Stimulation intensity was adjusted to elicit a half-maximal response. To verify that the isolated response was mediated purely by $GABA_A$ receptors, after some experiments the $GABA_A$ antagonist 6-imino-3-(4-methoxyphenyl)-1(6*H*)-pyridazinebutanoic acid hydrobromide (SR95531, 5 μM; Tocris) was applied.

Due to the hyperpolarization of the $GABA_A$ reversal potential with age (Ehrlich et al., 2013), stimulation responses were recorded in voltage clamp at holding potentials of -50 and -70 mV, and the potential with the larger amplitude responses was used. Decay time constant was calculated in Clampfit from the average of 5 sweeps, from just after the peak to baseline, using a one-term exponential (Equation 1).

Equation 1 $$f(t) = A \times e^{-t/\tau} + C$$

To measure short-term plasticity of $GABA_A$ PSCs, the response used to measure kinetics was elicited in trains of five pulses at 20 and 50 Hz, in five sweeps each at 0.1 Hz. Sweeps were averaged in Clampfit, and amplitudes were measured for each pulse from the 1 ms prior to the

stimulation artifact to the absolute peak deflection. The ratio of the amplitudes of pulse 5 to pulse 1 was calculated for each neuron at both stimulation frequencies.

5.3.5 Quantitative RT-PCR

BLA sections were harvested for PCR during the tissue preparation for electrophysiology. Bilateral BLA from a single coronal slice was microdissected and flash frozen. Quantitative PCR was performed as previously described (Hazra et al., 2011). Total RNA was isolated by homogenizing each sample in Trizol (Invitrogen, Carlsbad, CA, USA), and isolated RNA was reverse transcribed using a cocktail of 5 µl of 10x RT buffer, 10 mM dNTP mix, 10x random hexanucleotide and Multiscribe RT 5U/µl and RNAase free water. The mixture was incubated in a thermal cycler at 25° C for 10 min and then at 37° C for 120 min, and the resulting cDNA samples were stored at -20° C. All reagents were obtained from Applied Biosystems (Foster City, CA, USA).

Real-time PCR was performed using an Applied Biosystems 7500 Fast-Real Time PCR system (Applied Biosystems, Foster City, CA, USA). 2 µl of cDNA obtained from the isolated RNA were combined with Taqman probes specific for 18S rRNA (Accession No. X03205) or $GABA_A$ receptor α1 subunit (Accession No. NM_183326) and 1x Taqman universal PCR Master Mix (Applied Biosystems), and the reaction for each sample was performed in triplicate. The thermal cycling program consisted of: cycle 1 (20 min at 95° C) and cycles 2 through 40 (3 s at 95° C followed by 30 min at 60° C). Expression of the α1 subunit was normalized for all samples to expression of 18S rRNA. The $2^{-\Delta\Delta Ct}$ method of relative quantification was used to calculate the fold change in expression of genes, and these values were used for statistical analysis (Livak and Schmittgen, 2001).

5.3.6 Behavioral Testing

5.3.6.1 Elevated Plus-Maze

All behavioral tests were conducted during the light phase of a 12:12 hour light-dark cycle. The elevated plus-maze consisted of two open arms and two closed arms, each 50 x 11 cm and elevated to a height of 50 cm. Rats from ages P60-70 were placed for 5 min on the maze in a room illuminated by red lights suspended over the center of the maze. Videos of the session were recorded and analyzed offline. The durations of time spent in open and closed arms and maze center were measured using Topscan 2.00 (CleverSys Inc., Reston, VA, USA) with the following analysis parameters: animal size – 100 to 1000 px, max movement per frame - 200 px, animal detection threshold - contrast level 1. Center crossings and head dips (defined as extension of the head below the plane of the maze while the body is on an open arm) were counted manually by an experimenter blinded to animal group.

5.3.6.2 Sociability and Social Choice Test (SCT)

The SCT was conducted using a previously established paradigm for social discrimination and social novelty preference in rodents (van der Kooij and Sandi, 2012). On testing day, in a room illuminated with red light, rats were first acclimated for 5 min to the testing apparatus. The apparatus, made of clear plexiglass, consists of 3 adjacent chambers of dimensions 50x25x29 cm (LxWxH). Circular portals, 11 cm in diameter, on the inner walls allow access to between the chambers, and rats could freely explore the box. The corner of each outer chamber contained a wire mesh cage, of dimensions 22x14x18 cm, which was empty during acclimation. After acclimation, the test rat was removed from the apparatus and the 5 min sociability test was administered as follows: before the test rat was returned to the apparatus, into one of the wire mesh cages was placed an unfamiliar male conspecific of comparable age (C1), and into the other an inanimate object of comparable size to a P60 rat. The test rat was placed in the center chamber

of the testing apparatus, and its behavior was video recorded via an overhead camera. Following the sociability test, the test rat was removed and another conspecific (C2) was placed into the cage formerly containing the inanimate object. For the SCT, the test rat was placed back in the testing apparatus and behavior was recorded for 5 min. The conspecific rats C1 and C2 were used for up to 4 rounds of testing (4 test rats), alternating between being the first and second rat presented. Time spent interacting with the object and conspecific rats were scored by hand, offline, from overhead videos by a blinded experimenter.

5.3.6.3 Isolation-Induced Ultrasonic Vocalizations (USVs)

This test was based on the protocol described by Hofer et al. (2002). Pups were tested for USVs at P7 and P17. To minimize the separation stress to the pups, dams were left with the litters during habituation for 1 hour prior to testing. After habituation, pups were separated from the litter in series, and each was taken to another room and placed in a test cage with bedding for 5 min. The Sonotrack system (Metris, Kruisweg, Netherlands) was used to detect and analyze USVs, and the detector was mounted approximately 50 cm above the cage. The number of vocalizations was obtained for each pup offline with the following analysis parameters: discrimination factor: 10, width: 15 ms, and amplitude threshold: 22.13 dB. USVs with a mean frequency below 25kHz were excluded, and the detection ceiling was 90kHz.

5.3.7 Statistics

For all statistical tests, significance was assigned based on $\alpha = 0.05$. All data sets were tested for normality using the Shapiro–Wilk test ($\alpha = 0.05$) and for homoscedasticity using Levene's test ($\alpha = 0.0001$), implemented in Matlab. Comparisons of behavior in the EPM were made using Student's t-tests in Prism 4 (GraphPad, LaJolla, CA). Measures of open arm times and dips in the EPM failed the Shapiro-Wilk test, and were therefore analyzed with Mann-

Whitney U tests in Prism. For the social choice and interaction tests, time spent interacting with probe objects and conspecifics were analyzed with Two-way ANOVA, and preference indices were analyzed with a Student's t-test. Ultrasonic vocalization frequency was analyzed at both time points using a Student's t-test. The effects of age and stress on all electrophysiological properties were tested using Two-way ANOVAs in Prism and, if a significant main effect was observed, with Bonferroni post-tests. The following data were log-transformed before ANOVA to achieve homoscedasticity: body mass, input resistance, membrane time constant, AP half-width, 10-90% rise-time, 90-10% decay-time, rheobase, and current for maximum spike rate. Since only 5 neurons had a detectable fAHP at P14, this time point was excluded from analysis, allowing the data to meet the homoscedasticity assumption.

5.4 Results

Electrophysiological data were collected from 407 BLA neurons from 78 male rats on postnatal days (P)10, 14, 17, 21, 28, and 60, representing 23 distinct litters (at least 4 litters at each time-point/group). Neurons were divided into different datasets based on the recording configuration and patch solution, and a total of 238 neurons were recorded in voltage-clamp mode with a Cesium-based patch solution, and 169 neurons were recorded in current-clamp mode with a Potassium-based patch solution. Neurons were recorded in both configurations from most animals included in the study. A total of 203 neurons were recorded from PS animals and 204 from controls. From 3 animals sacrificed for electrophysiology in both groups at each time point, a portion of the BLA was microdissected for RT-PCR. Another 3 animals for both groups per time point were perfused for immunohistochemistry. In addition 37 male rats from 10 litters (5 PS and 5 control litters) were tested in the elevated plus-maze for anxiety-like behavior. Nine adult rats from 2 litters were used for social novelty testing, and 19 rats from 4 litters were tested for ultrasonic vocalizations. There was no effect of PS on litter size (11.7 ± 0.4 pups per control litter vs. 11.4 ± 0.6 pups per PS litter, Student's t-test, $p = 0.66$, $n = 18$), but body weight was significantly greater in PS offspring than controls (**Figure 5.2**; Two-way ANOVA, main effect of PS: $F_{1,69} = 4.09$; $p < 0.05$). At P60, there was a 10.2% increase in body weight due to PS (408.9 ± 40.7 g for PS vs. 371.1 ± 32.7 g for control).

5.4.1 Reduced emotionality in adult and juvenile PS rats

In light of previous findings on the effects of PS on emotional behavior in the offspring, specifically reports on contradictory findings of anxiogenic and anxiolytic effects (Estanislau and Morato, 2006; Richardson et al., 2006; Baker et al., 2008; Darnaudery and Maccari, 2008), we first tested the effect of our PS paradigm on offspring behavior. As illustrated in **Figure 5.3**, adult offspring of dams exposed to PS exhibited reduced anxiety-like behavior as measured in the

elevated plus-maze. PS rats at P60 spent significantly more time than controls in the open arms of the plus-maze (**Figure 5.3A**; 96.5 ± 10.6 s vs. 54.8 ± 6.9 s for controls; Mann-Whitney U test, U_{32} = 60, ** $p < 0.01$). PS rats also performed more head dips, indicative of reduced anxiety on the plus-maze (**Figure 5.3B**; 5.3 ± 0.6 vs. 3.3 ± 0.7 dips for controls; U_{32} = 85, * $p < 0.05$). PS rats did not exhibit any differences in terms of open arm entries (**Figure 5.3C**; 8.81± 0.6 vs. 7.2 ± 0.7 for controls; U_{32} = 96.5, $p = 0.104$) or locomotor activity, with a comparable number of center crossings for each group (**Figure 5.3D**; 11.9 ± 0.8 vs. 10.2 ± 1.0 crossings for controls; Student's t-test, t_{32} = 1.3, $p > 0.05$).

We also measured isolation-induced ultrasonic vocalization calls (USVs, **Figure 5.4**) to assess emotional behavior in developing rats. This under-powered experiment suggests USVs were comparable at P7 across groups (**Figure 5.4A**; 428.4 ± 63.6 vs. 406.8 ± 49.8 calls by controls; $t_{20} = 0.271$, $p > 0.05$; $10 \leq N \leq 12$), but tended to occur less frequently in PS rats compared to controls at P17 (**Figure 5.4B**; 153.3 ± 38.4 vs. 96.8 ± 23.8 calls in controls; t_{15} = 1.319, $p > 0.05$; $7 \leq N \leq 10$). On average, pups made many more USVs at P7 (416.6) than at P17 (120.1).

To test whether the anxiolytic effect of PS reflects reduced emotionality in the adult offspring, we measured sociability and social novelty preference (**Figure 5.5**). These experiments were also under-powered, but suggest sociability may be reduced in adult offspring of stressed dams. Both PS and control rats tended to spend more time with a novel conspecific than a novel object, but the social preference was weaker in PS rats (**Figure 5.5A, C**; Control total time interacting with conspecific: 101.8 ± 27.2 s, with object: 20.9 ± 3.1 s, sociability preference index: 0.64 ± 0.06; PS total time interacting with conspecific: 60.6 ± 7.6 s, with object: 22.1 ± 5.4 s, sociability preference index: 0.49 ± 0.11; Two-way ANOVA, interaction effect: $F_{1,14} = 0.90$, $p > 0.05$; $3 \leq N \leq 5$). When control rats were presented with a novel conspecific as well as the now familiar conspecific, they spent more time on average with the novel conspecific (**Figure 5.5B, C**; Control total time interacting with novel conspecific:51.2 ± 11.4 s, with familiar: 34.4 ± 3.2 s,

social novelty preference index: 0.15 ± 0.15; PS total time interacting with novel conspecific: 24.9 ± 9.3 s, with familiar:22.4 ± 10.6 s, social novelty preference index: 0.15 ± 0.18). Consistent with the sociability test, PS rats spent less time with either conspecific, but did not exhibit any difference from controls in their social novelty preference (**Figure 5.5C**, Two-way ANOVA, main effect of PS: $F_{1,14} = 4.04$, $p = 0.06$). Together, these behavioral findings suggest the altered emotionality in PS offspring emerges early in development and persists into adulthood.

5.4.2 PS altered intrinsic properties of BLA principal neurons during development

Having observed altered emotional behavior in PS offspring early in postnatal development, we assessed the effect of PS on the developmental trajectory of BLA principal neuron electrophysiology. **Figure 5.6** illustrates the typical developmental reduction in input resistance and membrane time constant, showing a nearly three-fold reduction in both measures between P10 and P28 (Ehrlich et al., 2012). We found no effect of PS on input resistance (**Figure 5.6A**; Two-way ANOVA: $F_{1,144} = 1.65$, $p > 0.05$) or membrane time constant (**Figure 5.6B**; $F_{1,142} = 0.07$, $p > 0.05$). However, we did find an effect of PS on resting membrane potential (RMP, **Figure 5.6C**), such that RMP was more hyperpolarized in PS animals across all ages, typically between 1 and 2 mV ($F_{1,148} = 4.63$, $p < 0.05$). As expected, there was a significant effect of age, with a RMP in control animals of -55.3 ± 1.0 mV at P10 that became hyperpolarized by P17, reaching the mature value of -62.9 ± 0.8 (Two-way ANOVA, main effect of age: $F_{5,148} = 17.3$, $p < 0.0001$).

The effects of PS on features of action potentials (APs) of BLA principal neurons are depicted in **Figure 5.7**, as we have previously shown APs change profoundly with age in this population (Ehrlich et al., 2012). AP threshold changed with age until around P21, as expected, but PS altered its developmental trajectory, reducing the threshold by 1-2 mV from P10 to P21 (**Figure 5.7A, B**; Two-way ANOVA: $F_{1,146} = 5.85$, $p < 0.05$). AP amplitude increased with age, from around 55 mV at P10 to 70 mV at P21-60, and was greater in PS animals (for example, at

P17: 71.4 ± 1.8 mV in PS animals vs. 61.8 ± 2.5 mV in controls), corresponding with the more hyperpolarized threshold (**Figure 5.7C**; Two-way ANOVA, main effect of stress: $F_{1,149} = 4.62$, $p < 0.05$).

We also investigated the fast afterhyperpolarization (fAHP) of the AP, which we have previously reported to emerge during development of BLA principal neurons (Ehrlich et al., 2012). In neurons expressing a fAHP, its peak voltage deflection became more hyperpolarized with age until P28, from around -38 mV at P10 to below -42 mV at P28 and P60 (**Figure 5.7A, D**). Beginning at P21 the fAHP peak was more hyperpolarized in neurons from PS animals relative to controls, and was approximately 2 mV more hyperpolarized in neurons from PS animals in adulthood (not significant, Two-way ANOVA, main effect of PS: $F_{1,66} = 2.34$, $p > 0.05$).

Unlike AP threshold and amplitude, AP kinetics did not change due to PS (**Figure 5.7E-G**). Half-width decreased approximately 40% from around 1.25 ms at P10 to around 0.75 ms at P28 (**Figure 5.7E**; Two-way ANOVA, main effect of age: $F_{5,149} = 42.18$, $p < 0.0001$), but was comparable in PS and control animals (main effect of PS: $F_{1,149} = 3.10$, $p > 0.05$). AP 10-90% rise time also decreased with age, around 25% from P10 to P21 (**Figure 5.7F**; Two-way ANOVA, main effect of age: $F_{5,150} = 25.97$, $p < 0.0001$) but exhibited no effect of PS ($F_{1,150} = 2.02$, $p > 0.05$). Similarly, AP 90-10% decay time decreased more than two-fold with age, from approximately 1.8 ms at P10 to approximately 0.7 ms at P28 and P60 (**Figure 5.7G**; Two-way ANOVA, main effect of age: $F_{5,149} = 53.28$, $p < 0.0001$). AP decay times tended to be faster at P28 and P60 in PS animals, but the effect was not significant (main effect of PS: $F_{1,149} = 3.09$, $p > 0.05$).

5.4.3 PS reduced excitability of BLA principal neurons in adulthood

We also measured neuronal excitability in patch clamped neurons by eliciting trains of action potentials with direct current injection (**Figure 5.8**). By injecting depolarizing current into

principal neurons at resting membrane potential, we were able to calculate rheobase, the minimum current required to elicit an action potential. We found an age-dependent increase in the rheobase. There was nearly a full order of magnitude increase in rheobase by P60 from initial values of 24.4 ± 4.3 pA in control pups and 28.8 ± 3.4 pA in PS pups at P10 (**Figure 5.8A**; Two-way ANOVA, main effect of age: $F_{5,135} = 53.55$, $p < 0.0001$). There was a significant interaction of age and PS, such that neurons from PS animals had a rheobase nearly twice as large as those from controls at P60 but not earlier (323.3 ± 32.0 pA vs. 176.3 ± 17.7 pA for controls, Bonferonni post-test, $p < 0.01$; Two-way ANOVA, interaction effect: $F_{5,135} = 3.24$, $p < 0.01$).

By increasing the magnitude of the direct current injections, we determined the maximum steady-state action potential frequency for BLA principal neurons (**Figure 5.8B**). There was a significant increase with age but no effect of PS (Two-way ANOVA, main effect of age: $F_{5,128} = 10.93$, $P < 0.0001$; main effect of stress: $F_{1,128} = 0.02$, $p > 0.05$). However, neurons from PS rats required more current to elicit the maximum spike rate, consistent with the reduced excitability already observed; this effect of PS was most evident at P60, when PS neurons required 44% more current than controls (**Figure 5.8C**; 1582 ± 113 pA vs. 1100 ± 184 pA for controls; Two-way ANOVA, main effect of stress: $F_{1,128} = 5.32$, $p < 0.05$). The reduced excitability in mature neurons from PS rats is clearly portrayed by their F-I curves, with right-shifted curves for PS neurons at P28 and P60 relative to controls (**Figure 5.8D**).

5.4.4 PS altered the developmental trajectory of GABAergic transmission in the BLA

Considering the role of GABAergic transmission in coordinating neural development, we sought to determine if early deficits in this neurotransmitter system were caused in the BLA by PS (**Figure 5.9**). We began by characterizing the waveforms of $GABA_A$ receptor-mediated postsynaptic currents (PSCs) in developing BLA principal neurons (**Figure 5.9A**). Stimulation-evoked $GABA_A$ PSCs from control animals had consistent kinetics across the first postnatal month but became slower in adulthood (**Figure 5.9B**; Two-way ANOVA, main effect of age:

$F_{5,142} = 3.9$, $p < 0.01$). Interestingly, $GABA_A$ PSCs were significantly slower in neurons from PS rats relative to those from control rats, specifically during a window early in the first postnatal month, but were faster than in neurons from control rats in adulthood. As shown in **Figure 5.9C**, at P14 the decay time constant of $GABA_A$ PSCs was 59% larger in neurons from PS animals (15.7 ± 2.3 ms) than those from controls (9.8 ± 1.8 ms, Bonferroni post-test, $p < 0.05$; Two-way ANOVA, interaction effect: $F_{5,142} = 2.79$, $p < 0.05$). **Figure 5.9D** depicts $GABA_A$ PSCs in neurons at P60, when the effect of PS is reversed compared to P14: decay time constants are 39% smaller in neurons from PS animals at P60 (10.7 ± 1.3 ms) than those from controls (17.4 ± 3.4 ms, Bonferroni post-test, $p > 0.05$).

We also investigated the effect of PS on synaptic plasticity of GABAergic transmission in the developing BLA (**Figure 5.10**). We have previously shown a developmental change in short-term plasticity of $GABA_A$ receptor-mediated PSCs in the BLA, such that immature PSCs exhibit short-term depression that is lost with age (Ehrlich et al., 2013). As expected, in neurons from control animals we found short-term depression of the fifth pulse of a train of 20Hz $GABA_A$ PSCs at P10 (66% of pulse 1), P14 (72% of pulse 1), and P17 (94% of pulse 1) that was lost by P21 (102% of pulse 1; **Figure 5.10A**; Two-way ANOVA, main effect of age: $F_{5,129} = 7.02$, $p < 0.0001$). However, short-term depression was also present at P60 (75% of pulse 1), creating an inverted-U of pulse ratio vs. age.

PS had no significant effect on short-term plasticity of $GABA_A$ receptor-mediated PSCs. However, PS tended to promote short-term facilitation during a specific developmental window, increasing the amplitude of pulse 5 relative to pulse 1 starting at P21 (**Figure 5.10A**; Two-way ANOVA, main effect of PS: $F_{1,129} = 2.59$, $P > 0.05$). As illustrated in **Figure 5.10B**, PSCs in a number of neurons from PS animals at P21 and P28 exhibited short-term facilitation, a phenomenon scarcely observed in neurons from control animals. At P21, only 1 of 9 control neurons exhibited PSCs with short-term facilitation greater than 15% (on average, 102 ± 18% of pulse 1) while 6 of 14 PS neurons exhibited such a facilitation (on average, 131 ± 27% of pulse

1). For trains of IPSCs elicited at 50Hz, a similar developmental trajectory to 20Hz trains was observed for both control and PS neurons, but short-term depression was present at all ages and in both groups, such that the curves were shifted lower on the y-axis (**Figure 5.10C**).

5.4.5 PS reduced BLA expression of the $GABA_A$ receptor α1 subunit during a development critical period

The timing of developmental critical periods is regulated by $GABA_A$ receptors containing the α1 subunit (Fagiolini et al., 2004). Having observed the postnatal emergence of some effects of PS on emotional behavior and BLA neuron physiology, namely principal neuron excitability and kinetics and plasticity of GABAergic transmission, we hypothesized early changes to α1 subunit expression in the BLA could contribute to the altered developmental trajectory following PS. We characterized expression of mRNA for the α1 subunit in the BLA of PS and control rats across postnatal development using quantitative RT-PCR (**Figure 5.11**). PS caused a significant and robust reduction in α1 expression, beginning around P17 (**Figure 5.11A**; Two-way ANOVA, main effect of PS: $F_{1,20} = 14.13$, $P < 0.01$). Expression of α1 subunit mRNA in the BLA at P10 and P14 was only reduced in PS animals by 1.17- and 1.27-fold, respectively; by P17, α1 expression was reduced by 2.47-fold in the BLA of PS animals relative to controls, and this reduction increased to 3.19- and 3.45-fold by P21 and P60, respectively (**Figure 5.11B**).

5.5 Discussion

We have provided the first evidence that amygdala electrophysiology is altered by ELS. By characterizing developmental trajectories, we identified age-specific changes to GABAergic transmission and receptor expression in the infant BLA due to PS. Considering the role of the GABA system in shaping circuit maturation, these effects of PS are likely to influence other aspects of amygdala development. In addition, we identified changes due to PS to neuronal intrinsic physiology as early as P10 and found reductions in BLA neuronal excitability that emerge in adolescence. Our PS paradigm reduced amygdala-dependent behavior, in agreement with reduced BLA principal neuron excitability, suggesting the effects of PS reported here may underlie the risk it confers for psychiatric disorders, including SZ and ASDs. The results of this study are summarized in **Figure 5.12**.

5.5.1 PS Reduces Anxiety-Like Behavior and May Reduce Sociability

We found that PS significantly reduced anxiety-like behavior in offspring, manifested as increased time spent on the open arms of the EPM and more head dips. While a number of studies have described anxiogenic studies of PS (Zagron and Weinstock, 2006; Baker et al., 2008; Darnaudery and Maccari, 2008), there is also a precedent for anxiolytic effects. For example, in one study PS throughout gestation had an anxiolytic effect on the EPM in male offspring, increasing the time spent in open arms (Estanislau and Morato, 2006). In another study, PS on the last 11 days of gestation significantly increased the number of head dips in the open arm of the plus maze (Mairesse et al., 2007). Reduced anxiety-like behavior in adulthood may be due to dampened amygdala activity, and we observed reduced excitability of BLA neurons in adult PS offspring. Interestingly, a study comparing predictable and unpredictable stress restricted to the last week of gestation found that the predictable stressor elicited the most robust increase in anxiety-like behavior and stress reactivity (Richardson et al., 2006), suggesting the effects we

observed here may be caused by unpredictable stress application late in gestation. Future studies will be required to address whether the anxiolytic effect of PS constitutes dampened emotionality, or instead reflects stress inoculation and increased resilience or increased risk-taking behavior.

We also found a trend toward reduced anxiety-like behavior in PS offspring as measured by isolation-induced USVs, considered an expression of anxiety-like states (Hofer et al., 2002). Although this data is preliminary, PS rats at P17 tended to exhibit fewer calls than age-matched controls upon separation from their litters. In contrast, at P7 very little difference was observed, raising the possibility that the anxiolytic effects of PS emerge between P7 and P17. Interestingly, alterations to GABAergic transmission in the BLA emerged around P17, which may underlie the effect on anxiety-like behavior. PS has been previously shown to suppress USVs in pups at P14, and was interpreted by Morgan and colleagues as an expression of behavioral inhibition (1999). Isolation-induced USVs are an inherently social behavior (Hofer et al., 2002; Harmon et al., 2008) and reduced USVs may alternatively reflect ASD-like deficits. Less frequent USVs have been previously reported in rodent models of ASDs (Umeda et al., 2010; Higashida et al., 2011). Diminished USVs in rat pups may model the lack of crying observed in some children with ASDs (Crawley, 2007).

As another indication of reduced social behavior in our PS animals, we found a trend towards decreased sociability. PS rats spent less time interacting with conspecifics in the social choice test, and may have reduced preference for a novel conspecific over a novel, inanimate object. Additional studies are needed to support this preliminary finding. If confirmed, these data would further suggest our PS paradigm reduces social behavior and models some aspects of ASDs (Moy et al., 2004; Moy et al., 2009; Mines et al., 2010; Ryan et al., 2010). Interestingly, reduction of BLA inhibition and ablation of a subset of interneurons corresponded with reduced sociability (Truitt et al., 2007), suggesting amygdala inhibition contributes to the proper function of the amygdala in social processing. We found alterations to GABAergic transmission in the

adult BLA and as early as P14, and identified potential deficits in social behavior at P17 and adulthood but not before P14.

5.5.2 PS Alters Electrophysiological Properties of Developing BLA Neurons

We identified a number of changes to electrophysiological properties of BLA neurons due to PS, some detectable throughout development and some beginning at specific ages. RMP and AP threshold typically become more hyperpolarized in BLA principal neurons across the first few postnatal weeks (Ehrlich et al., 2012), and both were more hyperpolarized in PS animals than controls throughout development. The effect of PS on RMP and AP threshold was around 1-2 mV on average at each time point. Corroborating the effect on AP threshold, AP amplitude was also increased due to PS, possibly reflecting greater expression of voltage-gated sodium currents mediating the AP. Conversely, there was no effect of PS on input resistance or membrane time constant; both properties exhibited the normative decrease with age until around P21.

Shifting RMP more hyperpolarized should serve to make BLA principal neurons less excitable, while the same change to AP threshold should increase excitability. Therefore, these two effects may negate each other, with no net change in neuron excitability. Supporting this notion, rheobase, a measure of neuronal excitability, was unaffected by PS in neurons before P28, despite the early changes to RMP and AP threshold. However, the effect of PS on AP threshold may function to shift the operational voltage range of these neurons, thereby reducing the influence on action potential generation of currents that are normally active near threshold, like I_T and I_A. The lack of effect of PS on rheobase suggests no direct effect on neuronal excitability, but interfering with the propensity to activate I_T and I_A may reduce the propensity of a neuron to exhibit membrane potential oscillations, which are critical for the mature function of BLA principal neurons (see **Chapter 6**).

PS also caused a non-significant increase in the amplitude of the fAHP at P28 and P60. The larger fAHP may be due to the larger AP amplitude, providing greater activation of voltage-

gated potassium channels that repolarize the AP and contribute to the AHP. However, the larger fAHP may also reflect direct alterations in the expression of those potassium channels, including the delayed rectifier, K_V3 family. A larger fAHP would be expected to increase maximum spike rate and the expression of high-frequency doublet firing. However, while maximum spike rate nearly doubled from P10 to P21, as we have previously reported (Ehrlich et al., 2012), we observed no difference in maximum spike rates due to PS.

As mentioned above, PS increased the rheobase of BLA principal neurons at P28 and P60 without any effect on maximum spike rate. Clearly illustrated in the F-I curves for neurons at P28 and P60, PS right-shifted the curves, reflecting greater current required to elicit any given spike rate. Reduced excitability was found at P28 and P60 despite no reduction of input resistance, suggesting voltage-gated currents regulating inter-spike intervals, like I_A, are altered in adulthood by PS. Diminished excitability of BLA output neurons at P60 may underlie the reduced anxiety observed in the EPM and trend towards reduced sociability, as amygdala activation is known to contribute to these behaviors. Importantly, SZ patients exhibit a deficit in amygdala activation to social and emotional stimuli (Schneider et al., 1998; Baas et al., 2008; Rasetti et al., 2009), and the effect of treatment to reduce the deficit in amygdala activation predicts the behavioral benefit for individual patients (Hooker et al., 2013). Amygdala hypo-activation in SZ may be recapitulated by the reduced BLA neuron excitability seen in our adult PS animals.

Interestingly, the reduction of BLA principal neuron excitability following PS was not observed until P28, suggesting it may occur downstream of earlier deficits. Specifically, increased rheobase may occur downstream of the reduction of $GABA_A$ receptor α1 subunit expression, initially observed around P17 and persisting into adulthood. Reduced α1 expression may lead to BLA principal neuron hyperexcitability, because α1-containing receptors are preferentially found in perisomatic inhibitory synapses with PV^+ terminals (Nusser et al., 1996; Fritschy et al., 1998; Pawelzik et al., 1999; Thomson et al., 2000; Nyiri et al., 2001; Klausberger

et al., 2002). The reduction in intrinsic excitability starting in late adolescence may be a homeostatic response to increased excitability due to loss of inhibitory synaptic transmission.

5.5.3 PS Alters GABAergic Transmission and Receptor Expression in the BLA

We found that stimulation-evoked IPSCs exhibited a different developmental trajectory from spontaneous IPSCs, which we reported previously. While spontaneous IPSCs in BLA principal neurons become faster from P14 to P21, corresponding with emergence of the $GABA_A$ receptor α1 subunit (Ehrlich et al., 2013), evoked IPSCs in control animals have consistent kinetics across the first postnatal month and are slower at P60. These data in the control condition constitute a novel finding, and are consistent with findings from a similar study in the developing visual cortex, in which $GABA_A$ receptor-mediated IPSCs were also recorded with local stimulation and pharmacological isolation (Jang et al., 2010). Jang and colleagues found an approximately two-fold increase in IPSC decay time constant from P21 to P60, comparable to the 1.98-fold increase we found across the same window. In addition, a study of GABAergic transmission in the developing hippocampus reported the emergence during the first postnatal month of a slow $GABA_A$ receptor-mediated IPSC. Like our slow IPSCs, these could be elicited with electrical stimulation, and the kinetics of this IPSC became slower with age (Banks et al., 2002).

The stimulation paradigm employed here and by Jang and colleagues clearly measures distinct aspects of GABAergic transmission than recording spontaneous IPSCs, and the underlying cause for slower IPSCs in adulthood is as of yet unknown. Maturation of stimulation-evoked IPSC kinetics is clearly not reflective of $GABA_A$ receptor subunit expression, but may rather reveal diminished efficiency of the GABA uptake system or increased activation of extrasynaptic GABA receptors (Roepstorff and Lambert, 1994). The slow IPSCs at P14 may reflect a shift of inhibitory synapses distally in the dendritic arbor, increasing filtering. A shift more distally could be caused by accelerated expansion of BLA principal neuron dendritic arbors

or a relative decrease of perisomatic inhibition due to delayed emergence of PV^+ interneurons. The number of perisomatic synapses is typically reduced at critical period onset (Katagiri et al., 2007), and this process may be exaggerated in PS animals. The slow, evoked IPSC in adulthood may also be due to a shift in the presynaptic population recruited by stimulation towards distal dendrite-targeting interneurons, either due to emergence of interneuron subtypes, maturation of axon collateralization, or changes to interneuron excitability. The electrophysiological properties and axon collateralization of PV^+ interneurons, for example, are known to change postnatally (Doischer et al., 2008; Kuhlman et al., 2010), which may influence their likelihood to be recruited by local stimulation or of synapsing on a given postsynaptic neuron. Interestingly, slow inhibition is mediated in the mature BLA by neurogliaform cells, a subset of interneurons (Manko et al., 2012). Neurogliaform cells may emerge between P28 and P60 to provide the slow inhibition we observed upon stimulation. Future studies will be required to measure spontaneous IPSCs, to determine whether a distinct population of slow IPSCs emerges after P28 or IPSCs become slower across the board.

The normative trajectory of development of IPSC kinetics was altered by PS. A transient expression of very slow IPSCs was found around P14 in BLA principal neurons from PS animals. The early expression of slow IPSCs will likely influence the excitatory-inhibitory balance in the developing BLA and may therefore alter the subsequent maturation of GABAergic synapses (for review, see Hensch, 2005). The change of IPSC kinetics at P14 due to PS may act upstream of the profound reduction of $GABA_A$ receptor α1 expression first observed at P17. In addition, the slow IPSCs normally expressed in adulthood were not observed in PS animals, which exhibited consistent kinetics from P21 to P60. These changes will likely influence the ability of IPSCs to regulate principal neuron activity in the mature BLA (see **Chapter 6**). Considering the explanations proposed above for the slow IPSCs observed at P60, PS may prevent the emergence of neurogliaform cells in the BLA or reduce GABA spillover and activation of extrasynaptic $GABA_A$ receptors. Diminished extrasynaptic $GABA_A$ receptor activation may contribute to the

pathophysiology of SZ, as activation of this receptor population reverses memory deficits in animal models (Damgaard et al., 2011). As stated above, the underlying causes of these changes to IPSC kinetics following PS are unknown. Future studies will be necessary to identify a structural correlate of the change in IPSC kinetics due to PS.

In addition to IPSC kinetics, PS tended to alter the development of short-term plasticity of IPSCs. We observed an increase in pulse ratio constituting a loss of short-term depression across the first postnatal month in control animals, as we reported previously (Ehrlich et al., 2013). In neurons from PS animals, IPSCs elicited at 20 Hz exhibited short-term facilitation at P21 and P28, which was not observed in control animals. In neurons from both PS and control animals, short-term depression re-emerged between P28 and P60, although the pulse ratio remained greater in the PS group. Previous studies did not proceed into adulthood to observe this novel re-emergence of synaptic depression. The same trajectory was observed for IPSCs elicited at 50 Hz, although pulse ratios were generally smaller, likely due to depletion of docked synaptic vesicles (Zucker and Regehr, 2002; Elfant et al., 2008). Short-term plasticity is known to influence information processing in neurons (Rothman et al., 2009), suggesting PS alters the function of GABA in the amygdala during adolescence. Short-term facilitation and depression occur simultaneously and act in direct opposition, and PS may act to either promote facilitation or block depression in adolescence.

The degree of synaptic facilitation is inversely correlated with the release probability of a synapse and generally also with neurotransmitter output (Dobrunz and Stevens, 1997; Zucker and Regehr, 2002), so GABAergic release in the BLA may be diminished starting at P21 in PS animals relative to controls. Sensory experience is known to trigger the loss of short-term depression of IPSCs during development (Jiang et al., 2010; Sanes and Kotak, 2011), and we suggest precocious activation of the BLA following ELS exposure may accelerate the typical developmental reduction of GABA release probability. Furthermore, parvalbumin is known to suppress short-term facilitation of GABAergic synapses (Caillard et al., 2000; Vreugdenhil et al.,

2003; Collin et al., 2005; Orduz et al., 2013) and begins to emerge in the BLA around P17, when short-term depression is lost (Berdel and Morys, 2000; Davila et al., 2008). We suggest PS interferes with the emergence of parvalbumin expression in the BLA, which could contribute to the short-term facilitation in PS animals that begins following P17. We found expression of the $GABA_A$ receptor α1 subunit, which is preferentially enriched at perisomatic inputs from PV^+ interneurons, is reduced starting at P17, which may also reflect the loss of parvalbumin (Nusser et al., 1996; Fritschy et al., 1998; Pawelzik et al., 1999; Thomson et al., 2000; Nyiri et al., 2001; Klausberger et al., 2002).

PS altered the expression of $GABA_A$ receptors, causing a reduction in the expression of the α1 subunit greater than two fold starting at P17. As mentioned above, this decrease is first observed when expression of α1 and parvalbumin typically emerge. These findings corroborate a recent study by Laloux and colleagues investigating $GABA_A$ receptor α1 protein expression in the amygdala (2012). Interestingly, Laloux and colleagues reported no effect at P14 but a trend towards reduction at P22, supporting the appearance of a PS effect around P17. They were investigating the whole amygdala and found a non-significant decrease in α1 expression, suggesting this effect of PS may be specific to the BLA, where we focused. Early postnatal stress has been shown to reduce expression of the α1 subunit in the adult amygdala and hippocampus, and our findings suggest the impact of ELS may begin well before adulthood (Caldji et al., 2003; Hsu et al., 2003). In transgenic mice lacking the α1 subunit, cortical circuits are impaired in their ability to organize gamma oscillations (Bosman et al., 2005a), which have been observed in the BLA during the expression of fear and are likely perturbed following PS (Madsen and Rainnie, 2009; Sangha et al., 2009; Pape and Pare, 2010). The reduction of α1 expression in the developing and adult BLA due to PS may therefore contribute to the reduced anxiety-like behavior we observed in those animals. Interestingly, human SZ patients exhibit reduced $GABA_A$ receptor α1 subunit expression (Glausier and Lewis, 2011) and a rodent model of Fragile X syndrome displays reduced α1 expression beginning around P17 (Vislay et al., 2013).

Furthermore, a rodent model of SZ including several aspects of disease pathophysiology is produced simply by $GABA_A$ receptor blockade in the BLA (Berretta and Benes, 2006). These findings suggest the effects of PS to reduce α1 expression in the developing BLA may influence emotional outcomes and contribute to ASD and SZ etiology.

The $GABA_A$ receptor α1 subunit plays a key role in regulating critical periods in development (Hensch, 2005). The reduction of α1 following PS may lead to delayed critical period closure in the BLA. Reducing excitability of PV^+ interneurons by disrupting PNNs causes re-opening of a developmental critical period (Pizzorusso et al., 2002), an effect mimicked simply by $GABA_A$ receptor antagonists (Harauzov et al., 2010). These studies suggest the reduction in α1 caused by PS in the developing BLA could extend a critical period for amygdala development. The closure of critical periods in the BLA, reflected by the emergence of PV^+ interneurons and PNNs, is known to trigger developmental changes to extinction learning (Gogolla et al., 2009). PS may therefore delay the emergence of mature forms of extinction learning, which has been shown following stress during infancy (Callaghan and Richardson, 2011, 2012). Changes to critical period timing may also influence plasticity in the adolescent BLA and have long-term impact on connectivity between the BLA and regions with late-developing inputs, like the PFC (Bouwmeester et al., 2002b; Cunningham et al., 2002, 2008). Finally, altered GABAergic transmission or critical period timing due to PS may perturb the excitability of the developing BLA, resulting in the reduction in BLA principal neuron excitability we observed starting at P28. Future studies will need to address the emergence of parvalbumin and PNNs in the BLA following PS.

The effects observed here may be unique to our PS paradigm, and future studies are required to elucidate the specific aspects of this paradigm, be they timing, intensity, predictability, or sex of the offspring, that contribute to the deficits we observed. Together, our findings on the effects of PS on amygdala development and offspring emotional behavior suggest dysfunction of the developing BLA contributes to emotional dysfunction and the etiology of

neurodevelopmental disorders like SZ and ASDs. PS is a known risk factor for a variety of other psychiatric disorders, including anxiety, depression, attention deficit hyperactivity disorder, many of which also involve amygdala dysfunction (Weinstock, 2001; O'Connor et al., 2003; Van den Bergh and Marcoen, 2004; Huizink et al., 2007; Ronald et al., 2010; Markham and Koenig, 2011). Together, these findings suggest early changes to BLA neuron excitability and GABAergic transmission contribute to later deficits in amygdala function and emotional behavior.

Looking ahead, hypotheses about how the changes due to PS influence the function of the amygdala must be considered in the context of the role of GABAergic transmission in shaping the function of the BLA network. As described in **Chapter 2**, the production of network oscillations in the BLA is critically involved in the generation of fear states and emotional learning. In **Chapter 6** we show that, while GABAergic transmission can function to reduce firing rates, it can also facilitate output of the BLA by organizing the activity of groups of neurons into network oscillations. By altering network oscillations in the BLA, changes to GABAergic transmission and principal neuron physiology may influence the development of the BLA and emotional behavior.

Figure 5.1 Prenatal Unpredictable Shock Stress Paradigm

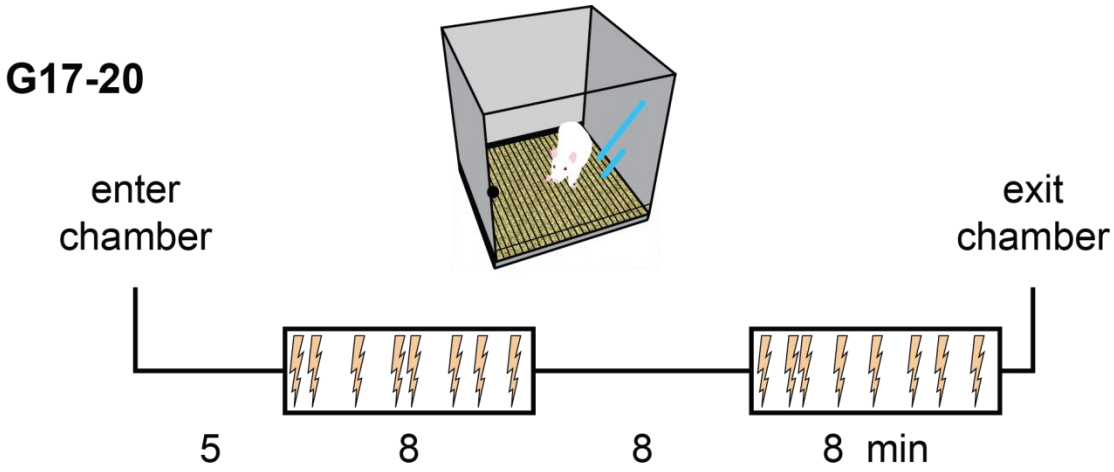

Figure 5.1 Prenatal Unpredictable Shock Stress Paradigm. Pregnant dams were placed in an operant conditioning chamber on embryonic days (E)17-20 to receive 16 pseudo-random footshocks, separated into two blocks as depicted. Non-stressed controls were placed in the chamber but received no shocks.

Figure 5.2 Increased body weight in PS rats.

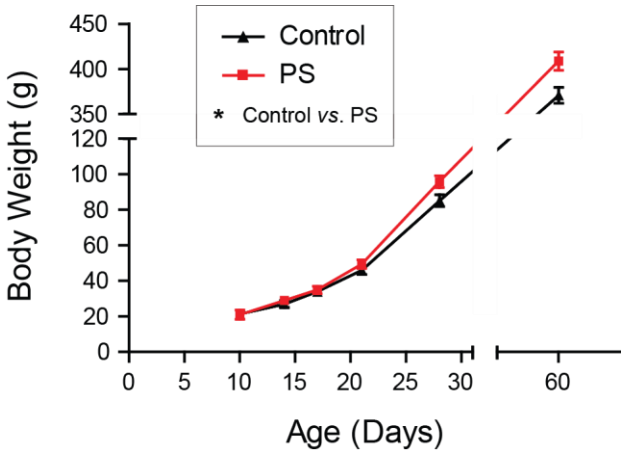

Figure 5.2 Increased body weight in PS rats. Body weight, depicted as a function of age, was significantly larger in PS rats than controls (Two-way ANOVA, main effect of PS: $F_{1,69} = 4.09$; $p < 0.05$). At P60, there was a 10.2% increase in body weight due to PS (408.9 ± 40.7 g for PS vs. 371.1 ± 32.7 g for control). 14 ≤ N 16.

Figure 5.3 PS had an anxiolytic effect in adult rats in the elevated plus-maze (EPM).

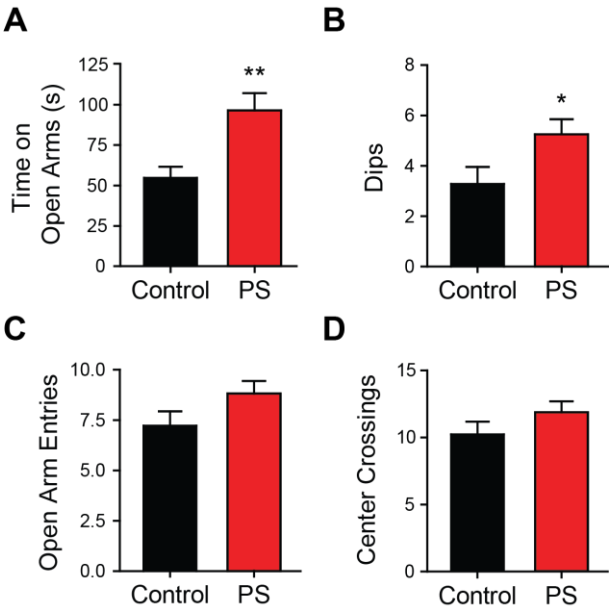

Figure 5.3 PS had an anxiolytic effect in adult rats in the elevated plus-maze (EPM). (A) Time spent in open arms was significantly greater in PS animals compared to non-stressed controls (Mann-Whitney U test, $U_{32} = 60$, ** $p < 0.01$). (**B**) The number of dips made on the plus-maze by PS animals was significantly higher than those made by controls ($U_{32} = 85$, * $p < 0.05$). (**C, D**) There was no effect of PS on open arm entries (C) or locomotor activity as measured by center crossings (D). $16 \leq N \leq 18$.

Figure 5.4 PS tends to reduce ultrasonic vocalization of isolated pups during a developmental critical period.

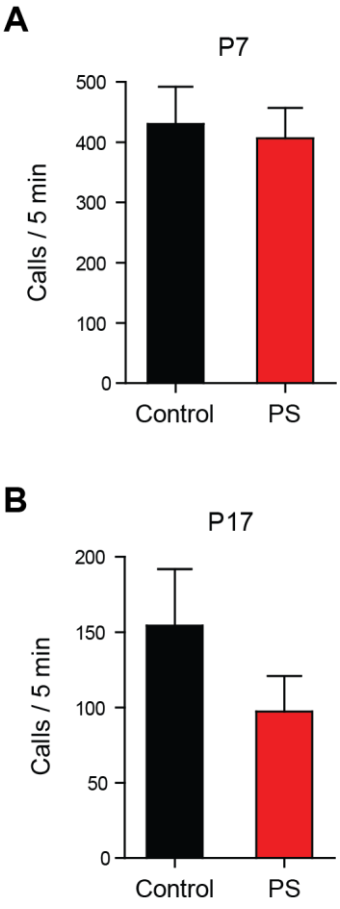

Figure 5.4 PS tends to reduce ultrasonic vocalization of isolated pups during a developmental critical period. (**A, B**) The number of USVs of the pups isolated from their litters are depicted for rats at P7 (A) and P17 (B). $7 \leq N \leq 12$.

Figure 5.5 Sociability in adult rat offspring exposed to PS.

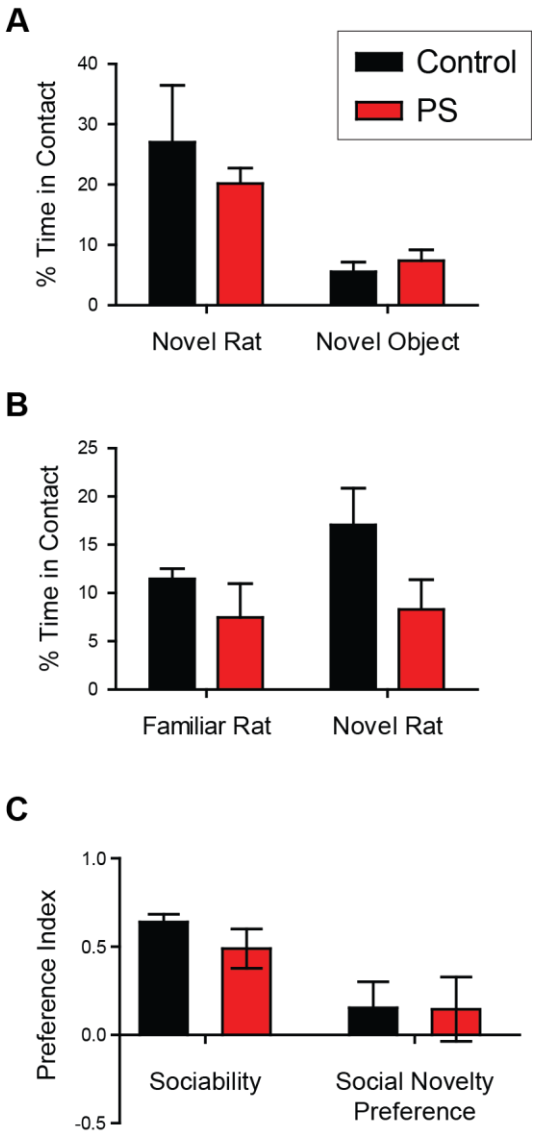

Figure 5.5 Sociability in adult rat offspring exposed to PS. (**A**) Interaction of control and PS rats with a novel object and conspecific is depicted from the sociability test. (**B**) PS rats spent less time interacting with other rats in the social choice test, and did not exhibit a preference for novel rats over familiar rats (Two-way ANOVA, main effect of PS: $F_{1,14} = 4.04$, $p = 0.06$). (**C**) Preference index is plotted for PS and control rats for the sociability and social choice tests. $4 \leq N \leq 5$.

Figure 5.6 The impact of PS on the developmental trajectory of intrinsic membrane properties of BLA principal neurons.

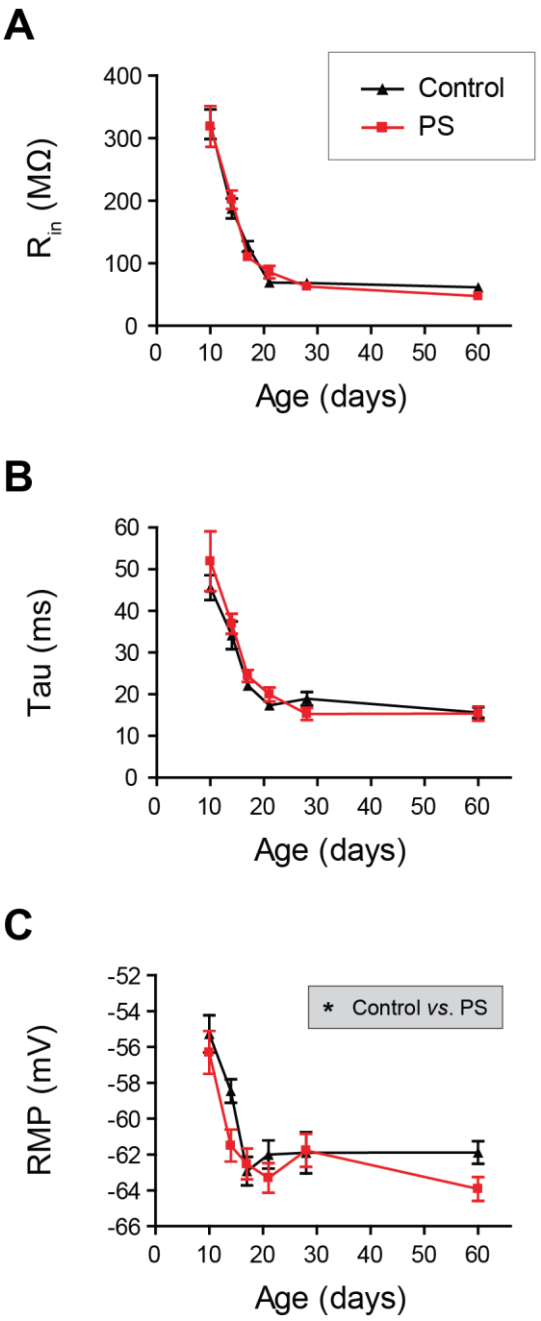

Figure 5.6 The impact of PS on the developmental trajectory of intrinsic membrane properties of BLA principal neurons. (**A, B**) There was no difference in the age-dependent changes to input resistance (R_{in}, A) or membrane time constant (B) in prenatally stressed rats compared to controls. (**C**) Resting membrane potential (RMP) was significantly more hyperpolarized across all ages in prenatally stressed rats compared to controls (Two-way ANOVA, main effect of stress: $F_{1,148} = 4.63$, $p < 0.05$). $7 \leq N \leq 19$.

Figure 5.7 The developmental trajectory of action potential (AP) properties of BLA principal neurons are altered by PS.

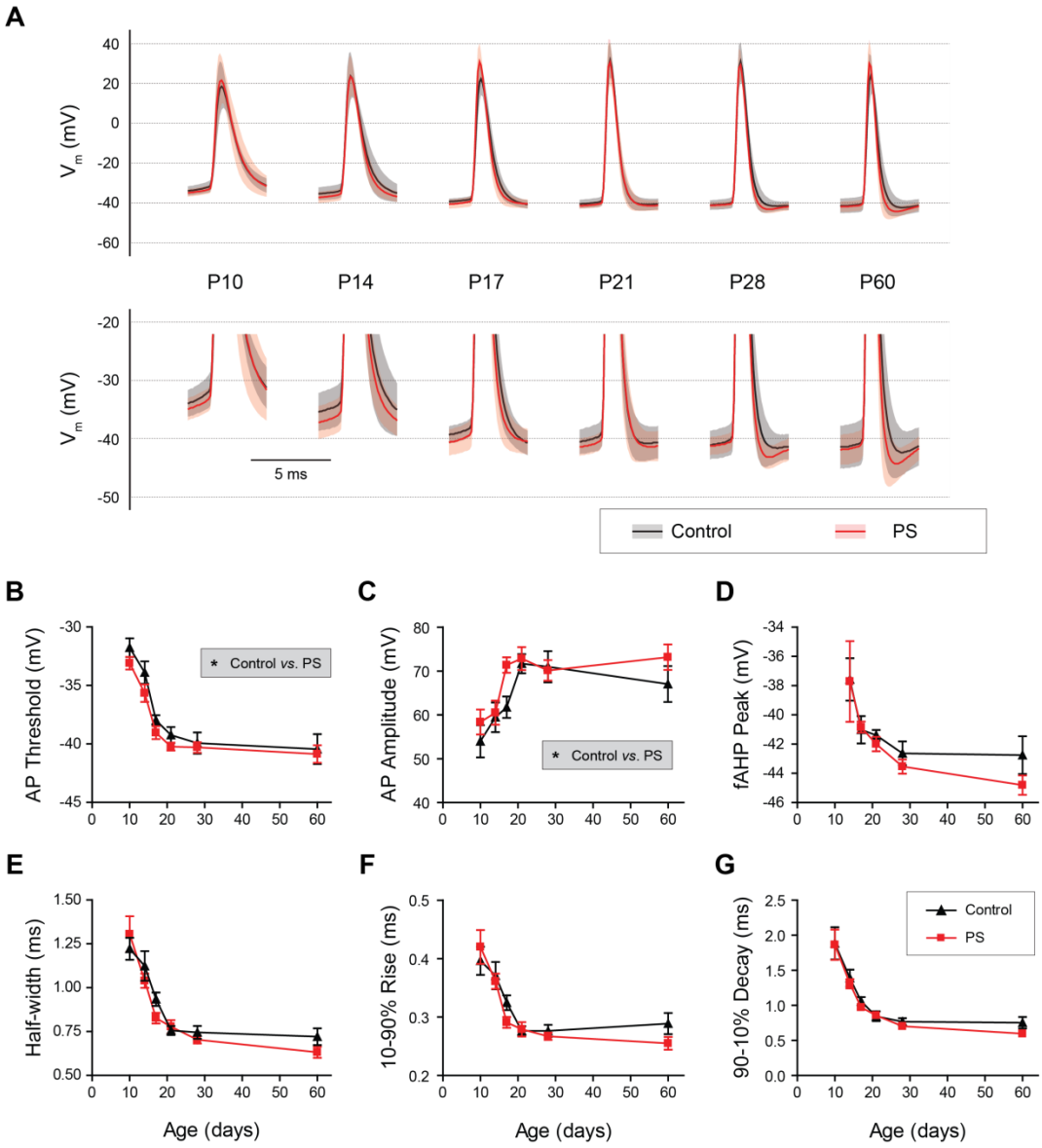

Figure 5.7 The developmental trajectory of action potential (AP) properties of BLA principal neurons are altered by PS. (**A**) AP waveforms, depicted as mean (solid line) and standard deviation (band), are shown for BLA principal neurons across postnatal development. The same data are shown at two resolutions to depict the full waveform (top) and the AP threshold and AHP (bottom). (**B**) AP threshold was significantly more hyperpolarized across all ages in PS animals (Two-way ANOVA, main effect of PS: $F_{1,146} = 5.85$, $p < 0.05$). (C) APs were significantly taller in PS animals ($F_{1,149} = 4.62$, $p < 0.05$). (D) The peak voltage deflection of the fAHP, for neurons in which one was detected, became more hyperpolarized with age but is unaffected by PS (Main effect of PS, $F_{1,66} = 2.34$, $p > 0.05$). (E-G) AP kinetics are plotted in terms of half-width (E), 10-90% rise time (F), and 90-10% decay time (G), but none of these metrics exhibit an effect of PS. $9 \leq N \leq 19$.

Figure 5.8 BLA principal neuron excitability was reduced in adulthood but not during development by PS.

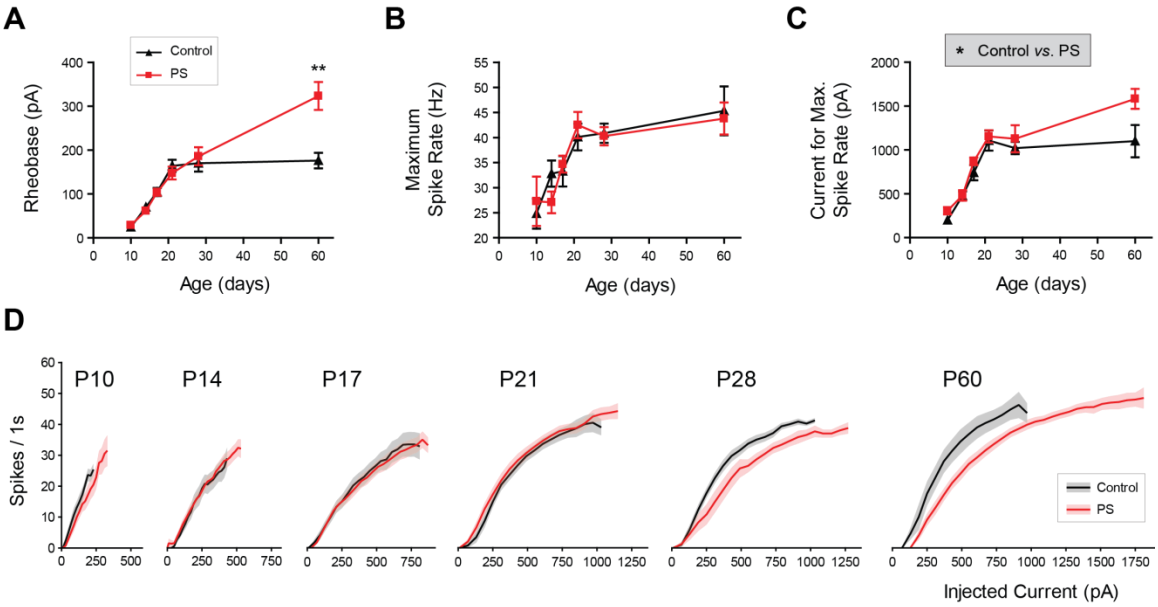

Figure 5.8 BLA principal neuron excitability was reduced in adulthood but not during development by PS. (**A**) The rheobase was significantly greater at P60 in neurons from offspring exposed to prenatal stress (Bonferroni post-test, ** $p < 0.01$; Two-way ANOVA, interaction effect: $F_{5,135} = 3.24$, $p < 0.01$). (**B**) The maximum spike rate increased with age but was not altered by prenatal stress. (**C**) The current injection required to elicit the maximum spike rate was greater for BLA principal neurons from PS rats (Two-way ANOVA, main effect of stress: $F_{1,128} = 5.32$, $p < 0.05$). (**D**) F-I curves are plotted for PS and control BLA principal neurons at each time point. Lines represent the mean and shaded bands represent the SEM for each group. $8 \leq N \leq 17$.

Figure 5.9 $GABA_A$ responses in BLA principal neurons are slower during development in PS rats.

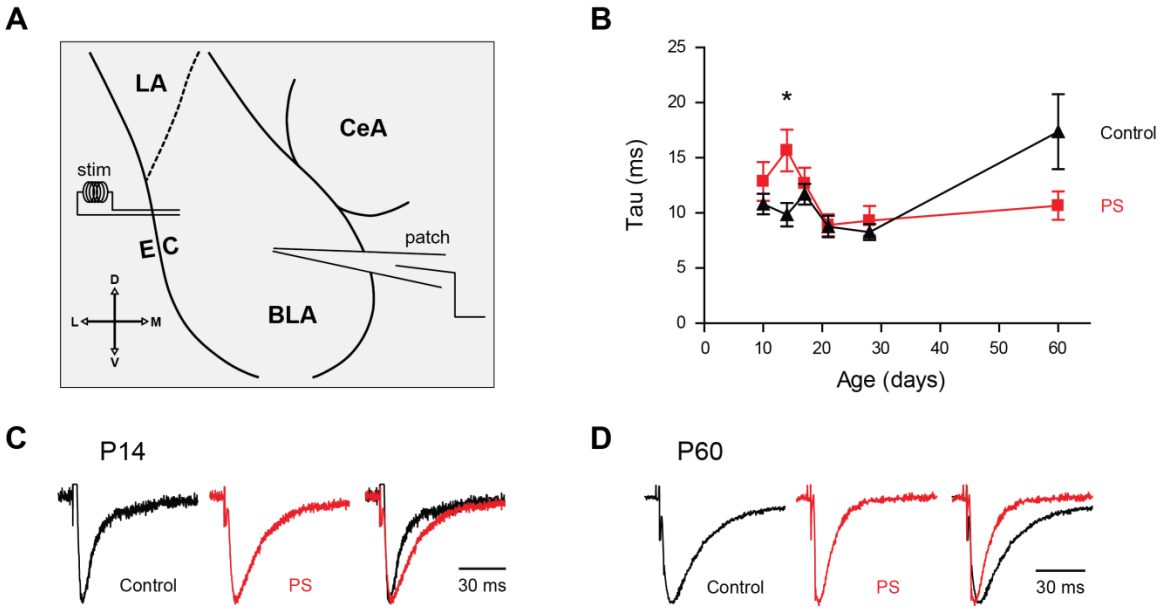

Figure 5.9 $GABA_A$ responses in BLA principal neurons are slower during development in PS rats. (**A**) Schematic of recording and stimulation sites. The stimulating electrode (stim) was placed medial to the external capsule (EC) within the BLA. The lateral nucleus (LA) and central nucleus (CeA) of the amygdala are also labeled. The compass gives directions for dorsal (D), ventral (V), lateral (L), and medial (M). (**B**) The decay time constant of stimulation-evoked IPSCs are depicted for BLA principal neurons across postnatal development. There was a significant interaction of age and prenatal stress (Two-way ANOVA, $F_{5,142} = 2.79$, $p < 0.05$). At P14, the decay time consant was significantly longer in neurons from prenatally stressed animals (Bonferroni post-test, * $p < 0.05$). $5 \leq N \leq 20$. (**C, D**) Representative PSCs (average of 5 sweeps) are illustrated for one PS and one control neuron at P14 (C) and P60 (D). Stimulation artifacts are cropped for clarity.

Figure 5.10 Effect of PS on short-term plasticity of $GABA_A$ PSCs.

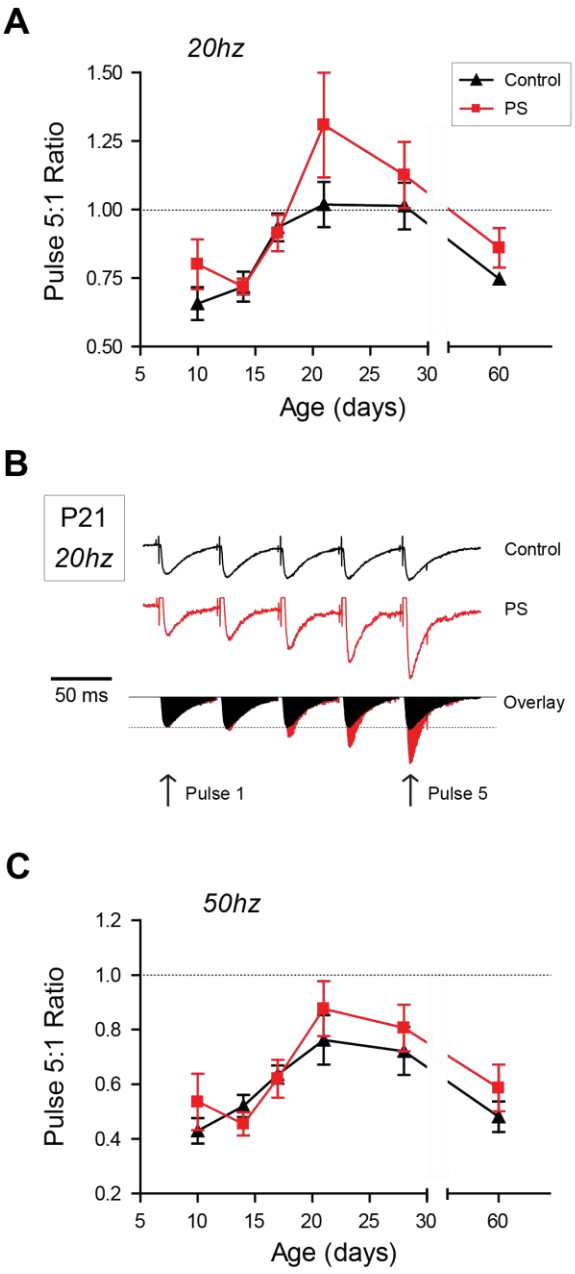

Figure 5.10 Effect of PS on short-term plasticity of $GABA_A$ PSCs. (**A**) Ratio of amplitudes of stimulation-evoked, $GABA_A$ receptor-mediated IPSCs in BLA principal neurons. The ratio of the peak amplitudes for pulse 5 and pulse 1 are depicted across postnatal development for neurons from prenatally stressed and control rats (not significant, Two-way ANOVA, main effect of stress: $F_{1,129} = 2.59$, $p = 0.11$). (**B**) Representative responses to 20hz stimulation for neurons from a prenatally stressed and control rat at P21. Stimulation artifacts were cropped for clarity. The area under the curve was filled to aid visual comparison across time points. (**C**) Similar to (A), ratios of the peak amplitudes of pulse 5 and pulse 1 are depicted for 50hz stimulation across postnatal development and for both groups. $2 \leq N \leq 9$.

Figure 5.11 PS reduces BLA expression of the $GABA_A$ receptor α1 subunit beginning at P17.

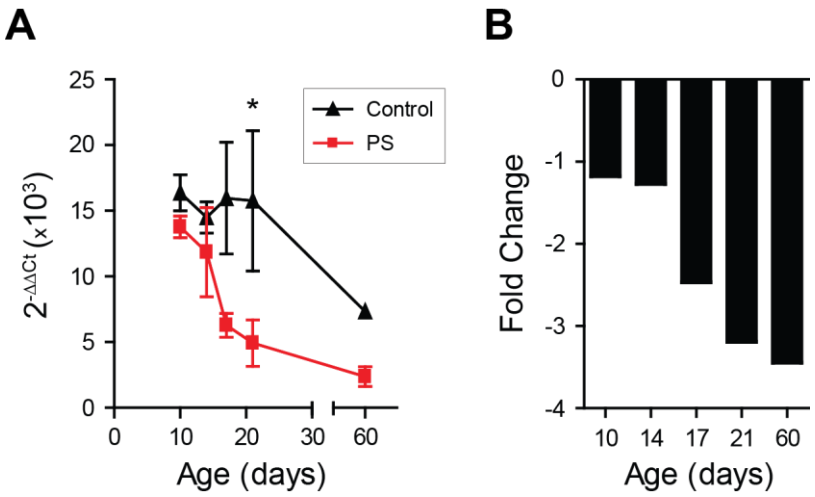

Figure 5.11 PS reduces BLA expression of the $GABA_A$ receptor α1 subunit from P17 onwards. (**A**) PS significantly reduced α1 subunit mRNA expression, depicted as $2^{-\Delta\,\Delta Ct}$, across all ages and specifically at P21, measured using real-time RT-PCR (Bonferroni post-test, * $p < 0.05$; Two-way ANOVA, main effect of stress: $F_{1,20} = 14.13$, $p < 0.01$). N = 3. (**B**) The effect of prenatal stress on α1 subunit mRNA is also expressed as fold change relative to controls.

Figure 5.12 Schematic of the effects of prenatal stress on BLA development

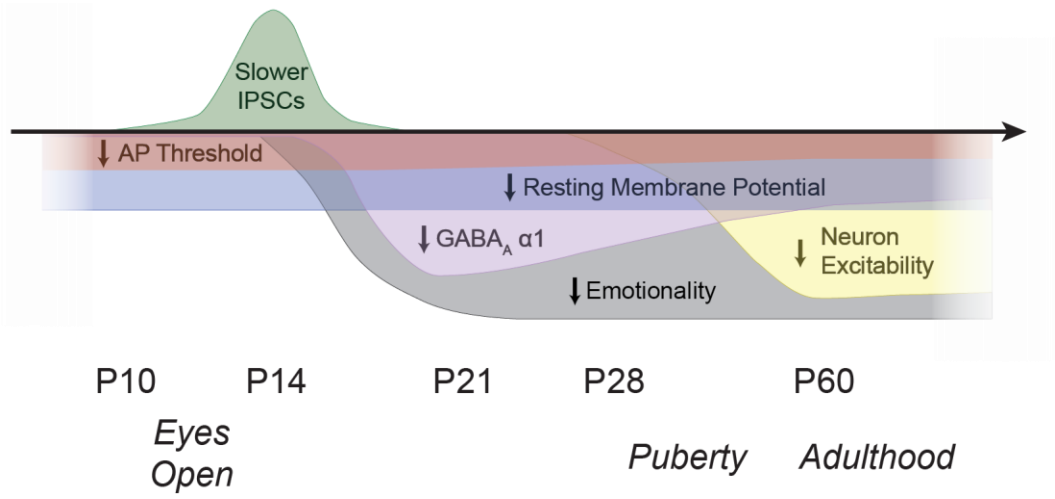

Figure 5.12 Schematic of the effects of prenatal stress on BLA development. The effects of prenatal stress in the BLA are represented as approximate trajectories, including increased duration of IPSCs around P14, reduced action potential (AP) threshold and resting membrane potential throughout development, decreased expression of the $GABA_A$ receptor α1 subunit, and reduced neuronal excitability starting around P28 and persisting into adulthood. Reduced emotionality is also included, based on reduced anxiety in the elevated plus-maze, decreased sociability in the social choice test, and fewer isolation-induced ultrasonic vocalizations.

Chapter 6: Spike-Timing Precision and Neuronal Synchrony are Enhanced by an Interaction between Synaptic Inhibition and Membrane Oscillations in the Amygdala[4]

[4] Adapted from Ryan SJ*, Ehrlich DE*, Jasnow AM*, Daftary S, Madsen TE, Rainnie DG (2012). Spike-timing precision and neuronal synchrony are enhanced by an interaction between synaptic inhibition and membrane oscillations in the amygdala. *PLoS One* 7 (4): e35320.

6.1 Abstract

The basolateral complex of the amygdala (BLA) is a critical component of the neural circuit regulating fear learning. During fear learning and recall, the amygdala and other brain regions, including the hippocampus and prefrontal cortex, exhibit phase-locked oscillations in the high delta / low theta frequency band (~2-6 Hz) that have been shown to contribute to the learning process. Network oscillations are commonly generated by inhibitory synaptic input that coordinates action potentials in groups of neurons. In the rat BLA, principal neurons spontaneously receive synchronized, inhibitory input in the form of compound, rhythmic, inhibitory postsynaptic potentials (IPSPs), likely originating from burst-firing parvalbumin interneurons. Here we investigated the role of compound IPSPs in the rat and rhesus macaque BLA in regulating action potential synchrony and spike-timing precision. Furthermore, because principal neurons exhibit intrinsic oscillatory properties and resonance between 4 and 5 Hz, in the same frequency band observed during fear, we investigated whether compound IPSPs and intrinsic oscillations interact to promote rhythmic activity in the BLA at this frequency. Using whole-cell patch clamp in brain slices, we demonstrate that compound IPSPs, which occur spontaneously and are synchronized across principal neurons in both the rat and primate BLA, significantly improve spike-timing precision in BLA principal neurons for a window of ~300 ms following each IPSP. We also show that compound IPSPs coordinate the firing of pairs of BLA principal neurons, and significantly improve spike synchrony for a window of ~130 ms. Compound IPSPs enhance a 5 Hz calcium-dependent membrane potential oscillation (MPO) in these neurons, likely contributing to the improvement in spike-timing precision and synchronization of spiking. Activation of the cAMP-PKA signaling cascade enhanced the MPO, and inhibition of this cascade blocked the MPO. We discuss these results in the context of spike-timing dependent plasticity and modulation by neurotransmitters important for fear learning, such as dopamine.

6.2 Introduction

The basolateral complex of the amygdala (BLA) is a critical part of the neural circuit regulating fear learning (Miserendino et al., 1990; Campeau et al., 1992; Davis, 2000; LeDoux, 2000; Rodrigues et al., 2001), and recent evidence suggests that oscillatory activity of neurons in this region plays a key role in regulating affect in awake, behaving animals (for review, see Pape and Pare, 2010). More specifically, it is now evident that the amygdala, hippocampus, and prefrontal cortex produce coordinated high delta / low theta (4-5 Hz) oscillations during acquisition (Madsen and Rainnie, 2009) and retrieval (Sangha et al., 2009) of learned fear, which then diminish over the course of subsequent extinction learning. Significantly, phase-locked theta stimulation applied simultaneously to the amygdala and hippocampus disrupts fear extinction and prolongs the expression of learned fear (Lesting et al., 2011), further supporting a role of synchronized neural activity in the processes of fear learning and extinction. Moreover, synchronous theta oscillations during REM sleep in the period between fear acquisition and retrieval correlate with changes in fear expression, suggesting that theta oscillations are critical for successful consolidation of fear memory (Popa et al., 2010). Despite the importance of these low frequency oscillations to amygdala function and emotional learning, the mechanisms by which the BLA circuit generates rhythmic activity are largely unknown.

A common mechanism for generating network oscillations utilizes coordinated inhibitory input across multiple neurons to synchronize their action potential firing (Soltesz and Deschenes, 1993; Buzsaki, 1997; Penttonen et al., 1998; Pouille and Scanziani, 2001; Person and Perkel, 2005; Sohal et al., 2006; Szucs et al., 2009). The BLA is organized to exploit this phenomenon through the rhythmic interaction of excitatory principal neurons and inhibitory interneurons. BLA principal neurons exhibit compound, rhythmic, inhibitory postsynaptic potentials (IPSPs) that occur at a baseline frequency of 0.5-4 Hz that is sensitive to modulation by dopamine and serotonin (Rainnie, 1999b; Loretan et al., 2004; Muly et al., 2009). These rhythmic IPSPs are

driven by action potentials in local, burst-firing interneurons, which we have previously shown to express parvalbumin (PV^+) (Rainnie et al., 2006). PV^+ interneurons have several characteristics that enable them to influence the activity of large networks of BLA principal neurons synchronously: first, these interneurons make up approximately 40% of the total interneuron population and are distributed throughout the BLA; second, each PV^+ interneuron can innervate the soma and axon hillock of approximately 150 principal neurons (McDonald et al., 2005); finally, these interneurons are coupled electrically by gap junctions to create a functional syncytium (Muller et al., 2005; Woodruff and Sah, 2007a, b). Significantly, we and others have shown that, in paired recordings of rat BLA principal neurons, spontaneous IPSPs are highly synchronized (Rainnie, 1999a; Popescu and Pare, 2011), suggesting that the output of PV^+ interneurons may coordinate the activity of large numbers of principal neurons.

Synchronous IPSPs in large groups of BLA principal neurons could also facilitate network oscillations by interacting with intrinsic oscillations in principal neurons to promote rhythmic firing. Synaptic inhibition has previously been shown to shift the phase of intrinsic membrane potential oscillations (MPOs) (Stiefel et al., 2010), suggesting synchronized IPSPs could coordinate oscillations across neurons. Intrinsic MPOs have been shown to improve spike-timing precision (Volgushev et al., 1998; Schaefer et al., 2006), which is, in turn, important for spike-timing dependent plasticity (Dan and Poo, 2004) and signal processing in neural networks (Mainen and Sejnowski, 1995). BLA principal neurons display a highly consistent MPO (Pare and Gaudreau, 1996; Pape et al., 1998) and an intrinsic resonance (Pape and Driesang, 1998), both in the same high delta / low theta frequency band as network oscillations observed during fear learning. If these MPOs were to occur synchronously in groups of BLA neurons, network activity should be promoted at this highly relevant frequency. Considering that groups of cells can have their firing activity entrained by synchronized IPSPs (Hasenstaub et al., 2005), we chose to investigate the possibility that synchronized, rhythmic IPSPs entrain and phase-lock MPOs and coordinate firing activity in BLA principal neurons. Furthermore, we examine the underlying

currents and intracellular signaling cascades regulating these phenomena and discuss potential links to synaptic plasticity and fear learning.

6.3 Methods

6.3.1 Animals and housing conditions

Whole cell patch clamp recordings were obtained from 76 neurons from 48 rodents, and 46 neurons from 13 primates. Rodent experiments were conducted on tissue from male Sprague-Dawley rats at 5-7 weeks of age. All rats were group-housed 4 per cage in Plexiglas cages with corn cob (Bed-O-Cob) bedding. Rats had access to food and water ad libitum, and were maintained in a temperature controlled colony room on a 12:12 light:dark cycle. The primate tissue for this study was obtained from juvenile (18-36 months) Macaca mulatta monkeys of both genders. Primates used in this study were born into the breeding colony housed at the Yerkes National Primate Research Center Field Station and raised in normal social groups. They were provided with ad libitum access to food and water and monitored by the Yerkes Veterinary Staff. Animals used in this study were selected for sacrifice by the veterinary staff for failure to thrive and/or chronic diarrhea refractory to treatment as part of the animal care end-points approved for our monkey colony. Once identified, the animals were moved to the Yerkes Main Station and scheduled for sacrifice within the week.

Experiments for Figures 6.1 & 6.2 were performed in both rat and primate tissue, and the remainder of experiments were performed exclusively in rat tissue (see figure legends for details). The care of the animals and all anesthesia and sacrifice procedures in this study were performed according to the National Institutes for Health Guide for the Care and Use of Laboratory Animals and were approved by the Institutional Animal Care and Use Committee of Emory University.

6.3.2 Electrophysiological procedures

6.3.2.1 Preparation of acute BLA slices.

To obtain slices from the rat basolateral amygdala, animals were decapitated under isoflurane anesthesia (Abbott Laboratories, North Chicago, IL). The brains were rapidly removed and placed in ice-cold kynurenic acid-based artificial cerebrospinal fluid (KA-ACSF), which contained (in mM): NaCl (130), KCl (3.5), KH_2PO4 (1.1), $MgCl_2$ (6.0), $CaCl_2$ (1.0), $NaHCO_3$ (30), glucose (10), thiourea (0.8), sodium pyruvate (2), ascorbic acid (0.4), and kynurenic acid (2). The glutamatergic antagonist kynurenic acid was included in the KA-ACSF to suppress any excitotoxic effects of glutamate release that may occur due to tissue slicing. A block of tissue containing the BLA was then mounted in a Leica VTS-1000 vibrating microtome (Leica Microsystems, Bannockburn, IL), and 350 μm coronal slices were cut. Slices were hemisected and hand-trimmed to remove excess tissue dorsal to the amygdala. For the primate basolateral amygdala, the animals were sacrificed with an overdose of pentobarbital (100 mg/kg) and hand-cut blocks of tissue from the medial temporal lobe were mounted in a vibratome and 400 μm coronal slices were cut as previously described (Muly et al., 2009). Slices from both species were transferred to a holding chamber containing KA-ACSF at 32°C and gassed with a 95%/5% O_2/CO_2 mixture for 40 min before being placed in oxygenated regular ACSF (ACSF) at room temperature containing (in mM): NaCl (130), KCl (3.5), KH_2PO_4 (1.1), $MgCl_2$ (1.3), $CaCl_2$ (2.5), $NaHCO_3$ (30), glucose (10), thiourea (0.8), sodium pyruvate (2), and ascorbic acid (0.4).

6.3.2.2 Recording procedures.

For recording, slices were placed in a Warner Series 20 recording chamber (Warner Instruments, Hamden, CT) mounted on the fixed stage of a Leica DM-LFS microscope (Leica Microsystems, Bannockburn, IL). Slices were fully submerged and continuously perfused at a rate of 1-2 mL/min with heated (32°C) and oxygenated ACSF. Neurons were selected for

recording under IR-DIC illumination with a 40X water immersion objective. Images were captured with a Hamamatsu Orca ER CCD camera (Hamamatsu, Tokyo, Japan) controlled by SimplePCI software (Compix, Sewickley, PA). Whole cell patch-clamp recordings were conducted using thin-walled borosilicate glass-patch electrodes (WPI, Sarasota, FL) which were pulled on a P-97 Flaming / Brown micropipette puller (Sutter Instruments, Novato, CA). Patch electrodes had resistances ranging from 4-7 MΩ when filled with standard patch solution that contained (in mM): K-gluconate (138), KCl (2), $MgCl_2$ (3), phosphocreatine (5), K-ATP (2) NaGTP (0.2), HEPES (10), and biocytin (3 mg/mL). The patch solution was adjusted to a pH of 7.3 with KOH and had a final osmolarity of approximately 280 mOsm. Junction potentials were offset manually prior to patching neurons. Access resistances were monitored throughout recordings and neurons with more than a 15% change were discarded. In the case of paired recordings, two neurons were selected for patching within a single 40X visual field. Neuronal types were pre-selected based on somatic morphology, and type was verified based on electrophysiological profile, as described previously for rat (Rainnie et al., 1993) and primate (Muly et al., 2009).

All recordings were performed in principal neurons of the basolateral nucleus of the amygdala, contained in the basolateral complex. Recordings were obtained using an Axopatch-700A amplifier (Molecular Devices, Sunnyvale, CA), a Digidata 1320A A/D interface, and pClamp 10 software (Molecular Devices). For all experiments, whole cell patch-clamp configuration was established, and cell responses were recorded in either current clamp or voltage clamp mode. Data were filtered at 5 kHz in current clamp and 2 kHz in voltage clamp, and sampled at a rate of 10 kHz. Neurons were excluded from analysis if their resting membrane potential (V_m) was more positive than -55 mV or if their action potentials did not surpass +5 mV.

6.3.2.3 Drug Application.

Drugs were applied by gravity perfusion at the required concentration in the circulating ACSF. Drugs used: cesium chloride (CsCl), 5 mM; nickel chloride ($NiCl_2$), 500 µM; 4-aminopyridine (4-AP), 100-500 µM; tetrodotoxin (TTX), 1 µM; tetraethylammonium chloride (TEA-Cl), 20 mM; forskolin, 10 µM; dideoxy-forskolin, 10 µM; 1,2-bis(o-aminophenoxy)ethane-N,N,N',N'-tetraacetic acid (BAPTA), 5 mM purchased from Sigma–Aldrich (St. Louis, MO); 6,7-dinitroquinoxaline-2,3-dione (DNQX), 20 µM; RS-CPP, 10 µM; CGP 52432, 2 µM; 4-(N-ethyl-N-phenylamino)-1,2-dimethyl-6-(methylamino) pyridinium chloride (ZD7228), 60 µM; (1R,4R,5S,6R)-4-amino-2-oxabicyclo[3.1.0]hexane-4,6-dicarboxylic acid (LY379268), 50 µM; 8-Br-cAMP, 5-10 µM; and (R)-adenosine, cyclic 3',5'-(hydrogenphosphorothioate) triethylammonium (cAMPs-RP), 25 µM purchased from Tocris (Ellisville, MO). All drugs were stored frozen as concentrated stock solutions in dH_2O except DNQX, which was made in 50% dimethyl sulfoxide and buffered to pH 7.3.

6.3.2.4 Spike-timing precision, resonance, and oscillations.

To assess the effect of IPSPs on spike-timing precision, repetitive action potentials were evoked with a depolarizing, square-wave current step of amplitude set to evoke 4-8 Hz firing from a holding potential of -60 mV. The current injections were repeated five times with an inter-event interval of 10 seconds. To examine the effect of synaptic inhibition on spike-timing precision, the current in the depolarizing step was transiently removed for 15 ms and then ramped back over 100 ms to the command amplitude to mimic compound spontaneous IPSPs observed in BLA principal neurons. Alternatively, pharmacologically isolated, compound, synaptic IPSPs were evoked using electrical stimulation within the dorsal BLA, just medial to the external capsule. The two IPSPs in each sweep were applied 550 and 1415 ms into the depolarizing step, separated by 865 ms start-to-start (~1.2 Hz), to mimic the frequency of spontaneous IPSPs previously observed in our laboratory.

To examine the membrane potential oscillation of BLA principal neurons, cells were held at -60 mV and injected with the same transient (2.5 s) square-wave depolarizing current pulse as described above. TTX (1 μM) was included in all experiments investigating the membrane oscillation. The voltage response to the DC current pulse was recorded and characterized in regular ACSF and also in varying drug conditions. The amplitude of the current pulse was adjusted such that the steady state membrane potential achieved during current injection was similar before and during drug application (between -40 and -30 mV). Any drug-induced changes in resting membrane potential were compensated for by DC current injection before initiating the transient square-wave depolarizing current pulse to assess the effect on membrane potential oscillations. To assess resonance frequency, principal neurons were held at -60 mV with DC current injection and a sinusoidal frequency sweep of constant current amplitude was injected, increasing from 1-12 Hz over a period of 8 seconds, and the voltage response of the cell was recorded.

6.3.3 Data and statistical analysis

The correlation of spontaneous IPSPs and burst-firing from paired recordings of BLA neurons were analyzed by first identifying event times using pClamp software and then using a Pearson product-moment correlation. Spike-timing precision was assessed using a correlation-based metric adapted from Schreiber et al. (2003). The correlation statistic (R_{corr}) was calculated for windows of 200 ms every 66 ms, using the equation (Equation 6.1) as published. Briefly, spike times from N traces were convolved with a Gaussian filter of pre-determined width (σ) to create spike vectors (*s*). For experiments involving artificial and evoked IPSPs, σ = 6 ms, and to prevent a floor effect due to lower spike rates, for experiments with spontaneous IPSPs, σ = 20 ms. The degree of correlation between the vectors (s_i, s_j) was calculated using a dot-product normalized to the product of their magnitudes and the number of comparisons being made.

Equation 6.1

$$R_{corr} = \frac{2}{N(N-1)} \sum_{i=1}^{N} \sum_{j=i+1}^{N} \frac{\vec{s}_i \cdot \vec{s}_j}{\left|\vec{s}_i\right|\left|\vec{s}_j\right|}$$

When calculating spike-timing precision within cells, all 5 traces (N = 5) were compared using this algorithm; when calculating across cells, only the 2 traces (N = 2) which occurred simultaneously were compared, and 5 comparisons were made and averaged. Statistical analyses were performed using a two-way Analysis of Variance (ANOVA), with Bonferroni post-tests to compare across windows and conditions.

Oscillations of the membrane potential of BLA principal neurons were analyzed by means of multi-taper spectral analysis using a custom program that was modified from the Chronux toolbox (Mitra and Bokil, 2008). The resonance frequency of BLA principal neurons was analyzed with fast Fourier transforms (FFT) in pClamp 10 (Molecular Devices) using a Hamming window. Power spectra (mV^2/Hz) were converted into standardized Z-scores and peak amplitudes were analyzed using a one-way ANOVA.

6.4 Results

6.4.1 Primate BLA principal neurons receive spontaneous, synchronized, rhythmic IPSPs that coordinate action potential timing.

We have shown previously that approximately 80% of principal neurons in slice preparations of the rat BLA receive spontaneous, compound IPSPs that occur rhythmically at frequencies ranging from 0.5-2 Hz, with a mean of 1.2 Hz, in control ACSF (Rainnie, 1999b). These compound IPSPs were observed in principal neurons with varying intrinsic properties (mean ± SD: input resistance 85 ± 28MΩ, action potential threshold -43 ± 3.5mV, action potential half width 0.8 ± 0.1ms, data not shown). Here we show that compound IPSPs are also observed in 67% of primate BLA slices with a frequency of 0.76 ± 0.33 Hz, similar to the rat (n = 46, **Figure 6.1A, B**). As in the rat BLA, compound IPSPs in the primate BLA were highly rhythmic, with a coefficient of variation of instantaneous frequency of 0.30 ± 0.09 (n = 12).

Compound IPSPs occur synchronously across multiple neurons in the rat BLA (Rainnie, 1999a; Popescu and Pare, 2011), and new analysis reveals they have a near perfect correlation in time across pairs of principal neurons (Pearson product-moment correlation, $R^2 = 0.999$; n = 11, data not shown). We extend this observation to show that compound IPSPs are also highly synchronized across pairs of primate neurons (**Figure 6.1A**; Pearson product-moment correlation, $R^2 = 1.0$; n = 5, data not shown), suggesting this is an evolutionarily conserved phenomenon.

Using paired recordings from a burst-firing interneuron and a principal neuron, we extend previous observations in the rat BLA (Rainnie, 1999a; Popescu and Pare, 2011) to the primate. Here we show that compound IPSPs observed in BLA principal neurons (**Figure 6.1C**, upper trace) coincide with rhythmic bursts of action potentials occurring in burst-firing interneurons (lower trace, n = 2**;** Pearson product-moment correlation, $R^2 = 0.999$, data not shown), which we have previously shown in the rat BLA to express the calcium-binding protein PV^+ (Rainnie et al., 2006). **Figure 6.1D** illustrates a typical burst-IPSP pair at higher temporal resolution. Compound IPSPs with a similar waveform can also be observed in principal neurons if an interneuron is driven to fire bursts of action potentials by direct current injection (**Figure 6.1E**). Previously, we have shown that these compound IPSPs were abolished by application of either the $GABA_A$ receptor antagonist, bicuculline, or the AMPA receptor antagonist, CNQX, suggesting glutamatergic input drives burst-firing PV^+ interneurons to release GABA at multiple sites onto BLA principal neurons (Rainnie, 1999a). Each parvalbumin interneuron can innervate more than 150 BLA principal neurons (Muller et al., 2006), further suggesting that spontaneous, compound IPSPs are highly synchronized across a larger population of principal neurons than the pairs we show here.

Elsewhere in the brain, IPSPs have been shown to interact with subthreshold membrane potential oscillations (MPOs) to improve stimulus discrimination and action potential precision in neurons (Mainen and Sejnowski, 1995; Schaefer et al., 2006). We were therefore interested in the ability of synchronized, compound IPSPs to coordinate firing activity within networks of

BLA principal neurons. As illustrated in **Figure 6.2**, compound IPSPs are capable of coordinating activity in the BLA, improving the temporal coherence of spontaneous action potentials between pairs of primate BLA principal neurons. When neurons were depolarized to threshold for action potential generation, action potentials occurring upon rebound from an IPSP-induced membrane hyperpolarization were highly coincident across cells (**Figure 6.2A**, shaded regions). To identify periods with consistent spike-timing across cells, we used a correlation-based metric with a sliding window (see Methods; Schreiber et al., 2003), where a value of 1 indicates identical spike-timing and a value of 0 indicates no timing correlation. Action potentials during a window directly following spontaneous, compound IPSPs had improved temporal coherence across pairs of neurons compared to those preceding IPSPs (**Figure 6.2B**). Interestingly, upon rebound from compound IPSPs, a subpopulation of primate BLA principal neurons (3/11 cells) exhibited an increased and more consistent firing rate (from 3.6 to 7.4 Hz, coefficient of variation from 0.56 to 0.28) (**Figure 6.2C**). Moreover, clusters of action potentials showing a consistent firing rate and high coherence following compound IPSPs were also observed in 2/6 paired recordings (**Figure 6.2D**). In the course of these experiments it was noted that compound IPSPs could elicit a damped oscillation on rebound, suggesting the observed effects on action potential patterning may be due to an interaction with an intrinsic MPO (**Figure 6.2E**).

Together these observations strongly suggest that compound IPSPs coordinate the firing activity of principal neurons in both the rat and primate BLA, and their prevalence and synchrony further suggest that this coordination extends across large groups of principal neurons. To better assess the interactions of compound IPSPs with intrinsic properties of BLA principal neurons, subsequent experiments examined the effects of IPSPs on spike trains in the absence of synaptic noise. Moreover, given the scarcity of primate tissue, all experiments were performed in the rat.

6.4.2 Compound IPSPs enhance spike-timing precision in rat BLA principal neurons.

We first examined the effect of IPSPs on the precision of action potential timing in a neuron depolarized to action potential threshold with DC current injection. In order to better isolate the effects of intrinsic currents on spike timing, we blocked synaptic currents with a mixture of glutamate and GABA receptor antagonists (see Methods). As illustrated in **Figure 6.3A**, BLA principal neurons displayed a regular action potential firing pattern when held at -45 mV. When ten sweeps from the same neuron were aligned using an action potential as the trigger (**Figure 6.3B**), it was apparent that subtle variations in inter-spike interval accumulated over the course of the train, such that the timing of spikes at the end of the train was less consistent than at the beginning. Conversely, when two simulated IPSPs were injected during 10 sweeps captured randomly in time (**Figure 6.3C**), the phase of spiking was reset and spike times became much more consistent across sweeps.

Having established that artificial IPSPs can improve spike-timing precision in free-firing neurons, we next sought to quantify this effect. Specifically, we used transient (2.5 s) steps of injected current to elicit a spike train and determine the effect of IPSPs on spike-timing precision in individual principal neurons, and between pairs of principal neurons. Similar to when neurons are free-firing, the timing of the first few spikes in a train was extremely consistent across sweeps, but the timing of subsequent spikes became less consistent as the train progressed because small variations in the inter-spike interval accumulated (**Figure 6.4A**). Here we used the same correlation-based metric as described for **Figure 6.2B**, adapted to compare across five sweeps recorded in a single neuron (see 6.3 Methods). This analysis revealed that, at the onset of the train, spike-timing was extremely precise with an initial correlation value of 0.75 ± 0.13 (mean ± SD), which then diminished to 0.26 ± 0.20 within 300 ms (**Figure 6.4D,** Control, n = 11).

We next evaluated spike-timing precision in the presence of stimulus-evoked IPSPs (**Figure 6.4B**). Electrical stimulation of the dorsolateral BLA in the presence of glutamate receptor antagonists elicited a monosynaptic IPSP in principal neurons that had a similar amplitude and duration to the spontaneous compound IPSPs. We also examined the effects of artificial IPSPs, elicited with hyperpolarizing current injection, on spike-timing precision (**Figure 6.4C**). Activation of either evoked or artificial IPSPs during the action potential train resulted in a significant improvement in spike-timing precision compared to the control condition (Two-way ANOVA with repeated measures, effect of group: $F_{2,800} = 136.3$, $p < 0.0001$). Both types of IPSPs significantly increased correlation values relative to the control condition for approximately 270 ms following each IPSP (effect of interaction: $F_{78,800} = 4.72$, $p < 0.0001$, Bonferroni post-tests). Evoked IPSPs improved correlation values from a baseline of 0.19 ± 0.11 to a peak of 0.47 ± 0.11 ($n = 11$) immediately following the IPSPs (**Figure 6.4D**). As illustrated in Figure 4F, artificial IPSPs had a more pronounced effect on spike-timing precision than evoked IPSPs, with a peak correlation value of approximately 0.71 ± 0.21 ($n = 11$) following each IPSP. Only at the peak points of the correlation, however, was there any significant difference in how the two IPSP manipulations affected spike-timing precision.

6.4.3 Compound IPSPs synchronize the firing activity of multiple BLA principal neurons.

We next quantified the ability of compound IPSPs to improve firing coherence across multiple BLA principal neurons, using a similar metric as above to measure the correlation of spike times in simultaneously recorded sweeps across the two neurons. In the absence of IPSPs, spike-timing across BLA neurons showed low coherence, such that the correlation-based metric reached an initial peak of only 0.27 ± 0.39 which then declined rapidly to 0.09 ± 0.07 ($n = 6$) within 300 ms (**Figure 6.5C**). The introduction of 2 evoked IPSPs was not able to significantly improve the coherence of spike times between neurons, likely due to the observed inconsistency in the amplitude and duration of the evoked IPSP waveform between neurons (data not shown).

Because artificial IPSPs have a highly consistent waveform across pairs of neurons and therefore mimic the consistency of spontaneous, compound IPSPs better than do evoked IPSPs, we also tested the effect of 2 artificial IPSPs on spike-timing. Artificial IPSPs significantly increased the coherence of spike times between pairs of neurons in the period immediately following the IPSPs (Two-way ANOVA with repeated measures, effect of interaction: $F_{39,200} = 2.123$, $p < 0.001$, Bonferroni post-tests), with an improvement from a baseline of 0.09 ± 0.12 to a peak of approximately 0.42 ± 0.27 ($n = 6$) in the correlation-based metric (**Figure 6.5B, D**). These data strongly suggest that synchronized IPSPs enhance spike-timing precision of BLA principal neurons and can serve to entrain the firing activity of multiple neurons, despite inherent differences in their intrinsic electrophysiological properties (e.g., membrane input resistance, time constants of membrane charging, and firing frequency). Based on our prior observation that spontaneous, compound IPSPs not only entrain action potential firing, but also promote rhythmic firing and unmask a damped membrane potential oscillation, we hypothesized that the ability of compound IPSPs to coordinate firing would be facilitated by an interaction with intrinsic oscillatory properties of principal neurons. Therefore, we next characterized the interaction of compound IPSPs with intrinsic oscillatory properties of BLA principal neurons.

6.4.4 Compound IPSPs facilitate an intrinsic membrane potential oscillation in BLA principal neurons.

Most central nervous system neurons exhibit a preferred resonance frequency that provides them with the ability to filter synaptic input based on frequency (Hutcheon et al., 1996a, b; Hutcheon and Yarom, 2000). Pape and colleagues have reported that principal neurons in the lateral amygdala of the cat have an intrinsic resonance frequency in the range of 1-3.5 Hz (1998). Here we extend these observations to show that BLA principal neurons of the rat also have an intrinsic resonance (**Figure 6.6A_1-D_1**, $n = 8$), with a preferred frequency at 4.2 ± 0.1 Hz (**Figure 6.6E**).

Many of the membrane currents that contribute to the resonant properties of neurons have also been implicated in mediating long-lasting, sub-threshold MPOs in the BLA as well as other brain regions (Hutcheon et al., 1994; Hutcheon et al., 1996a, b; Pape and Driesang, 1998; Pape et al., 1998). To determine whether compound IPSPs interact with an intrinsic MPO in principal neurons, we next examined the effect of IPSPs on membrane voltage in neurons depolarized to threshold in the presence of TTX (1 μM; n = 6). As illustrated in **Figure 6.6A$_2$**, depolarizing current injection evoked a transient depolarizing voltage deflection at the onset of current injection but did not elicit an MPO in BLA principal neurons. Furthermore, injection of artificial IPSPs evoked a similar depolarizing voltage deflection on the rebound of each IPSP, but did not elicit an MPO (**Figure 6.6A$_3$**). We hypothesized that the basal state of the neurons in the slice preparation might not be conducive to the expression of an MPO, and that modulation of intrinsic currents might be necessary to reveal the presence of an MPO.

6.4.5 The membrane potential oscillation is sensitive to modulation of its component currents.

Work by Pape and colleagues has shown that MPOs in the BLA can be enhanced by modulating a select population of voltage-activated currents including, but not limited to, the hyperpolarization-activated cation current (I_H) and the low-threshold Ca^{2+} current (I_T) (Pape et al., 2005). Significantly, an interaction between I_H and I_T is also thought to be a key element in the regulation of intrinsic resonance (Hutcheon et al., 1994; Hutcheon et al., 1996a, b). The I_T current is often opposed by the transient K^+ current, I_A (Russier et al., 2003; Molineux et al., 2005; Hammack et al., 2007; Anderson et al., 2010), which has been shown to regulate firing activity in BLA principal neurons (Gean and Shinnick-Gallagher, 1989). Thus, we reasoned that blocking I_A channels could effectively enhance I_T and thus facilitate resonance behavior in BLA principal neurons and unmask an MPO. Bath application of the non-selective I_A channel blocker, 4-aminopyridine (4-AP), at 100μM (**Figure 6.6E**) and 500μM (**Figure 6.6B$_1$, E**) both

significantly enhanced the amplitude of the peak resonance (One-way ANOVA, Tukey post-tests, $F_{3,46} = 8.763$, $p < 0.05$). Application of 500 µM 4-AP also enhanced the expression of the transient depolarizing voltage deflection and unmasked a small, transient MPO at the onset of the depolarizing step (**Figure 6.6B$_2$**). Furthermore, in the presence of 4-AP, the introduction of artificial IPSPs (**Figure 6.6B$_3$**) enhanced the amplitude of the MPO, which had peak power at approximately 5 Hz (**Figure 6.7A-C**, n = 6).

Importantly, I_T, I_H, and I_A channels are all substrates for phosphorylation by protein kinase-A (PKA), which decreases the conductance of I_A channels and increases the conductance of I_H and I_T channels (Kamp and Hell, 2000; Kim et al., 2006a; Ramadan et al., 2009) (Ingram and Williams, 1996; Hoffman and Johnston, 1998; Gerhardstein et al., 1999; Vargas and Lucero, 2002). Thus, we next examined the effects of the PKA activator, forskolin, on the resonance properties of BLA principal neurons. As illustrated in **Figure 6.6C$_1$**, bath application of forskolin (10 µM) in combination with 4-AP (500 µM) significantly increased the amplitude of the resonance peak compared to TTX controls (One-way ANOVA, Tukey post-test, $F_{3,46} = 8.763$, $p < 0.05$). However, the peak power of the resonance in 4-AP and forskolin was not significantly different than that observed in the presence of 4-AP alone (**Figure 6.6E**). In the context of the depolarizing step, the addition of forskolin (10 µM) in combination with 4-AP (500 µM) enhanced both the amplitude and duration of the MPO in all neurons tested (**Figure 6.6C$_2$**). The MPO resembled a damped oscillation (Pape and Driesang, 1998) and, as can be seen in **Figure 6.6F**, the power of the MPO was greatest at the onset of the depolarizing current injection and declined over time. In the majority of neurons the MPO was seen to terminate before the conclusion of the depolarizing current injection. The introduction of artificial IPSPs further enhanced the oscillation (**Figure 6.6C$_3$, G**) without changing the preferred frequency (**Figure 6.7E**, compared to **6.7C** and **6.7D**). Application of forskolin (10 µM) alone also unmasked an MPO, similar to the effects of 500 µM 4-AP, with a peak frequency at 4.8 Hz in all neurons

tested (n = 4) (**Figure 6.7D**). Hence, activation of the cAMP-signaling cascade alone can facilitate the expression of the MPO in BLA principal neurons.

In other brain regions, MPOs are partially dependent on the activation of I_T channels, and as the transient depolarizing voltage deflections observed upon rebound from the IPSPs were reminiscent of low-threshold calcium spikes, we next determined whether blocking I_T channels with 500 μM NiCl (Lee et al., 1999) would inhibit the combined response to forskolin and 4-AP. Application of NiCl diminished the resonant properties of BLA principal neurons (**Figure 6.6D$_1$**) and completely blocked the forskolin- and 4-AP-induced MPO in all neurons tested (n = 6) (**Figure 6.6D$_{2\text{-}3}$, 6.7F**), suggesting that an interaction between I_T and voltage-gated K^+ channels, most likely I_A channels, play a critical role in MPO expression in BLA neurons.

Application of high-micromolar 4-AP, however, can also block other K^+ channels, including several that are also sensitive to micromolar concentrations of TEA. Hence, to determine if the effects of 4-AP on the MPOs resulted from a non-selective blockade of K^+ channels, we repeated the experiments above in the presence of TEA (500 μM). As illustrated in **Figure 6.8**, application of TEA failed to mimic the 4-AP effect in either the presence or absence of simulated IPSPs. Moreover, concurrent application of forskolin (10 μM) and TEA also failed to unmask a significant increase in MPO amplitude over TEA alone (**Figure 6.8C**, n = 5), suggesting that the forskolin effect may only be observed when I_A channel activity is reduced by 4-AP.

To verify that the effects of forskolin were mediated by direct activation of the adenylyl cyclase-cAMP signaling cascade, we then examined the membrane response to application of the inactive forskolin isomer, dideoxy-forskolin (10 μM), in the presence of 4-AP. Dideoxy-forskolin failed to mimic the forskolin effect on MPOs in either the presence or absence of artificial IPSPs, suggesting that activation of the adenylyl cyclase-cAMP signaling cascade selectively facilitates IPSP-enhanced MPOs in principal neurons of the BLA (**Figure 6.8D**, n = 6).

Finally, we examined if modulation of intracellular Ca^{2+} levels also play a role in regulating the MPO. Here, inclusion of the Ca^{2+} chelator, BAPTA (5 mM), in the patch solution completely blocked the MPO induced by co-application of 4-AP (500μM) and forskolin (10μM) (**Figure 6.9A**, n = 6), suggesting that fluctuations in intracellular Ca^{2+} levels also play an important role in the expression of MPOs in BLA principal neurons. However, this result raised the possibility that the drug-induced MPO may be independent of activation of the cAMP-PKA signaling cascade. To address this question, we included the competitive antagonist of cAMP-induced PKA activation, cAMPs-RP, in the patch solution. Inclusion of cAMPs-RP (25 μM) completely blocked the MPO induced by forskolin (**Figure 6.9B**, n = 4). Conversely, inclusion of a non-hydrolysable cAMP analogue, 8-Br-cAMP (5-10 μM), in the patch pipette unmasked an MPO in the presence of TTX alone that was similar in magnitude to that induced by forskolin (**Figure 6.9C**, n = 6). Hence, Ca^{2+} influx through I_T channels, elevation of intracellular Ca^{2+}, and activation of the adenylyl cyclase-cAMP-PKA signaling cascade each play an important role in the expression of MPOs in BLA principal neurons.

The sensitivity of the MPO to modulation by intracellular Ca^{2+} and activation of the cAMP-PKA signaling cascade suggested that receptors coupled to $G_{\alpha s}$ would facilitate MPOs, whereas those coupled to $G_{\alpha i}$ would attenuate MPOs. To test this hypothesis, we examined the effect of prior application of the selective mGluR2/3 agonist, LY379268, on the 4-AP- and forskolin-induced MPOs. Principal neurons of the BLA express high levels of mGluR2/3 receptors (Rainnie et al., 1994; Muly et al., 2007), which couple to $G_{i/o}$ proteins to inhibit adenylyl cyclase activity (Pin and Duvoisin, 1995), and we reasoned that activation of these receptors would attenuate drug-induced MPOs. As illustrated in **Figure 6.9D** (n = 10), application of LY379268 (50 μM) completely blocked the MPOs.

6.5 Discussion

In the present study, we demonstrate that spontaneous, compound IPSPs function to increase spike-timing precision both within and across BLA principal neurons. Previous studies have shown that these IPSPs are driven by local, burst-firing PV^+ neurons (Rainnie, 1999b), which have a high level of connectivity with BLA principal neurons. These data suggest that spontaneous, compound IPSPs would function to synchronize action potentials in a large population of principal neurons. We also show that compound IPSPs promote and entrain a high delta / low theta frequency membrane potential oscillation (MPO) that is uncovered by activation of the cAMP-PKA signaling cascade. The oscillatory nature of BLA principal neurons is also manifested as a modifiable inherent resonance frequency. We propose that the interaction of compound IPSPs with the oscillatory properties of BLA principal neurons is a viable mechanism for synchronizing firing activity in this cell population, promoting network oscillations within the BLA, and enhancing coherent oscillations between the BLA and other brain regions involved in fear.

6.5.1 Synchronized inhibition drives coordinated activity of BLA principal neurons

Recent evidence suggests a wide variety of behaviors require synchronized neural activity and network oscillations, both of which are promoted by synaptic inhibition (Soltesz and Deschenes, 1993; Pouille and Scanziani, 2001; Person and Perkel, 2005; Sohal et al., 2006; Szucs et al., 2009). Here, we demonstrate that BLA principal neurons receive highly synchronized, rhythmic inhibition which, in turn, synchronizes firing activity among groups of BLA principal neurons. Importantly, spontaneous activity of interneurons in the prefrontal cortex at theta frequency entrains the firing of principal neurons to an ongoing network theta oscillation (Benchenane et al., 2010). This example from the prefrontal cortex suggests the coordination of principal neuron firing by inhibition is critical for salient output of some neural circuits. Through

coordinating the firing of large groups of BLA principal neurons, compound IPSPs should improve salience by promoting summation of output and leading to spike-timing dependent plasticity in both the BLA and its targets.

In order to study the effect of compound IPSPs on spike-timing precision, we used two proxies: artificial IPSPs generated by direct current injection at the soma, and compound IPSPs evoked by direct stimulation of interneurons in the BLA under glutamatergic blockade. We showed that spike-timing precision within single neurons is improved by spontaneous IPSPs, artificial IPSPs, and stimulation-evoked IPSPs, with artificial IPSPs being significantly more effective than evoked IPSPs. Furthermore, artificial IPSPs were able to significantly coordinate firing across neurons, but evoked IPSPs were not, due to the observed variability in the waveform. Spontaneous, compound IPSPs observed across pairs had a highly consistent waveform (evident in a representative pair in **Figure 6.1A**), likely because they are generated by burst-firing PV^+ interneurons, which innervate BLA principal neurons perisomatically and have their activity coordinated through a syncytium. In contrast, stimulation of the BLA to evoke IPSPs probably recruited multiple subtypes of GABAergic interneurons targeting multiple compartments of the principal neurons (McDonald and Betette, 2001; McDonald and Mascagni, 2002; Mascagni and McDonald, 2003) and hence introduced variability across cells in the IPSP waveform. While PV^+ interneurons seem uniquely positioned to generate synaptic inhibition that is ideal for interacting with an MPO and coordinating activity of BLA principal neurons, the possibility is not excluded that other inhibitory input, for instance feed-forward inhibition from cortical or thalamic sources (Rainnie et al., 1991b; Szinyei et al., 2000), could exert a similar coordinating influence.

The fact that artificial IPSPs were able to mimic the effects of evoked and spontaneous IPSPs on spike-timing precision without directly influencing the membrane conductance suggests they act primarily via membrane hyperpolarization. This hyperpolarization likely causes activation of I_H and de-inactivation of voltage-gated currents including I_T, which would contribute

to calcium spikes upon rebound (Hutcheon et al., 1994). Because I_T is typically inactive near resting membrane potential, the observed effect of compound IPSPs on spike timing is probably more applicable when BLA principal neurons are depolarized from rest. It is also important to consider that compound IPSPs occur amidst ongoing synaptic activity, not in the absence of synaptic input as when tested here. In the *in vivo* system, compound IPSPs may not produce spikes in the absence of excitatory transmission, but rather interact with ongoing synaptic activity to influence the timing of spikes.

The ability of compound IPSPs to coordinate spiking activity most likely occurs across large groups of BLA principal neurons due to the broad connectivity of PV^+ interneurons (Muller et al., 2006), the synchronization of PV^+ interneuron firing activity through a syncytium (Muller et al., 2005; Woodruff and Sah, 2007a, b), and, as shown here, the robustness of IPSP coordination of spike timing across principal neurons despite varying intrinsic properties. Although synchronizing large networks of principal neurons will improve potency of efferent signaling, it could also limit the specificity of signaling. Cortical inputs to the BLA are organized topographically (McDonald et al., 1999), and synchrony throughout the nucleus could weaken the specificity afforded by this topography. A loss of specificity in this circuit through excessive synchronization within the amygdala may lead to generalization of fear learning, which has been implicated in affective disorders such as post-traumatic stress disorder (Rainnie and Ressler, 2009). Furthermore, less than a quarter of BLA neurons appear to be incorporated into the engram for any specific fear memory (Han et al., 2007; Han et al., 2009). If encoding and recall of fear memories depend on network oscillations, there must be a mechanism to preferentially incorporate some neurons while excluding others. Some potential mechanisms include regulation of the extent of the syncytium or of projections from the PV^+ interneurons onto principal neurons, or, more interestingly, interactions between variability in the frequency of the network oscillation with variations in preferred resonance frequency of the principal cells.

Considering the prominent role inhibition appears to play in coordinating the activity of BLA principal neurons, it is likely that stimuli altering the frequency of IPSPs *in vivo* could drastically change the output activity of the BLA. For instance, activation of serotonin 2A or cholecystokinin B receptors, both of which are implicated in emotional learning (Chhatwal et al., 2009), increase the frequency of rhythmic IPSPs in BLA principal neurons through indirect excitation of interneurons (Rainnie, 1999b; Chung and Moore, 2007). A similar effect is observed in the BLA in response to local release of dopamine in mice (Loretan et al., 2004) and primates (Muly et al., 2009). Moreover, the BLA receives dopaminergic input from the ventral tegmental area, which also exhibits a network oscillation at 2-5 Hz during working memory tasks (Fujisawa and Buzsaki, 2011), raising important questions about the nature of the interaction of phasic dopamine release with a BLA circuit that itself generates rhythmic activity.

6.5.2 Resonance frequency and intrinsic membrane oscillations in BLA principal neurons

In the present study we have shown that BLA principal neurons in the rat have an intrinsic resonance that was extremely consistent, with nearly all neurons displaying a peak resonance between 4.2 and 4.4 Hz. This intrinsic resonance was insensitive to application of TTX (1 µM), whereas a previous study in guinea pigs reported neurons in the lateral and basolateral nuclei of the amygdala express a TTX-sensitive inherent resonance frequency at 2.5 Hz (Pape and Driesang, 1998). The difference in reported resonance frequencies is likely due to the different model species, as we have also seen differences in peak resonance frequency of principal neurons between rat and primate (unpublished observation). The difference in TTX sensitivity, however, is likely explained by the concentrations of TTX employed. In the study by Pape and colleagues the resonance frequency was abolished by 20 µM TTX, compared to the 1 µM TTX used here. High concentrations of TTX are known to block the persistent Na^+ current, and future studies should investigate whether it contributes to resonance in BLA principal neurons, as it does in LA neurons (Pape et al., 1998). Similar to our observations, hippocampal

principal neurons also display resonance that is insensitive to 1 μM TTX with a peak at 4.1 Hz (Pike et al., 2000).

In addition to selectively filtering synaptic input in high delta / low theta bands, BLA principal neurons also express high- and low-threshold MPOs in this frequency range, as described by Pape and colleagues (1998). Here we show the presence of an MPO that occurs at the peak resonance frequency of these neurons (~4-5 Hz) and seems to share some mechanisms with both previously described oscillations. Although Pape and colleagues found no effect of specific Ca^{2+} channel blockers on the high threshold membrane oscillations (Pape and Driesang, 1998), recordings with a BAPTA-containing electrode completely abolished the oscillation. In our hands, bath application of NiCl completely abolished the MPO, suggesting a strong influence of T-type Ca^{2+} channels. The Pape study also reported that high-threshold membrane oscillations were insensitive to 10 mM 4-AP, suggesting that voltage-gated K^+ channels were not involved in that membrane oscillation (1998) . We observed, however, that application of 100-500 μM 4-AP significantly enhanced the membrane oscillations, suggesting I_A may actively suppress the MPO, acting in opposition to I_T. This could also be related to changes in input resistance, but the lack of effect of 500 μM TEA suggests a specific role of I_A. A similar relationship between I_T and I_A has been shown in other systems (Pape et al., 2004; Molineux et al., 2005), and factors that either enhance I_T or reduce I_A could then unmask the expression of the intrinsic membrane oscillations. In agreement with Pape and colleagues, we did not find an effect on intrinsic membrane oscillations of blocking I_H with ZD7228 (60 μM, data not shown). While this is not an exhaustive pharmacological characterization, we believe we have identified the major currents involved in mediating this MPO. Other currents, including the persistent sodium current and calcium-activated potassium currents may also be involved (Pape and Driesang, 1998), and future study to illuminate their roles in this phenomenon would be valuable.

It is notable that the currents mentioned above (I_T, I_A, and I_H) are all sensitive to membrane hyperpolarization, particularly in the voltage range between rest and action potential

threshold (Rudy, 1988; Perez-Reyes, 2003; Robinson and Siegelbaum, 2003). Specifically, I_T channels are de-inactivated by hyperpolarization in this range and I_H channels are activated, while I_A channels are activated by depolarization in this range. We have shown that compound IPSPs facilitate the MPO in the absence of spiking, and this is likely due to hyperpolarization-mediated de-inactivation of I_T and activation of I_H. While we did not find an effect of I_H blockade on the MPO, it is possible this is an artifact of the degree to which we depolarize the membrane to enhance the MPO. The MPO is likely also active in a more subtle form at membrane potentials only slightly depolarized from rest, where I_T and I_A are active and I_H would enhance the rebound from an IPSP and may contribute directly to the MPO.

In addition, the conductances of these currents, and therefore the magnitude of the MPO itself, are not fixed but sensitive to modulation. Importantly, the channels mediating I_T and I_H increase their activity in response to PKA phosphorylation (Ingram and Williams, 1996; Gerhardstein et al., 1999; Kamp and Hell, 2000; Vargas and Lucero, 2002; Kim et al., 2006a; Ramadan et al., 2009). Conversely, activity of K^+ channels mediating I_A is decreased by PKA phosphorylation (Hoffman and Johnston, 1998). Together, these would enable neurotransmitter systems which modulate PKA activity to have synergistic effects to bi-directionally modulate the MPO.

The frequency of rhythmic, compound IPSPs is also sensitive to modulation. We have previously shown that dopamine acts to increase IPSP frequency into a range of 2-6 Hz (Rainnie, 1999b; Loretan et al., 2004; Muly et al., 2009). This would bring the IPSP frequency closer to the peak resonance frequency of BLA principal neurons, ensuring principal neurons respond to incoming rhythmic IPSPs with maximal voltage deflections and also serve to enhance the interaction with the MPO. In our hands, the oscillation does not occur spontaneously but is initiated by the IPSP and is naturally damped, quickly decaying from its initial amplitude. More frequent synchronized IPSPs would better reset drift in the phase relationship between cells and better maintain the amplitude of the oscillation.

It is interesting to note that the intracellular cascades activated by many of the neuromodulators that promote the MPO (e.g., G_s-coupled activation of cAMP and PKA) are also critical for synaptic plasticity. Through this mechanism, cells primed by neuromodulators to exhibit an MPO may be more likely to contribute to a fear memory engram.

6.5.3 Implications for learning and memory

Recent studies by several groups have emphasized the importance of amygdala network oscillations and synchronized oscillations across multiple brain regions in regulating long-term fear memory (Quirk et al., 1995; Collins et al., 2001; Pare et al., 2002; Seidenbecher et al., 2003; Pelletier and Pare, 2004; Pape et al., 2005; Bauer et al., 2007; Paz et al., 2008). Importantly, phase-locked stimulation of the amygdala and hippocampus at theta frequency during extinction training prolongs fear expression, suggesting synchronized network oscillations between these regions are an essential neurological component of fear memory (Lesting et al., 2011). The high delta / low theta oscillations in the LFPs of the BLA, hippocampus, and prefrontal cortex during fear acquisition and expression(Madsen and Rainnie, 2009; Sangha et al., 2009) match the frequency of the MPO and the peak resonance in BLA neurons, suggesting the intrinsic properties of BLA neurons contribute to the network oscillation. As we have argued, a candidate mechanism to promote these network oscillations is the interaction of synchronized IPSPs with MPOs in BLA principal neurons. MPOs could contribute to fear learning by promoting network oscillations, and by improving spike-timing precision they could support fear memory formation through enhanced spike-timing dependent plasticity (Dan and Poo, 2004; Jutras and Buffalo, 2010).

The sub-cellular mechanism of the intrinsic MPO is well-suited to facilitate plasticity in the BLA and thereby promote fear learning. The MPO requires activation of voltage-gated calcium currents (Pape and Driesang, 1998), causing calcium influx and subsequent activation of cAMP and PKA (Zaccolo and Pozzan, 2003). This can, in turn, reinforce the oscillation through

phosphorylation of ion channels. In fact, the oscillation is weak or nonexistent under our baseline experimental conditions, but must be uncovered by application of the PKA activator, forksolin. The close relationship of the MPO with the adenylyl cyclase-cAMP signaling cascade is particularly important because its downstream targets have been implicated in fear learning and memory (Schafe et al., 1999; Josselyn et al., 2001; Kida et al., 2002; Josselyn et al., 2004), and in regulating theta oscillations in the amygdala *in vivo* (Josselyn et al., 2001; Kida et al., 2002; Josselyn et al., 2004; Josselyn and Nguyen, 2005; Pape et al., 2005). It is also noteworthy that downstream targets of this signaling cascade, particularly the cAMP response element binding protein (CREB), have been used to identify those neurons activated specifically during fear memory formation (Han et al., 2007; Han et al., 2009).

One neurotransmitter receptor known to modulate the cAMP-PKA pathway, the dopamine D1 receptor, is also implicated in fear learning. Release of dopamine and subsequent activation of D1 receptors in the BLA are critically involved in the acquisition and consolidation of fear memory (Lamont and Kokkinidis, 1998; Greba et al., 2001). Additionally, we have recently shown that D1-receptor activation is necessary for long-term potentiation of sensory afferents to the BLA (Li et al., 2011). Aside from direct effects on synaptic plasticity, D1 receptor activation may promote fear learning by facilitating an MPO. Considering that the MPO must be uncovered by activation of PKA *in vitro*, D1-receptor activation could provide the requisite PKA activation to initiate a self-reinforcing high delta / low theta oscillation *in vivo*. Importantly, in the prefrontal cortex, application of dopamine mimics the effect of a working memory task to entrain firing of principal neurons to an ongoing theta oscillation (Benchenane et al., 2010). One possible explanation, which parallels our observations in the BLA *in vitro*, is that interneurons maintain a network oscillation by providing a background of rhythmic activity to which principal neurons are, at baseline, minimally sensitive. In this model, the principal neurons become more sensitive to rhythmic inhibitory input from the interneurons by activation of PKA, either directly (as in our hands, with forskolin) or with the introduction of dopamine (either

artificially or endogenously through a behavioral task) (Benchenane et al., 2010; Young, 2011). Interestingly, activation of D1 receptors has also been shown to enhance spike-timing dependent plasticity, potentially compounding with the effects of D1 activation on spike-timing precision via the MPO (Zhang et al., 2009).

We have shown that inhibition of adenylyl cyclase and cAMP production by activation of group II metabotropic glutamate receptors completely abolished the high amplitude MPO induced by forskolin and 4-AP. Activation of these receptors has been associated with reductions in fear learning, as well as de-potentation of synapses and long-term depression (Pin and Duvoisin, 1995; Lin et al., 2000; Lin et al., 2005), providing further support for a role for MPOs in BLA-dependent fear learning. Interestingly, the G_i-coupled type 1 cannabinoid receptor has been shown to reduce neural synchrony and dampen theta and gamma oscillations in the hippocampus (Robbe et al., 2006), further suggesting changes in cAMP levels can bi-directionally modulate the propensity of a network to oscillate.

While network oscillations contribute to normal brain functions, including fear learning, aberrant oscillations have been implicated in the pathophysiology of psychiatric disorders. For example, it is well established that diminished synchrony between pyramidal neurons, and consequently aberrant network oscillations in the gamma band, are involved in the pathophysiology of schizophrenia (Lewis et al., 2005). Interestingly, the changes in oscillations observed in schizophrenia have been specifically linked to diminished function in the PV^+ subpopulation of interneurons in the cortex (Lewis et al., 2005). It is worth noting that theta oscillations are thought to modulate the gain of gamma oscillations, and both are produced through the action of PV^+ interneurons (Canolty et al., 2006; Bartos et al., 2007; Jensen and Colgin, 2007). Gamma-frequency oscillations are observed in the BLA both *in vivo* and *in vitro* (Sinfield and Collins, 2006; Randall et al., 2011), and may be generated by similar mechanisms in the BLA as in the cortex due to their similar composition and architecture (Carlsen and Heimer, 1988). Considering the importance of neural oscillations and that compound IPSPs may

influence gamma oscillations through their effects on high delta / low theta oscillations, future studies should address changes in oscillations and PV^+ interneurons in the amygdala in various psychiatric disorders, particularly post-traumatic stress disorder and others linked to fear learning (Rainnie and Ressler, 2009).

Figure 6.1: Spontaneous, compound IPSPs in the BLA were synchronized across principal neurons and with bursts in inhibitory interneurons

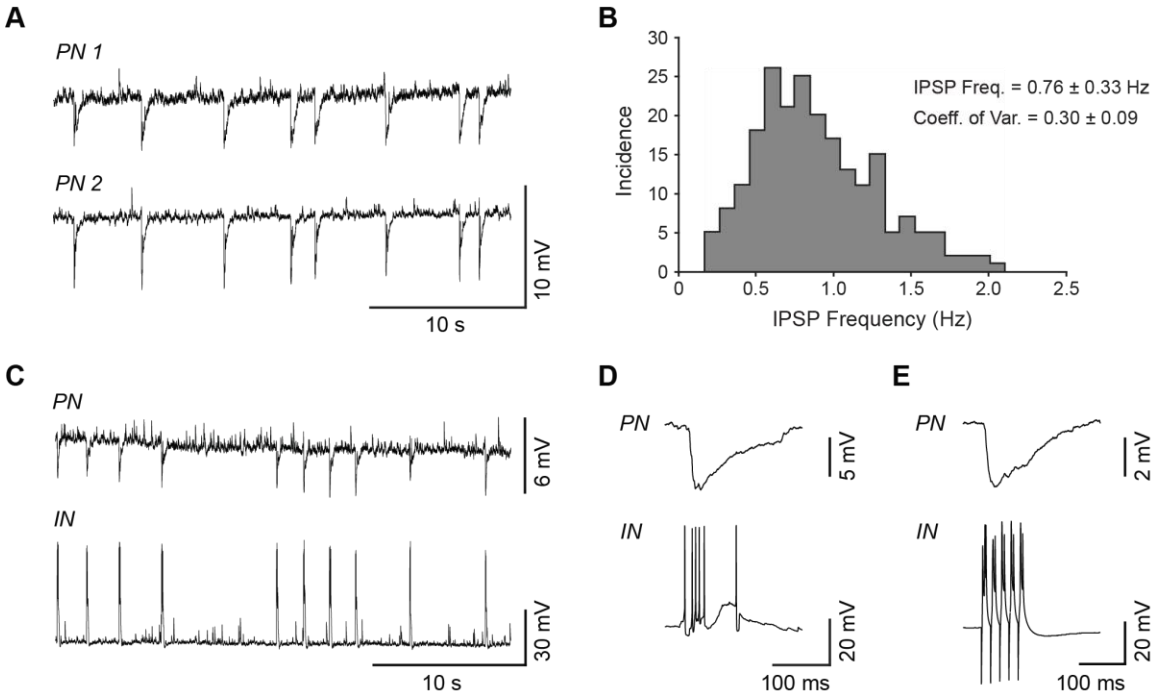

Figure 6.1: Spontaneous, compound IPSPs in the BLA were synchronized across principal neurons and with bursts in inhibitory interneurons. (A) A representative pair of primate BLA principal neurons, held at -60 mV, showing compound IPSPs that are rhythmic and highly synchronized, observed during gap-free recordings. (B) A histogram plotting instantaneous frequency of compound IPSPs during 30-second recordings from 12 primate BLA principal neurons. (C) Paired recordings in the primate BLA of a principal neuron receiving compound IPSPs and a burst-firing parvalbumin interneuron, both held at -60 mV. (D) An example of a burst-IPSP pair shown at higher temporal resolution. (E) A compound IPSP can be induced in a BLA principal neuron by using current injection to drive bursting activity in the interneuron.

Figure 6.2: Spontaneous, compound IPSPs coordinated spike timing and promoted rhythmic firing in the primate BLA

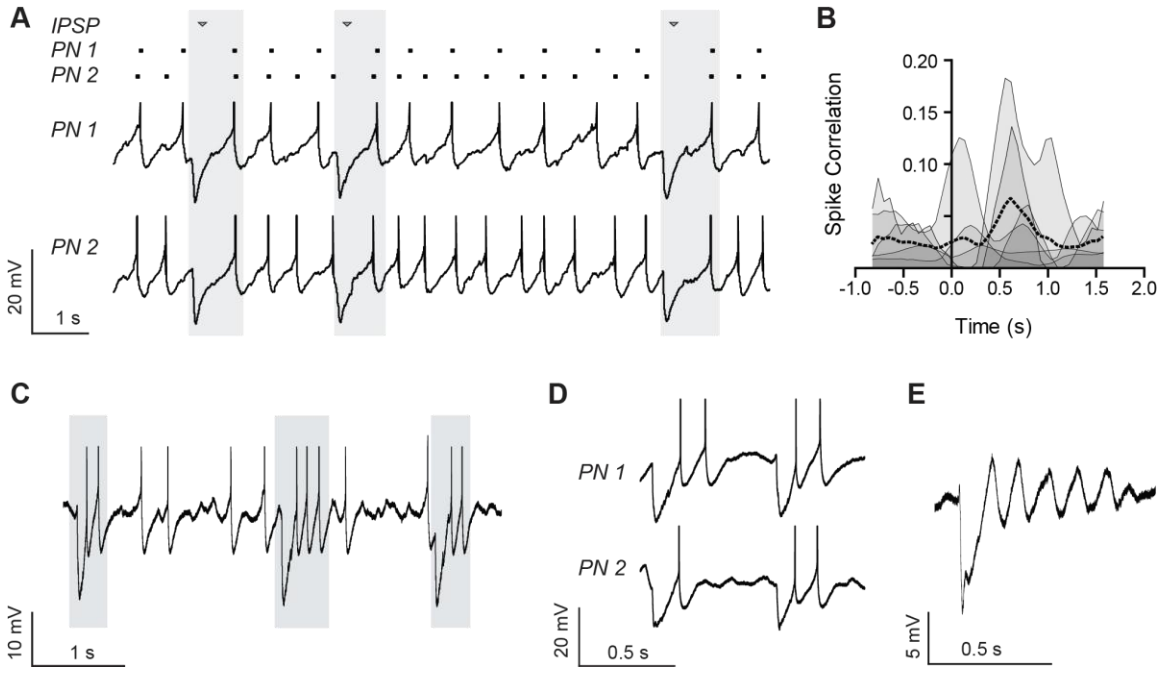

Figure 6.2: Spontaneous, compound IPSPs coordinated spike timing and promoted rhythmic firing in the primate BLA. (A) Spontaneous, compound IPSPs exhibited by a representative pair of primate BLA projection neurons, depolarized to action potential threshold (-45 to -40 mV) using a DC current injection. A raster plot highlights the relative synchrony of spikes following the IPSPs, highlighted in gray boxes. Action potentials are cropped at -30 mV (n = 6). (B) A spike correlation metric (see Methods) is plotted for 6 pairs of primate BLA principal neurons exhibiting compound IPSPs and depolarized to threshold, as in *A*. Correlation is plotted for each pair as an individual, smoothed trace (thin black lines) representing the mean correlation surrounding every spontaneous, compound IPSP, with the peak of each IPSP aligned to time 0. The mean of all 6 pairs is superimposed as a dotted black line. (C-D) A representative single (C, n = 4) and pair of (D, n = 2) primate BLA principal neurons exhibiting rhythmic firing upon rebound from spontaneous, compound IPSPs. Neurons were depolarized to threshold, as in *A*. IPSPs and rebound firing are highlighted with gray boxes in *C*. Action potentials were cropped at -30mV. (E) A primate BLA principal neuron, depolarized as in *A*, exhibiting a damped membrane potential oscillation in response to a spontaneous, compound IPSP.

Figure 6.3: Spike-timing precision diminishes in spike trains and is reset by compound IPSPs

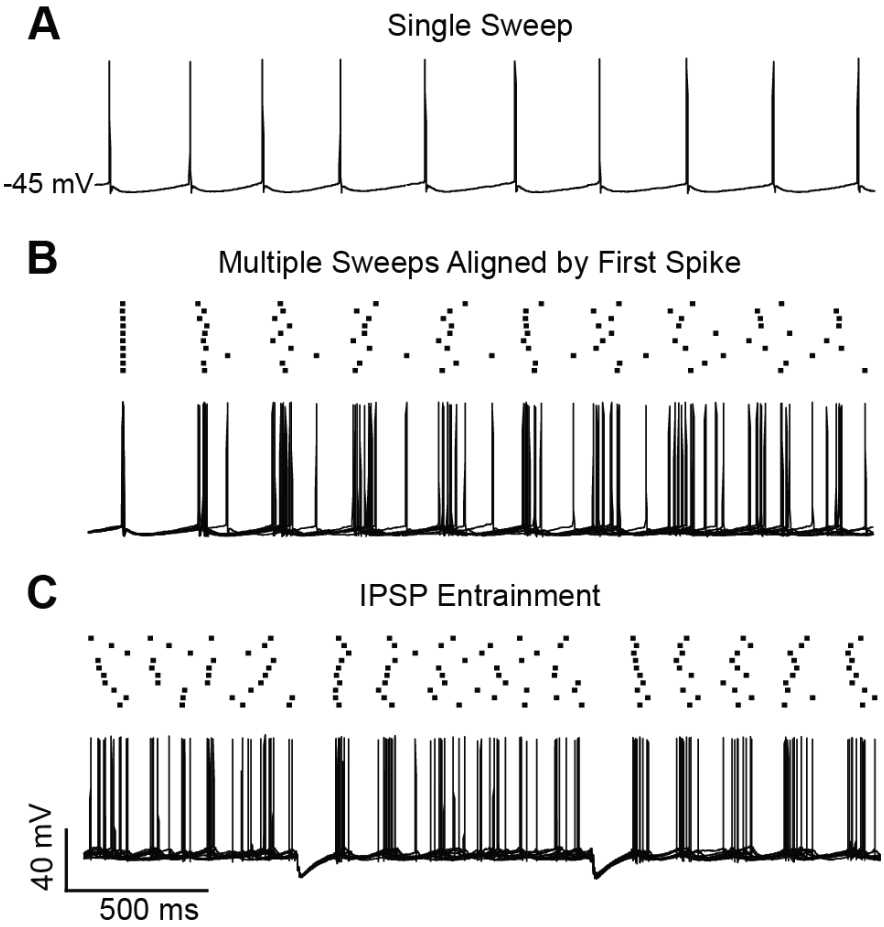

Figure 6.3: Spike-timing precision diminishes in spike trains and is reset by compound IPSPs. (A) A single sweep recorded from a spiking BLA principal neuron, held at -45 mV by steady-state current injection, displaying a typical regular firing pattern. (B) Multiple sweeps like that in *A* overlaid and aligned by their first spikes. A raster plot illustrates decay of spike-timing reliability. (C) Injection of artificial IPSPs recovers spike-timing precision.

Figure 6.4: Artificial and evoked compound IPSPs improved spike-timing precision in individual BLA principal neurons

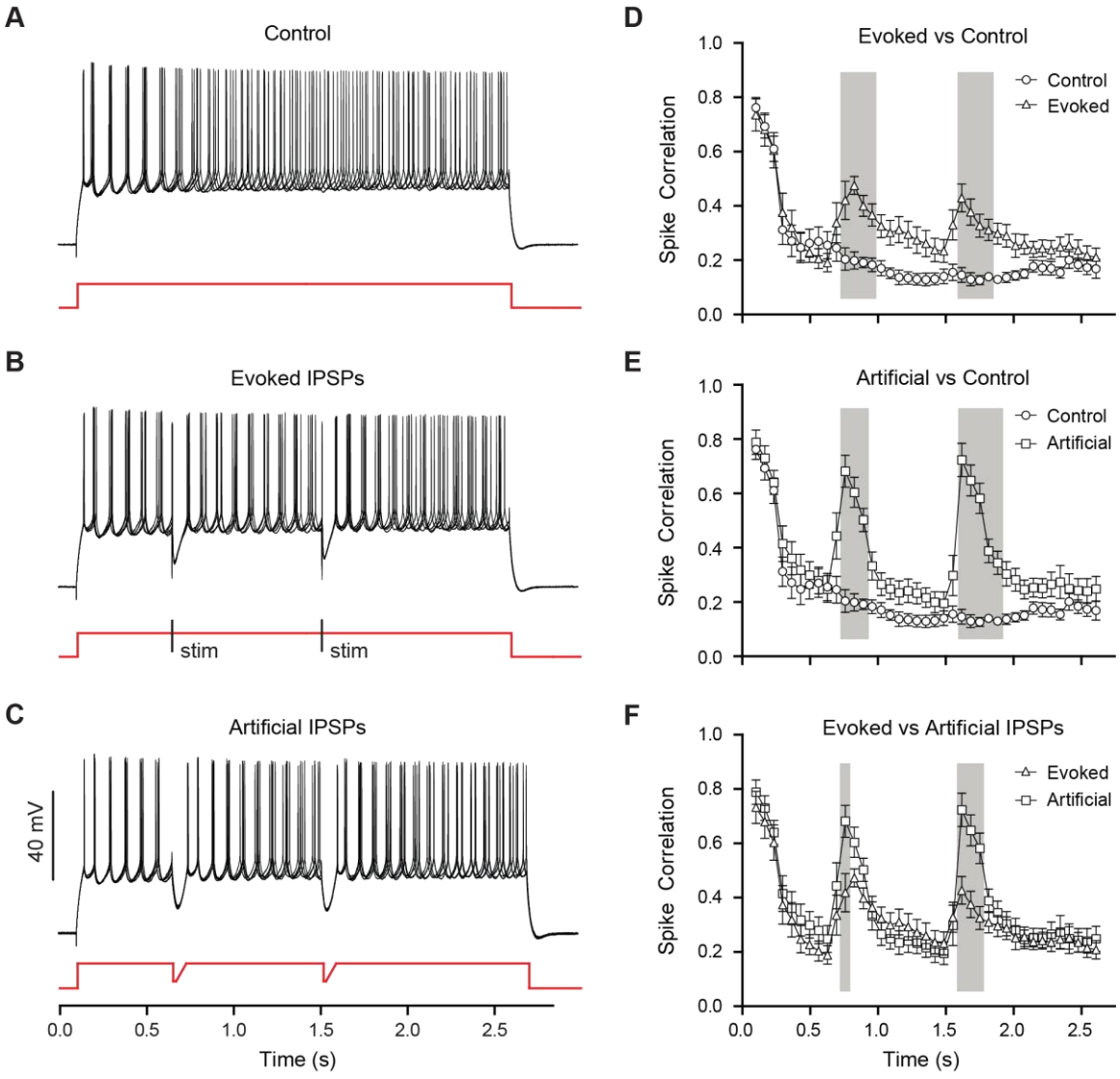

Figure 6.4: Artificial and evoked compound IPSPs improved spike-timing precision in individual BLA principal neurons. (A) Five superimposed traces from a representative principal neuron, held at -60 mV, showing a train of action potentials in response to a depolarizing current step in the presence of DNQX (20 μM), RS-CPP (10 μM) and CGP (2 μM); note the loss of spike-timing precision as the spike train progresses. (B, C) Similar traces to *A* with the injection of evoked (B) or artificial (C) compound IPSPs to demonstrate improvement of spike-timing precision following a compound IPSP. (D, E, F) Comparisons of spike-timing precision for neurons with no IPSPs (Control, n = 11), evoked IPSPs (n = 11), and artificial IPSPs (n = 11), assessed with a spike correlation metric (see Methods) and plotted as mean ± SEM. Comparisons were made using a two-way ANOVA (see Results), and windows of significant differences ($p < 0.05$) in spike correlation are denoted with grey boxes.

Figure 6.5: Artificial, compound IPSPs coordinated spike timing across pairs of BLA principal neurons

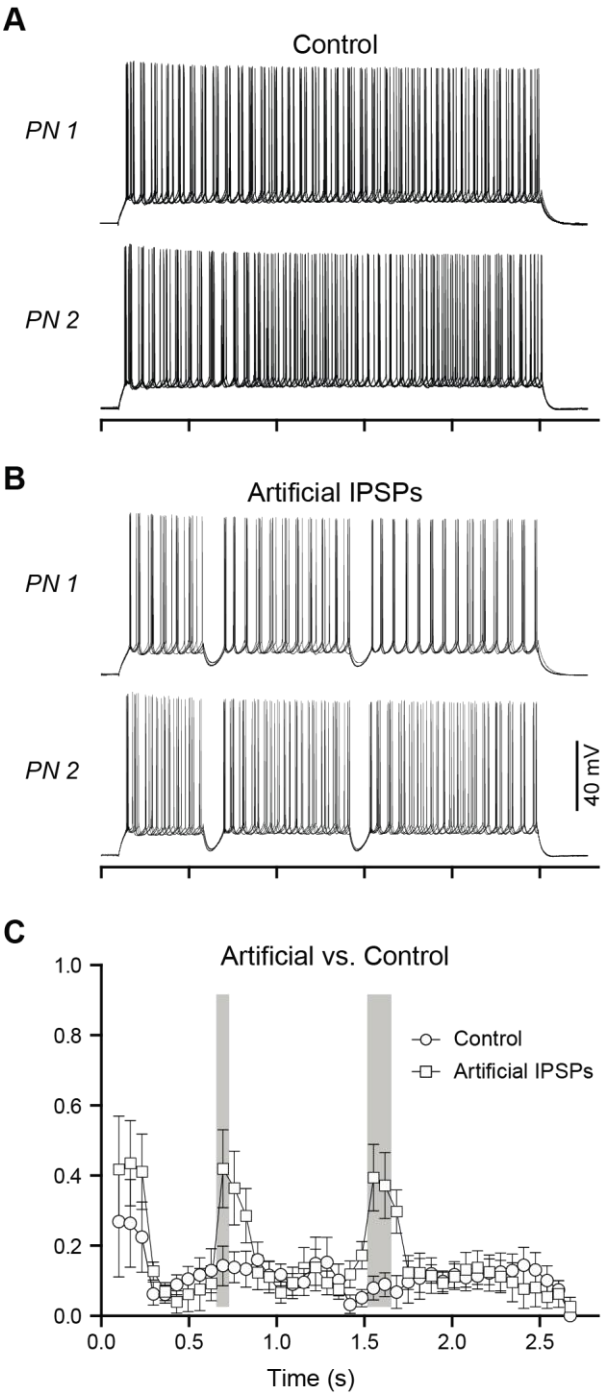

Figure 6.5: Artificial, compound IPSPs coordinated spike timing across pairs of BLA principal neurons. (A) Five overlaid, consecutive traces of action potentials during paired recordings of BLA principal neurons, held at -60 mV, in response to a depolarizing current injection without IPSPs and (B) with two IPSPs. (C) Spike correlation metric calculated across pairs of neurons when artificial IPSPs are injected compared to the control condition ($n = 6$ pairs), plotted against time. Comparisons were made using a two-way ANOVA (see Results), and grey boxes denote windows of significant differences ($p < 0.05$) in spike correlation.

Figure 6.6: BLA principal neurons exhibited a modifiable intrinsic resonance and a membrane potential oscillation that was facilitated by compound IPSPs

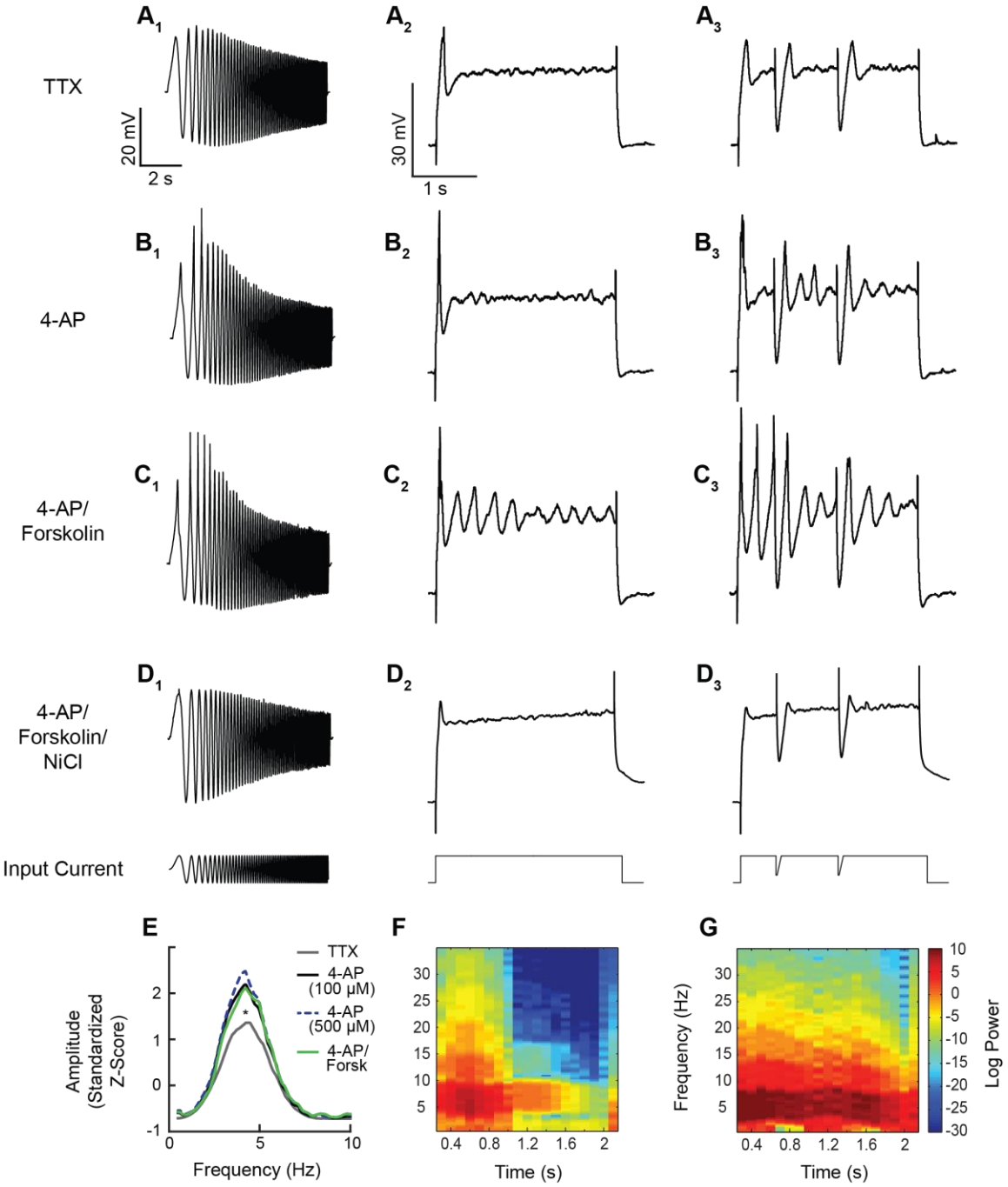

Figure 6.6: BLA principal neurons exhibited a modifiable intrinsic resonance and a membrane potential oscillation that was facilitated by compound IPSPs. (A1-D1) Principal neuron membrane potential response to injection of a sinusoidal current with constant amplitude and linearly changing frequency (0-12 Hz) in the presence of various drug cocktails. All neurons were held at baseline of -60 mV. (A1) Typical voltage response to the sinusoidal current in TTX (1 μM). The resonance of BLA principal neurons can be enhanced by application of 4-AP (B1, 500 μM) and the adenylyl cyclase activator, forskolin (C1, 10 μM), and is abolished by application of NiCl (500 μM, D1). Analysis of power spectra (E) shows that the enhancement of resonance by 4-AP and forskolin is significantly different from baseline ($p < 0.05$). (A2-D3) Intrinsic membrane oscillations of BLA principal neurons, held at -60 mV, in response to a steady depolarizing current injection (A2-D2) and in response to the same current injection with superimposed IPSPs (A3-D3). Similar to resonant properties, membrane oscillations are enhanced by application of 4-AP and forskolin, and abolished in NiCl. Injection of artificial IPSPs in A3-D3 significantly enhanced the amplitude and duration of oscillations (F and G; spectrograms illustrate data from C2 and C3 respectively).

Figure 6.7: The peak power of the membrane potential oscillation was sensitive to modulation of I_A and I_T and activation of PKA

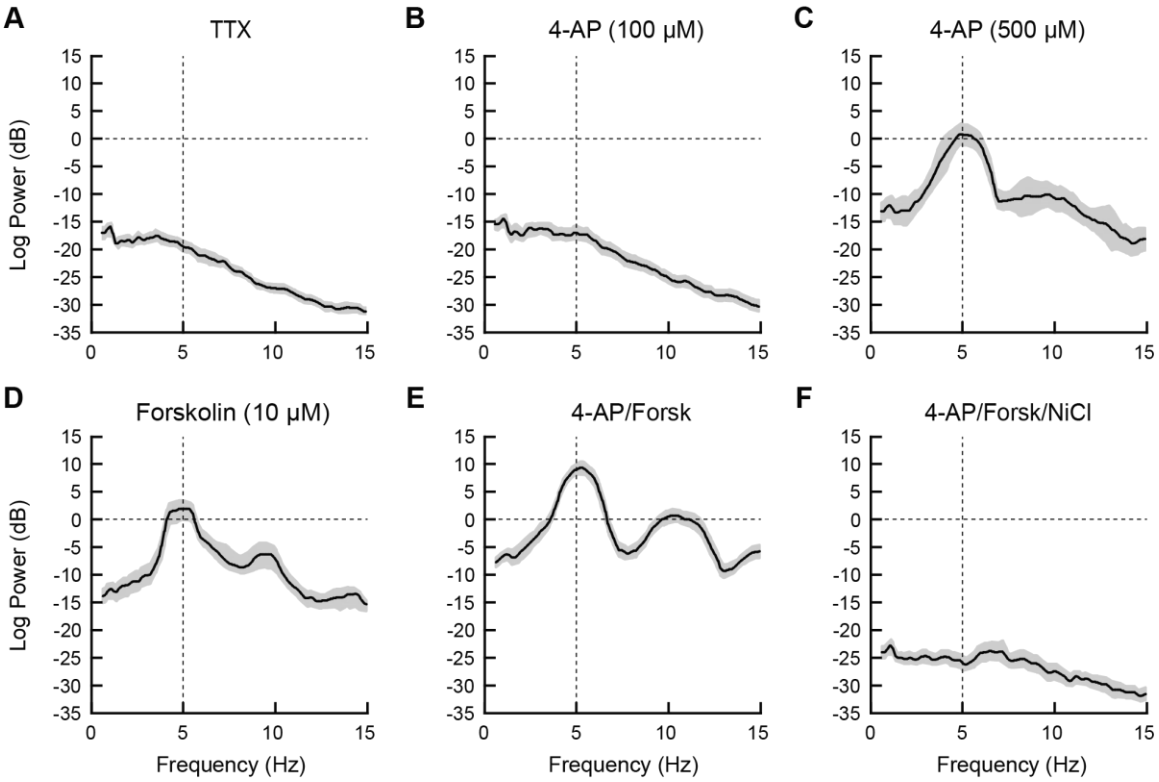

Figure 6.7: The peak power of the membrane potential oscillation was sensitive to modulation of I_A and I_T and activation of PKA. Power spectra of MPOs in BLA PNs in response to a depolarizing step with artificial IPSPs, with mean (solid lines) and 95% confidence intervals (shaded region). Frequencies at which the 95% confidence intervals do not overlap indicate statistically significant differences among the plots. (A) In the presence of TTX, neurons exhibit a weak MPO. (B,C) MPOs were not enhanced by bath application of 100 µM 4-AP (B) but were significantly enhanced by 500 µM 4-AP, with peak power at 4.9 Hz (C). (D) Application of forksolin, an activator of the c-AMP cascade, at 10 µM also enhanced a MPO with peak power at 4.8 Hz. (E) The MPO was significantly enhanced by a combination of 500 µM 4-AP and 10 µM forskolin, with peak power greater than for either drug alone but occurring at a similar frequency. (F) The MPO observed in forskolin and 4-AP was completely abolished by co-application of NiCl (500 µM) to block low-threshold calcium channels.

Figure 6.8: Forskolin and 4-AP modulation of the membrane potential oscillation were not mimicked by dideoxy-forskolin and TEA, respectively

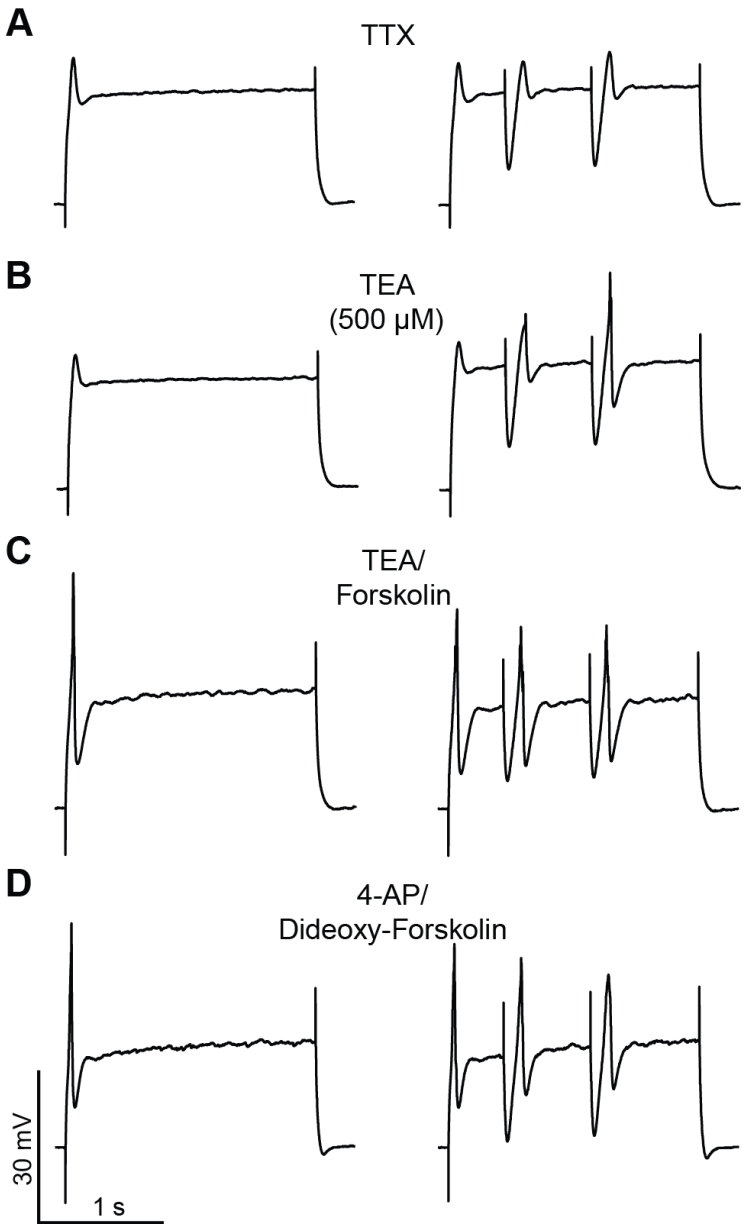

Figure 6.8: Forskolin and 4-AP modulation of the membrane potential oscillation were not mimicked by dideoxy-forskolin and TEA, respectively. Intrinsic membrane oscillations of BLA principal neurons, held at -60 mV, in response to a steady depolarizing current injection with and without artificial IPSPs. (A) Shows typical small membrane oscillations in TTX during the depolarizing current injection. In the presence of 1 μM TTX, the introduction of IPSPs evoked a transient depolarizing deflection at the termination of each IPSP, but failed to unmask a MPO. (B) MPOs are not enhanced by application of TEA (500 μM). (C) The addition of 10 μM forskolin had a small enhancing effect on MPOs in the presence of TEA. (D) Application of the inactive isomer dideoxy-forskolin in the presence of 4-AP did not enhance the MPO as observed previously with forskolin.

Figure 6.9: Membrane potential oscillations in the BLA were bi-directionally modulated by the adenylyl cyclase signaling cascade

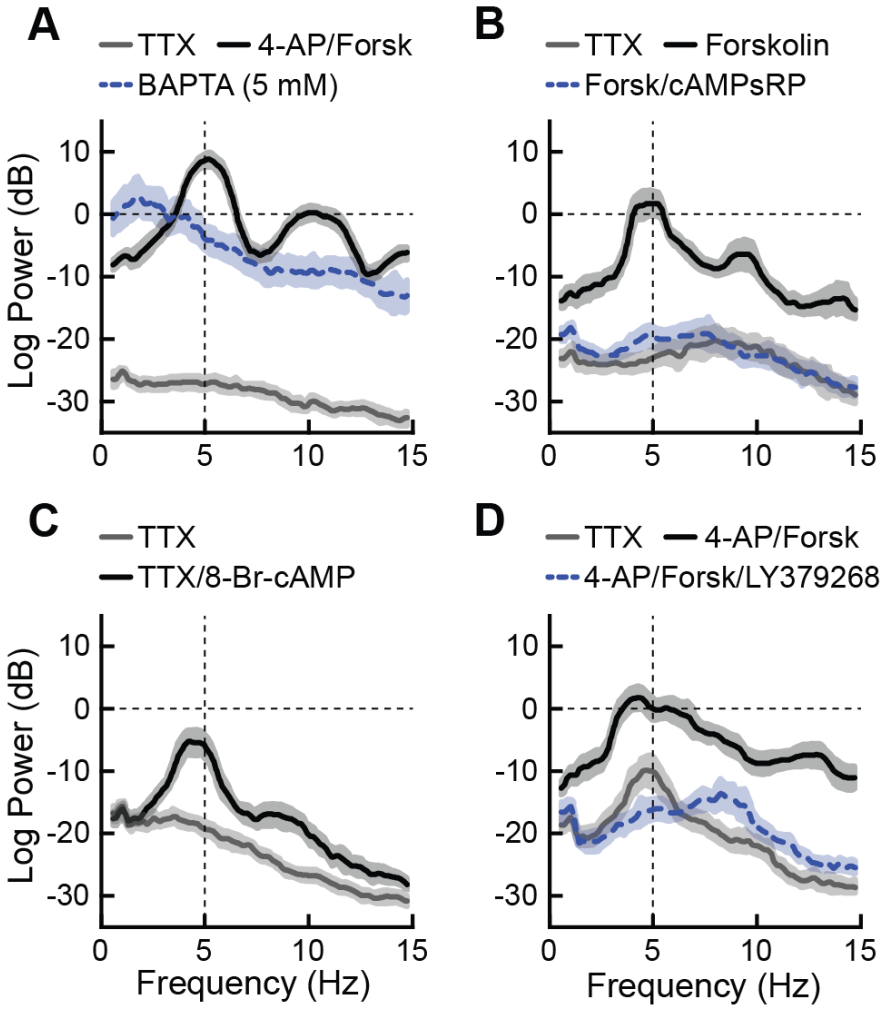

Figure 6.9: Membrane potential oscillations in the BLA were bi-directionally modulated by the adenylyl cyclase signaling cascade. Cumulative power spectra of intrinsic theta frequency MPOs in BLA principal neurons. Responses are plotted as mean (solid lines) and 95% confidence intervals (shaded regions). Frequencies at which the 95% confidence intervals do not overlap indicate statistically significant differences among the plots. (A) BAPTA-containing patch solutions disorganized the frequency tuning of 4-AP- and forskolin-induced MPOs. (B) Inhibiting PKA activation completely abolishes forskolin-induced MPOs. (C) Activation of PKA with the cAMP analog 8Br-cAMP induces MPOs in TTX alone that are similar to those observed in response to forskolin. (D) Activation of mGluR II glutamate receptors with LY379268 completely blocked 4-AP and forskolin-induced theta MPOs.

Chapter 7: Discussion

7.1 Summary of Results

The work presented here represents three major contributions to the state of knowledge concerning the function and development of the amygdala: 1) supporting a novel function of the neurotransmitter GABA in the BLA to facilitate network activation, 2) providing the first evidence that BLA neurons and GABAergic transmission are physiologically distinct in juveniles and adults, and 3) identifying effects of prenatal stress on the developmental trajectory of the BLA, including GABAergic transmission, that may underlie the conferred risk for psychiatric illness. The results of the studies on the normative development of BLA physiology and morphology are summarized in **Figure 7.1**.

In terms of GABAergic function in the adult BLA, we hypothesized that BLA neurons rebounding from GABAergic inhibition would exhibit membrane potential oscillations that would regulate their action potential firing. We found that rhythmic inhibition, which is synchronized across BLA principal neurons, can coordinate the spiking within and across neurons. Furthermore, we suggest that this coordinated firing is a mechanism utilized by the adult circuit for the generation of network oscillations. This novel mechanism should influence the way we conceptualize GABA in the BLA, because this neurotransmitter has been classically treated as a singular system that functions solely to dampen activity and suppress fear (Quirk and Gehlert, 2003; Ehrlich et al., 2009). Because rhythmic inhibition is driven by parvalbumin-expressing interneurons, these findings argue for heterogeneity of BLA interneurons that should influence how we understand the effects of neuromodulators in the BLA. Considering the BLA circuit in terms of its capacity to generate network oscillations, the developmental changes we report in the BLA circuit are likely of great consequence for BLA function. Implications are discussed in **Section 7.2.2**.

We observed a wealth of interrelated changes to BLA neurons during postnatal development. These changes, which often covered an order of magnitude or more, occur

throughout a period of emotional development that includes the emergence of and transitions to many amygdala-dependent behaviors. We propose that the maturation of amygdala function and emotional behavior occurs downstream of the changes to individual BLA neurons and synaptic transmission during the first postnatal month, which include: extension and expansion of dendrites, an approximately 10-fold increase in dendritic spine density, large reductions in input resistance and membrane time constant, faster action potentials with more hyperpolarized thresholds, larger and faster afterhyperpolarizations, higher spike rates, higher resonance frequency and greater propensity to oscillate, shifting subunits of ion channels that contribute to intrinsic properties and oscillations, the emergence of inhibitory GABA and a feed-forward shunt of cortical inputs, faster synaptic GABA responses that do not exhibit short-term synaptic depression, and changes to $GABA_A$ receptor subunit expression.

As stated above, we also showed that PS alters the developmental trajectory of many of these properties and concomitantly perturbs emotional behavior. Specifically, BLA principal neurons in PS animals had a more hyperpolarized resting membrane potential and action potential threshold across all ages, received slower GABAergic PSCs in a specific window around P14, did not exhibit the typical slow IPSCs in adulthood, and had reduced excitability starting at P28. Furthermore, PS reduced the expression of $GABA_A$ receptor α1 subunit mRNA across all ages, and by at least 2 fold starting at P17. Finally, PS animals exhibited reduced anxiety-like behavior in adulthood, a trend toward reduced anxiety-like behavior at P17, and a trend toward reduced sociability. These effects of PS are consistent with many findings or models of amygdala deficits in autism spectrum disorders and schizophrenia, suggesting perturbation of BLA development following PS contributes to the etiology of neurodevelopmental disorders.

7.2 Integration of Findings

7.2.1 Importance of Studying Developmental Trajectories

Neuroconstructivist theory suggests that brain function, genes, and environmental factors actively interact to shape brain development (Karmiloff-Smith, 2009). While a very simplistic and intuitive idea, the consequences can be profound and easily overlooked. For instance, researchers have long attempted to study neurodevelopmental disorders from the perspective of the adult brain, generally unsuccessfully. As Insel contends, the last century has seen little change in the prevalence or societal burden of mental illness, all the while diseases including tuberculosis and leprosy have seen great advances in treatment. One explanation for the relative difficulty in pinpointing the pathology and etiology of these disorders is that their neurodevelopmental basis adds many layers of complexity (2010). The classical (and understandably necessary) way of initially approaching neural function, where brain regions are modular and relatively insular (Karmiloff-Smith, 2009), is now outdated and has probably contributed to this stagnation.

Our findings of marked developmental change to BLA neurons support the idea that the amygdala is not a single module – for instance, a "fear center" – but likely has distinct functions throughout development. These changes occur at the precise ages when disorders like anxiety, depression, autism, and schizophrenia are thought to be instantiated, at least in part. Therefore, understanding the normative trajectory is an absolute necessity for identifying where perturbations arise and how they contribute to disease onset.

The findings we present on the effects of PS on amygdala development perfectly illustrate the importance of studying developmental trajectories. We identified a number of transient changes and precise ages of onset for alterations due to prenatal stress. These include a change to GABAergic transmission that came and went completely within a 7 day window from P10 to P17, and a shift in GABA receptor gene expression from a reduction of approximately 20% at P14 to nearly 60% by P17. Such a thorough examination of developmental trajectories

was required to gain this level of precision in detection. Furthermore, had we not started with a systematic characterization of normative development of the brain systems of interest, we would not have been able to focus on windows of highest plasticity that are likely most vulnerable to perturbation. Without the thorough analysis employed here, we would have less precise knowledge regarding ages of onset for the effects of PS, and may have completely overlooked the transient change in GABAergic transmission around P14.

Section 1.4.1 outlines a number of changes to the amygdala cause by PS, a number of which were only measured in adulthood. While changes to the adult system provide a valuable starting point, it is extremely difficult to build a working model of how these changes – for instance, increased density of PV^+ interneurons – influences adult amygdala function, when developmental processes may be altered. An important future direction will be to apply thorough detection methods during early development for effects of early life risk factors only observed in adulthood, to better identify when changes occur. However, there will still be limitations to interpretation until we better understand how relevant neural systems function in the immature brain.

7.2.2 Potential Impact of Prenatal Stress on Emotion Via Amygdala Network Oscillations

In **Section 1.2.3.2** we described a number of studies implicating network oscillations in the BLA in emotional processing. The findings presented in **Chapter 6** illustrate how GABA in the BLA may contribute to the generation of network oscillations, through interactions with intrinsic oscillations in BLA neurons. Interestingly, many aspects of the BLA circuit that contribute to the GABA-oscillation interaction are altered in the immature BLA and exhibit convergent maturation. For instance, spontaneous membrane potential oscillations become much more prominent around P21, reflecting changes to active membrane currents that likely also drive the concurrent shift of resonance frequency into the adult range, and the frequency of BLA network oscillations expressed during fear (**Section 2.5.2**).

Around the same time, the GABAergic circuit is becoming refined. PV^+ interneurons, which provide the synchronized, rhythmic inhibition that coordinates BLA principal neurons, are first detected in the BLA around the same age (Berdel and Morys, 2000). In **Section 4.4.3**, we showed that $GABA_A$ receptors first become inhibitory around P14, suggesting that at younger ages the activity of interneurons would not be able to provide the requisite inhibition to enable a rebound and enhance neuronal oscillations. Furthermore, $GABA_A$ receptor-mediated currents become faster from P14 to P21 (**Section 4.4.2**). The kinetics of individual IPSCs should influence their effect on spike timing (Pouille and Scanziani, 2001) and are known to regulate the ability of GABAergic afferents to entrain postsynaptic oscillations (Tamas et al., 2004). Therefore, the near simultaneous shift towards faster, more inhibitory IPSCs with the emergence of oscillatory properties in BLA principal neurons represents both sides of the circuit assuming their mature properties, becoming able to promote network oscillations. In support of this model, no discernible network oscillations were observed in the BLA from birth through P14 in an electroencephalography study (Snead and Stephens, 1983). Prominent oscillations emerge by P14 age in other regions including cortex, hippocampus and thalamus, suggesting network oscillations in the BLA develop relatively late, driven by the maturation of BLA neurons and GABAergic transmission.

To determine whether kinetics influence the ability of synchronized IPSCs to entrain spiking and coordinate BLA neurons, we performed the following pilot study. Similar to the studies in **Section 6.4.2**, individual adult BLA principal neurons were patch clamped and injected with a depolarizing current step, and artificial IPSCs were injected to improve spike timing precision (Figure 7.2). In this study, we varied the slope of the decay of the artificial IPSC, to model changes in the kinetics of rhythmic IPSCs. While this data is very preliminary (n = 6), we found that the kinetics of the IPSC moderate its effects on spike timing. Specifically, IPSCs with a decay time constant (here defined as 63.2% of the duration of the off-ramp) of ~250 ms were best at improving spike timing, with a variance across 5 sweeps summed for the first 5 spikes of

291 ms^2. By comparison, a faster decay of ~125 ms and a slower decay of ~630 ms yielded much larger spike timing variance of 899 and 904 ms^2, respectively.

These preliminary data suggest changes to the kinetics of IPSCs will moderate the ability of PV^+ interneurons to organize network oscillations. We propose that IPSCs that are too fast or too slow do not de-inactive and activate calcium currents enough, respectively, to promote oscillations. We will test these hypotheses with future studies.

With these data in mind, the effects we describe in Section 5.4.4 – that PS alters IPSC kinetics in the BLA at P14 and in adulthood – may reflect a change in the capacity of the BLA to generate network oscillations related to fear expression. It is important to keep in mind those effects were observed for single events and not the compound events that make up a rhythmic IPSC, and were not specific to afferents of PV^+ interneurons, but the effect on kinetics may very well translate to rhythmic IPSCs. Future studies should therefore also address whether the reduced anxiety-like behavior we observed in PS animals reflects diminished production of network oscillations in the BLA.

7.2.3 Applying Critical Period Concepts to BLA Development

One potential criticism of the arguments made herein is that assumptions are made about the applicability of the concept of critical periods to the amygdala. The concept was first described for visual cortical development, after all. The BLA is considered a "cortical-like" structure, with a similar complement of neurons and physiology to the visual cortex (Carlsen and Heimer, 1988). It is important to acknowledge this major hypothesis going forward - that critical periods of plasticity in the BLA are of consequence for emotion.

In the visual system, the term 'critical period' refers to a specific phenomenon: a window when sensory stimuli are capable of causing gross reorganization of the cortex. This concept lends itself nicely to considering 'sensitive periods' for the amygdala, when acute exposure to external stimuli like stress might cause gross reorganization of the amygdala. However, we

extended the concept of critical periods to refer simply to periods of abundant plasticity, not necessarily to sensitivity to external stimuli. In this model, periods of heightened plasticity represent sensitivity to the effects not simply of acutely encountered environmental stimuli, but to cascades set in motion early in development by early life risk factors or genetically encoded alterations to basic developmental processes. Critical periods in the development of the amygdala may thereby constitute windows when risk is translated to perturbations of physiology or behavior. Critical periods could be the key to the etiology of neurodevelopmental disorders that can emerge abruptly, like autism or schizophrenia, and help explain periods of dormancy between exposure to environmental risk factors, like prenatal stress, and the manifestation of symptoms. Several groups have broadly argued for this interpretation (Pine, 2002; Monk, 2008; King et al., 2013), but it is still theoretical.

In light of the yet theoretical nature of critical period in amygdala development, it is important to consider deficits that may be conferred by changes to the timing of developmental processes in the amygdala. Identifying specific hypotheses for the impact of changes to GABA-dependent circuit maturation will be important for further characterizing our prenatal stress model. Even in the absence of a discrete "critical period" for a developmental process, akin to ocular dominance plasticity, there may be profound effects of alterations to the timing of maturation of plasticity of inputs or balancing excitation and inhibition. In general, mismatched timing of the maturation of brain regions is thought to underlie developmental changes to emotional processing. For instance, as described in **Section 1.2.1**, the amygdala achieving a mature state and coming "online" before the prefrontal cortex is thought to result in limited top-down suppression and hyper-activation of the amygdala during adolescence. This imbalance in developmental processes is also thought to underlie the susceptibility to psychiatric disease onset during adolescence (Drevets, 2003; Yurgelun-Todd, 2007; Casey et al., 2010; Somerville et al., 2010). Precocious maturation of the amygdala could effectively prolong the "adolescent" period of heightened emotionality.

Another proposed effect of changes to the timing of amygdala development is closely related to plasticity of inputs during visual cortical critical periods. As described in **Section 1.4.1.1**, we propose accelerated closing of windows of plasticity due to early amygdala activation results in altered long-range connections of the BLA. Shifting the window of plasticity early may render BLA neurons unreceptive to inputs that arrive late in development, after the window has prematurely closed. Outlined in **Section 1.3.3.1**, late developing inputs to the BLA include those from the frontal cortices, meaning precocious amygdala maturation may reduce the resulting connectivity of the BLA and PFC in adulthood. This model is potentially applicable to anxiety disorders, which may involve diminished top-down control and hyperactivity of the amygdala in adolescence (Correll et al., 2005; Casey et al., 2010). Importantly, ELS has been shown to diminish the integrity of the uncinate fasciculus, which connects the BLA and PFC (Eluvathingal et al., 2006; Govindan et al., 2010), suggesting stressors may influence the amygdala in the proposed manner. Conversely, delayed closure of plasticity windows may provide exaggerated sensitivity to inputs from frontal cortices, which could lead to excessive suppression of the amygdala in adulthood and the flat affect characteristic of schizophrenia. Delayed closure of critical period plasticity, a potential consequence of the diminished $GABA_A$ receptor α1 expression we reported in our novel PS model (**Chapter 5**), may explain the reduced anxiety-like behavior observed in PS animals.

In general, we have employed a bottom-up approach, and started by identifying effects on BLA development of a risk factor for a variety of neurodevelopmental disorders. By beginning to understand how the consequences of prenatal stress we described alter amygdala function and its integration into limbic circuitry, with attention paid to the dynamic nature of those interactions through development, the hope is to engender fresh hypotheses for specific deficits that underlie these complex disorders.

Figure 7.1 Summary of Normative Development of BLA Principal Neurons

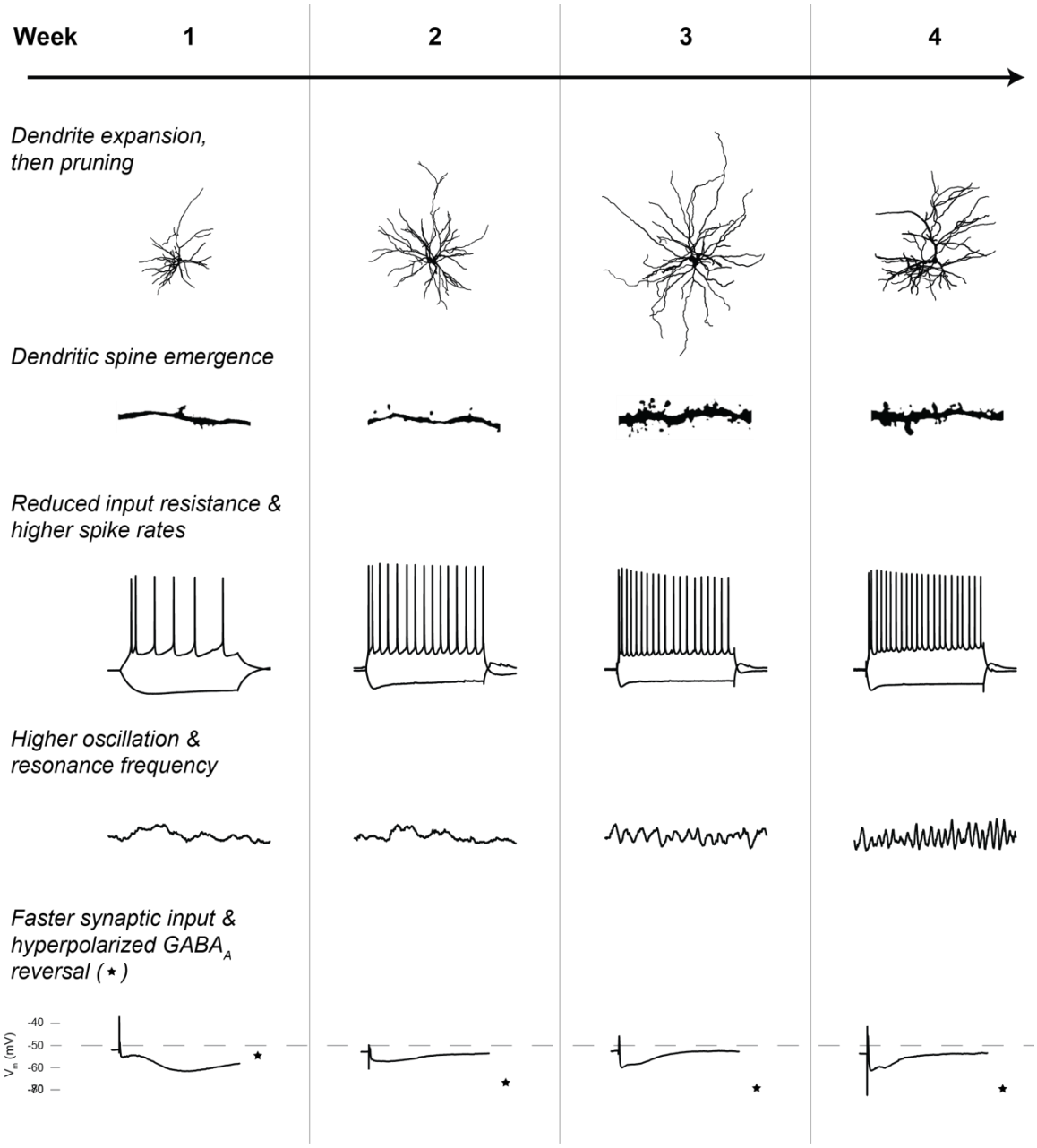

Figure 7.1 Summary of Normative Development of BLA Principal Neurons. Schematic illustrating the representative phenotype of BLA principal neurons at 1, 2, 3, and 4 weeks of age in terms of dendritic morphology, electrophysiological responses to hyperpolarizing and depolarizing current steps, spontaneous oscillations, and synaptic transmission.

Figure 7.2 Ability of IPSCs to Organize Spiking May Be Moderated by IPSC Kinetics

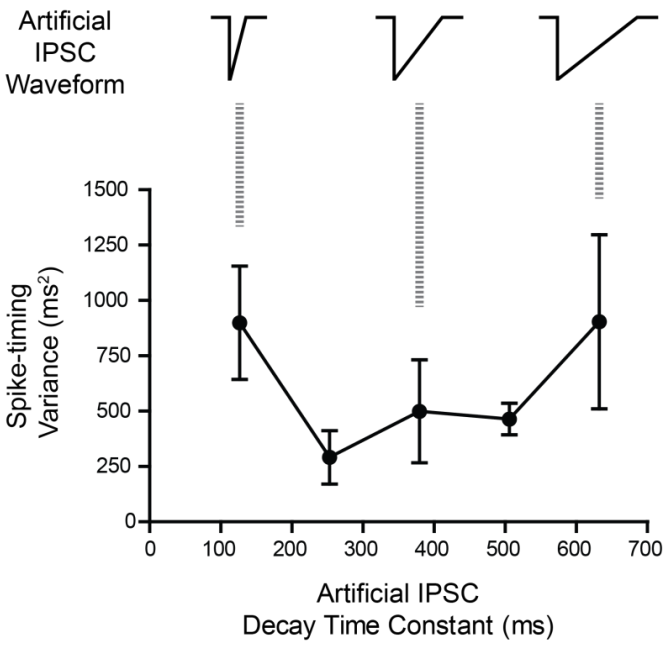

Figure 7.2 Ability of IPSCs to Organize Spiking May Be Moderated by IPSC Kinetics. The effects of artificial IPSC decay kinetics on the ability to organize spiking were tested. Action potential trains were elicited in adult, BLA principal neurons from resting membrane potential using 1s depolarizing current steps. Artificial IPSCs were injected during the step to hyperpolarize the neuron, and the variance of spike times across 5 sweeps was calculated for the first 5 action potentials following the IPSC. The duration of the off-ramp of the IPSC was varied for each injected neuron, with the various stimuli injected in a random order. These preliminary results suggest the variability of spike times depend on the kinetics of the preceding IPSC. n = 6.

References

Abbott LF, Regehr WG (2004) Synaptic computation. Nature 431:796-803.

Adolphs R (2010) What does the amygdala contribute to social cognition? Annals of the New York Academy of Sciences 1191:42-61.

Adolphs R, Tranel D, Damasio AR (1998) The human amygdala in social judgment. Nature 393:470-474.

Adolphs R, Tranel D, Denburg N (2000) Impaired emotional declarative memory following unilateral amygdala damage. Learn Mem 7:180-186.

Adolphs R, Baron-Cohen S, Tranel D (2002) Impaired recognition of social emotions following amygdala damage. Journal of cognitive neuroscience 14:1264-1274.

Adolphs R, Tranel D, Damasio H, Damasio A (1994) Impaired recognition of emotion in facial expressions following bilateral damage to the human amygdala. Nature 372:669-672.

Aggleton JP, Saunders RC (2000) The amygdala - what's happened in the last decade? In: The Amygdala: A Functional Analysis (Aggleton JP, ed). London: Oxford University Press.

Akerman CJ, Cline HT (2007) Refining the roles of GABAergic signaling during neural circuit formation. Trends in neurosciences 30:382-389.

Akirav I, Raizel H, Maroun M (2006) Enhancement of conditioned fear extinction by infusion of the GABA(A) agonist muscimol into the rat prefrontal cortex and amygdala. The European journal of neuroscience 23:758-764.

Aleman A, Kahn RS (2005) Strange feelings: do amygdala abnormalities dysregulate the emotional brain in schizophrenia? Progress in neurobiology 77:283-298.

Amaral DG, Schumann CM, Nordahl CW (2008) Neuroanatomy of autism. Trends in neurosciences 31:137-145.

Ambroggi F, Ishikawa A, Fields HL, Nicola SM (2008) Basolateral amygdala neurons facilitate reward-seeking behavior by exciting nucleus accumbens neurons. Neuron 59:648-661.

Andersen SL, Tomada A, Vincow ES, Valente E, Polcari A, Teicher MH (2008) Preliminary evidence for sensitive periods in the effect of childhood sexual abuse on regional brain development. J Neuropsychiatry Clin Neurosci 20:292-301.

Anderson D, Mehaffey WH, Iftinca M, Rehak R, Engbers JD, Hameed S, Zamponi GW, Turner RW (2010) Regulation of neuronal activity by Cav3-Kv4 channel signaling complexes. Nature neuroscience 13:333-337.

Anderson SA, Classey JD, Conde F, Lund JS, Lewis DA (1995) Synchronous development of pyramidal neuron dendritic spines and parvalbumin-immunoreactive chandelier neuron axon terminals in layer III of monkey prefrontal cortex. Neuroscience 67:7-22.

Arborelius L, Owens MJ, Plotsky PM, Nemeroff CB (1999) The role of corticotropin-releasing factor in depression and anxiety disorders. J Endocrinol 160:1-12.

Atkinson SE, Williams SR (2009) Postnatal development of dendritic synaptic integration in rat neocortical pyramidal neurons. Journal of neurophysiology 102:735-751.

Avishai-Eliner S, Yi SJ, Baram TZ (1996) Developmental profile of messenger RNA for the corticotropin-releasing hormone receptor in the rat limbic system. Brain research Developmental brain research 91:159-163.

Baas D, Aleman A, Vink M, Ramsey NF, de Haan EH, Kahn RS (2008) Evidence of altered cortical and amygdala activation during social decision-making in schizophrenia. NeuroImage 40:719-727.

Baas PW, Lin S (2011) Hooks and comets: The story of microtubule polarity orientation in the neuron. Developmental neurobiology 71:403-418.

Bachevalier J, Malkova L (2006) The amygdala and development of social cognition: theoretical comment on Bauman, Toscano, Mason, Lavenex, and Amaral (2006). Behavioral neuroscience 120:989-991.

Bachevalier J, Loveland KA (2006) The orbitofrontal-amygdala circuit and self-regulation of social-emotional behavior in autism. Neurosci Biobehav Rev 30:97-117.

Baimbridge KG, Celio MR, Rogers JH (1992) Calcium-binding proteins in the nervous system. Trends in neurosciences 15:303-308.

Baird AA, Gruber SA, Fein DA, Maas LC, Steingard RJ, Renshaw PF, Cohen BM, Yurgelun-Todd DA (1999) Functional magnetic resonance imaging of facial affect recognition in children and adolescents. Journal of the American Academy of Child and Adolescent Psychiatry 38:195-199.

Baker S, Chebli M, Rees S, Lemarec N, Godbout R, Bielajew C (2008) Effects of gestational stress: 1. Evaluation of maternal and juvenile offspring behavior. Brain research 1213:98-110.

Balmer TS, Carels VM, Frisch JL, Nick TA (2009) Modulation of perineuronal nets and parvalbumin with developmental song learning. The Journal of neuroscience : the official journal of the Society for Neuroscience 29:12878-12885.

Banks MI, Hardie JB, Pearce RA (2002) Development of GABA(A) receptor-mediated inhibitory postsynaptic currents in hippocampus. Journal of neurophysiology 88:3097-3107.

Barad M, Gean PW, Lutz B (2006) The role of the amygdala in the extinction of conditioned fear. Biological psychiatry 60:322-328.

Baram TZ, Schultz L (1991) Corticotropin-releasing hormone is a rapid and potent convulsant in the infant rat. Brain research Developmental brain research 61:97-101.

Barbazanges A, Piazza PV, Le Moal M, Maccari S (1996) Maternal glucocorticoid secretion mediates long-term effects of prenatal stress. The Journal of neuroscience : the official journal of the Society for Neuroscience 16:3943-3949.

Barlow SM, Knight AF, Sullivan FM (1978) Delay in postnatal growth and development of offspring produced by maternal restraint stress during pregnancy in the rat. Teratology 18:211-218.

Barnet RC, Hunt PS (2005) Trace and long-delay fear conditioning in the developing rat. Learn Behav 33:437-443.

Barnet RC, Hunt PS (2006) The expression of fear-potentiated startle during development: integration of learning and response systems. Behavioral neuroscience 120:861-872.

Baron-Cohen S, Ring HA, Bullmore ET, Wheelwright S, Ashwin C, Williams SC (2000) The amygdala theory of autism. Neurosci Biobehav Rev 24:355-364.

Barr GA, Moriceau S, Shionoya K, Muzny K, Gao P, Wang S, Sullivan RM (2009) Transitions in infant learning are modulated by dopamine in the amygdala. Nature neuroscience 12:1367-1369.

Bartos M, Elgueta C (2012) Functional characteristics of parvalbumin- and cholecystokinin-expressing basket cells. The Journal of physiology 590:669-681.

Bartos M, Vida I, Jonas P (2007) Synaptic mechanisms of synchronized gamma oscillations in inhibitory interneuron networks. Nature reviews Neuroscience 8:45-56.

Bartos M, Vida I, Frotscher M, Meyer A, Monyer H, Geiger JR, Jonas P (2002) Fast synaptic inhibition promotes synchronized gamma oscillations in hippocampal interneuron networks. Proceedings of the National Academy of Sciences of the United States of America 99:13222-13227.

Bauer EP, Paz R, Pare D (2007) Gamma oscillations coordinate amygdalo-rhinal interactions during learning. The Journal of neuroscience : the official journal of the Society for Neuroscience 27:9369-9379.

Bayer SA, Altman J, Russo RJ, Zhang X (1993) Timetables of neurogenesis in the human brain based on experimentally determined patterns in the rat. Neurotoxicology 14:83-144.

Beckel-Mitchener A, Greenough WT (2004) Correlates across the structural, functional, and molecular phenotypes of fragile X syndrome. Mental retardation and developmental disabilities research reviews 10:53-59.

Beenhakker MP, Huguenard JR (2010) Astrocytes as gatekeepers of GABAB receptor function. The Journal of neuroscience : the official journal of the Society for Neuroscience 30:15262-15276.

Beesdo-Baum K, Knappe S (2012) Developmental epidemiology of anxiety disorders. Child Adolesc Psychiatr Clin N Am 21:457-478.

Bellani M, Calderoni S, Muratori F, Brambilla P (2013) Brain anatomy of autism spectrum disorders II. Focus on amygdala. Epidemiol Psychiatr Sci:1-4.

Ben-Ari Y (2002) Excitatory actions of gaba during development: the nature of the nurture. Nature reviews Neuroscience 3:728-739.

Ben-Ari Y, Khalilov I, Kahle KT, Cherubini E (2012) The GABA Excitatory/Inhibitory Shift in Brain Maturation and Neurological Disorders. The Neuroscientist : a review journal bringing neurobiology, neurology and psychiatry 18:467-486.

Ben-Ari Y, Khazipov R, Leinekugel X, Caillard O, Gaiarsa JL (1997) GABAA, NMDA and AMPA receptors: a developmentally regulated 'menage a trois'. Trends in neurosciences 20:523-529.

Benchenane K, Peyrache A, Khamassi M, Tierney PL, Gioanni Y, Battaglia FP, Wiener SI (2010) Coherent theta oscillations and reorganization of spike timing in the hippocampal-prefrontal network upon learning. Neuron 66:921-936.

Bender RA, Baram TZ (2008) Hyperpolarization activated cyclic-nucleotide gated (HCN) channels in developing neuronal networks. Progress in neurobiology 86:129-140.

Bender RA, Brewster A, Santoro B, Ludwig A, Hofmann F, Biel M, Baram TZ (2001) Differential and age-dependent expression of hyperpolarization-activated, cyclic nucleotide-gated cation channel isoforms 1-4 suggests evolving roles in the developing rat hippocampus. Neuroscience 106:689-698.

Benes FM (2010) Amygdalocortical circuitry in schizophrenia: from circuits to molecules. Neuropsychopharmacology : official publication of the American College of Neuropsychopharmacology 35:239-257.

Benevento LA, Bakkum BW, Cohen RS (1995) gamma-Aminobutyric acid and somatostatin immunoreactivity in the visual cortex of normal and dark-reared rats. Brain research 689:172-182.

Berdel B, Morys J (2000) Expression of calbindin-D28k and parvalbumin during development of rat's basolateral amygdaloid complex. International journal of developmental neuroscience : the official journal of the International Society for Developmental Neuroscience 18:501-513.

Berdel B, Morys J, Maciejewska B (1997a) Neuronal changes in the basolateral complex during development of the amygdala of the rat. International journal of developmental neuroscience : the official journal of the International Society for Developmental Neuroscience 15:755-765.

Berdel B, Morys J, Maciejewska B, Dziewiatkowski J (1997b) Volume and topographical changes of the basolateral complex during the development of the rat's amygdaloid body. Folia morphologica 56:1-11.

Bergado-Acosta JR, Sangha S, Narayanan RT, Obata K, Pape HC, Stork O (2008) Critical role of the 65-kDa isoform of glutamic acid decarboxylase in consolidation and generalization of Pavlovian fear memory. Learn Mem 15:163-171.

Berghuis P, Dobszay MB, Sousa KM, Schulte G, Mager PP, Hartig W, Gorcs TJ, Zilberter Y, Ernfors P, Harkany T (2004) Brain-derived neurotrophic factor controls functional differentiation and microcircuit formation of selectively isolated fast-spiking GABAergic interneurons. The European journal of neuroscience 20:1290-1306.

Bergman K, Sarkar P, O'Connor TG, Modi N, Glover V (2007) Maternal stress during pregnancy predicts cognitive ability and fearfulness in infancy. Journal of the American Academy of Child and Adolescent Psychiatry 46:1454-1463.

Berretta S, Benes FM (2006) A rat model for neural circuitry abnormalities in schizophrenia. Nat Protoc 1:833-839.

Beversdorf DQ, Manning SE, Hillier A, Anderson SL, Nordgren RE, Walters SE, Nagaraja HN, Cooley WC, Gaelic SE, Bauman ML (2005) Timing of prenatal stressors and autism. J Autism Dev Disord 35:471-478.

Bischop DP, Orduz D, Lambot L, Schiffmann SN, Gall D (2012) Control of neuronal excitability by calcium binding proteins: a new mathematical model for striatal fast-spiking interneurons. Frontiers in molecular neuroscience 5:78.

Blackford JU, Pine DS (2012) Neural substrates of childhood anxiety disorders: a review of neuroimaging findings. Child Adolesc Psychiatr Clin N Am 21:501-525.

Boehlen A, Heinemann U, Erchova I (2010) The range of intrinsic frequencies represented by medial entorhinal cortex stellate cells extends with age. The Journal of neuroscience : the official journal of the Society for Neuroscience 30:4585-4589.

Bokil H, Andrews P, Kulkarni JE, Mehta S, Mitra PP (2010) Chronux: a platform for analyzing neural signals. Journal of neuroscience methods 192:146-151.

Bony G, Szczurkowska J, Tamagno I, Shelly M, Contestabile A, Cancedda L (2013) Non-hyperpolarizing GABAB receptor activation regulates neuronal migration and neurite growth and specification by cAMP/LKB1. Nat Commun 4:1800.

Bosman L, Lodder JC, van Ooyen A, Brussaard AB (2005a) Role of synaptic inhibition in spatiotemporal patterning of cortical activity. Progress in brain research 147:201-204.

Bosman LW, Rosahl TW, Brussaard AB (2002) Neonatal development of the rat visual cortex: synaptic function of GABAA receptor alpha subunits. The Journal of physiology 545:169-181.

Bosman LW, Heinen K, Spijker S, Brussaard AB (2005b) Mice lacking the major adult GABAA receptor subtype have normal number of synapses, but retain juvenile IPSC kinetics until adulthood. Journal of neurophysiology 94:338-346.

Bourgeois JP, Goldman-Rakic PS, Rakic P (1994) Synaptogenesis in the prefrontal cortex of rhesus monkeys. Cereb Cortex 4:78-96.

Bouton ME, Westbrook RF, Corcoran KA, Maren S (2006) Contextual and temporal modulation of extinction: behavioral and biological mechanisms. Biological psychiatry 60:352-360.

Bouwmeester H, Wolterink G, van Ree JM (2002a) Neonatal development of projections from the basolateral amygdala to prefrontal, striatal, and thalamic structures in the rat. The Journal of comparative neurology 442:239-249.

Bouwmeester H, Smits K, Van Ree JM (2002b) Neonatal development of projections to the basolateral amygdala from prefrontal and thalamic structures in rat. The Journal of comparative neurology 450:241-255.

Boyle LM (2013) A neuroplasticity hypothesis of chronic stress in the basolateral amygdala. Yale J Biol Med 86:117-125.

Breiter HC, Etcoff NL, Whalen PJ, Kennedy WA, Rauch SL, Buckner RL, Strauss MM, Hyman SE, Rosen BR (1996) Response and habituation of the human amygdala during visual processing of facial expression. Neuron 17:875-887.

Bremner JD (2007) Neuroimaging in posttraumatic stress disorder and other stress-related disorders. Neuroimaging Clin N Am 17:523-538, ix.

Bremner JD, Randall P, Vermetten E, Staib L, Bronen RA, Mazure C, Capelli S, McCarthy G, Innis RB, Charney DS (1997) Magnetic resonance imaging-based measurement of hippocampal volume in posttraumatic stress disorder related to childhood physical and sexual abuse--a preliminary report. Biological psychiatry 41:23-32.

Brummelte S, Teuchert-Noodt G (2006) Postnatal development of dopamine innervation in the amygdala and the entorhinal cortex of the gerbil (Meriones unguiculatus). Brain research 1125:9-16.

Brummelte S, Witte V, Teuchert-Noodt G (2007) Postnatal development of GABA and calbindin cells and fibers in the prefrontal cortex and basolateral amygdala of gerbils (Meriones unguiculatus). International journal of developmental neuroscience : the official journal of the International Society for Developmental Neuroscience 25:191-200.

Brunson KL, Chen Y, Avishai-Eliner S, Baram TZ (2003) Stress and the developing hippocampus: a double-edged sword? Mol Neurobiol 27:121-136.

Buonomano DV (2000) Decoding temporal information: A model based on short-term synaptic plasticity. The Journal of neuroscience : the official journal of the Society for Neuroscience 20:1129-1141.

Burton BG, Economo MN, Lee GJ, White JA (2008) Development of theta rhythmicity in entorhinal stellate cells of the juvenile rat. Journal of neurophysiology 100:3144-3157.

Buss C, Davis EP, Shahbaba B, Pruessner JC, Head K, Sandman CA (2012) Maternal cortisol over the course of pregnancy and subsequent child amygdala and hippocampus volumes and affective problems. Proceedings of the National Academy of Sciences of the United States of America 109:E1312-1319.

Buzsaki G (1997) Functions for interneuronal nets in the hippocampus. Can J Physiol Pharmacol 75:508-515.

Caillard O, Moreno H, Schwaller B, Llano I, Celio MR, Marty A (2000) Role of the calcium-binding protein parvalbumin in short-term synaptic plasticity. Proceedings of the National Academy of Sciences of the United States of America 97:13372-13377.

Calabrese B, Wilson MS, Halpain S (2006) Development and regulation of dendritic spine synapses. Physiology (Bethesda) 21:38-47.

Caldji C, Diorio J, Meaney MJ (2003) Variations in maternal care alter GABA(A) receptor subunit expression in brain regions associated with fear. Neuropsychopharmacology : official publication of the American College of Neuropsychopharmacology 28:1950-1959.

Caldji C, Francis D, Sharma S, Plotsky PM, Meaney MJ (2000) The effects of early rearing environment on the development of GABAA and central benzodiazepine receptor levels and novelty-induced fearfulness in the rat. Neuropsychopharmacology : official publication of the American College of Neuropsychopharmacology 22:219-229.

Callaghan BL, Richardson R (2011) Maternal separation results in early emergence of adult-like fear and extinction learning in infant rats. Behavioral neuroscience 125:20-28.

Callaghan BL, Richardson R (2012) The effect of adverse rearing environments on persistent memories in young rats: removing the brakes on infant fear memories. Transl Psychiatry 2:e138.

Callaghan BL, Graham BM, Li S, Richardson R (2013) From resilience to vulnerability: mechanistic insights into the effects of stress on transitions in critical period plasticity. Front Psychiatry 4:90.

Camp LL, Rudy JW (1988) Changes in the categorization of appetitive and aversive events during postnatal development of the rat. Developmental psychobiology 21:25-42.

Campbell BA, Ampuero MX (1985) Dissociation of autonomic and behavioral components of conditioned fear during development in the rat. Behavioral neuroscience 99:1089-1102.

Campeau S, Miserendino MJ, Davis M (1992) Intra-amygdala infusion of the N-methyl-D-aspartate receptor antagonist AP5 blocks acquisition but not expression of fear-potentiated startle to an auditory conditioned stimulus. Behavioral neuroscience 106:569-574.

Cancedda L, Fiumelli H, Chen K, Poo MM (2007) Excitatory GABA action is essential for morphological maturation of cortical neurons in vivo. The Journal of neuroscience : the official journal of the Society for Neuroscience 27:5224-5235.

Canolty RT, Knight RT (2010) The functional role of cross-frequency coupling. Trends in cognitive sciences 14:506-515.

Canolty RT, Edwards E, Dalal SS, Soltani M, Nagarajan SS, Kirsch HE, Berger MS, Barbaro NM, Knight RT (2006) High gamma power is phase-locked to theta oscillations in human neocortex. Science 313:1626-1628.

Carlsen J, Heimer L (1988) The basolateral amygdaloid complex as a cortical-like structure. Brain research 441:377-380.

Cartwright-Hatton S (2006) Anxiety of childhood and adolescence: Challenges and opportunities. Clin Psychol Rev 26:813-816.

Cartwright-Hatton S, McNicol K, Doubleday E (2006) Anxiety in a neglected population: prevalence of anxiety disorders in pre-adolescent children. Clin Psychol Rev 26:817-833.

Casey BJ, Giedd JN, Thomas KM (2000) Structural and functional brain development and its relation to cognitive development. Biol Psychol 54:241-257.

Casey BJ, Jones RM, Hare TA (2008) The adolescent brain. Annals of the New York Academy of Sciences 1124:111-126.

Casey BJ, Jones RM, Levita L, Libby V, Pattwell SS, Ruberry EJ, Soliman F, Somerville LH (2010) The storm and stress of adolescence: insights from human imaging and mouse genetics. Developmental psychobiology 52:225-235.

Chandy GK, Grissmer S, Gutman GA, Lazdunski M, McKinnon D, Pardo LA, Robertson GA, Rudy B, Sanguineti MC, Stuhmer W, Wang X (2012a) Voltage-gated potassium channels: Kv1.4. In: IUPHAR database.

Chandy GK, Grissmer S, Gutman GA, Lazdunski M, McKinnon D, Pardo LA, Robertson GA, Rudy B, Sanguineti MC, Stuhmer W, Wang X (2012b) Voltage-gated potassium channels: Kv3.4. In: IUPHAR database.

Chareyron LJ, Lavenex PB, Lavenex P (2012) Postnatal development of the amygdala: a stereological study in rats. The Journal of comparative neurology 520:3745-3763.

Charney DS, Deutch A (1996) A functional neuroanatomy of anxiety and fear: implications for the pathophysiology and treatment of anxiety disorders. Critical reviews in neurobiology 10:419-446.

Chattopadhyaya B, Cristo GD (2012) GABAergic circuit dysfunctions in neurodevelopmental disorders. Front Psychiatry 3:51.

Chattopadhyaya B, Di Cristo G, Higashiyama H, Knott GW, Kuhlman SJ, Welker E, Huang ZJ (2004) Experience and activity-dependent maturation of perisomatic GABAergic innervation in primary visual cortex during a postnatal critical period. The Journal of neuroscience : the official journal of the Society for Neuroscience 24:9598-9611.

Chattopadhyaya B, Di Cristo G, Wu CZ, Knott G, Kuhlman S, Fu Y, Palmiter RD, Huang ZJ (2007) GAD67-mediated GABA synthesis and signaling regulate inhibitory synaptic innervation in the visual cortex. Neuron 54:889-903.

Chavez CM, McGaugh JL, Weinberger NM (2013) Activation of the basolateral amygdala induces long-term enhancement of specific memory representations in the cerebral cortex. Neurobiology of learning and memory 101:8-18.

Chen Y, Li H, Jin Z, Shou T, Yu H (2013) Feedback of the amygdala globally modulates visual response of primary visual cortex in the cat. NeuroImage 84C:775-785.

Chhatwal JP, Gutman AR, Maguschak KA, Bowser ME, Yang Y, Davis M, Ressler KJ (2009) Functional interactions between endocannabinoid and CCK neurotransmitter systems may be critical for extinction learning. Neuropsychopharmacology : official publication of the American College of Neuropsychopharmacology 34:509-521.

Chrousos GP, Gold PW (1992) The concepts of stress and stress system disorders. Overview of physical and behavioral homeostasis. JAMA : the journal of the American Medical Association 267:1244-1252.

Chung L, Moore SD (2007) Cholecystokinin enhances GABAergic inhibitory transmission in basolateral amygdala. Neuropeptides 41:453-463.

Cobb SR, Buhl EH, Halasy K, Paulsen O, Somogyi P (1995) Synchronization of neuronal activity in hippocampus by individual GABAergic interneurons. Nature 378:75-78.

Coe CL, Shirtcliff EA (2004) Growth trajectory evident at birth affects age of first delivery in female monkeys. Pediatr Res 55:914-920.

Cohen AS, Lin DD, Coulter DA (2000) Protracted postnatal development of inhibitory synaptic transmission in rat hippocampal area CA1 neurons. Journal of neurophysiology 84:2465-2476.

Cohen J (1988) Statistical Power Analysis for the Behavioral Sciences, 2nd ed. Edition. United States of America: Lawrence Erlbaum Associates.

Cohen NA, Brenman JE, Snyder SH, Bredt DS (1996) Binding of the inward rectifier K+ channel Kir 2.3 to PSD-95 is regulated by protein kinase A phosphorylation. Neuron 17:759-767.

Coles ME, Heimberg RG (2002) Memory biases in the anxiety disorders: current status. Clin Psychol Rev 22:587-627.

Collin T, Chat M, Lucas MG, Moreno H, Racay P, Schwaller B, Marty A, Llano I (2005) Developmental changes in parvalbumin regulate presynaptic Ca2+ signaling. The Journal of neuroscience : the official journal of the Society for Neuroscience 25:96-107.

Collins DR, Pelletier JG, Pare D (2001) Slow and fast (gamma) neuronal oscillations in the perirhinal cortex and lateral amygdala. Journal of neurophysiology 85:1661-1672.

Cook CJ (2004) Stress induces CRF release in the paraventricular nucleus, and both CRF and GABA release in the amygdala. Physiology & behavior 82:751-762.

Cork LC, Walker LC (1993) Age-Related Lesions, Nervous System. In: Nonhuman Primates II (Jones TC, Mohr U, Hunt RD, eds). New York: Springer-Verlag.

Correll CM, Rosenkranz JA, Grace AA (2005) Chronic cold stress alters prefrontal cortical modulation of amygdala neuronal activity in rats. Biological psychiatry 58:382-391.

Costafreda SG, Brammer MJ, David AS, Fu CH (2008) Predictors of amygdala activation during the processing of emotional stimuli: a meta-analysis of 385 PET and fMRI studies. Brain Res Rev 58:57-70.

Cowan CS, Callaghan BL, Richardson R (2013) Acute early-life stress results in premature emergence of adult-like fear retention and extinction relapse in infant rats. Behavioral neuroscience 127:703-711.

Cratty MS, Ward HE, Johnson EA, Azzaro AJ, Birkle DL (1995) Prenatal stress increases corticotropin-releasing factor (CRF) content and release in rat amygdala minces. Brain research 675:297-302.

Crawley JN (2007) Mouse behavioral assays relevant to the symptoms of autism. Brain Pathol 17:448-459.

Cressman VL, Balaban J, Steinfeld S, Shemyakin A, Graham P, Parisot N, Moore H (2010) Prefrontal cortical inputs to the basal amygdala undergo pruning during late adolescence in the rat. The Journal of comparative neurology 518:2693-2709.

Cui H, Sakamoto H, Higashi S, Kawata M (2008) Effects of single-prolonged stress on neurons and their afferent inputs in the amygdala. Neuroscience 152:703-712.

Cunningham MG, Bhattacharyya S, Benes FM (2002) Amygdalo-cortical sprouting continues into early adulthood: implications for the development of normal and abnormal function during adolescence. The Journal of comparative neurology 453:116-130.

Cunningham MG, Bhattacharyya S, Benes FM (2008) Increasing Interaction of amygdalar afferents with GABAergic interneurons between birth and adulthood. Cereb Cortex 18:1529-1535.

Curley AA, Lewis DA (2012) Cortical basket cell dysfunction in schizophrenia. The Journal of physiology 590:715-724.

Damgaard T, Plath N, Neill JC, Hansen SL (2011) Extrasynaptic GABAA receptor activation reverses recognition memory deficits in an animal model of schizophrenia. Psychopharmacology 214:403-413.

Dan Y, Poo MM (2004) Spike timing-dependent plasticity of neural circuits. Neuron 44:23-30.
Darnaudery M, Maccari S (2008) Epigenetic programming of the stress response in male and female rats by prenatal restraint stress. Brain Res Rev 57:571-585.
Davila JC, Olmos L, Legaz I, Medina L, Guirado S, Real MA (2008) Dynamic patterns of colocalization of calbindin, parvalbumin and GABA in subpopulations of mouse basolateral amygdalar cells during development. Journal of chemical neuroanatomy 35:67-76.
Davis AM, Penschuck S, Fritschy JM, McCarthy MM (2000) Developmental switch in the expression of GABA(A) receptor subunits alpha(1) and alpha(2) in the hypothalamus and limbic system of the rat. Brain research Developmental brain research 119:127-138.
Davis M (2000) The role of the amygdala in conditioned and unconditioned fear and anxiety. In: The Amygdala: A Functional Analysis (Aggleton JP, ed). London: Oxford University Press.
Davis M, Whalen PJ (2001) The amygdala: vigilance and emotion. Molecular psychiatry 6:13-34.
Davis M, Rainnie D, Cassell M (1994) Neurotransmission in the rat amygdala related to fear and anxiety. Trends in neurosciences 17:208-214.
Davis M, Walker DL, Myers KM (2003) Role of the amygdala in fear extinction measured with potentiated startle. Annals of the New York Academy of Sciences 985:218-232.
De Bellis MD, Keshavan MS, Clark DB, Casey BJ, Giedd JN, Boring AM, Frustaci K, Ryan ND (1999) A.E. Bennett Research Award. Developmental traumatology. Part II: Brain development. Biological psychiatry 45:1271-1284.
De Felipe J, Marco P, Fairen A, Jones EG (1997) Inhibitory synaptogenesis in mouse somatosensory cortex. Cereb Cortex 7:619-634.
de Lima AD, Opitz T, Voigt T (2004) Irreversible loss of a subpopulation of cortical interneurons in the absence of glutamatergic network activity. The European journal of neuroscience 19:2931-2943.
Dedovic K, Duchesne A, Andrews J, Engert V, Pruessner JC (2009) The brain and the stress axis: the neural correlates of cortisol regulation in response to stress. NeuroImage 47:864-871.
Del Cerro MC, Perez-Laso C, Ortega E, Martin JL, Gomez F, Perez-Izquierdo MA, Segovia S (2010) Maternal care counteracts behavioral effects of prenatal environmental stress in female rats. Behavioural brain research 208:593-602.
Deoni SC, Mercure E, Blasi A, Gasston D, Thomson A, Johnson M, Williams SC, Murphy DG (2011) Mapping infant brain myelination with magnetic resonance imaging. The Journal of neuroscience : the official journal of the Society for Neuroscience 31:784-791.
Desmaisons D, Vincent JD, Lledo PM (1999) Control of action potential timing by intrinsic subthreshold oscillations in olfactory bulb output neurons. The Journal of neuroscience : the official journal of the Society for Neuroscience 19:10727-10737.
Di Cristo G (2007) Development of cortical GABAergic circuits and its implications for neurodevelopmental disorders. Clinical genetics 72:1-8.
Dickerson PA, Lally BE, Gunnel E, Birkle DL, Salm AK (2005) Early emergence of increased fearful behavior in prenatally stressed rats. Physiology & behavior 86:586-593.
Diorio J, Meaney MJ (2007) Maternal programming of defensive responses through sustained effects on gene expression. Journal of psychiatry & neuroscience : JPN 32:275-284.
Dityatev A, Bruckner G, Dityateva G, Grosche J, Kleene R, Schachner M (2007) Activity-dependent formation and functions of chondroitin sulfate-rich extracellular matrix of perineuronal nets. Developmental neurobiology 67:570-588.
Dobrunz LE, Stevens CF (1997) Heterogeneity of release probability, facilitation, and depletion at central synapses. Neuron 18:995-1008.
Doischer D, Hosp JA, Yanagawa Y, Obata K, Jonas P, Vida I, Bartos M (2008) Postnatal differentiation of basket cells from slow to fast signaling devices. The Journal of neuroscience : the official journal of the Society for Neuroscience 28:12956-12968.

Dorrn AL, Yuan K, Barker AJ, Schreiner CE, Froemke RC (2010) Developmental sensory experience balances cortical excitation and inhibition. Nature 465:932-936.

Draguhn A, Heinemann U (1996) Different mechanisms regulate IPSC kinetics in early postnatal and juvenile hippocampal granule cells. Journal of neurophysiology 76:3983-3993.

Drevets WC (2003) Neuroimaging abnormalities in the amygdala in mood disorders. Annals of the New York Academy of Sciences 985:420-444.

Driesang RB, Pape HC (2000) Spike doublets in neurons of the lateral amygdala: mechanisms and contribution to rhythmic activity. Neuroreport 11:1703-1708.

Driessen M, Herrmann J, Stahl K, Zwaan M, Meier S, Hill A, Osterheider M, Petersen D (2000) Magnetic resonance imaging volumes of the hippocampus and the amygdala in women with borderline personality disorder and early traumatization. Archives of general psychiatry 57:1115-1122.

Dunn AJ, Berridge CW (1990) Physiological and behavioral responses to corticotropin-releasing factor administration: is CRF a mediator of anxiety or stress responses? Brain Res Brain Res Rev 15:71-100.

Dunning DD, Hoover CL, Soltesz I, Smith MA, O'Dowd DK (1999) GABA(A) receptor-mediated miniature postsynaptic currents and alpha-subunit expression in developing cortical neurons. Journal of neurophysiology 82:3286-3297.

Duvarci S, Pare D (2007) Glucocorticoids enhance the excitability of principal basolateral amygdala neurons. The Journal of neuroscience : the official journal of the Society for Neuroscience 27:4482-4491.

Edge MD, Ramel W, Drabant EM, Kuo JR, Parker KJ, Gross JJ (2009) For better or worse? Stress inoculation effects for implicit but not explicit anxiety. Depression and anxiety 26:831-837.

Eggermann E, Jonas P (2012) How the 'slow' Ca(2+) buffer parvalbumin affects transmitter release in nanodomain-coupling regimes. Nature neuroscience 15:20-22.

Ehrlich DE, Ryan SJ, Rainnie DG (2012) Postnatal development of electrophysiological properties of principal neurons in the rat basolateral amygdala. The Journal of physiology 590:4819-4838.

Ehrlich DE, Ryan SJ, Hazra R, Guo JD, Rainnie DG (2013) Postnatal maturation of GABAergic transmission in the rat basolateral amygdala. Journal of neurophysiology 110:926-941.

Ehrlich I, Humeau Y, Grenier F, Ciocchi S, Herry C, Luthi A (2009) Amygdala inhibitory circuits and the control of fear memory. Neuron 62:757-771.

Eippert F, Veit R, Weiskopf N, Erb M, Birbaumer N, Anders S (2007) Regulation of emotional responses elicited by threat-related stimuli. Hum Brain Mapp 28:409-423.

Elfant D, Pal BZ, Emptage N, Capogna M (2008) Specific inhibitory synapses shift the balance from feedforward to feedback inhibition of hippocampal CA1 pyramidal cells. The European journal of neuroscience 27:104-113.

Eluvathingal TJ, Chugani HT, Behen ME, Juhasz C, Muzik O, Maqbool M, Chugani DC, Makki M (2006) Abnormal brain connectivity in children after early severe socioemotional deprivation: a diffusion tensor imaging study. Pediatrics 117:2093-2100.

Engel AK, Fries P, Singer W (2001) Dynamic predictions: oscillations and synchrony in top-down processing. Nature reviews Neuroscience 2:704-716.

Erchova I, Kreck G, Heinemann U, Herz AV (2004) Dynamics of rat entorhinal cortex layer II and III cells: characteristics of membrane potential resonance at rest predict oscillation properties near threshold. The Journal of physiology 560:89-110.

Ernst M, Fudge JL (2009) A developmental neurobiological model of motivated behavior: anatomy, connectivity and ontogeny of the triadic nodes. Neurosci Biobehav Rev 33:367-382.

Errington AC, Renger JJ, Uebele VN, Crunelli V (2010) State-dependent firing determines intrinsic dendritic Ca2+ signaling in thalamocortical neurons. The Journal of neuroscience : the official journal of the Society for Neuroscience 30:14843-14853.

Escobar C, Salas M (1993) Neonatal undernutrition and amygdaloid nuclear complex development: an experimental study in the rat. Experimental neurology 122:311-318.

Estanislau C, Morato S (2005) Prenatal stress produces more behavioral alterations than maternal separation in the elevated plus-maze and in the elevated T-maze. Behavioural brain research 163:70-77.

Estanislau C, Morato S (2006) Behavior ontogeny in the elevated plus-maze: prenatal stress effects. International journal of developmental neuroscience : the official journal of the International Society for Developmental Neuroscience 24:255-262.

Eyre MD, Renzi M, Farrant M, Nusser Z (2012) Setting the time course of inhibitory synaptic currents by mixing multiple GABA(A) receptor alpha subunit isoforms. The Journal of neuroscience : the official journal of the Society for Neuroscience 32:5853-5867.

Faber ES, Sah P (2002) Physiological role of calcium-activated potassium currents in the rat lateral amygdala. The Journal of neuroscience : the official journal of the Society for Neuroscience 22:1618-1628.

Fagiolini M, Fritschy JM, Low K, Mohler H, Rudolph U, Hensch TK (2004) Specific GABAA circuits for visual cortical plasticity. Science 303:1681-1683.

Faul F, Erdfelder E, Lang AG, Buchner A (2007) G*Power 3: a flexible statistical power analysis program for the social, behavioral, and biomedical sciences. Behav Res Methods 39:175-191.

Fendt M, Fanselow MS (1999) The neuroanatomical and neurochemical basis of conditioned fear. Neurosci Biobehav Rev 23:743-760.

Field T, Diego M (2008) Cortisol: the culprit prenatal stress variable. Int J Neurosci 118:1181.

Fiorentino H, Kuczewski N, Diabira D, Ferrand N, Pangalos MN, Porcher C, Gaiarsa JL (2009) GABA(B) receptor activation triggers BDNF release and promotes the maturation of GABAergic synapses. The Journal of neuroscience : the official journal of the Society for Neuroscience 29:11650-11661.

Fortune ES, Rose GJ (2001) Short-term synaptic plasticity as a temporal filter. Trends in neurosciences 24:381-385.

Francis DD, Champagne FA, Liu D, Meaney MJ (1999a) Maternal care, gene expression, and the development of individual differences in stress reactivity. Annals of the New York Academy of Sciences 896:66-84.

Francis DD, Caldji C, Champagne F, Plotsky PM, Meaney MJ (1999b) The role of corticotropin-releasing factor--norepinephrine systems in mediating the effects of early experience on the development of behavioral and endocrine responses to stress. Biological psychiatry 46:1153-1166.

Freund TF, Katona I (2007) Perisomatic inhibition. Neuron 56:33-42.

Fride E, Weinstock M (1984) The effects of prenatal exposure to predictable or unpredictable stress on early development in the rat. Developmental psychobiology 17:651-660.

Fritschy JM, Weinmann O, Wenzel A, Benke D (1998) Synapse-specific localization of NMDA and GABA(A) receptor subunits revealed by antigen-retrieval immunohistochemistry. The Journal of comparative neurology 390:194-210.

Fritschy JM, Panzanelli P, Kralic JE, Vogt KE, Sassoe-Pognetto M (2006) Differential dependence of axo-dendritic and axo-somatic GABAergic synapses on GABAA receptors containing the alpha1 subunit in Purkinje cells. The Journal of neuroscience : the official journal of the Society for Neuroscience 26:3245-3255.

Fritschy JM, Meskenaite V, Weinmann O, Honer M, Benke D, Mohler H (1999) GABAB-receptor splice variants GB1a and GB1b in rat brain: developmental regulation, cellular

distribution and extrasynaptic localization. The European journal of neuroscience 11:761-768.

Fuchs EC, Zivkovic AR, Cunningham MO, Middleton S, Lebeau FE, Bannerman DM, Rozov A, Whittington MA, Traub RD, Rawlins JN, Monyer H (2007) Recruitment of parvalbumin-positive interneurons determines hippocampal function and associated behavior. Neuron 53:591-604.

Fujisawa S, Buzsaki G (2011) A 4 Hz oscillation adaptively synchronizes prefrontal, VTA, and hippocampal activities. Neuron 72:153-165.

Gabbott PL, Stewart MG (1987) Quantitative morphological effects of dark-rearing and light exposure on the synaptic connectivity of layer 4 in the rat visual cortex (area 17). Experimental brain research Experimentelle Hirnforschung Experimentation cerebrale 68:103-114.

Gao Y, Raine A, Venables PH, Dawson ME, Mednick SA (2010) The development of skin conductance fear conditioning in children from ages 3 to 8 years. Dev Sci 13:201-212.

Gean PW, Shinnick-Gallagher P (1989) The transient potassium current, the A-current, is involved in spike frequency adaptation in rat amygdala neurons. Brain research 480:160-169.

Geoffroy PA, Etain B, Houenou J (2013) Gene X Environment Interactions in Schizophrenia and Bipolar Disorder: Evidence from Neuroimaging. Front Psychiatry 4:136.

George AA, Lyons-Warren AM, Ma X, Carlson BA (2011) A diversity of synaptic filters are created by temporal summation of excitation and inhibition. The Journal of neuroscience : the official journal of the Society for Neuroscience 31:14721-14734.

Gerhardstein BL, Puri TS, Chien AJ, Hosey MM (1999) Identification of the sites phosphorylated by cyclic AMP-dependent protein kinase on the beta 2 subunit of L-type voltage-dependent calcium channels. Biochemistry 38:10361-10370.

Giachino C, Canalia N, Capone F, Fasolo A, Alleva E, Riva MA, Cirulli F, Peretto P (2007) Maternal deprivation and early handling affect density of calcium binding protein-containing neurons in selected brain regions and emotional behavior in periadolescent rats. Neuroscience 145:568-578.

Giedd JN, Vaituzis AC, Hamburger SD, Lange N, Rajapakse JC, Kaysen D, Vauss YC, Rapoport JL (1996) Quantitative MRI of the temporal lobe, amygdala, and hippocampus in normal human development: ages 4-18 years. The Journal of comparative neurology 366:223-230.

Giesbrecht CJ, Mackay JP, Silveira HB, Urban JH, Colmers WF (2010) Countervailing modulation of Ih by neuropeptide Y and corticotrophin-releasing factor in basolateral amygdala as a possible mechanism for their effects on stress-related behaviors. The Journal of neuroscience : the official journal of the Society for Neuroscience 30:16970-16982.

Gillespie CF, Phifer J, Bradley B, Ressler KJ (2009) Risk and resilience: genetic and environmental influences on development of the stress response. Depression and anxiety 26:984-992.

Glausier JR, Lewis DA (2011) Selective pyramidal cell reduction of GABA(A) receptor alpha1 subunit messenger RNA expression in schizophrenia. Neuropsychopharmacology : official publication of the American College of Neuropsychopharmacology 36:2103-2110.

Gleich O, Strutz J (2002) Age dependent changes in the medial nucleus of the trapezoid body in gerbils. Hearing research 164:166-178.

Glover V (2011) Annual Research Review: Prenatal stress and the origins of psychopathology: an evolutionary perspective. Journal of child psychology and psychiatry, and allied disciplines 52:356-367.

Glover V, O'Connor TG, O'Donnell K (2010) Prenatal stress and the programming of the HPA axis. Neurosci Biobehav Rev 35:17-22.
Goddard GV (1964) Amygdaloid Stimulation and Learning in the Rat. J Comp Physiol Psychol 58:23-30.
Gogolla N, Caroni P, Luthi A, Herry C (2009) Perineuronal nets protect fear memories from erasure. Science 325:1258-1261.
Goldberg EM, Jeong HY, Kruglikov I, Tremblay R, Lazarenko RM, Rudy B (2011) Rapid developmental maturation of neocortical FS cell intrinsic excitability. Cereb Cortex 21:666-682.
Goldin PR, Manber T, Hakimi S, Canli T, Gross JJ (2009) Neural bases of social anxiety disorder: emotional reactivity and cognitive regulation during social and physical threat. Archives of general psychiatry 66:170-180.
Goldstein LE, Rasmusson AM, Bunney BS, Roth RH (1996) Role of the amygdala in the coordination of behavioral, neuroendocrine, and prefrontal cortical monoamine responses to psychological stress in the rat. The Journal of neuroscience : the official journal of the Society for Neuroscience 16:4787-4798.
Gonzalez-Islas C, Chub N, Wenner P (2009) NKCC1 and AE3 appear to accumulate chloride in embryonic motoneurons. Journal of neurophysiology 101:507-518.
Gourley SL, Olevska A, Warren MS, Taylor JR, Koleske AJ (2012) Arg kinase regulates prefrontal dendritic spine refinement and cocaine-induced plasticity. The Journal of neuroscience : the official journal of the Society for Neuroscience 32:2314-2323.
Govindan RM, Behen ME, Helder E, Makki MI, Chugani HT (2010) Altered water diffusivity in cortical association tracts in children with early deprivation identified with Tract-Based Spatial Statistics (TBSS). Cereb Cortex 20:561-569.
Graham YP, Heim C, Goodman SH, Miller AH, Nemeroff CB (1999) The effects of neonatal stress on brain development: implications for psychopathology. Development and psychopathology 11:545-565.
Gray TS, Bingaman EW (1996) The amygdala: corticotropin-releasing factor, steroids, and stress. Critical reviews in neurobiology 10:155-168.
Greba Q, Gifkins A, Kokkinidis L (2001) Inhibition of amygdaloid dopamine D2 receptors impairs emotional learning measured with fear-potentiated startle. Brain research 899:218-226.
Green MK, Rani CS, Joshi A, Soto-Pina AE, Martinez PA, Frazer A, Strong R, Morilak DA (2011) Prenatal stress induces long term stress vulnerability, compromising stress response systems in the brain and impairing extinction of conditioned fear after adult stress. Neuroscience 192:438-451.
Griffin WC, 3rd, Skinner HD, Salm AK, Birkle DL (2003) Mild prenatal stress in rats is associated with enhanced conditioned fear. Physiology & behavior 79:209-215.
Guan D, Horton LR, Armstrong WE, Foehring RC (2011) Postnatal development of A-type and Kv1- and Kv2-mediated potassium channel currents in neocortical pyramidal neurons. Journal of neurophysiology 105:2976-2988.
Gulledge AT, Stuart GJ (2003) Excitatory actions of GABA in the cortex. Neuron 37:299-309.
Gullone E (2000) The development of normal fear: a century of research. Clin Psychol Rev 20:429-451.
Gunnar M, Quevedo K (2007) The neurobiology of stress and development. Annu Rev Psychol 58:145-173.
Guo YY, Liu SB, Cui GB, Ma L, Feng B, Xing JH, Yang Q, Li XQ, Wu YM, Xiong LZ, Zhang W, Zhao MG (2012) Acute stress induces down-regulation of large-conductance Ca2+-activated potassium channels in the lateral amygdala. The Journal of physiology 590:875-886.

Gutfreund Y, yarom Y, Segev I (1995) Subthreshold oscillations and resonant frequency in guinea-pig cortical neurons: physiology and modelling. The Journal of physiology 483 (Pt 3):621-640.

Guyer AE, Monk CS, McClure-Tone EB, Nelson EE, Roberson-Nay R, Adler AD, Fromm SJ, Leibenluft E, Pine DS, Ernst M (2008) A developmental examination of amygdala response to facial expressions. Journal of cognitive neuroscience 20:1565-1582.

Hale MW, Johnson PL, Westerman AM, Abrams JK, Shekhar A, Lowry CA (2010) Multiple anxiogenic drugs recruit a parvalbumin-containing subpopulation of GABAergic interneurons in the basolateral amygdala. Prog Neuropsychopharmacol Biol Psychiatry 34:1285-1293.

Hamann SB, Adolphs R (1999) Normal recognition of emotional similarity between facial expressions following bilateral amygdala damage. Neuropsychologia 37:1135-1141.

Hammack SE, Mania I, Rainnie DG (2007) Differential expression of intrinsic membrane currents in defined cell types of the anterolateral bed nucleus of the stria terminalis. Journal of neurophysiology 98:638-656.

Han JH, Kushner SA, Yiu AP, Cole CJ, Matynia A, Brown RA, Neve RL, Guzowski JF, Silva AJ, Josselyn SA (2007) Neuronal competition and selection during memory formation. Science 316:457-460.

Han JH, Kushner SA, Yiu AP, Hsiang HL, Buch T, Waisman A, Bontempi B, Neve RL, Frankland PW, Josselyn SA (2009) Selective erasure of a fear memory. Science 323:1492-1496.

Harauzov A, Spolidoro M, DiCristo G, De Pasquale R, Cancedda L, Pizzorusso T, Viegi A, Berardi N, Maffei L (2010) Reducing intracortical inhibition in the adult visual cortex promotes ocular dominance plasticity. The Journal of neuroscience : the official journal of the Society for Neuroscience 30:361-371.

Hare TA, Tottenham N, Galvan A, Voss HU, Glover GH, Casey BJ (2008) Biological substrates of emotional reactivity and regulation in adolescence during an emotional go-nogo task. Biological psychiatry 63:927-934.

Harmon KM, Cromwell HC, Burgdorf J, Moskal JR, Brudzynski SM, Kroes RA, Panksepp J (2008) Rats selectively bred for low levels of 50 kHz ultrasonic vocalizations exhibit alterations in early social motivation. Developmental psychobiology 50:322-331.

Hartig W, Bruckner G, Brauer K, Schmidt C, Bigl V (1995) Allocation of perineuronal nets and parvalbumin-, calbindin-D28k- and glutamic acid decarboxylase-immunoreactivity in the amygdala of the rhesus monkey. Brain research 698:265-269.

Hasenstaub A, Shu Y, Haider B, Kraushaar U, Duque A, McCormick DA (2005) Inhibitory postsynaptic potentials carry synchronized frequency information in active cortical networks. Neuron 47:423-435.

Hazra R, Guo JD, Dabrowska J, Rainnie DG (2012) Differential distribution of serotonin receptor subtypes in BNST(ALG) neurons: modulation by unpredictable shock stress. Neuroscience 225:9-21.

Hazra R, Guo JD, Ryan SJ, Jasnow AM, Dabrowska J, Rainnie DG (2011) A transcriptomic analysis of type I-III neurons in the bed nucleus of the stria terminalis. Molecular and cellular neurosciences 46:699-709.

Heim C, Nemeroff CB (2002) Neurobiology of early life stress: clinical studies. Seminars in clinical neuropsychiatry 7:147-159.

Heim C, Mletzko T, Purselle D, Musselman DL, Nemeroff CB (2008) The dexamethasone/corticotropin-releasing factor test in men with major depression: role of childhood trauma. Biological psychiatry 63:398-405.

Heldt SA, Ressler KJ (2007) Training-induced changes in the expression of GABAA-associated genes in the amygdala after the acquisition and extinction of Pavlovian fear. The European journal of neuroscience 26:3631-3644.

Heldt SA, Ressler KJ (2010) Amygdala-specific reduction of alpha1-GABAA receptors disrupts the anticonvulsant, locomotor, and sedative, but not anxiolytic, effects of benzodiazepines in mice. The Journal of neuroscience : the official journal of the Society for Neuroscience 30:7139-7151.

Hendry SH, Jones EG (1986) Reduction in number of immunostained GABAergic neurones in deprived-eye dominance columns of monkey area 17. Nature 320:750-753.

Hennenlotter A, Schroeder U, Erhard P, Castrop F, Haslinger B, Stoecker D, Lange KW, Ceballos-Baumann AO (2005) A common neural basis for receptive and expressive communication of pleasant facial affect. NeuroImage 26:581-591.

Hensch TK (2005) Critical period plasticity in local cortical circuits. Nature reviews Neuroscience 6:877-888.

Hensch TK, Fagiolini M, Mataga N, Stryker MP, Baekkeskov S, Kash SF (1998) Local GABA circuit control of experience-dependent plasticity in developing visual cortex. Science 282:1504-1508.

Herman JP, Cullinan WE (1997) Neurocircuitry of stress: central control of the hypothalamo-pituitary-adrenocortical axis. Trends in neurosciences 20:78-84.

Herman JP, Figueiredo H, Mueller NK, Ulrich-Lai Y, Ostrander MM, Choi DC, Cullinan WE (2003) Central mechanisms of stress integration: hierarchical circuitry controlling hypothalamo-pituitary-adrenocortical responsiveness. Front Neuroendocrinol 24:151-180.

Hevers W, Luddens H (2002) Pharmacological heterogeneity of gamma-aminobutyric acid receptors during development suggests distinct classes of rat cerebellar granule cells in situ. Neuropharmacology 42:34-47.

Hibino H, Inanobe A, Furutani K, Murakami S, Findlay I, Kurachi Y (2010) Inwardly rectifying potassium channels: their structure, function, and physiological roles. Physiological reviews 90:291-366.

Hicks BM, DiRago AC, Iacono WG, McGue M (2009) Gene-environment interplay in internalizing disorders: consistent findings across six environmental risk factors. Journal of child psychology and psychiatry, and allied disciplines 50:1309-1317.

Higashida H, Yokoyama S, Munesue T, Kikuchi M, Minabe Y, Lopatina O (2011) CD38 gene knockout juvenile mice: a model of oxytocin signal defects in autism. Biol Pharm Bull 34:1369-1372.

Hofer MA, Shair HN, Brunelli SA (2002) Ultrasonic vocalizations in rat and mouse pups. Curr Protoc Neurosci Chapter 8:Unit 8 14.

Hoffman DA, Johnston D (1998) Downregulation of transient K+ channels in dendrites of hippocampal CA1 pyramidal neurons by activation of PKA and PKC. The Journal of neuroscience : the official journal of the Society for Neuroscience 18:3521-3528.

Hollrigel GS, Soltesz I (1997) Slow kinetics of miniature IPSCs during early postnatal development in granule cells of the dentate gyrus. The Journal of neuroscience : the official journal of the Society for Neuroscience 17:5119-5128.

Hooker CI, Bruce L, Fisher M, Verosky SC, Miyakawa A, D'Esposito M, Vinogradov S (2013) The influence of combined cognitive plus social-cognitive training on amygdala response during face emotion recognition in schizophrenia. Psychiatry research 213:99-107.

Hornung JP, Fritschy JM (1996) Developmental profile of GABAA-receptors in the marmoset monkey: expression of distinct subtypes in pre- and postnatal brain. The Journal of comparative neurology 367:413-430.

Hsu FC, Zhang GJ, Raol YS, Valentino RJ, Coulter DA, Brooks-Kayal AR (2003) Repeated neonatal handling with maternal separation permanently alters hippocampal GABAA receptors and behavioral stress responses. Proceedings of the National Academy of Sciences of the United States of America 100:12213-12218.

Hu H, Vervaeke K, Storm JF (2002) Two forms of electrical resonance at theta frequencies, generated by M-current, h-current and persistent Na+ current in rat hippocampal pyramidal cells. The Journal of physiology 545:783-805.

Huang ZJ (2009) Activity-dependent development of inhibitory synapses and innervation pattern: role of GABA signalling and beyond. The Journal of physiology 587:1881-1888.

Huang ZJ, Scheiffele P (2008) GABA and neuroligin signaling: linking synaptic activity and adhesion in inhibitory synapse development. Curr Opin Neurobiol 18:77-83.

Huang ZJ, Kirkwood A, Pizzorusso T, Porciatti V, Morales B, Bear MF, Maffei L, Tonegawa S (1999) BDNF regulates the maturation of inhibition and the critical period of plasticity in mouse visual cortex. Cell 98:739-755.

Hubbard DT, Blanchard DC, Yang M, Markham CM, Gervacio A, Chun IL, Blanchard RJ (2004) Development of defensive behavior and conditioning to cat odor in the rat. Physiology & behavior 80:525-530.

Huizink AC, Robles de Medina PG, Mulder EJ, Visser GH, Buitelaar JK (2003) Stress during pregnancy is associated with developmental outcome in infancy. Journal of child psychology and psychiatry, and allied disciplines 44:810-818.

Huizink AC, Dick DM, Sihvola E, Pulkkinen L, Rose RJ, Kaprio J (2007) Chernobyl exposure as stressor during pregnancy and behaviour in adolescent offspring. Acta psychiatrica Scandinavica 116:438-446.

Humphrey T (1968) The development of the human amygdala during early embryonic life. The Journal of comparative neurology 132:135-165.

Hunt PS (1999) A further investigation of the developmental emergence of fear-potentiated startle in rats. Developmental psychobiology 34:281-291.

Hunt PS, Richardson R, Campbell BA (1994) Delayed development of fear-potentiated startle in rats. Behavioral neuroscience 108:69-80.

Huntsman MM, Isackson PJ, Jones EG (1994) Lamina-specific expression and activity-dependent regulation of seven GABAA receptor subunit mRNAs in monkey visual cortex. The Journal of neuroscience : the official journal of the Society for Neuroscience 14:2236-2259.

Hutcheon B, Yarom Y (2000) Resonance, oscillation and the intrinsic frequency preferences of neurons. Trends in neurosciences 23:216-222.

Hutcheon B, Miura RM, Puil E (1996a) Models of subthreshold membrane resonance in neocortical neurons. Journal of neurophysiology 76:698-714.

Hutcheon B, Miura RM, Puil E (1996b) Subthreshold membrane resonance in neocortical neurons. Journal of neurophysiology 76:683-697.

Hutcheon B, Fritschy JM, Poulter MO (2004) Organization of GABA receptor alpha-subunit clustering in the developing rat neocortex and hippocampus. The European journal of neuroscience 19:2475-2487.

Hutcheon B, Miura RM, Yarom Y, Puil E (1994) Low-threshold calcium current and resonance in thalamic neurons: a model of frequency preference. Journal of neurophysiology 71:583-594.

Inanobe A, Fujita A, Ito M, Tomoike H, Inageda K, Kurachi Y (2002) Inward rectifier K+ channel Kir2.3 is localized at the postsynaptic membrane of excitatory synapses. Am J Physiol Cell Physiol 282:C1396-1403.

Ingram SL, Williams JT (1996) Modulation of the hyperpolarization-activated current (Ih) by cyclic nucleotides in guinea-pig primary afferent neurons. The Journal of physiology 492 (Pt 1):97-106.

Insel TR (2010) Rethinking schizophrenia. Nature 468:187-193.

Isomoto S, Kondo C, Kurachi Y (1997) Inwardly rectifying potassium channels: their molecular heterogeneity and function. Jpn J Physiol 47:11-39.

Ito W, Pan BX, Yang C, Thakur S, Morozov A (2009) Enhanced generalization of auditory conditioned fear in juvenile mice. Learn Mem 16:187-192.

Izhikevich EM (2002) Resonance and selective communication via bursts in neurons having subthreshold oscillations. Bio Systems 67:95-102.

Jacobson-Pick S, Elkobi A, Vander S, Rosenblum K, Richter-Levin G (2008) Juvenile stress-induced alteration of maturation of the GABAA receptor alpha subunit in the rat. Int J Neuropsychopharmacol 11:891-903.

Jang HJ, Cho KH, Park SW, Kim MJ, Yoon SH, Rhie DJ (2010) The development of phasic and tonic inhibition in the rat visual cortex. Korean J Physiol Pharmacol 14:399-405.

Jankord R, Herman JP (2008) Limbic regulation of hypothalamo-pituitary-adrenocortical function during acute and chronic stress. Annals of the New York Academy of Sciences 1148:64-73.

Jarolimek W, Lewen A, Misgeld U (1999) A furosemide-sensitive K+-Cl- cotransporter counteracts intracellular Cl- accumulation and depletion in cultured rat midbrain neurons. The Journal of neuroscience : the official journal of the Society for Neuroscience 19:4695-4704.

Jensen O, Colgin LL (2007) Cross-frequency coupling between neuronal oscillations. Trends in cognitive sciences 11:267-269.

Jiang B, Huang S, de Pasquale R, Millman D, Song L, Lee HK, Tsumoto T, Kirkwood A (2010) The maturation of GABAergic transmission in visual cortex requires endocannabinoid-mediated LTD of inhibitory inputs during a critical period. Neuron 66:248-259.

Jiao Y, Zhang C, Yanagawa Y, Sun QQ (2006) Major effects of sensory experiences on the neocortical inhibitory circuits. The Journal of neuroscience : the official journal of the Society for Neuroscience 26:8691-8701.

Joels M, Baram TZ (2009) The neuro-symphony of stress. Nature reviews Neuroscience 10:459-466.

Johnson SA, Wang JF, Sun X, McEwen BS, Chattarji S, Young LT (2009) Lithium treatment prevents stress-induced dendritic remodeling in the rodent amygdala. Neuroscience 163:34-39.

Josselyn SA, Nguyen PV (2005) CREB, synapses and memory disorders: past progress and future challenges. Curr Drug Targets CNS Neurol Disord 4:481-497.

Josselyn SA, Kida S, Silva AJ (2004) Inducible repression of CREB function disrupts amygdala-dependent memory. Neurobiology of learning and memory 82:159-163.

Josselyn SA, Shi C, Carlezon WA, Jr., Neve RL, Nestler EJ, Davis M (2001) Long-term memory is facilitated by cAMP response element-binding protein overexpression in the amygdala. The Journal of neuroscience : the official journal of the Society for Neuroscience 21:2404-2412.

Juster RP, McEwen BS, Lupien SJ (2010) Allostatic load biomarkers of chronic stress and impact on health and cognition. Neurosci Biobehav Rev 35:2-16.

Jutras MJ, Buffalo EA (2010) Synchronous neural activity and memory formation. Curr Opin Neurobiol 20:150-155.

Kamp TJ, Hell JW (2000) Regulation of cardiac L-type calcium channels by protein kinase A and protein kinase C. Circulation research 87:1095-1102.

Kanyshkova T, Pawlowski M, Meuth P, Dube C, Bender RA, Brewster AL, Baumann A, Baram TZ, Pape HC, Budde T (2009) Postnatal expression pattern of HCN channel isoforms in thalamic neurons: relationship to maturation of thalamocortical oscillations. The Journal of neuroscience : the official journal of the Society for Neuroscience 29:8847-8857.

Karmiloff-Smith A (2009) Nativism versus neuroconstructivism: rethinking the study of developmental disorders. Dev Psychol 45:56-63.

Katagiri H, Fagiolini M, Hensch TK (2007) Optimization of somatic inhibition at critical period onset in mouse visual cortex. Neuron 53:805-812.

Kaufmann WE, Moser HW (2000) Dendritic anomalies in disorders associated with mental retardation. Cereb Cortex 10:981-991.

Kemppainen S, Pitkanen A (2000) Distribution of parvalbumin, calretinin, and calbindin-D(28k) immunoreactivity in the rat amygdaloid complex and colocalization with gamma-aminobutyric acid. The Journal of comparative neurology 426:441-467.

Kessler RC, Berglund P, Demler O, Jin R, Merikangas KR, Walters EE (2005) Lifetime prevalence and age-of-onset distributions of DSM-IV disorders in the National Comorbidity Survey Replication. Archives of general psychiatry 62:593-602.

Khashan AS, Abel KM, McNamee R, Pedersen MG, Webb RT, Baker PN, Kenny LC, Mortensen PB (2008) Higher risk of offspring schizophrenia following antenatal maternal exposure to severe adverse life events. Archives of general psychiatry 65:146-152.

Khurana S, Liu Z, Lewis AS, Rosa K, Chetkovich D, Golding NL (2012) An essential role for modulation of hyperpolarization-activated current in the development of binaural temporal precision. The Journal of neuroscience : the official journal of the Society for Neuroscience 32:2814-2823.

Kida S, Josselyn SA, Pena de Ortiz S, Kogan JH, Chevere I, Masushige S, Silva AJ (2002) CREB required for the stability of new and reactivated fear memories. Nature neuroscience 5:348-355.

Kilb W (2012) Development of the GABAergic system from birth to adolescence. The Neuroscientist : a review journal bringing neurobiology, neurology and psychiatry 18:613-630.

Killgore WD, Yurgelun-Todd DA (2004) Sex-related developmental differences in the lateralized activation of the prefrontal cortex and amygdala during perception of facial affect. Perceptual and motor skills 99:371-391.

Kim-Cohen J, Caspi A, Moffitt TE, Harrington H, Milne BJ, Poulton R (2003) Prior juvenile diagnoses in adults with mental disorder: developmental follow-back of a prospective-longitudinal cohort. Archives of general psychiatry 60:709-717.

Kim JA, Park JY, Kang HW, Huh SU, Jeong SW, Lee JH (2006a) Augmentation of Cav3.2 T-type calcium channel activity by cAMP-dependent protein kinase A. J Pharmacol Exp Ther 318:230-237.

Kim JH, Richardson R (2007) A developmental dissociation in reinstatement of an extinguished fear response in rats. Neurobiology of learning and memory 88:48-57.

Kim JH, Richardson R (2008) The effect of temporary amygdala inactivation on extinction and reextinction of fear in the developing rat: unlearning as a potential mechanism for extinction early in development. The Journal of neuroscience : the official journal of the Society for Neuroscience 28:1282-1290.

Kim JH, Richardson R (2010) New findings on extinction of conditioned fear early in development: theoretical and clinical implications. Biological psychiatry 67:297-303.

Kim JH, McNally GP, Richardson R (2006b) Recovery of fear memories in rats: role of gamma-amino butyric acid (GABA) in infantile amnesia. Behavioral neuroscience 120:40-48.

Kim JH, Hamlin AS, Richardson R (2009) Fear extinction across development: the involvement of the medial prefrontal cortex as assessed by temporary inactivation and immunohistochemistry. The Journal of neuroscience : the official journal of the Society for Neuroscience 29:10802-10808.

Kim U, Sanchez-Vives MV, McCormick DA (1997) Functional dynamics of GABAergic inhibition in the thalamus. Science 278:130-134.

King EC, Pattwell SS, Glatt CE, Lee FS (2013) Sensitive periods in fear learning and memory. Stress.

Kinney DK, Munir KM, Crowley DJ, Miller AM (2008) Prenatal stress and risk for autism. Neurosci Biobehav Rev 32:1519-1532.

Klausberger T, Roberts JD, Somogyi P (2002) Cell type- and input-specific differences in the number and subtypes of synaptic GABA(A) receptors in the hippocampus. The Journal of neuroscience : the official journal of the Society for Neuroscience 22:2513-2521.

Kling A, Lancaster J, Benitone J (1970) Amygdalectomy in the free-ranging vervet (Cercopithecus aethiops). J Psychiatr Res 7:191-199.

Koenig JI, Kirkpatrick B, Lee P (2002) Glucocorticoid hormones and early brain development in schizophrenia. Neuropsychopharmacology : official publication of the American College of Neuropsychopharmacology 27:309-318.

Kofman O (2002) The role of prenatal stress in the etiology of developmental behavioural disorders. Neurosci Biobehav Rev 26:457-470.

Kolber BJ, Boyle MP, Wieczorek L, Kelley CL, Onwuzurike CC, Nettles SA, Vogt SK, Muglia LJ (2010) Transient early-life forebrain corticotropin-releasing hormone elevation causes long-lasting anxiogenic and despair-like changes in mice. The Journal of neuroscience : the official journal of the Society for Neuroscience 30:2571-2581.

Konig N, Roch G, Marty R (1975) The onset of synaptogenesis in rat temporal cortex. Anat Embryol (Berl) 148:73-87.

Koob GF, Volkow ND (2010) Neurocircuitry of addiction. Neuropsychopharmacology : official publication of the American College of Neuropsychopharmacology 35:217-238.

Korosi A, Baram TZ (2008) The central corticotropin releasing factor system during development and adulthood. European journal of pharmacology 583:204-214.

Korosi A, Baram TZ (2009) The pathways from mother's love to baby's future. Front Behav Neurosci 3:27.

Kraszpulski M, Dickerson PA, Salm AK (2006) Prenatal stress affects the developmental trajectory of the rat amygdala. Stress 9:85-95.

Kuhlman SJ, Lu J, Lazarus MS, Huang ZJ (2010) Maturation of GABAergic inhibition promotes strengthening of temporally coherent inputs among convergent pathways. PLoS computational biology 6:e1000797.

Kulik A, Nakadate K, Nyiri G, Notomi T, Malitschek B, Bettler B, Shigemoto R (2002) Distinct localization of GABA(B) receptors relative to synaptic sites in the rat cerebellum and ventrobasal thalamus. The European journal of neuroscience 15:291-307.

Ladd CO, Huot RL, Thrivikraman KV, Nemeroff CB, Plotsky PM (2004) Long-term adaptations in glucocorticoid receptor and mineralocorticoid receptor mRNA and negative feedback on the hypothalamo-pituitary-adrenal axis following neonatal maternal separation. Biological psychiatry 55:367-375.

Laloux C, Mairesse J, Van Camp G, Giovine A, Branchi I, Bouret S, Morley-Fletcher S, Bergonzelli G, Malagodi M, Gradini R, Nicoletti F, Darnaudery M, Maccari S (2012) Anxiety-like behaviour and associated neurochemical and endocrinological alterations in male pups exposed to prenatal stress. Psychoneuroendocrinology 37:1646-1658.

Lamont EW, Kokkinidis L (1998) Infusion of the dopamine D1 receptor antagonist SCH 23390 into the amygdala blocks fear expression in a potentiated startle paradigm. Brain research 795:128-136.

Lampl I, Yarom Y (1997) Subthreshold oscillations and resonant behavior: two manifestations of the same mechanism. Neuroscience 78:325-341.

Landers MS, Sullivan RM (2012) The development and neurobiology of infant attachment and fear. Dev Neurosci 34:101-114.

Langton JM, Kim JH, Nicholas J, Richardson R (2007) The effect of the NMDA receptor antagonist MK-801 on the acquisition and extinction of learned fear in the developing rat. Learn Mem 14:665-668.

Lazarus MS, Huang ZJ (2011) Distinct maturation profiles of perisomatic and dendritic targeting GABAergic interneurons in the mouse primary visual cortex during the critical period of ocular dominance plasticity. Journal of neurophysiology 106:775-787.

Le Magueresse C, Monyer H (2013) GABAergic interneurons shape the functional maturation of the cortex. Neuron 77:388-405.

Le Magueresse C, Alfonso J, Khodosevich K, Arroyo Martin AA, Bark C, Monyer H (2011) "Small axonless neurons": postnatally generated neocortical interneurons with delayed functional maturation. The Journal of neuroscience : the official journal of the Society for Neuroscience 31:16731-16747.

LeBlanc JJ, Fagiolini M (2011) Autism: a "critical period" disorder? Neural Plast 2011:921680.

Lebrand C, Cases O, Wehrle R, Blakely RD, Edwards RH, Gaspar P (1998) Transient developmental expression of monoamine transporters in the rodent forebrain. The Journal of comparative neurology 401:506-524.

LeDoux J (2000) The amygdala and emotion: a view through fear. In: The Amygdala: A Functional Analysis (Aggleton JP, ed). London: Oxford University Press.

LeDoux J (2007) The amygdala. Current biology : CB 17:R868-874.

Lee JH, Gomora JC, Cribbs LL, Perez-Reyes E (1999) Nickel block of three cloned T-type calcium channels: low concentrations selectively block alpha1H. Biophysical journal 77:3034-3042.

Lee KF, Soares C, Beique JC (2012) Examining form and function of dendritic spines. Neural Plast 2012:704103.

Legaz I, Olmos L, Real MA, Guirado S, Davila JC, Medina L (2005) Development of neurons and fibers containing calcium binding proteins in the pallial amygdala of mouse, with special emphasis on those of the basolateral amygdalar complex. The Journal of comparative neurology 488:492-513.

Lesting J, Narayanan RT, Kluge C, Sangha S, Seidenbecher T, Pape HC (2011) Patterns of coupled theta activity in amygdala-hippocampal-prefrontal cortical circuits during fear extinction. PloS one 6:e21714.

Levine S (1967) Maternal and environmental influences on the adrenocortical response to stress in weanling rats. Science 156:258-260.

Levine S (2001) Primary social relationships influence the development of the hypothalamic--pituitary--adrenal axis in the rat. Physiology & behavior 73:255-260.

Levine S (2005) Developmental determinants of sensitivity and resistance to stress. Psychoneuroendocrinology 30:939-946.

Lewis DA, Hashimoto T, Volk DW (2005) Cortical inhibitory neurons and schizophrenia. Nature reviews Neuroscience 6:312-324.

Li C, Dabrowska J, Hazra R, Rainnie DG (2011) Synergistic activation of dopamine D1 and TrkB receptors mediate gain control of synaptic plasticity in the basolateral amygdala. PloS one 6:e26065.

Liao CC, Lee LJ (2012) Evidence for structural and functional changes of subplate neurons in developing rat barrel cortex. Brain structure & function 217:275-292.

Lin CH, Lee CC, Huang YC, Wang SJ, Gean PW (2005) Activation of group II metabotropic glutamate receptors induces depotentiation in amygdala slices and reduces fear-potentiated startle in rats. Learn Mem 12:130-137.

Lin HC, Mao SC, Gean PW (2009) Block of gamma-aminobutyric acid-A receptor insertion in the amygdala impairs extinction of conditioned fear. Biological psychiatry 66:665-673.

Lin HC, Wang SJ, Luo MZ, Gean PW (2000) Activation of group II metabotropic glutamate receptors induces long-term depression of synaptic transmission in the rat amygdala. The Journal of neuroscience : the official journal of the Society for Neuroscience 20:9017-9024.

Lisman JE (1997) Bursts as a unit of neural information: making unreliable synapses reliable. Trends in neurosciences 20:38-43.

Lissek S, Powers AS, McClure EB, Phelps EA, Woldehawariat G, Grillon C, Pine DS (2005) Classical fear conditioning in the anxiety disorders: a meta-analysis. Behaviour research and therapy 43:1391-1424.

Livak KJ, Schmittgen TD (2001) Analysis of relative gene expression data using real-time quantitative PCR and the 2(-Delta Delta C(T)) Method. Methods 25:402-408.

Llinas RR, Grace AA, Yarom Y (1991) In vitro neurons in mammalian cortical layer 4 exhibit intrinsic oscillatory activity in the 10- to 50-Hz frequency range. Proceedings of the National Academy of Sciences of the United States of America 88:897-901.

Loretan K, Bissiere S, Luthi A (2004) Dopaminergic modulation of spontaneous inhibitory network activity in the lateral amygdala. Neuropharmacology 47:631-639.

LoTurco JJ, Owens DF, Heath MJ, Davis MB, Kriegstein AR (1995) GABA and glutamate depolarize cortical progenitor cells and inhibit DNA synthesis. Neuron 15:1287-1298.

Luhmann HJ, Prince DA (1991) Postnatal maturation of the GABAergic system in rat neocortex. Journal of neurophysiology 65:247-263.

Lujan R, Shigemoto R (2006) Localization of metabotropic GABA receptor subunits GABAB1 and GABAB2 relative to synaptic sites in the rat developing cerebellum. The European journal of neuroscience 23:1479-1490.

Luk KC, Sadikot AF (2001) GABA promotes survival but not proliferation of parvalbumin-immunoreactive interneurons in rodent neostriatum: an in vivo study with stereology. Neuroscience 104:93-103.

Lupien SJ, McEwen BS, Gunnar MR, Heim C (2009) Effects of stress throughout the lifespan on the brain, behaviour and cognition. Nature reviews Neuroscience 10:434-445.

Lyons DM, Parker KJ, Katz M, Schatzberg AF (2009) Developmental cascades linking stress inoculation, arousal regulation, and resilience. Front Behav Neurosci 3:32.

Ma DQ, Whitehead PL, Menold MM, Martin ER, Ashley-Koch AE, Mei H, Ritchie MD, Delong GR, Abramson RK, Wright HH, Cuccaro ML, Hussman JP, Gilbert JR, Pericak-Vance MA (2005) Identification of significant association and gene-gene interaction of GABA receptor subunit genes in autism. Am J Hum Genet 77:377-388.

Mabandla MV, Dobson B, Johnson S, Kellaway LA, Daniels WM, Russell VA (2008) Development of a mild prenatal stress rat model to study long term effects on neural function and survival. Metab Brain Dis 23:31-42.

Maccari S, Morley-Fletcher S (2007) Effects of prenatal restraint stress on the hypothalamus-pituitary-adrenal axis and related behavioural and neurobiological alterations. Psychoneuroendocrinology 32 Suppl 1:S10-15.

Maccari S, Piazza PV, Kabbaj M, Barbazanges A, Simon H, Le Moal M (1995) Adoption reverses the long-term impairment in glucocorticoid feedback induced by prenatal stress. The Journal of neuroscience : the official journal of the Society for Neuroscience 15:110-116.

MacDermott AB, Role LW, Siegelbaum SA (1999) Presynaptic ionotropic receptors and the control of transmitter release. Annual review of neuroscience 22:443-485.

Machado CJ, Bachevalier J (2003) Non-human primate models of childhood psychopathology: the promise and the limitations. Journal of child psychology and psychiatry, and allied disciplines 44:64-87.

MacMillan HL, Fleming JE, Streiner DL, Lin E, Boyle MH, Jamieson E, Duku EK, Walsh CA, Wong MY, Beardslee WR (2001) Childhood abuse and lifetime psychopathology in a community sample. The American journal of psychiatry 158:1878-1883.

Madsen TE, Rainnie DG (2009) Local field potentials in the rat basolateral amygdala and medial prefrontal cortex show coherent oscillations in multiple frequency bands during fear. Society for Neuroscience Annual Meeting, Chicago, IL, Oct 18, 2009.

Maheu FS, Dozier M, Guyer AE, Mandell D, Peloso E, Poeth K, Jenness J, Lau JY, Ackerman JP, Pine DS, Ernst M (2010) A preliminary study of medial temporal lobe function in

youths with a history of caregiver deprivation and emotional neglect. Cogn Affect Behav Neurosci 10:34-49.
Mainen ZF, Sejnowski TJ (1995) Reliability of spike timing in neocortical neurons. Science 268:1503-1506.
Mainen ZF, Sejnowski TJ (1996) Influence of dendritic structure on firing pattern in model neocortical neurons. Nature 382:363-366.
Mairesse J, Viltart O, Salome N, Giuliani A, Catalani A, Casolini P, Morley-Fletcher S, Nicoletti F, Maccari S (2007) Prenatal stress alters the negative correlation between neuronal activation in limbic regions and behavioral responses in rats exposed to high and low anxiogenic environments. Psychoneuroendocrinology 32:765-776.
Mana S, Paillere Martinot ML, Martinot JL (2010) Brain imaging findings in children and adolescents with mental disorders: a cross-sectional review. Eur Psychiatry 25:345-354.
Manent JB, Demarque M, Jorquera I, Pellegrino C, Ben-Ari Y, Aniksztejn L, Represa A (2005) A noncanonical release of GABA and glutamate modulates neuronal migration. The Journal of neuroscience : the official journal of the Society for Neuroscience 25:4755-4765.
Manko M, Bienvenu TC, Dalezios Y, Capogna M (2012) Neurogliaform cells of amygdala: a source of slow phasic inhibition in the basolateral complex. The Journal of physiology 590:5611-5627.
Marcelin B, Liu Z, Chen Y, Lewis AS, Becker A, McClelland S, Chetkovich DM, Migliore M, Baram TZ, Esclapez M, Bernard C (2012) Dorsoventral differences in intrinsic properties in developing CA1 pyramidal cells. The Journal of neuroscience : the official journal of the Society for Neuroscience 32:3736-3747.
Maren S (2003) What the amygdala does and doesn't do in aversive learning. Learn Mem 10:306-308.
Maren S (2005) Synaptic mechanisms of associative memory in the amygdala. Neuron 47:783-786.
Markham JA, Koenig JI (2011) Prenatal stress: role in psychotic and depressive diseases. Psychopharmacology 214:89-106.
Marowsky A, Fritschy JM, Vogt KE (2004) Functional mapping of GABA A receptor subtypes in the amygdala. The European journal of neuroscience 20:1281-1289.
Marowsky A, Yanagawa Y, Obata K, Vogt KE (2005) A specialized subclass of interneurons mediates dopaminergic facilitation of amygdala function. Neuron 48:1025-1037.
Martina M, Royer S, Pare D (2001) Cell-type-specific GABA responses and chloride homeostasis in the cortex and amygdala. Journal of neurophysiology 86:2887-2895.
Mascagni F, McDonald AJ (2003) Immunohistochemical characterization of cholecystokinin containing neurons in the rat basolateral amygdala. Brain research 976:171-184.
Mascagni F, McDonald AJ (2009) Parvalbumin-immunoreactive neurons and GABAergic neurons of the basal forebrain project to the rat basolateral amygdala. Neuroscience 160:805-812.
Matsui F, Morimoto M, Yoshimoto K, Nakatomi Y, Syoji H, Nishimura A, Isoda K, Tanda K, Hosoi H (2010) Effects of stress of postnatal development on corticosterone, serotonin and behavioral changes. Brain Dev 32:517-523.
McCormick DA, Prince DA (1987) Post-natal development of electrophysiological properties of rat cerebral cortical pyramidal neurones. The Journal of physiology 393:743-762.
McDonald AJ (1985) Immunohistochemical identification of gamma-aminobutyric acid-containing neurons in the rat basolateral amygdala. Neuroscience letters 53:203-207.
McDonald AJ (1996) Localization of AMPA glutamate receptor subunits in subpopulations of non-pyramidal neurons in the rat basolateral amygdala. Neuroscience letters 208:175-178.
McDonald AJ (1998) Cortical pathways to the mammalian amygdala. Progress in neurobiology 55:257-332.

McDonald AJ, Pearson JC (1989) Coexistence of GABA and peptide immunoreactivity in non-pyramidal neurons of the basolateral amygdala. Neuroscience letters 100:53-58.
McDonald AJ, Mascagni F (2001) Colocalization of calcium-binding proteins and GABA in neurons of the rat basolateral amygdala. Neuroscience 105:681-693.
McDonald AJ, Betette RL (2001) Parvalbumin-containing neurons in the rat basolateral amygdala: morphology and co-localization of Calbindin-D(28k). Neuroscience 102:413-425.
McDonald AJ, Mascagni F (2002) Immunohistochemical characterization of somatostatin containing interneurons in the rat basolateral amygdala. Brain research 943:237-244.
McDonald AJ, Shammah-Lagnado SJ, Shi C, Davis M (1999) Cortical afferents to the extended amygdala. Annals of the New York Academy of Sciences 877:309-338.
McDonald AJ, Mascagni F, Mania I, Rainnie DG (2005) Evidence for a perisomatic innervation of parvalbumin-containing interneurons by individual pyramidal cells in the basolateral amygdala. Brain research 1035:32-40.
McEwen BS (2003) Early life influences on life-long patterns of behavior and health. Mental retardation and developmental disabilities research reviews 9:149-154.
McEwen BS (2004) Protection and damage from acute and chronic stress: allostasis and allostatic overload and relevance to the pathophysiology of psychiatric disorders. Annals of the New York Academy of Sciences 1032:1-7.
McEwen BS (2007) Physiology and neurobiology of stress and adaptation: central role of the brain. Physiological reviews 87:873-904.
McKernan MG, Shinnick-Gallagher P (1997) Fear conditioning induces a lasting potentiation of synaptic currents in vitro. Nature 390:607-611.
Mehta MA, Golembo NI, Nosarti C, Colvert E, Mota A, Williams SC, Rutter M, Sonuga-Barke EJ (2009) Amygdala, hippocampal and corpus callosum size following severe early institutional deprivation: the English and Romanian Adoptees study pilot. Journal of child psychology and psychiatry, and allied disciplines 50:943-951.
Merlo Pich E, Lorang M, Yeganeh M, Rodriguez de Fonseca F, Raber J, Koob GF, Weiss F (1995) Increase of extracellular corticotropin-releasing factor-like immunoreactivity levels in the amygdala of awake rats during restraint stress and ethanol withdrawal as measured by microdialysis. The Journal of neuroscience : the official journal of the Society for Neuroscience 15:5439-5447.
Micheva KD, Beaulieu C (1995) Neonatal sensory deprivation induces selective changes in the quantitative distribution of GABA-immunoreactive neurons in the rat barrel field cortex. The Journal of comparative neurology 361:574-584.
Miles R, Toth K, Gulyas AI, Hajos N, Freund TF (1996) Differences between somatic and dendritic inhibition in the hippocampus. Neuron 16:815-823.
Miller GE, Chen E, Zhou ES (2007) If it goes up, must it come down? Chronic stress and the hypothalamic-pituitary-adrenocortical axis in humans. Psychol Bull 133:25-45.
Mines MA, Yuskaitis CJ, King MK, Beurel E, Jope RS (2010) GSK3 influences social preference and anxiety-related behaviors during social interaction in a mouse model of fragile X syndrome and autism. PloS one 5:e9706.
Miserendino MJ, Sananes CB, Melia KR, Davis M (1990) Blocking of acquisition but not expression of conditioned fear-potentiated startle by NMDA antagonists in the amygdala. Nature 345:716-718.
Mitra P, Bokil H (2008) Observed brain dynamics, 2nd ed. Edition. New York: Oxford University Press.
Miyoshi G, Butt SJ, Takebayashi H, Fishell G (2007) Physiologically distinct temporal cohorts of cortical interneurons arise from telencephalic Olig2-expressing precursors. The Journal of neuroscience : the official journal of the Society for Neuroscience 27:7786-7798.

Miyoshi G, Hjerling-Leffler J, Karayannis T, Sousa VH, Butt SJ, Battiste J, Johnson JE, Machold RP, Fishell G (2010) Genetic fate mapping reveals that the caudal ganglionic eminence produces a large and diverse population of superficial cortical interneurons. The Journal of neuroscience : the official journal of the Society for Neuroscience 30:1582-1594.

Mizukawa K, Tseng IM, Otsuka N (1989) Quantitative electron microscopic analysis of postnatal development of zinc-positive nerve endings in the rat amygdala using Timm's sulphide silver technique. Brain research Developmental brain research 50:197-203.

Moffitt TE, Caspi A, Harrington H, Milne BJ, Melchior M, Goldberg D, Poulton R (2007) Generalized anxiety disorder and depression: childhood risk factors in a birth cohort followed to age 32. Psychological medicine 37:441-452.

Mohajerani MH, Cherubini E (2006) Role of giant depolarizing potentials in shaping synaptic currents in the developing hippocampus. Critical reviews in neurobiology 18:13-23.

Mohler H, Fritschy JM, Crestani F, Hensch T, Rudolph U (2004) Specific GABA(A) circuits in brain development and therapy. Biochemical pharmacology 68:1685-1690.

Molineux ML, Fernandez FR, Mehaffey WH, Turner RW (2005) A-type and T-type currents interact to produce a novel spike latency-voltage relationship in cerebellar stellate cells. The Journal of neuroscience : the official journal of the Society for Neuroscience 25:10863-10873.

Monk CS (2008) The development of emotion-related neural circuitry in health and psychopathology. Development and psychopathology 20:1231-1250.

Monk CS, McClure EB, Nelson EE, Zarahn E, Bilder RM, Leibenluft E, Charney DS, Ernst M, Pine DS (2003a) Adolescent immaturity in attention-related brain engagement to emotional facial expressions. NeuroImage 20:420-428.

Monk CS, Grillon C, Baas JM, McClure EB, Nelson EE, Zarahn E, Charney DS, Ernst M, Pine DS (2003b) A neuroimaging method for the study of threat in adolescents. Developmental psychobiology 43:359-366.

Monk CS, Telzer EH, Mogg K, Bradley BP, Mai X, Louro HM, Chen G, McClure-Tone EB, Ernst M, Pine DS (2008) Amygdala and ventrolateral prefrontal cortex activation to masked angry faces in children and adolescents with generalized anxiety disorder. Archives of general psychiatry 65:568-576.

Monteggia LM, Eisch AJ, Tang MD, Kaczmarek LK, Nestler EJ (2000) Cloning and localization of the hyperpolarization-activated cyclic nucleotide-gated channel family in rat brain. Brain research Molecular brain research 81:129-139.

Monteiro RA, Henrique RM, Oliveira MH, Silva MW, Rocha E (2005) Postnatal cerebellar granule cells of the white rat (Rattus norvegicus): a quantitative study, using design-based stereology. Ann Anat 187:161-173.

Monteiro RA, Henrique RM, Rocha E, Marini-Abreu MM, Oliveira MH, Silva MW (1998) Age-related changes in the volume of somata and organelles of cerebellar granule cells. Neurobiology of aging 19:325-332.

Morgan KN, Thayer JE, Frye CA (1999) Prenatal stress suppresses rat pup ultrasonic vocalization and myoclonic twitching in response to separation. Developmental psychobiology 34:205-215.

Moriceau S, Sullivan RM (2006) Maternal presence serves as a switch between learning fear and attraction in infancy. Nature neuroscience 9:1004-1006.

Moriceau S, Roth TL, Okotoghaide T, Sullivan RM (2004) Corticosterone controls the developmental emergence of fear and amygdala function to predator odors in infant rat pups. International journal of developmental neuroscience : the official journal of the International Society for Developmental Neuroscience 22:415-422.

Moriceau S, Wilson DA, Levine S, Sullivan RM (2006) Dual circuitry for odor-shock conditioning during infancy: corticosterone switches between fear and attraction via

amygdala. The Journal of neuroscience : the official journal of the Society for Neuroscience 26:6737-6748.
Moriceau S, Shionoya K, Jakubs K, Sullivan RM (2009) Early-life stress disrupts attachment learning: the role of amygdala corticosterone, locus ceruleus corticotropin releasing hormone, and olfactory bulb norepinephrine. The Journal of neuroscience : the official journal of the Society for Neuroscience 29:15745-15755.
Morys J, Berdel B, Kowianski P, Dziewiatkowski J (1998) The pattern of synaptophysin changes during the maturation of the amygdaloid body and hippocampal hilus in the rat. Folia neuropathologica / Association of Polish Neuropathologists and Medical Research Centre, Polish Academy of Sciences 36:15-23.
Moy SS, Nonneman RJ, Young NB, Demyanenko GP, Maness PF (2009) Impaired sociability and cognitive function in Nrcam-null mice. Behavioural brain research 205:123-131.
Moy SS, Nadler JJ, Perez A, Barbaro RP, Johns JM, Magnuson TR, Piven J, Crawley JN (2004) Sociability and preference for social novelty in five inbred strains: an approach to assess autistic-like behavior in mice. Genes Brain Behav 3:287-302.
Moye TB, Rudy JW (1987) Ontogenesis of trace conditioning in young rats: dissociation of associative and memory processes. Developmental psychobiology 20:405-414.
Mueller BR, Bale TL (2008) Sex-specific programming of offspring emotionality after stress early in pregnancy. The Journal of neuroscience : the official journal of the Society for Neuroscience 28:9055-9065.
Mukhopadhyay A, McGuire T, Peng CY, Kessler JA (2009) Differential effects of BMP signaling on parvalbumin and somatostatin interneuron differentiation. Development 136:2633-2642.
Muller JF, Mascagni F, McDonald AJ (2005) Coupled networks of parvalbumin-immunoreactive interneurons in the rat basolateral amygdala. The Journal of neuroscience : the official journal of the Society for Neuroscience 25:7366-7376.
Muller JF, Mascagni F, McDonald AJ (2006) Pyramidal cells of the rat basolateral amygdala: synaptology and innervation by parvalbumin-immunoreactive interneurons. The Journal of comparative neurology 494:635-650.
Muller JF, Mascagni F, McDonald AJ (2009) Dopaminergic innervation of pyramidal cells in the rat basolateral amygdala. Brain structure & function 213:275-288.
Muly EC, Mania I, Guo JD, Rainnie DG (2007) Group II metabotropic glutamate receptors in anxiety circuitry: correspondence of physiological response and subcellular distribution. The Journal of comparative neurology 505:682-700.
Muly EC, Senyuz M, Khan ZU, Guo JD, Hazra R, Rainnie DG (2009) Distribution of D1 and D5 dopamine receptors in the primate and rat basolateral amygdala. Brain structure & function 213:375-393.
Myers KM, Davis M (2007) Mechanisms of fear extinction. Molecular psychiatry 12:120-150.
Nair HP, Berndt JD, Barrett D, Gonzalez-Lima F (2001) Maturation of extinction behavior in infant rats: large-scale regional interactions with medial prefrontal cortex, orbitofrontal cortex, and anterior cingulate cortex. The Journal of neuroscience : the official journal of the Society for Neuroscience 21:4400-4407.
Narabayashi H, Nagao T, Saito Y, Yoshida M, Nagahata M (1963) Stereotaxic amygdalotomy for behavior disorders. Arch Neurol 9:1-16.
Nemeroff CB (2004) Neurobiological consequences of childhood trauma. J Clin Psychiatry 65 Suppl 1:18-28.
Nemeroff CB, Vale WW (2005) The neurobiology of depression: inroads to treatment and new drug discovery. J Clin Psychiatry 66 Suppl 7:5-13.
Neuhaus E, Beauchaine TP, Bernier R (2010) Neurobiological correlates of social functioning in autism. Clin Psychol Rev 30:733-748.

Nishio H, Kasuga S, Ushijima M, Harada Y (2001) Prenatal stress and postnatal development of neonatal rats--sex-dependent effects on emotional behavior and learning ability of neonatal rats. International journal of developmental neuroscience : the official journal of the International Society for Developmental Neuroscience 19:37-45.

Nolan MF, Malleret G, Dudman JT, Buhl DL, Santoro B, Gibbs E, Vronskaya S, Buzsaki G, Siegelbaum SA, Kandel ER, Morozov A (2004) A behavioral role for dendritic integration: HCN1 channels constrain spatial memory and plasticity at inputs to distal dendrites of CA1 pyramidal neurons. Cell 119:719-732.

Notomi T, Shigemoto R (2004) Immunohistochemical localization of Ih channel subunits, HCN1-4, in the rat brain. The Journal of comparative neurology 471:241-276.

Nowicka D, Soulsby S, Skangiel-Kramska J, Glazewski S (2009) Parvalbumin-containing neurons, perineuronal nets and experience-dependent plasticity in murine barrel cortex. The European journal of neuroscience 30:2053-2063.

Nusser Z, Sieghart W, Benke D, Fritschy JM, Somogyi P (1996) Differential synaptic localization of two major gamma-aminobutyric acid type A receptor alpha subunits on hippocampal pyramidal cells. Proceedings of the National Academy of Sciences of the United States of America 93:11939-11944.

Nyiri G, Freund TF, Somogyi P (2001) Input-dependent synaptic targeting of alpha(2)-subunit-containing GABA(A) receptors in synapses of hippocampal pyramidal cells of the rat. The European journal of neuroscience 13:428-442.

O'Connor TG, Heron J, Golding J, Glover V (2003) Maternal antenatal anxiety and behavioural/emotional problems in children: a test of a programming hypothesis. Journal of child psychology and psychiatry, and allied disciplines 44:1025-1036.

O'Donnell K, O'Connor TG, Glover V (2009) Prenatal stress and neurodevelopment of the child: focus on the HPA axis and role of the placenta. Dev Neurosci 31:285-292.

Ochsner KN, Gross JJ (2005) The cognitive control of emotion. Trends in cognitive sciences 9:242-249.

Okada M, Onodera K, Van Renterghem C, Sieghart W, Takahashi T (2000) Functional correlation of GABA(A) receptor alpha subunits expression with the properties of IPSCs in the developing thalamus. The Journal of neuroscience : the official journal of the Society for Neuroscience 20:2202-2208.

Ono M, Kikusui T, Sasaki N, Ichikawa M, Mori Y, Murakami-Murofushi K (2008) Early weaning induces anxiety and precocious myelination in the anterior part of the basolateral amygdala of male Balb/c mice. Neuroscience 156:1103-1110.

Orduz D, Bischop DP, Schwaller B, Schiffmann SN, Gall D (2013) Parvalbumin tunes spike-timing and efferent short-term plasticity in striatal fast spiking interneurons. The Journal of physiology 591:3215-3232.

Overstreet LS, Jones MV, Westbrook GL (2000) Slow desensitization regulates the availability of synaptic GABA(A) receptors. The Journal of neuroscience : the official journal of the Society for Neuroscience 20:7914-7921.

Owens DF, Kriegstein AR (2002) Is there more to GABA than synaptic inhibition? Nature reviews Neuroscience 3:715-727.

Owens DF, Boyce LH, Davis MB, Kriegstein AR (1996) Excitatory GABA responses in embryonic and neonatal cortical slices demonstrated by gramicidin perforated-patch recordings and calcium imaging. The Journal of neuroscience : the official journal of the Society for Neuroscience 16:6414-6423.

Owens MJ, Nemeroff CB (1991) Physiology and pharmacology of corticotropin-releasing factor. Pharmacol Rev 43:425-473.

Padival MA, Blume SR, Rosenkranz JA (2013) Repeated restraint stress exerts different impact on structure of neurons in the lateral and basal nuclei of the amygdala. Neuroscience 246:230-242.

Pan BX, Ito W, Morozov A (2009) Divergence between thalamic and cortical inputs to lateral amygdala during juvenile-adult transition in mice. Biological psychiatry 66:964-971.
Pantazopoulos H, Murray EA, Berretta S (2008) Total number, distribution, and phenotype of cells expressing chondroitin sulfate proteoglycans in the normal human amygdala. Brain research 1207:84-95.
Pape HC, Driesang RB (1998) Ionic mechanisms of intrinsic oscillations in neurons of the basolateral amygdaloid complex. Journal of neurophysiology 79:217-226.
Pape HC, Pare D (2010) Plastic synaptic networks of the amygdala for the acquisition, expression, and extinction of conditioned fear. Physiological reviews 90:419-463.
Pape HC, Pare D, Driesang RB (1998) Two types of intrinsic oscillations in neurons of the lateral and basolateral nuclei of the amygdala. Journal of neurophysiology 79:205-216.
Pape HC, Munsch T, Budde T (2004) Novel vistas of calcium-mediated signalling in the thalamus. Pflugers Arch 448:131-138.
Pape HC, Budde T, Mager R, Kisvarday ZF (1994) Prevention of Ca(2+)-mediated action potentials in GABAergic local circuit neurones of rat thalamus by a transient K+ current. The Journal of physiology 478 Pt 3:403-422.
Pape HC, Narayanan RT, Smid J, Stork O, Seidenbecher T (2005) Theta activity in neurons and networks of the amygdala related to long-term fear memory. Hippocampus 15:874-880.
Pare D, Gaudreau H (1996) Projection cells and interneurons of the lateral and basolateral amygdala: distinct firing patterns and differential relation to theta and delta rhythms in conscious cats. The Journal of neuroscience : the official journal of the Society for Neuroscience 16:3334-3350.
Pare D, Collins DR, Pelletier JG (2002) Amygdala oscillations and the consolidation of emotional memories. Trends in cognitive sciences 6:306-314.
Pattwell SS, Bath KG, Casey BJ, Ninan I, Lee FS (2011) Selective early-acquired fear memories undergo temporary suppression during adolescence. Proceedings of the National Academy of Sciences of the United States of America 108:1182-1187.
Patz S, Grabert J, Gorba T, Wirth MJ, Wahle P (2004) Parvalbumin expression in visual cortical interneurons depends on neuronal activity and TrkB ligands during an Early period of postnatal development. Cereb Cortex 14:342-351.
Pawelzik H, Bannister AP, Deuchars J, Ilia M, Thomson AM (1999) Modulation of bistratified cell IPSPs and basket cell IPSPs by pentobarbitone sodium, diazepam and Zn2+: dual recordings in slices of adult rat hippocampus. The European journal of neuroscience 11:3552-3564.
Payne C, Machado CJ, Bliwise NG, Bachevalier J (2010) Maturation of the hippocampal formation and amygdala in Macaca mulatta: a volumetric magnetic resonance imaging study. Hippocampus 20:922-935.
Paz R, Bauer EP, Pare D (2008) Theta synchronizes the activity of medial prefrontal neurons during learning. Learn Mem 15:524-531.
Pellegrino L (1968) Amygdaloid lesions and behavioral inhibition in the rat. J Comp Physiol Psychol 65:483-491.
Pelletier JG, Pare D (2004) Role of amygdala oscillations in the consolidation of emotional memories. Biological psychiatry 55:559-562.
Pena F, Amuzescu B, Neaga E, Flonta ML (2006) Thermodynamic properties of hyperpolarization-activated current (Ih) in a subgroup of primary sensory neurons. Experimental brain research Experimentelle Hirnforschung Experimentation cerebrale 173:282-290.
Penttonen M, Kamondi A, Acsady L, Buzsaki G (1998) Gamma frequency oscillation in the hippocampus of the rat: intracellular analysis in vivo. The European journal of neuroscience 10:718-728.

Perez-Reyes E (2003) Molecular physiology of low-voltage-activated t-type calcium channels. Physiological reviews 83:117-161.

Person AL, Perkel DJ (2005) Unitary IPSPs drive precise thalamic spiking in a circuit required for learning. Neuron 46:129-140.

Pessoa L, Adolphs R (2010) Emotion processing and the amygdala: from a 'low road' to 'many roads' of evaluating biological significance. Nature reviews Neuroscience 11:773-783.

Pfister JP, Dayan P, Lengyel M (2010) Synapses with short-term plasticity are optimal estimators of presynaptic membrane potentials. Nature neuroscience 13:1271-1275.

Pike FG, Goddard RS, Suckling JM, Ganter P, Kasthuri N, Paulsen O (2000) Distinct frequency preferences of different types of rat hippocampal neurones in response to oscillatory input currents. The Journal of physiology 529 Pt 1:205-213.

Pillai AG, de Jong D, Kanatsou S, Krugers H, Knapman A, Heinzmann JM, Holsboer F, Landgraf R, Joels M, Touma C (2012) Dendritic morphology of hippocampal and amygdalar neurons in adolescent mice is resilient to genetic differences in stress reactivity. PloS one 7:e38971.

Pin JP, Duvoisin R (1995) The metabotropic glutamate receptors: structure and functions. Neuropharmacology 34:1-26.

Pine DS (2002) Brain development and the onset of mood disorders. Seminars in clinical neuropsychiatry 7:223-233.

Pine DS, Cohen P, Gurley D, Brook J, Ma Y (1998) The risk for early-adulthood anxiety and depressive disorders in adolescents with anxiety and depressive disorders. Archives of general psychiatry 55:56-64.

Pizzorusso T, Medini P, Berardi N, Chierzi S, Fawcett JW, Maffei L (2002) Reactivation of ocular dominance plasticity in the adult visual cortex. Science 298:1248-1251.

Plotkin JL, Wu N, Chesselet MF, Levine MS (2005) Functional and molecular development of striatal fast-spiking GABAergic interneurons and their cortical inputs. The European journal of neuroscience 22:1097-1108.

Ponomarev I, Rau V, Eger EI, Harris RA, Fanselow MS (2010) Amygdala transcriptome and cellular mechanisms underlying stress-enhanced fear learning in a rat model of posttraumatic stress disorder. Neuropsychopharmacology : official publication of the American College of Neuropsychopharmacology 35:1402-1411.

Popa D, Duvarci S, Popescu AT, Lena C, Pare D (2010) Coherent amygdalocortical theta promotes fear memory consolidation during paradoxical sleep. Proceedings of the National Academy of Sciences of the United States of America 107:6516-6519.

Popescu AT, Pare D (2011) Synaptic interactions underlying synchronized inhibition in the basal amygdala: evidence for existence of two types of projection cells. Journal of neurophysiology 105:687-696.

Pouille F, Scanziani M (2001) Enforcement of temporal fidelity in pyramidal cells by somatic feed-forward inhibition. Science 293:1159-1163.

Pouzat C, Hestrin S (1997) Developmental regulation of basket/stellate cell-->Purkinje cell synapses in the cerebellum. The Journal of neuroscience : the official journal of the Society for Neuroscience 17:9104-9112.

Prather MD, Lavenex P, Mauldin-Jourdain ML, Mason WA, Capitanio JP, Mendoza SP, Amaral DG (2001) Increased social fear and decreased fear of objects in monkeys with neonatal amygdala lesions. Neuroscience 106:653-658.

Prescott SA, Sejnowski TJ (2008) Spike-rate coding and spike-time coding are affected oppositely by different adaptation mechanisms. The Journal of neuroscience : the official journal of the Society for Neuroscience 28:13649-13661.

Puram SV, Kim AH, Ikeuchi Y, Wilson-Grady JT, Merdes A, Gygi SP, Bonni A (2011) A CaMKIIbeta signaling pathway at the centrosome regulates dendrite patterning in the brain. Nature neuroscience 14:973-983.

Qin S, Young CB, Supekar K, Uddin LQ, Menon V (2012) Immature integration and segregation of emotion-related brain circuitry in young children. Proceedings of the National Academy of Sciences of the United States of America 109:7941-7946.

Quinn R (2005) Comparing rat's to human's age: how old is my rat in people years? Nutrition 21:775-777.

Quirk GJ, Gehlert DR (2003) Inhibition of the amygdala: key to pathological states? Annals of the New York Academy of Sciences 985:263-272.

Quirk GJ, Repa C, LeDoux JE (1995) Fear conditioning enhances short-latency auditory responses of lateral amygdala neurons: parallel recordings in the freely behaving rat. Neuron 15:1029-1039.

Racine RJ, Gartner JG, Burnham WM (1972) Epileptiform activity and neural plasticity in limbic structures. Brain research 47:262-268.

Raimondo JV, Markram H, Akerman CJ (2012) Short-term ionic plasticity at GABAergic synapses. Frontiers in synaptic neuroscience 4:5.

Raineki C, De Souza MA, Szawka RE, Lutz ML, De Vasconcellos LF, Sanvitto GL, Izquierdo I, Bevilaqua LR, Cammarota M, Lucion AB (2009) Neonatal handling and the maternal odor preference in rat pups: involvement of monoamines and cyclic AMP response element-binding protein pathway in the olfactory bulb. Neuroscience 159:31-38.

Rainnie DG (1999a) Synchronous inhibitory synaptic potentials in simultaneously recorded neurons of the basolateral amygdala. Society for Neuroscience Annual Meeting, Miami Beach, FL, Oct 1999.

Rainnie DG (1999b) Serotonergic modulation of neurotransmission in the rat basolateral amygdala. Journal of neurophysiology 82:69-85.

Rainnie DG, Ressler KJ (2009) Physiology of the Amygdala: Implications for PTSD. In: Post-Traumatic Stress Disorder (LeDoux JE, Keane T, Shiromani P, eds). New York: Humana Press.

Rainnie DG, Asprodini EK, Shinnick-Gallagher P (1991a) Inhibitory transmission in the basolateral amygdala. Journal of neurophysiology 66:999-1009.

Rainnie DG, Asprodini EK, Shinnick-Gallagher P (1991b) Excitatory transmission in the basolateral amygdala. Journal of neurophysiology 66:986-998.

Rainnie DG, Fernhout BJ, Shinnick-Gallagher P (1992) Differential actions of corticotropin releasing factor on basolateral and central amygdaloid neurones, in vitro. J Pharmacol Exp Ther 263:846-858.

Rainnie DG, Asprodini EK, Shinnick-Gallagher P (1993) Intracellular recordings from morphologically identified neurons of the basolateral amygdala. Journal of neurophysiology 69:1350-1362.

Rainnie DG, Holmes KH, Shinnick-Gallagher P (1994) Activation of postsynaptic metabotropic glutamate receptors by trans-ACPD hyperpolarizes neurons of the basolateral amygdala. The Journal of neuroscience : the official journal of the Society for Neuroscience 14:7208-7220.

Rainnie DG, Mania I, Mascagni F, McDonald AJ (2006) Physiological and morphological characterization of parvalbumin-containing interneurons of the rat basolateral amygdala. The Journal of comparative neurology 498:142-161.

Rainnie DG, Bergeron R, Sajdyk TJ, Patil M, Gehlert DR, Shekhar A (2004) Corticotrophin releasing factor-induced synaptic plasticity in the amygdala translates stress into emotional disorders. The Journal of neuroscience : the official journal of the Society for Neuroscience 24:3471-3479.

Rakic P (1995) The development of the frontal lobe. A view from the rear of the brain. Advances in neurology 66:1-6; discussion 6-8.

Ramadan O, Qu Y, Wadgaonkar R, Baroudi G, Karnabi E, Chahine M, Boutjdir M (2009) Phosphorylation of the consensus sites of protein kinase A on alpha1D L-type calcium channel. The Journal of biological chemistry 284:5042-5049.

Ramakers GJ, van Galen H, Feenstra MG, Corner MA, Boer GJ (1994) Activity-dependent plasticity of inhibitory and excitatory amino acid transmitter systems in cultured rat cerebral cortex. International journal of developmental neuroscience : the official journal of the International Society for Developmental Neuroscience 12:611-621.

Ramamoorthi K, Lin Y (2011) The contribution of GABAergic dysfunction to neurodevelopmental disorders. Trends Mol Med 17:452-462.

Ramoa AS, McCormick DA (1994) Developmental changes in electrophysiological properties of LGNd neurons during reorganization of retinogeniculate connections. The Journal of neuroscience : the official journal of the Society for Neuroscience 14:2089-2097.

Randall FE, Whittington MA, Cunningham MO (2011) Fast oscillatory activity induced by kainate receptor activation in the rat basolateral amygdala in vitro. The European journal of neuroscience 33:914-922.

Rasetti R, Mattay VS, Wiedholz LM, Kolachana BS, Hariri AR, Callicott JH, Meyer-Lindenberg A, Weinberger DR (2009) Evidence that altered amygdala activity in schizophrenia is related to clinical state and not genetic risk. The American journal of psychiatry 166:216-225.

Reinblatt SP, Riddle MA (2007) The pharmacological management of childhood anxiety disorders: a review. Psychopharmacology 191:67-86.

Rescorla RA (2001) Retraining of extinguished Pavlovian stimuli. J Exp Psychol Anim Behav Process 27:115-124.

Reyes A, Sakmann B (1999) Developmental switch in the short-term modification of unitary EPSPs evoked in layer 2/3 and layer 5 pyramidal neurons of rat neocortex. The Journal of neuroscience : the official journal of the Society for Neuroscience 19:3827-3835.

Reznikov LR, Reagan LP, Fadel JR (2008) Activation of phenotypically distinct neuronal subpopulations in the anterior subdivision of the rat basolateral amygdala following acute and repeated stress. The Journal of comparative neurology 508:458-472.

Richardson HN, Zorrilla EP, Mandyam CD, Rivier CL (2006) Exposure to repetitive versus varied stress during prenatal development generates two distinct anxiogenic and neuroendocrine profiles in adulthood. Endocrinology 147:2506-2517.

Richardson MJ, Brunel N, Hakim V (2003) From subthreshold to firing-rate resonance. Journal of neurophysiology 89:2538-2554.

Richardson R, Paxinos G, Lee J (2000) The ontogeny of conditioned odor potentiation of startle. Behavioral neuroscience 114:1167-1173.

Rinaman L, Levitt P, Card JP (2000) Progressive postnatal assembly of limbic-autonomic circuits revealed by central transneuronal transport of pseudorabies virus. The Journal of neuroscience : the official journal of the Society for Neuroscience 20:2731-2741.

Robbe D, Montgomery SM, Thome A, Rueda-Orozco PE, McNaughton BL, Buzsaki G (2006) Cannabinoids reveal importance of spike timing coordination in hippocampal function. Nature neuroscience 9:1526-1533.

Robinson RB, Siegelbaum SA (2003) Hyperpolarization-activated cation currents: from molecules to physiological function. Annual review of physiology 65:453-480.

Rodrigues SM, Schafe GE, LeDoux JE (2001) Intra-amygdala blockade of the NR2B subunit of the NMDA receptor disrupts the acquisition but not the expression of fear conditioning. The Journal of neuroscience : the official journal of the Society for Neuroscience 21:6889-6896.

Rodrigues SM, Schafe GE, LeDoux JE (2004) Molecular mechanisms underlying emotional learning and memory in the lateral amygdala. Neuron 44:75-91.

Rodrigues SM, LeDoux JE, Sapolsky RM (2009) The influence of stress hormones on fear circuitry. Annual review of neuroscience 32:289-313.

Rodriguez Manzanares PA, Isoardi NA, Carrer HF, Molina VA (2005) Previous stress facilitates fear memory, attenuates GABAergic inhibition, and increases synaptic plasticity in the rat basolateral amygdala. The Journal of neuroscience : the official journal of the Society for Neuroscience 25:8725-8734.

Roepstorff A, Lambert JD (1994) Factors contributing to the decay of the stimulus-evoked IPSC in rat hippocampal CA1 neurons. Journal of neurophysiology 72:2911-2926.

Romand S, Wang Y, Toledo-Rodriguez M, Markram H (2011) Morphological development of thick-tufted layer v pyramidal cells in the rat somatosensory cortex. Front Neuroanat 5:5.

Romeo RD, Bellani R, Karatsoreos IN, Chhua N, Vernov M, Conrad CD, McEwen BS (2006) Stress history and pubertal development interact to shape hypothalamic-pituitary-adrenal axis plasticity. Endocrinology 147:1664-1674.

Ronald A, Pennell CE, Whitehouse AJ (2010) Prenatal Maternal Stress Associated with ADHD and Autistic Traits in early Childhood. Front Psychol 1:223.

Roozendaal B, McEwen BS, Chattarji S (2009) Stress, memory and the amygdala. Nature reviews Neuroscience 10:423-433.

Roozendaal B, Brunson KL, Holloway BL, McGaugh JL, Baram TZ (2002) Involvement of stress-released corticotropin-releasing hormone in the basolateral amygdala in regulating memory consolidation. Proceedings of the National Academy of Sciences of the United States of America 99:13908-13913.

Rosvold HE, Mirsky AF, Pribram KH (1954) Influence of amygdalectomy on social behavior in monkeys. J Comp Physiol Psychol 47:173-178.

Rothman JS, Cathala L, Steuber V, Silver RA (2009) Synaptic depression enables neuronal gain control. Nature 457:1015-1018.

Royer S, Zemelman BV, Losonczy A, Kim J, Chance F, Magee JC, Buzsaki G (2012) Control of timing, rate and bursts of hippocampal place cells by dendritic and somatic inhibition. Nature neuroscience 15:769-775.

Rubinow MJ, Juraska JM (2009) Neuron and glia numbers in the basolateral nucleus of the amygdala from preweaning through old age in male and female rats: a stereological study. The Journal of comparative neurology 512:717-725.

Rudy B (1988) Diversity and ubiquity of K channels. Neuroscience 25:729-749.

Rudy JW (1993) Contextual conditioning and auditory cue conditioning dissociate during development. Behavioral neuroscience 107:887-891.

Russier M, Carlier E, Ankri N, Fronzaroli L, Debanne D (2003) A-, T-, and H-type currents shape intrinsic firing of developing rat abducens motoneurons. The Journal of physiology 549:21-36.

Rutherford LC, DeWan A, Lauer HM, Turrigiano GG (1997) Brain-derived neurotrophic factor mediates the activity-dependent regulation of inhibition in neocortical cultures. The Journal of neuroscience : the official journal of the Society for Neuroscience 17:4527-4535.

Ryan BC, Young NB, Crawley JN, Bodfish JW, Moy SS (2010) Social deficits, stereotypy and early emergence of repetitive behavior in the C58/J inbred mouse strain. Behavioural brain research 208:178-188.

Ryan SJ, Ehrlich DE, Jasnow AJ, Daftary S, Madsen TE, Rainnie DG (2012) Spike-Timing Precision and Neuronal Synchrony Are Enhanced by an Interaction between Synaptic Inhibition and Membrane Oscillations in the Amygdala. PloS one 7:e35320.

Sadler TR, Nguyen PT, Yang J, Givrad TK, Mayer EA, Maarek JM, Hinton DR, Holschneider DP (2011) Antenatal maternal stress alters functional brain responses in adult offspring during conditioned fear. Brain research 1385:163-174.

Sajdyk TJ, Schober DA, Gehlert DR, Shekhar A (1999) Role of corticotropin-releasing factor and urocortin within the basolateral amygdala of rats in anxiety and panic responses. Behavioural brain research 100:207-215.

Sanchez MM (2006) The impact of early adverse care on HPA axis development: nonhuman primate models. Hormones and behavior 50:623-631.

Sanchez MM, Ladd CO, Plotsky PM (2001) Early adverse experience as a developmental risk factor for later psychopathology: evidence from rodent and primate models. Development and psychopathology 13:419-449.

Sancristobal B, Sancho JM, Garcia-Ojalvo J (2010) Phase-response approach to firing-rate selectivity in neurons with subthreshold oscillations. Physical review E, Statistical, nonlinear, and soft matter physics 82:041908.

Sanders SK, Shekhar A (1995) Regulation of anxiety by GABAA receptors in the rat amygdala. Pharmacology, biochemistry, and behavior 52:701-706.

Sanders SK, Morzorati SL, Shekhar A (1995) Priming of experimental anxiety by repeated subthreshold GABA blockade in the rat amygdala. Brain research 699:250-259.

Sandford JJ, Argyropoulos SV, Nutt DJ (2000) The psychobiology of anxiolytic drugs. Part 1: Basic neurobiology. Pharmacol Ther 88:197-212.

Sanes DH, Kotak VC (2011) Developmental plasticity of auditory cortical inhibitory synapses. Hearing research 279:140-148.

Sangha S, Narayanan RT, Bergado-Acosta JR, Stork O, Seidenbecher T, Pape HC (2009) Deficiency of the 65 kDa isoform of glutamic acid decarboxylase impairs extinction of cued but not contextual fear memory. The Journal of neuroscience : the official journal of the Society for Neuroscience 29:15713-15720.

Sapolsky RM, Meaney MJ (1986) Maturation of the adrenocortical stress response: neuroendocrine control mechanisms and the stress hyporesponsive period. Brain research 396:64-76.

Sauer JF, Bartos M (2010) Recruitment of early postnatal parvalbumin-positive hippocampal interneurons by GABAergic excitation. The Journal of neuroscience : the official journal of the Society for Neuroscience 30:110-115.

Scanziani M (2000) GABA spillover activates postsynaptic GABA(B) receptors to control rhythmic hippocampal activity. Neuron 25:673-681.

Schaefer AT, Angelo K, Spors H, Margrie TW (2006) Neuronal oscillations enhance stimulus discrimination by ensuring action potential precision. PLoS Biol 4:e163.

Schafe GE, Nadel NV, Sullivan GM, Harris A, LeDoux JE (1999) Memory consolidation for contextual and auditory fear conditioning is dependent on protein synthesis, PKA, and MAP kinase. Learn Mem 6:97-110.

Schmahl CG, Vermetten E, Elzinga BM, Douglas Bremner J (2003) Magnetic resonance imaging of hippocampal and amygdala volume in women with childhood abuse and borderline personality disorder. Psychiatry research 122:193-198.

Schneider F, Weiss U, Kessler C, Salloum JB, Posse S, Grodd W, Muller-Gartner HW (1998) Differential amygdala activation in schizophrenia during sadness. Schizophrenia research 34:133-142.

Schreiber S, Fellous JM, Whitmer D, Tiesinga P, Sejnowski TJ (2003) A new correlation-based measure of spike timing reliability. Neurocomputing 52-54:925-931.

Schultz RT (2005) Developmental deficits in social perception in autism: the role of the amygdala and fusiform face area. International journal of developmental neuroscience : the official journal of the International Society for Developmental Neuroscience 23:125-141.

Schulze L, Domes G, Kruger A, Berger C, Fleischer M, Prehn K, Schmahl C, Grossmann A, Hauenstein K, Herpertz SC (2011) Neuronal correlates of cognitive reappraisal in borderline patients with affective instability. Biological psychiatry 69:564-573.

Schumann CM, Barnes CC, Lord C, Courchesne E (2009) Amygdala enlargement in toddlers with autism related to severity of social and communication impairments. Biological psychiatry 66:942-949.

Schwaller B, Meyer M, Schiffmann S (2002) 'New' functions for 'old' proteins: the role of the calcium-binding proteins calbindin D-28k, calretinin and parvalbumin, in cerebellar physiology. Studies with knockout mice. Cerebellum 1:241-258.

Seidel K, Helmeke C, Poeggel G, Braun K (2008) Repeated neonatal separation stress alters the composition of neurochemically characterized interneuron subpopulations in the rodent dentate gyrus and basolateral amygdala. Developmental neurobiology 68:1137-1152.

Seidenbecher T, Laxmi TR, Stork O, Pape HC (2003) Amygdalar and hippocampal theta rhythm synchronization during fear memory retrieval. Science 301:846-850.

Serodio P, Rudy B (1998) Differential expression of Kv4 K+ channel subunits mediating subthreshold transient K+ (A-type) currents in rat brain. Journal of neurophysiology 79:1081-1091.

Sgado P, Dunleavy M, Genovesi S, Provenzano G, Bozzi Y (2011) The role of GABAergic system in neurodevelopmental disorders: a focus on autism and epilepsy. Int J Physiol Pathophysiol Pharmacol 3:223-235.

Shaban H, Humeau Y, Herry C, Cassasus G, Shigemoto R, Ciocchi S, Barbieri S, van der Putten H, Kaupmann K, Bettler B, Luthi A (2006) Generalization of amygdala LTP and conditioned fear in the absence of presynaptic inhibition. Nature neuroscience 9:1028-1035.

Shaw P, Brierley B, David AS (2005) A critical period for the impact of amygdala damage on the emotional enhancement of memory? Neurology 65:326-328.

Shayegan DK, Stahl SM (2005) Emotion processing, the amygdala, and outcome in schizophrenia. Prog Neuropsychopharmacol Biol Psychiatry 29:840-845.

Shekhar A, Sajdyk TJ, Gehlert DR, Rainnie DG (2003) The amygdala, panic disorder, and cardiovascular responses. Annals of the New York Academy of Sciences 985:308-325.

Shekhar A, Truitt W, Rainnie D, Sajdyk T (2005) Role of stress, corticotrophin releasing factor (CRF) and amygdala plasticity in chronic anxiety. Stress 8:209-219.

Sheng M, Tsaur ML, Jan YN, Jan LY (1992) Subcellular segregation of two A-type K+ channel proteins in rat central neurons. Neuron 9:271-284.

Shepherd GM (1996) The dendritic spine: a multifunctional integrative unit. Journal of neurophysiology 75:2197-2210.

Shin LM, Rauch SL, Pitman RK (2006) Amygdala, medial prefrontal cortex, and hippocampal function in PTSD. Annals of the New York Academy of Sciences 1071:67-79.

Shu W, Cho JY, Jiang Y, Zhang M, Weisz D, Elder GA, Schmeidler J, De Gasperi R, Sosa MA, Rabidou D, Santucci AC, Perl D, Morrisey E, Buxbaum JD (2005) Altered ultrasonic vocalization in mice with a disruption in the Foxp2 gene. Proceedings of the National Academy of Sciences of the United States of America 102:9643-9648.

Shu Y, Hasenstaub A, McCormick DA (2003) Turning on and off recurrent balanced cortical activity. Nature 423:288-293.

Sieghart W, Sperk G (2002) Subunit composition, distribution and function of GABA(A) receptor subtypes. Current topics in medicinal chemistry 2:795-816.

Sinfield JL, Collins DR (2006) Induction of synchronous oscillatory activity in the rat lateral amygdala in vitro is dependent on gap junction activity. The European journal of neuroscience 24:3091-3095.

Singer W (2009) Distributed processing and temporal codes in neuronal networks. Cognitive neurodynamics 3:189-196.

Smagin GN, Heinrichs SC, Dunn AJ (2001) The role of CRH in behavioral responses to stress. Peptides 22:713-724.

Snead OC, 3rd, Stephens HI (1983) Ontogeny of cortical and subcortical electroencephalographic events in unrestrained neonatal and infant rats. Experimental neurology 82:249-269.
Sohal VS, Pangratz-Fuehrer S, Rudolph U, Huguenard JR (2006) Intrinsic and synaptic dynamics interact to generate emergent patterns of rhythmic bursting in thalamocortical neurons. The Journal of neuroscience : the official journal of the Society for Neuroscience 26:4247-4255.
Sohal VS, Zhang F, Yizhar O, Deisseroth K (2009) Parvalbumin neurons and gamma rhythms enhance cortical circuit performance. Nature 459:698-702.
Soltesz I, Deschenes M (1993) Low- and high-frequency membrane potential oscillations during theta activity in CA1 and CA3 pyramidal neurons of the rat hippocampus under ketamine-xylazine anesthesia. Journal of neurophysiology 70:97-116.
Somerville LH, Jones RM, Casey BJ (2010) A time of change: behavioral and neural correlates of adolescent sensitivity to appetitive and aversive environmental cues. Brain Cogn 72:124-133.
Somogyi P, Kisvarday ZF, Martin KA, Whitteridge D (1983) Synaptic connections of morphologically identified and physiologically characterized large basket cells in the striate cortex of cat. Neuroscience 10:261-294.
Sotres-Bayon F, Quirk GJ (2010) Prefrontal control of fear: more than just extinction. Curr Opin Neurobiol 20:231-235.
Southwell DG, Froemke RC, Alvarez-Buylla A, Stryker MP, Gandhi SP (2010) Cortical plasticity induced by inhibitory neuron transplantation. Science 327:1145-1148.
Spear LP (2009) Heightened stress responsivity and emotional reactivity during pubertal maturation: Implications for psychopathology. Development and psychopathology 21:87-97.
Spitzer NC, Debaca RC, Allen KA, Holliday J (1993) Calcium dependence of differentiation of GABA immunoreactivity in spinal neurons. The Journal of comparative neurology 337:168-175.
State MW, Levitt P (2011) The conundrums of understanding genetic risks for autism spectrum disorders. Nature neuroscience 14:1499-1506.
Stein MB, Koverola C, Hanna C, Torchia MG, McClarty B (1997) Hippocampal volume in women victimized by childhood sexual abuse. Psychological medicine 27:951-959.
Steinberg L (2005) Cognitive and affective development in adolescence. Trends in cognitive sciences 9:69-74.
Stiefel KM, Fellous JM, Thomas PJ, Sejnowski TJ (2010) Intrinsic subthreshold oscillations extend the influence of inhibitory synaptic inputs on cortical pyramidal neurons. The European journal of neuroscience 31:1019-1026.
Storm JF (1989) An after-hyperpolarization of medium duration in rat hippocampal pyramidal cells. The Journal of physiology 409:171-190.
Stuber GD, Sparta DR, Stamatakis AM, van Leeuwen WA, Hardjoprajitno JE, Cho S, Tye KM, Kempadoo KA, Zhang F, Deisseroth K, Bonci A (2011) Excitatory transmission from the amygdala to nucleus accumbens facilitates reward seeking. Nature 475:377-380.
Sullivan RM, Landers M, Yeaman B, Wilson DA (2000) Good memories of bad events in infancy. Nature 407:38-39.
Surges R, Freiman TM, Feuerstein TJ (2004) Input resistance is voltage dependent due to activation of Ih channels in rat CA1 pyramidal cells. Journal of neuroscience research 76:475-480.
Surges R, Brewster AL, Bender RA, Beck H, Feuerstein TJ, Baram TZ (2006) Regulated expression of HCN channels and cAMP levels shape the properties of the h current in developing rat hippocampus. The European journal of neuroscience 24:94-104.
Sweeten TL, Posey DJ, Shekhar A, McDougle CJ (2002) The amygdala and related structures in the pathophysiology of autism. Pharmacology, biochemistry, and behavior 71:449-455.

Szinyei C, Heinbockel T, Montagne J, Pape HC (2000) Putative cortical and thalamic inputs elicit convergent excitation in a population of GABAergic interneurons of the lateral amygdala. The Journal of neuroscience : the official journal of the Society for Neuroscience 20:8909-8915.

Sztainberg Y, Kuperman Y, Tsoory M, Lebow M, Chen A (2010) The anxiolytic effect of environmental enrichment is mediated via amygdalar CRF receptor type 1. Molecular psychiatry 15:905-917.

Szucs A, Huerta R, Rabinovich MI, Selverston AI (2009) Robust microcircuit synchronization by inhibitory connections. Neuron 61:439-453.

Takahashi LK (1992) Ontogeny of behavioral inhibition induced by unfamiliar adult male conspecifics in preweanling rats. Physiology & behavior 52:493-498.

Takahashi LK, Rubin WW (1993) Corticosteroid induction of threat-induced behavioral inhibition in preweanling rats. Behavioral neuroscience 107:860-866.

Takahashi LK, Turner JG, Kalin NH (1991) Development of stress-induced responses in preweanling rats. Developmental psychobiology 24:341-360.

Takatoh J, Wang F (2012) Axonally translated SMADs link up BDNF and retrograde BMP signaling. Neuron 74:3-5.

Talge NM, Neal C, Glover V (2007) Antenatal maternal stress and long-term effects on child neurodevelopment: how and why? Journal of child psychology and psychiatry, and allied disciplines 48:245-261.

Talley EM, Cribbs LL, Lee JH, Daud A, Perez-Reyes E, Bayliss DA (1999) Differential distribution of three members of a gene family encoding low voltage-activated (T-type) calcium channels. The Journal of neuroscience : the official journal of the Society for Neuroscience 19:1895-1911.

Tamas G, Buhl EH, Somogyi P (1997) Fast IPSPs elicited via multiple synaptic release sites by different types of GABAergic neurone in the cat visual cortex. The Journal of physiology 500 (Pt 3):715-738.

Tamas G, Szabadics J, Lorincz A, Somogyi P (2004) Input and frequency-specific entrainment of postsynaptic firing by IPSPs of perisomatic or dendritic origin. The European journal of neuroscience 20:2681-2690.

Tang HH, McNally GP, Richardson R (2007) The effects of FG7142 on two types of forgetting in 18-day-old rats. Behavioral neuroscience 121:1421-1425.

Teicher MH, Andersen SL, Polcari A, Anderson CM, Navalta CP, Kim DM (2003) The neurobiological consequences of early stress and childhood maltreatment. Neurosci Biobehav Rev 27:33-44.

Thomas CG, Tian H, Diamond JS (2011) The relative roles of diffusion and uptake in clearing synaptically released glutamate change during early postnatal development. The Journal of neuroscience : the official journal of the Society for Neuroscience 31:4743-4754.

Thomas KM, Drevets WC, Whalen PJ, Eccard CH, Dahl RE, Ryan ND, Casey BJ (2001a) Amygdala response to facial expressions in children and adults. Biological psychiatry 49:309-316.

Thomas KM, Drevets WC, Dahl RE, Ryan ND, Birmaher B, Eccard CH, Axelson D, Whalen PJ, Casey BJ (2001b) Amygdala response to fearful faces in anxious and depressed children. Archives of general psychiatry 58:1057-1063.

Thompson JV, Sullivan RM, Wilson DA (2008) Developmental emergence of fear learning corresponds with changes in amygdala synaptic plasticity. Brain research 1200:58-65.

Thomson AM, Bannister AP, Hughes DI, Pawelzik H (2000) Differential sensitivity to Zolpidem of IPSPs activated by morphologically identified CA1 interneurons in slices of rat hippocampus. The European journal of neuroscience 12:425-436.

Tohidi V, Nadim F (2009) Membrane resonance in bursting pacemaker neurons of an oscillatory network is correlated with network frequency. The Journal of neuroscience : the official journal of the Society for Neuroscience 29:6427-6435.

Torres-Garcia ME, Solis O, Patricio A, Rodriguez-Moreno A, Camacho-Abrego I, Limon ID, Flores G (2012) Dendritic morphology changes in neurons from the prefrontal cortex, hippocampus and nucleus accumbens in rats after lesion of the thalamic reticular nucleus. Neuroscience 223:429-438.

Tosevski J, Malikovic A, Mojsilovic-Petrovic J, Lackovic V, Peulic M, Sazdanovic P, Alexopulos C (2002) Types of neurons and some dendritic patterns of basolateral amygdala in humans--a golgi study. Ann Anat 184:93-103.

Tottenham N, Sheridan MA (2009) A review of adversity, the amygdala and the hippocampus: a consideration of developmental timing. Frontiers in human neuroscience 3:68.

Tottenham N, Hare TA, Millner A, Gilhooly T, Zevin JD, Casey BJ (2011) Elevated amygdala response to faces following early deprivation. Dev Sci 14:190-204.

Tottenham N, Hertzig ME, Gillespie-Lynch K, Gilhooly T, Millner AJ, Casey BJ (2013) Elevated amygdala response to faces and gaze aversion in autism spectrum disorder. Soc Cogn Affect Neurosci.

Tottenham N, Hare TA, Quinn BT, McCarry TW, Nurse M, Gilhooly T, Millner A, Galvan A, Davidson MC, Eigsti IM, Thomas KM, Freed PJ, Booma ES, Gunnar MR, Altemus M, Aronson J, Casey BJ (2010) Prolonged institutional rearing is associated with atypically large amygdala volume and difficulties in emotion regulation. Dev Sci 13:46-61.

Tritsch NX, Bergles DE (2010) Developmental regulation of spontaneous activity in the Mammalian cochlea. The Journal of neuroscience : the official journal of the Society for Neuroscience 30:1539-1550.

Truitt WA, Sajdyk TJ, Dietrich AD, Oberlin B, McDougle CJ, Shekhar A (2007) From anxiety to autism: spectrum of abnormal social behaviors modeled by progressive disruption of inhibitory neuronal function in the basolateral amygdala in Wistar rats. Psychopharmacology 191:107-118.

Tseng HA, Nadim F (2010) The membrane potential waveform of bursting pacemaker neurons is a predictor of their preferred frequency and the network cycle frequency. The Journal of neuroscience : the official journal of the Society for Neuroscience 30:10809-10819.

Tsoory MM, Guterman A, Richter-Levin G (2010) "Juvenile stress" alters maturation-related changes in expression of the neural cell adhesion molecule L1 in the limbic system: relevance for stress-related psychopathologies. Journal of neuroscience research 88:369-380.

Tully K, Li Y, Tsvetkov E, Bolshakov VY (2007) Norepinephrine enables the induction of associative long-term potentiation at thalamo-amygdala synapses. Proceedings of the National Academy of Sciences of the United States of America 104:14146-14150.

Tyzio R, Minlebaev M, Rheims S, Ivanov A, Jorquera I, Holmes GL, Zilberter Y, Ben-Ari Y, Khazipov R (2008) Postnatal changes in somatic gamma-aminobutyric acid signalling in the rat hippocampus. The European journal of neuroscience 27:2515-2528.

Ugolini A, Sokal DM, Arban R, Large CH (2008) CRF1 receptor activation increases the response of neurons in the basolateral nucleus of the amygdala to afferent stimulation. Front Behav Neurosci 2:2.

Ulfig N, Setzer M, Bohl J (2003) Ontogeny of the human amygdala. Annals of the New York Academy of Sciences 985:22-33.

Umeda T, Takashima N, Nakagawa R, Maekawa M, Ikegami S, Yoshikawa T, Kobayashi K, Okanoya K, Inokuchi K, Osumi N (2010) Evaluation of Pax6 mutant rat as a model for autism. PloS one 5:e15500.

Vacher H, Diochot S, Bougis PE, Martin-Eauclaire MF, Mourre C (2006) Kv4 channels sensitive to BmTX3 in rat nervous system: autoradiographic analysis of their distribution during brain ontogenesis. The European journal of neuroscience 24:1325-1340.

Vale W, Spiess J, Rivier C, Rivier J (1981) Characterization of a 41-residue ovine hypothalamic peptide that stimulates secretion of corticotropin and beta-endorphin. Science 213:1394-1397.

Valeeva G, Abdullin A, Tyzio R, Skorinkin A, Nikolski E, Ben-Ari Y, Khazipov R (2010) Temporal coding at the immature depolarizing GABAergic synapse. Front Cell Neurosci 4.

Van den Bergh BR, Marcoen A (2004) High antenatal maternal anxiety is related to ADHD symptoms, externalizing problems, and anxiety in 8- and 9-year-olds. Child Dev 75:1085-1097.

Van den Bergh BR, Mulder EJ, Mennes M, Glover V (2005) Antenatal maternal anxiety and stress and the neurobehavioural development of the fetus and child: links and possible mechanisms. A review. Neurosci Biobehav Rev 29:237-258.

van der Kooij MA, Sandi C (2012) Social memories in rodents: methods, mechanisms and modulation by stress. Neurosci Biobehav Rev 36:1763-1772.

van Dongen J, Boomsma DI (2013) The evolutionary paradox and the missing heritability of schizophrenia. Am J Med Genet B Neuropsychiatr Genet 162B:122-136.

Van Eden CG, Uylings HB (1985) Postnatal volumetric development of the prefrontal cortex in the rat. The Journal of comparative neurology 241:268-274.

Vargas G, Lucero MT (2002) Modulation by PKA of the hyperpolarization-activated current (Ih) in cultured rat olfactory receptor neurons. The Journal of membrane biology 188:115-125.

Vasilyev DV, Barish ME (2002) Postnatal development of the hyperpolarization-activated excitatory current Ih in mouse hippocampal pyramidal neurons. The Journal of neuroscience : the official journal of the Society for Neuroscience 22:8992-9004.

Verwer RW, Van Vulpen EH, Van Uum JF (1996) Postnatal development of amygdaloid projections to the prefrontal cortex in the rat studied with retrograde and anterograde tracers. The Journal of comparative neurology 376:75-96.

Vicini S, Ferguson C, Prybylowski K, Kralic J, Morrow AL, Homanics GE (2001) GABA(A) receptor alpha1 subunit deletion prevents developmental changes of inhibitory synaptic currents in cerebellar neurons. The Journal of neuroscience : the official journal of the Society for Neuroscience 21:3009-3016.

Vidal L, Ruiz C, Villena A, Diaz F, Perez de Vargas I (2004) Quantitative age-related changes in dorsal lateral geniculate nucleus relay neurons of the rat. Neurosci Res 48:387-396.

Vislay RL, Martin BS, Olmos-Serrano JL, Kratovac S, Nelson DL, Corbin JG, Huntsman MM (2013) Homeostatic responses fail to correct defective amygdala inhibitory circuit maturation in fragile X syndrome. The Journal of neuroscience : the official journal of the Society for Neuroscience 33:7548-7558.

Volgushev M, Chistiakova M, Singer W (1998) Modification of discharge patterns of neocortical neurons by induced oscillations of the membrane potential. Neuroscience 83:15-25.

Volk DW, Lewis DA (2013) Prenatal ontogeny as a susceptibility period for cortical GABA neuron disturbances in schizophrenia. Neuroscience 248C:154-164.

Vreugdenhil M, Jefferys JG, Celio MR, Schwaller B (2003) Parvalbumin-deficiency facilitates repetitive IPSCs and gamma oscillations in the hippocampus. Journal of neurophysiology 89:1414-1422.

Vyas A, Jadhav S, Chattarji S (2006) Prolonged behavioral stress enhances synaptic connectivity in the basolateral amygdala. Neuroscience 143:387-393.

Vyas A, Mitra R, Shankaranarayana Rao BS, Chattarji S (2002) Chronic stress induces contrasting patterns of dendritic remodeling in hippocampal and amygdaloid neurons.

The Journal of neuroscience : the official journal of the Society for Neuroscience 22:6810-6818.
Walker DL, Davis M (2008) Role of the extended amygdala in short-duration versus sustained fear: a tribute to Dr. Lennart Heimer. Brain structure & function 213:29-42.
Wang C, Wilson WA, Moore SD (2001) Role of NMDA, non-NMDA, and GABA receptors in signal propagation in the amygdala formation. Journal of neurophysiology 86:1422-1429.
Wang CW, Chan CL, Ho RT (2013) Prevalence and trajectory of psychopathology among child and adolescent survivors of disasters: a systematic review of epidemiological studies across 1987-2011. Soc Psychiatry Psychiatr Epidemiol 48:1697-1720.
Wang Y, Gupta A, Toledo-Rodriguez M, Wu CZ, Markram H (2002) Anatomical, physiological, molecular and circuit properties of nest basket cells in the developing somatosensory cortex. Cereb Cortex 12:395-410.
Washburn MS, Moises HC (1992) Inhibitory responses of rat basolateral amygdaloid neurons recorded in vitro. Neuroscience 50:811-830.
Weinstock M (2001) Alterations induced by gestational stress in brain morphology and behaviour of the offspring. Progress in neurobiology 65:427-451.
Weinstock M (2008) The long-term behavioural consequences of prenatal stress. Neurosci Biobehav Rev 32:1073-1086.
Weisskopf MG, Bauer EP, LeDoux JE (1999) L-type voltage-gated calcium channels mediate NMDA-independent associative long-term potentiation at thalamic input synapses to the amygdala. The Journal of neuroscience : the official journal of the Society for Neuroscience 19:10512-10519.
Welberg LA, Seckl JR (2001) Prenatal stress, glucocorticoids and the programming of the brain. Journal of neuroendocrinology 13:113-128.
Welberg LA, Seckl JR, Holmes MC (2000) Inhibition of 11beta-hydroxysteroid dehydrogenase, the foeto-placental barrier to maternal glucocorticoids, permanently programs amygdala GR mRNA expression and anxiety-like behaviour in the offspring. The European journal of neuroscience 12:1047-1054.
Welberg LA, Seckl JR, Holmes MC (2001) Prenatal glucocorticoid programming of brain corticosteroid receptors and corticotrophin-releasing hormone: possible implications for behaviour. Neuroscience 104:71-79.
White LE, Price JL (1993) The functional anatomy of limbic status epilepticus in the rat. I. Patterns of 14C-2-deoxyglucose uptake and Fos immunocytochemistry. The Journal of neuroscience : the official journal of the Society for Neuroscience 13:4787-4809.
Wiedenmayer CP (2009) Plasticity of defensive behavior and fear in early development. Neurosci Biobehav Rev 33:432-441.
Wiesel TN, Hubel DH (1963) Effects of Visual Deprivation on Morphology and Physiology of Cells in the Cats Lateral Geniculate Body. Journal of neurophysiology 26:978-993.
Wills TJ, Cacucci F, Burgess N, O'Keefe J (2010) Development of the hippocampal cognitive map in preweanling rats. Science 328:1573-1576.
Wiltgen BJ, Godsil BP, Peng Z, Saab F, June HL, Linn ML, Cook JM, Houser CR, O'Dell TJ, Homanics GE, Fanselow MS (2009) The alpha1 subunit of the GABA(A) receptor modulates fear learning and plasticity in the lateral amygdala. Front Behav Neurosci 3:37.
Wolterink G, Daenen LE, Dubbeldam S, Gerrits MA, van Rijn R, Kruse CG, Van Der Heijden JA, Van Ree JM (2001) Early amygdala damage in the rat as a model for neurodevelopmental psychopathological disorders. European neuropsychopharmacology : the journal of the European College of Neuropsychopharmacology 11:51-59.
Woodruff AR, Sah P (2007a) Inhibition and synchronization of basal amygdala principal neuron spiking by parvalbumin-positive interneurons. Journal of neurophysiology 98:2956-2961.

Woodruff AR, Sah P (2007b) Networks of parvalbumin-positive interneurons in the basolateral amygdala. The Journal of neuroscience : the official journal of the Society for Neuroscience 27:553-563.

Wu N, Hsiao CF, Chandler SH (2001) Membrane resonance and subthreshold membrane oscillations in mesencephalic V neurons: participants in burst generation. The Journal of neuroscience : the official journal of the Society for Neuroscience 21:3729-3739.

Yajeya J, de la Fuente Juan A, Merchan MA, Riolobos AS, Heredia M, Criado JM (1997) Cholinergic responses of morphologically and electrophysiologically characterized neurons of the basolateral complex in rat amygdala slices. Neuroscience 78:731-743.

Yamada D, Miyajima M, Ishibashi H, Wada K, Seki K, Sekiguchi M (2012) Adult-like action potential properties and abundant GABAergic synaptic responses in amygdala neurons from newborn marmosets. The Journal of physiology.

Yap CS, Richardson R (2007) The ontogeny of fear-potentiated startle: effects of earlier-acquired fear memories. Behavioral neuroscience 121:1053-1062.

Yehuda R (2001) Biology of posttraumatic stress disorder. J Clin Psychiatry 62 Suppl 17:41-46.

Yilmazer-Hanke DM, Faber-Zuschratter H, Linke R, Schwegler H (2002) Contribution of amygdala neurons containing peptides and calcium-binding proteins to fear-potentiated startle and exploration-related anxiety in inbred Roman high- and low-avoidance rats. The European journal of neuroscience 15:1206-1218.

Young CK (2011) Behavioral significance of hippocampal theta oscillations: looking elsewhere to find the right answers. Journal of neurophysiology 106:497-499.

Yurgelun-Todd D (2007) Emotional and cognitive changes during adolescence. Curr Opin Neurobiol 17:251-257.

Zaccolo M, Pozzan T (2003) CAMP and Ca2+ interplay: a matter of oscillation patterns. Trends in neurosciences 26:53-55.

Zagron G, Weinstock M (2006) Maternal adrenal hormone secretion mediates behavioural alterations induced by prenatal stress in male and female rats. Behavioural brain research 175:323-328.

Zarrow MX, Philpott JE, Denenberg VH (1970) Passage of 14C-4-corticosterone from the rat mother to the foetus and neonate. Nature 226:1058-1059.

Zhang J, Muller JF, McDonald AJ (2013) Noradrenergic innervation of pyramidal cells in the rat basolateral amygdala. Neuroscience 228:395-408.

Zhang JC, Lau PM, Bi GQ (2009) Gain in sensitivity and loss in temporal contrast of STDP by dopaminergic modulation at hippocampal synapses. Proceedings of the National Academy of Sciences of the United States of America 106:13028-13033.

Zhang JH, Sato M, Araki T, Tohyama M (1992) Postnatal ontogenesis of neurons containing GABAA alpha 1 subunit mRNA in the rat forebrain. Brain research Molecular brain research 16:193-203.

Zhang TY, Parent C, Weaver I, Meaney MJ (2004) Maternal programming of individual differences in defensive responses in the rat. Annals of the New York Academy of Sciences 1032:85-103.

Zhang TY, Bagot R, Parent C, Nesbitt C, Bredy TW, Caldji C, Fish E, Anisman H, Szyf M, Meaney MJ (2006) Maternal programming of defensive responses through sustained effects on gene expression. Biol Psychol 73:72-89.

Zhang W, Rosenkranz JA (2012) Repeated restraint stress increases basolateral amygdala neuronal activity in an age-dependent manner. Neuroscience 226:459-474.

Zhang W, Rosenkranz JA (2013) Repeated restraint stress enhances cue-elicited conditioned freezing and impairs acquisition of extinction in an age-dependent manner. Behavioural brain research 248:12-24.

Zhang ZW (2004) Maturation of layer V pyramidal neurons in the rat prefrontal cortex: intrinsic properties and synaptic function. Journal of neurophysiology 91:1171-1182.

Zucker RS, Regehr WG (2002) Short-term synaptic plasticity. Annual review of physiology 64:355-405.